



National Library
of Canada

Canadian Theses Service

Ottawa, Canada
K1A 0N4

Bibliothèque nationale
du Canada

Services des thèses canadiennes

CANADIAN THESES

NOTICE

The quality of this microfiche is heavily dependent upon the quality of the original thesis submitted for microfilming. Every effort has been made to ensure the highest quality of reproduction possible.

If pages are missing, contact the university which granted the degree.

Some pages may have indistinct print especially if the original pages were typed with a poor typewriter ribbon or if the university sent us an inferior photocopy.

Previously copyrighted materials (journal articles, published tests, etc.) are not filmed.

Reproduction in full or in part of this film is governed by the Canadian Copyright Act, R.S.C. 1970, c. C-30.

**THIS DISSERTATION
HAS BEEN MICROFILMED
EXACTLY AS RECEIVED**

THÈSES CANADIENNES

AVIS

La qualité de cette microfiche dépend grandement de la qualité de la thèse soumise au microfilmage. Nous avons tout fait pour assurer une qualité supérieure de reproduction.

S'il manque des pages, veuillez communiquer avec l'université qui a conféré le grade.

La qualité d'impression de certaines pages peut laisser à désirer, surtout si les pages originales ont été dactylographiées à l'aide d'un ruban usé ou si l'université nous a fait parvenir une photocopie de qualité inférieure.

Les documents qui font déjà l'objet d'un droit d'auteur (articles de revue, examens publiés, etc.) ne sont pas microfilmés.

La reproduction, même partielle, de ce microfilm est soumise à la Loi canadienne, sur le droit d'auteur, SRC 1970, c. C-30.

**LA THÈSE A ÉTÉ
MICROFILMÉE TELLE QUE
NOUS L'AVONS REÇUE**

**Simulation and Analysis of Dynamic Loads
on Cylindrical Gears and
An Improved Method for Fatigue Damage Assessment**

Selva Kumar Arumugam

A Thesis

in

The Department

of

Mechanical Engineering

**Presented in Partial Fulfillment of the Requirements
for the Degree of Doctor of Philosophy at
Concordia University
Montréal, Québec, Canada**

March 1986


© Selva Kumar Arumugam, 1986

Permission has been granted to the National Library of Canada to microfilm this thesis and to lend or sell copies of the film.

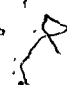
The author (copyright owner) has reserved other publication rights, and neither the thesis nor extensive extracts from it may be printed or otherwise reproduced without his/her written permission.

L'autorisation a été accordée à la Bibliothèque nationale du Canada de microfilmer cette thèse et de prêter ou de vendre des exemplaires du film.

L'auteur (titulaire du droit d'auteur) se réserve les autres droits de publication; ni la thèse ni de longs extraits de celle-ci ne doivent être imprimés ou autrement reproduits sans son autorisation écrite.



ISBN 0-315-30694-7



ABSTRACT

Simulation and Analysis of Dynamic Loads on Cylindrical Gears and An Improved Method for Fatigue Damage Assessment

Selva Kumar Arumugam, Ph.D.
Concordia University, 1986

In this thesis, modelling and solution procedures for the estimation of gear dynamic loads and the resulting fatigue damage in cylindrical gears are presented. Non-linear, non-stationary mathematical models incorporating the effects of the variable mesh stiffness, the transmission errors, the backlash, the friction between the teeth as well as the coupling between the torsional and lateral modes, are developed. Both deterministic and stochastic input characterizations are considered. The mathematical models are solved for the dynamic response and hence the dynamic force, using state-space technique. The use of state-space technique results in reduced computational effort and at the same time provides useful information regarding the dynamic stability of gear system modelled with minimal additional effort. Also, as a part of this thesis, a new modelling and solution scheme for analysing large dynamic systems is developed and is applied to gear system dynamics problem.

The fatigue damage and the fatigue life of modelled gears are then estimated with the use of local stress-strain

fatigue approach. The required local strain history at the critical location in the fillet is computed by the application of Boundary Element Methods to gear tooth stress analysis problem. To include the effect of multi-axial stress conditions at the fillet, an equivalent strain quantity is defined and used as the controlling variable. The fatigue damage due to the equivalent strain excursions is computed based on strain-life curve and accumulated with the use of Miner's rule. For this purpose, a computer simulation program, incorporating a simple cycle counting procedure, and the non-linear functional relationships between the local stresses and strains, is implemented. The program breaks any complex random strain history into individual cycles, so that constant loading fatigue data can be used for damage evaluation. In contrast to any existing program, the presented simulation program is concise and does not require the entire strain history to start the simulation, which makes it ideal for micro-processor based real time, on-line damage evaluation and monitoring applications.

At each stage of the thesis, the results from the simulation are compared with the available experimental and numerical results to validate the developed simulation and analysis procedures.

ACKNOWLEDGEMENTS

The author is deeply indebted to his supervisors Dr.M.O.M.Osman and Dr.T.S.Sankar for their encouragement and continued guidance during the course of this investigation.

The author wishes to acknowledge the financial support provided by Concordia University graduate fellowship, the Department of Mechanical Engineering, and other agencies during the course of this research.

Finally, the author wishes to thank his family and friends for their patience and continued encouragement during the course of this research.

TABLE OF CONTENTS

ABSTRACT	iii
ACKNOWLEDGEMENTS	v
TABLE OF CONTENTS	vi
LIST OF FIGURES	xi
LIST OF TABLES	xiv
NOMENCLATURE	xv

CHAPTER 1

INTRODUCTION AND LITERATURE REVIEW

1.1 General	1
1.2 Fatigue design of gears	3
1.3 Literature review	5
1.3.1 Gear dynamics	6
1.3.2 Gear tooth stress estimation	7
1.3.3 Gear fatigue	8
1.3.4 New approaches in fatigue analysis	9
1.3.5 Computer aided design of gears	13
1.4 Scope of the investigation	14

CHAPTER 2

IDENTIFICATION AND MODELLING OF THE FACTORS THAT INFLUENCE GEAR DYNAMIC BEHAVIOUR

2.1 Introduction	19
2.2 Classification of the influencing factors	21
2.2.1 Gear transmission error	22
2.2.2 Variable mesh stiffness	23
2.2.3 Non-linear backlash element	37

2.2.4 System inertias and shaft elasticities	39
2.2.5 Damping in the system	40
2.2.6 Input torque fluctuations	40
2.2.7 Variation in contact ratio	41
2.2.8 Coupling between torsional and lateral modes	44
2.2.9 Effect of friction	45
2.3 Summary	50

CHAPTER 3

DYNAMIC LOAD ESTIMATION - DETERMINISTIC APPROACH

3.1 Introduction	51
3.2 Modelling of the gear system	53
3.2.1 Schematic configuration of the gear system	55
3.2.2 Modelling of the configured gear system	55
3.3 Solution procedure	62
3.3.1 Selection of initial conditions	66
3.4 Dynamic load estimation	68
3.5 Verification of the simulator	69
3.6 Dynamic load variation	77
3.7 Stability analysis	81
3.8 Summary	85

CHAPTER 4

DYNAMIC LOAD ESTIMATION - STOCHASTIC APPROACH

4.1 Introduction	87
4.2 The mathematical model	89
4.2.1 Gear transmission error representation	90

4.2.2 Mathematical model	92
4.2.3 Selection of initial conditions	97
4.3 Dynamic load analysis	99
4.4 Summary	108

CHAPTER 5

DISCRETE - TIME TRANSFER MATRIX METHOD (DT-TMM)
AND ITS APPLICATION TO GEAR SYSTEM DYNAMICS

5.1 Introduction	109
5.2 Formulation of the DT-TMM	113
5.2.1 Basis of the methodology	113
5.2.2 Formulation of the method	118
5.2.3 Algorithm for response computation	122
5.2.4 Time step selection	123
5.2.5 Sources of error	125
5.2.6 Highlights of the method	126
5.2.7 Validation of the proposed methodology	127
5.3 DT-TMM as applied to gear dynamics	134
5.3.1 Massless shaft module	136
5.3.2 Lumped mass module	136
5.3.3 Disc module	136
5.3.4 Bearing module	137
5.3.5 Gear pair module	143
5.4 TM for other system components	147
5.5 Solution procedure	147
5.6 Validation of the proposed methodology	151
5.7 Summary	152

CHAPTER 6

ESTIMATION OF GEAR FATIGUE LIFE

6.1 Introduction	158
6.2 Computation of the stress-strain history	161
6.2.1 Static Vs Dynamic analysis	164
6.2.2 Boundary element analysis procedure	165
6.2.3 The boundary element model	165
6.2.4 Boundary conditions	166
6.2.5 Loading conditions	168
6.2.6 Output from the boundary element analysis	171
6.2.7 Validation of boundary element results	174
6.3 Construction of duty cycles	175
6.4 Simulation and accumulation of fatigue damage	179
6.5 Cyclic behaviour of metals	179
6.5.1 Cyclic stress-strain curve	179
6.5.2 Shape of stress-strain hysteresis loop	183
6.5.3 Memory effect	184
6.5.4 Cycle dependent properties	185
6.6 Computer simulation of the material behaviour	189
6.6.1 Proposed simulation model	192
6.7 Damage computation	197
6.8 Damage accumulation and life estimation	201
6.9 Summary	202

CHAPTER 7

EXTENSION TO HELICAL AND OTHER TYPES OF CYLINDRICAL GEARS

7.1 General	205
7.2 Helical gear dynamics	205
7.2.1 Variable mesh stiffness	206
7.2.2 Mathematical model	207
7.3 Extension to other types of cylindrical gears	214
7.4 Summary	216

CHAPTER 8

CONCLUSIONS AND RECOMMENDATIONS FOR FUTURE WORK

8.1 General	217
8.2 Specific conclusions	217
8.2.1 Gear dynamic load estimation	217
8.2.2 Stochastic estimation of gear dynamic load	218
8.2.3 Discrete time transfer matrix method	219
8.2.4 Estimation of gear fatigue life	220
8.3 Recommendations for future work	222

REFERENCES	224
------------	-----

APPENDIX I

BOUNDARY ELEMENT METHOD	245
-------------------------	-----

APPENDIX II

AN AUTOMATIC GEAR MESH GENERATOR (AGMG)	251
---	-----

APPENDIX III

SELECTION OF SHAPING FILTER PARAMETERS	273
--	-----

APPENDIX IV

FORTRAN PROGRAM FOR FATIGUE SIMULATION	276
--	-----

LIST OF FIGURES

- Fig. 2.1: Gear geometry
- Fig. 2.2: Hertz contact deformation and load distribution
- Fig. 2.3: BE model of a spur gear tooth
- Fig. 2.4: Calculated and approximated compliance
- Fig. 2.5: Gear tooth load pattern [42]
- Fig. 2.6: Comparison of tooth deflection values computed by various methods
- Fig. 2.7: Gear tooth backlash model
- Fig. 2.8: Gear tooth deflection under load
- Fig. 2.9: Forces acting between tooth pair in contact
- Fig. 3.1: Schematic of the dynamic load simulator
- Fig. 3.2: A typical spur gear system
- Fig. 3.3: Equivalent vibration system
- Fig. 3.4: Composition of matrices $K(t)$ and $C(t)$
- Fig. 3.5: Experimental set-up [127]
- Fig. 3.6: Comparison of simulator and experimental results
- Fig. 3.7: Comparison of simulator and photoelasticity results
- Fig. 3.8: Comparison of simulator and photoelasticity results
- Fig. 3.9: Variation of D.F. along contact position
- Fig. 3.10: Variation of maximum D.F. with operating speed
- Fig. 3.11: Stability chart for the given gear system
- Fig. 4.1: Typical gear transmission error signal
- Fig. 4.2: Symmetric backlash characteristics
- Fig. 4.3: Variation of mean and variance of D.F. with contact position, at 1500 R.P.M.
- Fig. 4.4: Variation of mean and variance of D.F. with contact position, at 3000 R.P.M.

- Fig. 4.5: Variation of mean and variance of D.F. with contact position, at 9200 R.P.M.
- Fig. 4.6: Variation of mean and variance of D.F. with operating speed
- Fig. 4.7: Comparison of mean of D.F. computed using different methods
- Fig. 5.1: A typical gear system
- Fig. 5.2: Discretization of a continuous structure into sub-systems
- Fig. 5.3: Algorithm for DT-TMM formulation
- Fig. 5.4: Model of an undamped system with multi degrees of freedom
- Fig. 5.5: Comparison of response values computed using direct integration and DT-TMM
- Fig. 5.6: Comparison of computing time of DT-TMM and numerical integration
- Fig. 5.7: Relative response between two gears modelled
- Fig. 5.8: Model of the support bearings
- Fig. 5.9: Schematics of different modules
- Fig. 5.10: Transfer matrix of a gear system component
- Fig. 5.11: Gear pair module
- Fig. 5.12: Schematic representations of solution techniques
- Fig. 5.13: Model of the given gear system
- Fig. 5.14: Comparison of simulator results
- Fig. 5.15: Comparison of simulator results
- Fig. 6.1: Schematic of local stress-strain fatigue life prediction process
- Fig. 6.2: Basis of local stress-strain approach
- Fig. 6.3: Boundary element model of a spur gear tooth
- Fig. 6.4: Boundary conditions for thick and thin rim gears
- Fig. 6.5: Discretization of dynamic load acting on the tooth
- Fig. 6.6: Hofer's angle to define the critical location in the fillet

- Fig. 6.7: Variation of principal stress values within the fillet region
- Fig. 6.8: Variation of equivalent strain at the critical location
- Fig. 6.9: Definition of cyclic stress-strain curve
- Fig. 6.10: Cyclic stress-strain hysteresis curve
- Fig. 6.11: Construction of hysteresis curve
- Fig. 6.12: Material memory characteristics
- Fig. 6.13: Typical cyclic stress-strain variation corresponding to random strain excursions
- Fig. 6.14: Cyclic hardening and softening behaviour of materials [92]
- Fig. 6.15: Martin's rheological model [91]
- Fig. 6.16: Wetzel's piecewise linear model [92]
- Fig. 6.17: Logic diagram for the fatigue damage simulator
- Fig. 6.18: Strain-life characteristics
- Fig. 7.1: Helical gear set model
- Fig. I.1: Definition of domain and boundary
- Fig. II.1: Element library in AGMG
- Fig. II.2: Equivalent rectangular mesh
- Fig. II.3: Different numbering schemes
- Fig. II.4: Coordinates used for involute profile generation
- Fig. II.5: Different smoothing schemes
- Fig. II.6: Helical gear construction
- Fig. II.7: AGMG - main menu
- Fig. II.8: AGMG - geometry data table
- Fig. II.9: AGMG - mesh data table
- Fig. II.10: Examples of different meshes generated with AGMG
- Fig. III.1: Autocorrelation and PSD plots for a second order Markov process

LIST OF TABLES

- Table 2.1: Spur gear data [42]
- Table 3.1: Parameters of the experimental set-up
- Table 4.1: Salient parameters of the gear system
- Table 5.1: Table of coefficients for different integration schemes
- Table 5.2: Parameters of the system shown in Fig. 5.4
- Table 5.3: Parameters of the system shown in Fig. 3.3
- Table 5.4: Parameters of the system shown in Fig. 5.13

NOMENCLATURE

a_1, a_2	coefficients in shaping filter equation
$A(t)$	system matrix
$A_a(t)$	augmented system matrix
$A_f(t)$	shaping filter system matrix
A_n, B_n, C_n, D_n	linear coefficients used in the approximation of acceleration and velocity quantities
b_1, b_2	fatigue strength and ductility exponents
$b(t)$	deterministic input forcing vector
$b_a(t)$	augmented system input forcing vector
$b_d(t_i)$	deterministic discrete time input forcing vector
B	face width
BL	backlash
c	damping, in general
$c_{pg}(t)$	variable mesh damping
c_x	damping coefficient of the bearing along X direction.
c_y	damping coefficient of the bearing along Y direction

lower case bold letter denotes a vector.

upper case bold letter denotes a matrix.

c_z	damping coefficient of the bearing along Z direction
c_γ	damping coefficient of the gear in the tipping mode
$C(t)$	damping matrix
C_0	tooth pair compliance at the pitch radius
C_1	proportionality constant
C_p	compliance of pinion tooth
C_{pg}	$C_p + C_g$ = tooth pair compliance
C_g	compliance of gear tooth
CR	contact ratio
$d(t_m)$	combined forcing vector at the end of mesh cycle
$d_i, i=1,2,..$	coefficients obtained through curve fitting
D	accumulated damage
$D(t_m)$	combined forcing matrix at the end of mesh cycle
D_i	damage fraction corresponding to the i^{th} closed hysteresis loop
DCTF	number of duty cycles to failure
DF	dynamic factor
$e(t)$	transmission error
e_r	random component of transmission error
E	modulus of elasticity of the gear material

E_e	equivalent modulus of elasticity
$f(t)$	input forcing function vector
F	field matrix
g_a	augmented vector of white noise intensity
g_f	shaping filter vector of white noise intensity
G	submatrix of $A_a(t)$
h	lubricant film thickness, m
I	area moment of inertia
I_T	transverse moment of inertia
J	polar moment of inertia in torsional mode
J_y	moment of inertia in tipping mode
k	stiffness, in general
k'	cyclic strength coefficient
$k_{pg}(t)$	variable mesh stiffness
k_x	stiffness of the bearing along X direction
k_y	stiffness of the bearing along Y direction
k_z	stiffness of the bearing along Z direction
k_y	stiffness of the gear in the tipping mode
$K(t)$	stiffness matrix
l	half width of contact
L	length of shaft
m	mass
m_v	mean vector
M	bending moment

n	gear ratio
n'	cyclic strain hardening exponent
N_f	cycles to failure
0	null matrix or vector
p	distributed load at the contact of two cylinders
p_b	base pitch
P	point matrix
P_{vv}	covariance matrix
$Q(t)$	intensity of white noise
$Q_d(t_i)$	discrete time white noise intensity
r	the number of terms used to truncate the Taylor series
R_1, R_2	radius of curvature at the point of contact
R_b	base radius
R_e	effective radius of curvature at contact point
R_j	radius of curvature at the contact point of the j^{th} tooth pair
s	dummy variable
S	normalized contact position
t	time
t_i	discrete time instants
t_0	time instant at the start of a mesh cycle
t_m	time instant at the end of a mesh cycle

T	transfer matrix
T	external torque applied
T_r	torque due to the rolling friction force
T_s	torque due to the sliding friction force
u	relative displacement along the line of contact
U	mass unbalance
$v(t)$	state vector
$v_a(t)$	augmented system state vector
$v_f(t)$	shaping filter state vector
V	shear force
V_m	mean surface speed, m/s
V_r	rolling velocity, m/s
V_s	sliding velocity, m/s
$w(t)$	white noise signal
$w_d(t_i)$	discrete time white noise
W	normal load, N
W_d	total normal dynamic load
W_{dj}	normal dynamic load at the contact of j^{th} tooth pair
W_r	rolling friction force
W_s	sliding friction force
x	displacement along X direction
y	displacement along Y direction
z	displacement along Z direction.

α	pressure angle
β	angle used to locate the line joining the centres of a gear pair
γ	angular displacement in the tipping mode
ρ	transformation angle used in the construction of helical gears
δ	deflection of the tooth in the direction of the applied normal load
$\delta(\cdot)$	delta function
ϵ	strain
η	lubricant absolute viscosity, 10^{-3} N.s/m ²
η	pressure viscosity coefficient, m ² /N
θ	torsional displacement
λ_0	helix angle
λ	helix angle on the base cylinder
μ	coefficient of friction
ν	Poisson's ratio of gear material
ξ	damping ratio
σ	stress
σ_e	standard deviation of the random error component
σ_0	mean stress
τ	internal torque
ψ	slope in XZ plane
x	internal force

ϕ	slope in YZ plane
ω	frequency, rad./sec
ΔT	time step
Φ	state transition matrix
Ψ	auto correlation function
θ	Hofer's angle used to define the critical location in the fillet
σ'_f	fatigue strength coefficient
ϵ'_f	fatigue ductility coefficient
$\Delta\epsilon^e$	the elastic strain range
$\Delta\epsilon^p$	the plastic strain range
$\Delta\epsilon$	total local strain range
Δ	the stress range
ϵ_a^e	$\Delta\epsilon^e/2$ = the elastic strain amplitude
ϵ_a^p	$\Delta\epsilon^p/2$ = the plastic strain amplitude
ϵ_a	$\Delta\epsilon/2$ = total local strain amplitude
σ_a	$\Delta\sigma/2$ = the stress amplitude
< >	expected value of enclosed variable

Subscripts

d	denotes dynamic nature of parameters
e	denotes equivalent parameters
g	denotes gear parameters
i	index used to denote different time instants
j	index denoting the number of tooth pairs in contact at any given time

n denotes different sub-systems in a system
p denotes pinion parameters
pg and gp denotes parameters associated with both pinion and gear
x denotes parameters related to X direction
y denotes parameters related to Y direction
z denotes parameters related to Z direction

Superscripts

a denotes amplitude
e denotes elastic component
p denotes plastic component
L denotes parameters at the left of a sub-system or module
R denotes parameters at the right of a sub-system or module
T denotes transpose of a matrix or a vector

CHAPTER 1

INTRODUCTION AND LITERATURE REVIEW

1.1 General

Gears, generally defined as toothed members transmitting rotary motion and/or power from one shaft to another, are among the oldest of mechanical devices and are generally the most rugged and durable. They form the vital elements of main and ancillary mechanisms in many machines used in such diverse industries as aerospace, process, refinery, construction, mining, marine, and transportation. In all such applications, there has been a continuing demand towards higher reliability and higher efficiency at a lower cost. Gear designers and, the gear industry in general, are responding to this trend by constantly refining their analytical, design and manufacturing techniques. Clearly, overdesigning for better reliability is no longer acceptable and hence optimal designs which satisfy the constraints of improved reliability and light-weight configuration are being sought. But the present gear design methods which are based on empiricism and conservative design principles are not formulated to obtain optimal designs and thus at best result in designs which are heavier than necessary and at worst result in unpredictable and catastrophic failure modes. Also, the most optimal design may not necessarily lie in the design space defined by the existing gear design standards [1-3]. Thus, a methodology is needed which would not only

aid in the evaluation of existing designs but would, in addition, apply accumulated field data directly and quickly to new designs in order to achieve optimal design.

Towards this goal, a new computer based methodology for a reliable estimation of fatigue life of modern industrial gears using measured, simulated, or stochastically estimated loading data, is proposed in this investigation. This methodology can be used for either for simulating existing gear sets or systems, or for synthesising new designs. Broadly, the methodology developed consists of the following three steps:

- 1) computation of gear dynamic loads using realistic analytical models,
- 2) computation of gear dynamic stresses at critical locations using boundary element methods,
- 3) computation of gear tooth fatigue life based on local stress-strain approach.

Even though the proposed methodology is applicable, in principle, to analyse any type of cylindrical gears, spur gears of both standard and non-standard types are used in this investigation extensively as case studies. Because of this, it should be noted here that, unless otherwise mentioned the term 'gear' in this thesis always denotes 'spur gear'.

A complete gear system which includes the mating gears, the shafts and the support bearings, the seals and the housing may fail in many different ways. However, most such failures manifest themselves in the failure of the gear teeth. The American Gear Manufacturers Association (AGMA) [4] cites 21 modes of gear tooth failure. Of these, metal fatigue alone accounts for more than 50% of all gear failures. In gears, metal fatigue manifests itself as surface fatigue and bending fatigue. Though phenomenologically both type of failures are the same, the influencing factors are different. This investigation primarily deals with bending fatigue only. However, the proposed methodology is equally applicable to the surface fatigue life prediction.

1.2 Fatigue design of gears

The dynamic loads acting on the gear teeth, as a result of the gear system dynamics, cause stress fluctuations at critical locations eventually leading to fatigue failure. The recommended standard [1-3] procedures for fatigue design of gears is based on the classical S-N curve analysis. In essence, the fatigue design of gears is carried out by ensuring that the bending stress at the critical location computed using the modified Lewis equation and the surface stress computed using the Hertz contact theory are well below the endurance limit of the gear material. Some of the shortcomings of these methods are outlined in this section.

Even though gears represent a high level of engineering achievement, conventional design methods [5,6] based on simple strength of material stress models coupled with empirical correction factors lack consistency and universality. Basically, in the conventional design methods, the success of a design is ensured with the use of numerous modifying factors which provide enough margin of safety. However, most correction factors are loosely defined, have no or little analytical backing, and are mostly based on experience rather than scientific experiments. Therefore any application outside the average routine design range is not supported either by theory, or by empirical data currently available. In such cases, the design process is augmented by repetitive and expensive testing of prototypes. Also the conventional design process is based on tooth type and does not take into account the variations in gear type. For example, it does not differentiate the external gear design from internal gear design or gears with thin rims from gears with thick rims even though experience has shown otherwise [7]. In addition, current design methods consider only the maximum stress level value, while ignoring the stress recursions occurring at various critical regions.

In spite of these deficiencies and in spite of the several other alternatives proposed by various investigators, the conventional gear design methods based on the modified Lewis equation had stood the test of time and

continue to date to be the basis for all the accepted standards such as AGMA [1], ISO [2], DIN [3], etc.. The reasons for this continued acceptance are: the inherent simplicity, low cost computation requirements, reasonable correlation with test results in routine applications, and ease of day to day engineering use. However, the current design procedures are inadequate for the design of modern gears [7] which have to satisfy the conflicting requirements of higher reliability and performance at lower cost. This inadequacy is borne out by the fact that all the gear design standards recommend the use of prototype testing for new or unique gear designs.

In this investigation, new analyses and simulation methodologies are developed and applied for estimation of fatigue life of gears. The underlying principle behind the methodology is to include all the factors of technological advances in all the related fields, but only to the extent that both the cost and reliability can be justified for day to day engineering solution of gear problems in industry.

1.3 Literature review

A review of relevant literature is presented in the following subsections, grouped in a sequence so as to develop the scope of the investigation presented in this thesis.

1.3.1 Gear dynamics

Most of the pre-1940 investigators were primarily concerned with component strength and not with reliability and cost. The earlier efforts of Lewis [8], Buckingham [9], and many others are too wellknown to review again here. Essentially, they evolved designs to operate gears indefinitely at stresses calculated to be less than the endurance limit. The calculated stresses, however, varied according to numerous assumptions especially those related to stress concentration, shape factors, and load sharing among the teeth. Also during this period, the presence of dynamic loads on gear tooth was identified and incorporated into the design procedures in the form of dynamic factors.

Between 1940 and 1950's, another era in analysing the dynamic loads in gear teeth developed. The studies conducted during this period utilized more detailed information on gear teeth deflection, and in addition made use of lumped mass-spring models under wedge, cam, or sinusoidal type of excitations. [10,11]. In general, this group of analyses could be considered as using an equivalent constant mesh stiffness model.

In the gear dynamic models developed after the late 1950's [12-17], the excitations due to tooth profile errors, pitch errors together with the effect of periodic variation in mesh stiffness were introduced. Cornell et.al. [18]

improved and extended the previous models to High Contact Ratio (HCR) gears with and without backlash. And Kasuba et.al. [19] introduced the variable-variable mesh stiffness concept wherein the profile errors and tooth deflection under static load are taken into account in the formulation of mesh stiffness. Also, Tobe et.al. [20-22] carried out a statistical analysis of the gear dynamic loads. In recent years, a number of models [23-29] incorporating the coupling between the torsional and flexural modes are also introduced. In addition to these studies on the subject of dynamic load estimation, several investigations on compliance/stiffness estimation [30-33] and gear system stability [34-36] have also been reported during the last decade. However, none of the gear dynamic models proposed so far are complete enough to simulate or synthesize complex industrial gear sets or systems.

1.3.2 Gear tooth stress estimation

In the conventional design methods, the bending stresses due to gear tooth loads are estimated using modified Lewis equation, which is based on the cantilever beam theory. However, the cantilever beam assumption is valid only for the conventional thick rim, external gears and hence application of modified Lewis equation outside this classification results in inaccurate stress values. To overcome this, recently Finite Element Methods (FEM) [37-45], Boundary Element Methods (BEM) [46-50] and other

rigorous transformation methods like Complex Potential Method (CPM) [33,51,52] are all attempted. Of these, inspite of the excessive amount of computations involved, FEM is being increasingly deployed in gear stress analysis, because of its ability to model standard as well as non-standard gear systems. The BEM being relatively new and still in the developmental stage, is not as widely used as FEM, whereas CPM is found to be too complex to be used in design practice [60]. In addition to these analytical and numerical studies, a number of experimental studies [53-59] using various strain and/or stress measurement techniques have also been undertaken to evaluate gear tooth stresses. In this study, BEM is employed for stress computation, because of the computational and modelling advantages it offers.

The foregoing review on gear dynamics considers only those studies which are most relevant to the present investigation. More information on gear dynamics investigation can be found in [60] and [61].

1.3.3 Gear fatigue

Most of the studies on gear fatigue reported in literature are of experimental nature. Typically, in these studies [62-71], the effects of various profile parameters such as addendum, profile errors and profile changes due to wear on the fatigue strength of gear tooth are studied. In

one instance [72], even the effect of vacuum on the bending strength of gears was investigated. Recently, with the increased use of plastic gears, a number of studies [73,74] on the fatigue strength of such non-metallic gears have been also reported.

1.3.4 New approaches in fatigue analysis

Eversince the pioneering fatigue studies conducted by Wohler between 1857 and 1869, a large number of investigations on different aspects of fatigue had been undertaken and published in open literature. As an indication of the overwhelming interest in mechanical fatigue failures by researchers, Manson [75] notes: "It is quite clear that, if a person wished to keep up with the literature and read one report per working day, he would fall behind on the order of one year for every year that he read. This would be true if he started with a knowledge of the existing literature; catching up on the backlog would be almost impossible." Thus a thorough review of literature on all aspects of fatigue analysis is beyond the scope of this investigation. Instead a brief summary of salient features of common methods of fatigue analysis is presented in the following sections. These methods can be grouped into two broad categories, namely, the stochastic or the random process approach and the direct approach.

Random process approach

Fatigue failures being essentially a random process, this approach uses the theory of stochastic processes to analyze the statistical characteristics of fatigue behaviour. The dynamic characteristics of the system are generally assumed to be deterministic while the excitation is taken to be a random process. The objective here is to determine the reliability of the structure or component to withstand random excitations and to predict its service life [76-79].

This approach requires the knowledge of the stress process (e.g. narrow or wide band process) and the statistical parameters of the peak stress envelope distribution. In general, the probability density function (PDF) of the peak stress envelope cannot be easily derived except for under some simplistic loading conditions [77]. Thus the random process approach is not very practical and hence is not widely used in practice.

Direct methods

These methods are essentially deterministic and the variations in fatigue life data are not explicitly included in the analysis. The classical S-N curve analysis and the relatively new local stress-strain and fracture mechanics approaches belong to this classification. Although there are significant differences in the level of sophistication

and accuracy of these methods, all are based on the critical location stress/strain concept.

Classical S-N curve analysis

The stress-life (S-N) curves introduced by Wohler in the 1850's have for years been the only fatigue criterion used for the basic fatigue design of machine elements and machine structures [6,80,81]. Over the years, the effects of mean stress, stress concentration, and notch sensitivity were all incorporated into the S-N curve analysis for better accuracy. Though the S-N curves are widely used for both finite life as well as infinite life designs, it has been reported that in the low cycle or finite life region the S-N curve analysis invariably fails [80]. This is due to its inherent inability to account for the plastic strain present at the critical locations.

New approaches

The evolution of computers over the past decade has allowed the development of increasingly sophisticated analysis procedures based on the newly developed disciplines, namely, the local stress-strain concept [80,82-87] and the fracture mechanics approach [88,89]. For this purpose the fatigue process is divided into two regions: i) crack initiation and ii) crack propagation to fracture. Currently, the fatigue crack initiation and crack propagation lives are estimated independently based on local

stress-strain and fracture mechanics concepts, respectively. No unified approach has yet been developed to combine these two estimates.

Local stress-strain approaches

These approaches, used for the evaluation of crack initiation life, have been developed over many years. Essentially these methods involve first estimation of local stresses and strains as a function of the applied loads or nominal stresses on reversal by reversal basis. Then by assuming that both the deformation response and the fatigue life behaviour at the critical location are identical to those of a reference smooth specimen forced through the same critical location deformation history, damage is computed [81]. Here the specimen is viewed as a filament of material located in the critical location of a complex structure or component and the life of the specimen is considered equivalent to the life of the component.

Initial advances in this field were made through the application of computerized cyclic deformation models [90-92], cycle counting methods [93-95], notch analysis [84,85], and fatigue damage computations under variable amplitude loading [96,97]. It has been reported that when care is taken to completely and accurately determine local stresses and strains in notched specimens then fatigue crack initiation life can be accurately predicted using these

methods [92,96,97]. Although the reliability of this approach for design of actual machine components under service load conditions has been successfully demonstrated by various investigators [86,96-101], industrial applications of these techniques have been relatively rare. This is because the purely research oriented computer methods have not yet been converted to a more general and easily accessible format. Also the precise testing techniques that are required to define the needed fatigue and cyclic deformation properties of materials have only recently become practical with the development of servo-hydraulic testing equipment and advances in instrumentation and micro-electronics. In addition, these properties, once evaluated, have not been widely circulated to all industrial designers. Furthermore, some of the concepts utilized in these methods represent new additions to the traditional engineering fatigue design philosophy. However this situation is slowly changing and a number of large design organizations [99-104] have already started using these techniques for day to day applications. These state of art fatigue analysis procedures are incorporated into the proposed gear design methodology.

1.3.5 Computer aided design of gears

Almost all the aspects of routine mechanical design procedures including gear design are now computerized through customized software. A number of interactive,

computer graphics oriented computer aided design (CAD) software [106-108] based on conventional gear design procedures have been introduced recently. These programs, in general, automate and speed up the routine calculations that are required in the conventional design process. And some of them have built-in data bases consisting of material data as well as semi-empirical load and geometry data. In addition to these, there are few general purpose interactive fatigue design software [109,110] available, which can also be used for fatigue design of gears. Basically these software are all based on classical S-N curve analysis and so far no attempts have been made to include the recent developments in the fatigue analysis area.

Since all the component parts of the present investigation, namely, dynamic load simulation, boundary element stress analysis, and local stress-strain fatigue analysis, require the use of computers and to facilitate the use of the proposed methodology on a day to day basis, a computer aided gear design software is proposed as part of this investigation.

1.4 Scope of the investigation

The objective of this investigation is to develop a computer aided analysis and simulation procedure, so as to reduce the empiricism involved in the current methods of gear design. Broadly this is achieved through the following

four steps:

- 1) computation of gear dynamic loads using more realistic analytical models,
- 2) computation of gear dynamic stresses at critical locations using boundary element methods,
- 3) computation of gear tooth fatigue life based on local stress-strain approach.
- 4) formulation of computer aided design software for gear design based on the previous three steps.

To estimate or compute the dynamic loads on the gear tooth, the complete gear system with its various components is considered. And mathematical models incorporating most of the important factors that influence the gear system dynamics, are formulated. Based on these mathematical models, three different dynamic load simulators are developed. Two of the dynamic load simulators, one deterministic and the other stochastic, are applicable to small gear systems and may also be used for preliminary design of large gear systems. The third simulator based on a new method of modelling and solution technique, namely, discrete time transfer matrix method, is used to simulate large, complex, and practical gear systems. Provision to use either the actual measured transmission error records or the statistical properties of the error records are provided.

Boundary element models of the gear tooth are then formulated and solved for stress quantities at the critical locations in the fillet using the simulated dynamic loads as input. The stress history obtained is then processed through a newly developed cycle counting algorithm to break the entire history into a series of individual cycles. Fatigue damage is then computed for each cycle and accumulated using Miner's rule.

In chapter 2, the gear system factors that influence the gear dynamics are identified and reviewed. Mathematical expressions characterizing the influence of these factors on gear dynamics are derived.

In chapter 3, mathematical models including most of the factors identified and discussed in the previous chapter are formulated for a spur gear set along with its supports. Both torsional and lateral motions are considered. A dynamic load simulation procedure based on the mathematical model is introduced. The actual measured error records are used as an input to the simulation. The results of the simulation are compared with the experimental results reported in the literature.

In chapter 4, a dynamic load simulator using stochastic error representation is introduced for the cases wherein the actual transmission error record is not available. For this

purpose the system equations formulated in chapter 3 are augmented with a linear stochastic differential equation representing a second order Markov process. The state equations of the augmented system are then discretized and the mean and covariance propagation equations are written. Once again state space technique is used to solve the resultant linear stochastic difference equations. The results of the simulator are then compared with the results obtained with other techniques.

In chapter 5, a new method of modelling and solution scheme referred to as "discrete time transfer matrix method" is introduced. The feasibility of the proposed method for simulating large practical gear systems with many transmission line components is investigated.

In chapter 6, using the dynamic load history record obtained from the simulators described in the previous chapters as loading data, the strain history at the critical locations in the gear tooth fillet is computed using BEM. The results of the BEM are compared with the experimental and numerical results obtained from a related study. Also, a new cycle counting algorithm which is used to break the complex strain history waveforms into individual closed cycles is presented. A fatigue damage parameter is then computed for each individual cycle and the damage is accumulated using the Miner's rule. And, design of a

micro-processor based on-line damage monitoring system is also discussed.

In chapter 7, the extension of the dynamic load simulators and the fatigue damage simulator to the cases of helical gears and non-standard cylindrical gears is discussed and described.

Finally, the conclusions, the highlights and recommendations for future work are presented in chapter 8.

CHAPTER 2

IDENTIFICATION AND MODELLING OF THE FACTORS

THAT INFLUENCE GEAR DYNAMIC BEHAVIOUR

2.1 Introduction

In this chapter, mathematical models characterizing the various major factors that influence the gear dynamics are formulated. A proper identification of the influencing factors is necessary since most of these factors are inter-dependent and some of them are dependent on complex processes such as gear lubrication, which are not yet completely understood. Also, these influencing characteristics should be classified in the order of importance to gear dynamic load estimation, since the more the number of factors considered the more will be the complexity and computation requirements of the simulators. Thus in the following sections, the factors that affect the gear dynamics are first classified into two groups and then reviewed. Expressions relating the influences of these factors are also derived to facilitate their inclusion into the mathematical models developed subsequently in the following chapters. The geometric quantities used in the derivations are given in Fig. 2.1.

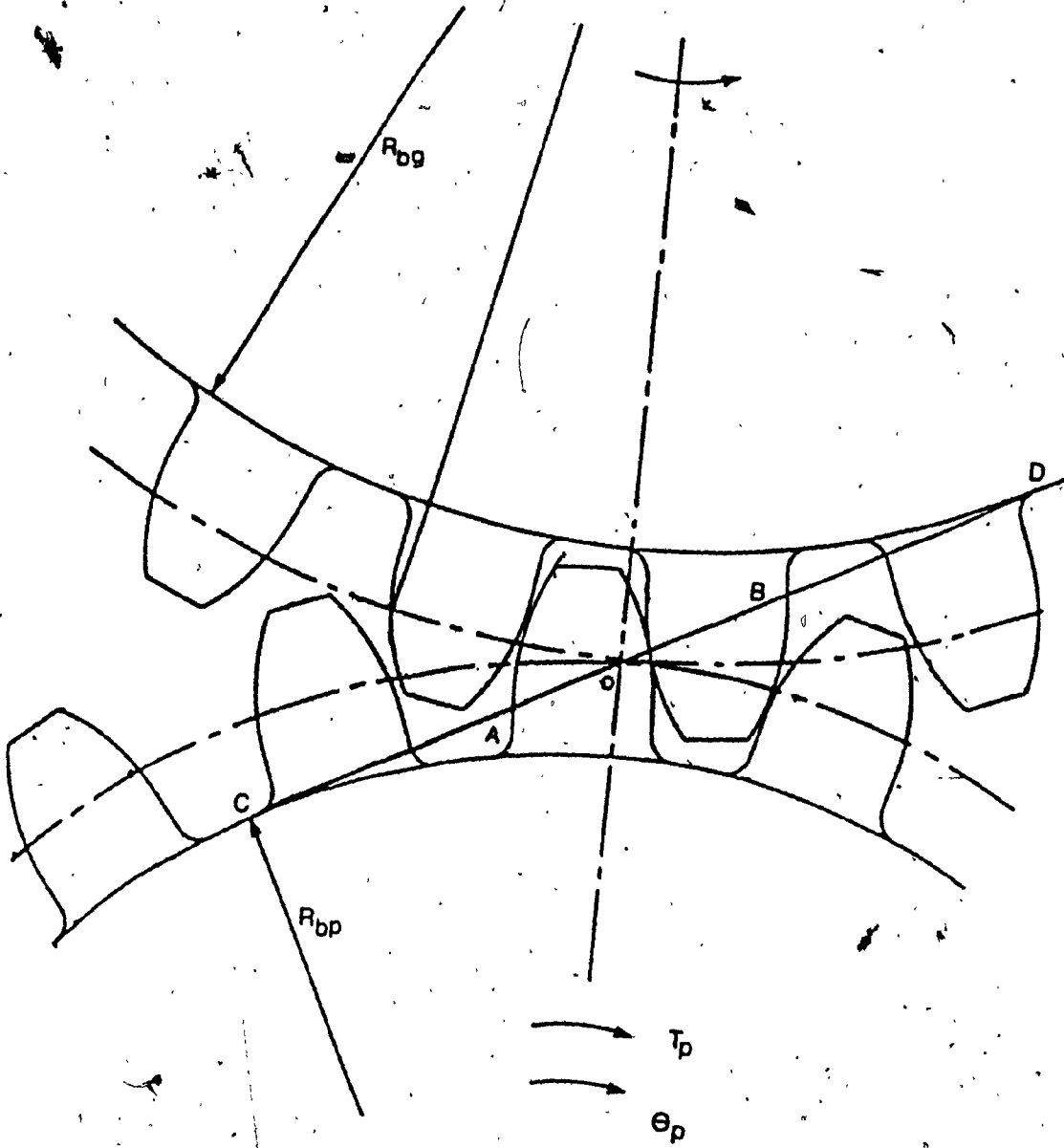


Fig. 2.1: Gear geometry.

2.2 Classification of the influencing factors

Factors that affect the gear dynamics can be broadly grouped into two categories, namely, primary and secondary. The primary factors are those which influence the meshing action directly and are inherent in any gear pair, irrespective of the gear type and gear system configuration. They constitute the dynamic excitation to the gear system. All other factors are grouped under the second category. The primary and secondary factors are first listed and detailed description of these factors and the governing relationships are presented in the following subsections.

Primary factors:

1. Gear transmission errors
2. Variable mesh stiffness
3. Non-linear backlash element

Secondary factors:

1. Shaft elasticities
2. System inertias
3. Damping in the system
4. Input torque fluctuations
5. Variation in contact ratio
6. Coupling between torsional and lateral modes
7. Sliding and rolling friction at the contact
8. Non-linearities from other components in the gear system (e.g. coupling characteristics, bearing clearances, etc.)

2.2.1 Gear transmission error

The gear transmission error, which is the total error consisting of the manufacturing errors, mounting errors, and the tooth deflection under the applied load, is the principal cause of noise and vibration in gears. This combined error is considered to be of dynamic in nature and is defined, for any instantaneous position of one gear, as the departure of the mating gear from the position it would occupy if the system were ideal, with constant velocity ratio, and constant contact ratio [16].

That is,

$$e(t) = \theta_p - n \theta_g \quad (2.1)$$

where,

- $e(t)$ = transmission error,
- n = gear ratio,
- θ_p = angular position of pinion,
- θ_g = angular position of gear.

A continuous time record of this transmission error is required to form the dynamic excitation to gear dynamic system simulators. Recently introduced computerized measuring techniques and equipments [111-113] such as the Automatic Gear Accuracy Measuring Instrument (AGAMI) [112] or the optical encoded measuring apparatus described in [113] make it possible to measure this error precisely.

These new measuring equipments give the transmission error as a function of successive angular positions of the gear rotation and can be converted to a time scale for any given rotational speed. In cases where the transmission error records are not available, a procedure to use the statistical information on transmission errors instead of the actual transmission errors is given in chapter 4. The required statistical information on transmission errors can either be extracted from the error records of similar gear systems in existence or can be constructed [114,115] from the measured records of the component errors that constitute the transmission error.

2.2.2 Variable mesh stiffness

The stiffness of a teeth-pair in mesh is primarily a function of contact or load position and hence referred to as variable mesh stiffness. The variation of teeth pair stiffness with load position, and hence with time acts as a parametric excitation to gear system. Also, the load sharing between the teeth when more than one pair of teeth are in contact is influenced by the variable mesh stiffness. Thus an accurate evaluation of the actual pattern of stiffness variation is essential for proper simulation. Although much work [19,30-33] has been done on this subject, a complete and accurate method, covering all the factors has not yet been achieved.

The current procedures for gear teeth pair stiffness estimation can be classified into three groups, namely,

1. the classical approach [32],
2. the analytical methods, like conformal mapping [31] and complex potential methods [30,33].

and

3. the numerical procedures such as FEM or BEM [40,50],

In this investigation, the third category, namely, the numerical procedure is used to compute the tooth stiffness and the teeth pair stiffness. All the component sources of deflections, including the local compression and rim deflection can be accounted for with this procedure by proper modelling. The main advantage of numerical procedure is its flexibility. That is, the procedure can be used irrespective of the gear type (e.g. thin rim, thick rim, or internal), and gear tooth type (e.g. involute, circular or non standard). This flexibility is achieved at the cost of increasing computation time since each new evaluation requires a proper FE or BE model. However, this cost can be somewhat reduced by the use of special purpose automatic mesh generator software. Also a provision to obtain an adequate series approximation of the compliance or inverse stiffness variation curve based on a small, finite number of analyses, as suggested in [32], is provided. The coefficients of this approximate function can then be retained for future use. Thus, for a given pair of gears, a

complete stiffness estimation is to be performed only for a small, finite number of times.

Finite elements versus Boundary elements

Having decided on the use of numerical methods for stiffness evaluation of the gear tooth, a choice has to be made between the FEM and the BEM. The FEM is by far the most popular numerical method used for structural analysis, nowadays. The inherent versatility of the method along with the recent developments in modern computer hardware make this method a very powerful and useful tool. It has been used successfully in the recent past, to compute stresses and deflections of various types of gear teeth. But, for a proper stress and deflection analysis of a gear tooth, the FE mesh at the regions of large stress gradients like the fillets and at the contact regions [42] on the surface along the path of the contact should be very fine. This, in addition to the requirement of FEM that the entire gear tooth be discretized, makes a proper analysis prohibitively costly for day to day use in design applications.

The above factor has led to the introduction of BEM for gear stress and deflection analysis [47-50]. BEM, while having its origin in classical elasticity, have only in recent years began to play a significant role in solid mechanics. The main advantage of BEM is that the dimensionality of the problem is reduced by one. This

reduction in dimension leads to savings in modelling time as well as computation time. At the same time, the accuracy of BEM is comparable to that of FEM as can be seen from the numerous examples available in literature [46,48,50]. In addition, it is ideally suited for plane contact problems and problems involving large stress gradients. The analysis of gear tooth falls into this category, and thus BEM is preferred and has been chosen over the FEM in this study. Mathematical formulation of the method is given in the Appendix I.

BE model for stiffness evaluation

The first step in BE modelling is to discretize the gear tooth and the gear blank. This is done in this study using a newly developed Automatic Gear Mesh Generator (AGMG) described in Appendix II. Briefly, the AGMG first generates the tooth profile and blank configuration from the given geometry data and then uses the model data specified by the user to discretize the gear. For proper stiffness evaluation, the hub region should also be modelled to account for the torsional deflection of the web under operating loading conditions. It is very important to choose the correct reference datum to account for the web deflection correctly. In most of the earlier studies, the inner radius of the hub is taken to be the reference radius. However, in this study the centroid radius is used as reference radius. This choice is made based on the

experimental results obtained recently [59]. Also, the mesh around contact or loading point should be fine enough to account for the local compression. This can be achieved through AGMG using the user defined element option. That is, the user can instruct the AGMG to place a particular element of specified size at a user specified location in the model. AGMG automatically rearranges the surrounding elements to accommodate the user specified element. The dimension of the element at the point of contact can be calculated using the following procedure.

In the case of spur gears, since the radius of curvature is constant along the line of contact, the contact would be Hertzian. Thus for a given concentrated load of W , according to Hertz contact theory [6], the half width of contact l , is given by

$$l = \left[\frac{8W}{\pi B} \frac{R_1 R_2}{R_1 + R_2} \frac{1 - \nu^2}{E} \right]^{\frac{1}{2}} \quad (2.2)$$

where,

- B = face width,
- R_1, R_2 = radius of curvature at the point of contact,
- ν = Poisson's ratio of the gear material,
- E = Young's modulus of the gear material.

Using the user defined element option in the AGMG, an element with $2l$ length can then be placed at the required location.

In contrast to the FEM, BEM also requires that the load on the element be distributed rather than concentrated. Once again using the Hertz contact theory, the load distribution on the boundary element can be computed as follows. The elliptically distributed load due to the concentrated load W at the point of contact, as shown in Fig. 2.2, is [6],

$$p = \frac{2W}{\pi l B} [1 - (x/l)^2]^{\frac{1}{2}} \quad (2.3)$$

Fig. 2.3 shows a typical BE grid pattern for a single tooth attached to the rim of a gear wheel. Using these grids and the equivalent distributed loads obtained from the previous analysis as input, one can readily compute the deflection δ under a load W applied at the point of contact. The compliance or the inverse stiffness of the gear tooth at that point of contact is then given by,

$$C_p = \frac{\delta}{W} \quad (2.4)$$

which could be rewritten in a non-dimensional form as,

$$C_p = \frac{\delta E B}{W} \quad (2.5)$$

Here,

δ = deflection of the tooth along the line of action,

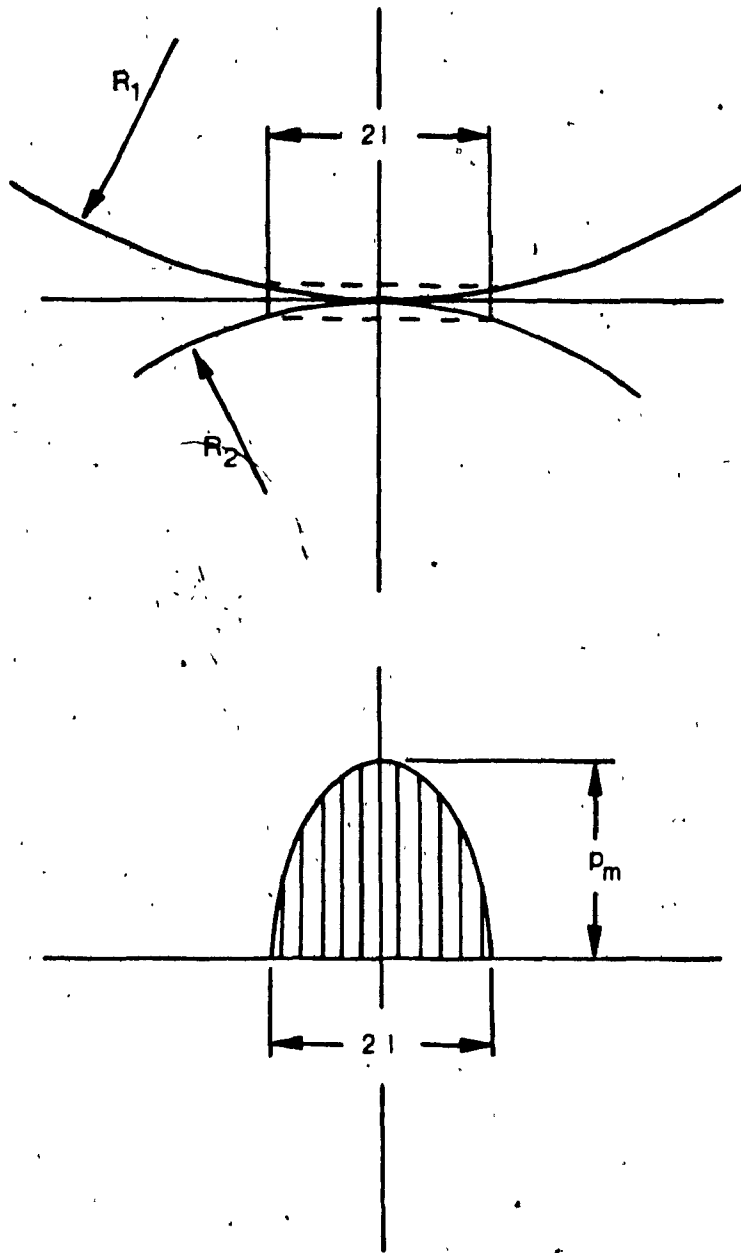


Fig. 2.2: Hertz contact deformation and load distribution

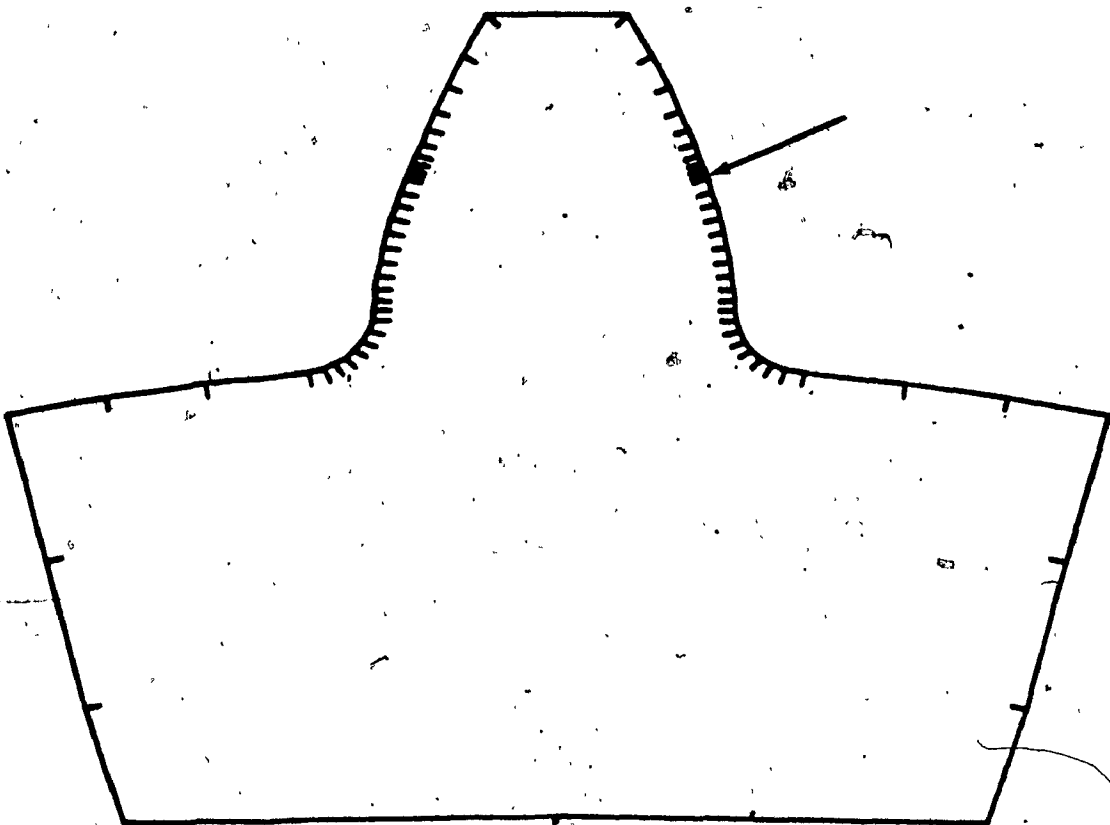


Fig. 2.3: BE model of a spur gear tooth

W = load acting on the gear tooth,
B = face width,
E = Young's modulus of elasticity of the gear material.

Similarly the compliance of the meshing gear tooth C_g can also be computed. The overall compliance C_{pg} is then obtained by summing up the individual compliances of the two meshing teeth at various contact points. The variation of the compliance along the line of action is then approximated by a five term power series [32] as,

$$C_{pg} = C_o [1 + d_1(S) + d_2(S)^2 + d_3(S)^3 + d_4(S)^4] \quad (2.6)$$

where,

C_o = tooth pair compliance at the pitch radius,
 d_i = coefficients obtained through curve fitting,
 $i=1,2,3,4$
 S = normalized contact position.

The coefficients of this equation are then stored for future use in the mathematical models. Fig. 2.4 shows the variation of the computed values of C_p , C_g , C_{pg} as well as the approximate function for C_{pg} , for a given gear. As can be seen from this figure, the approximate function which is obtained through least square curve fitting duplicates the computed compliance variations for the entire region of

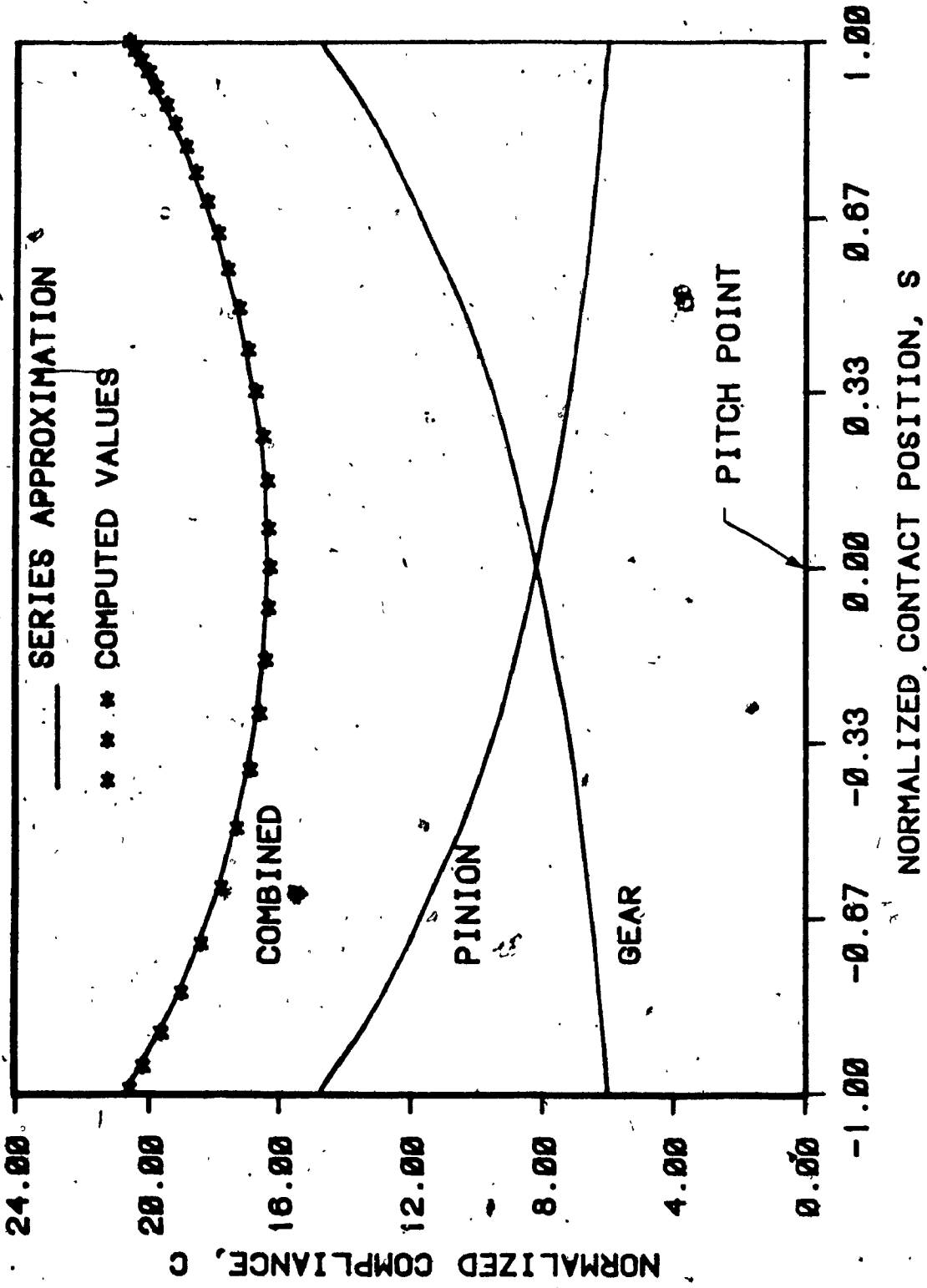


Fig. 2.4: Calculated and approximated compliance

interest. The tooth pair compliance C_{pg} is symmetrical about the pitch point, since the gear and the pinion are taken to be of same size in this particular case. In cases where the pinion and the gear are not of the same size, the compliance variation curve will not be symmetric and hence the coefficients d_1 and d_3 will not be equal to zero.

In order to check the viability of the procedure proposed above for gear tooth stiffness evaluation, the deflections obtained with BEM are compared with those obtained from other techniques. For this purpose, the study by Coy et.al. [42], wherein a detailed comparison of the deflections obtained from their fine mesh FE model along with those obtained from a coarse FE model [40] and the Cornell's classical approach [32] was carried out, is chosen. The loading pattern and the gear geometry given in Fig. 2.5, and Table 2.1, respectively are reproduced from [42]. Using these data and based on the analysis given earlier, the deflections along the line of action are computed at different loading points. Fig. 2.6 shows deflection obtained from the BEM along with those reproduced from [42]. As can be seen from the Fig. 2.6, the deflection values computed by the proposed analysis method compares well with those of Cornell and is slightly less than those obtained from the FE analysis. This difference is due to the different reference radius chosen in the FE analysis, whereas Cornell's method and the present study uses

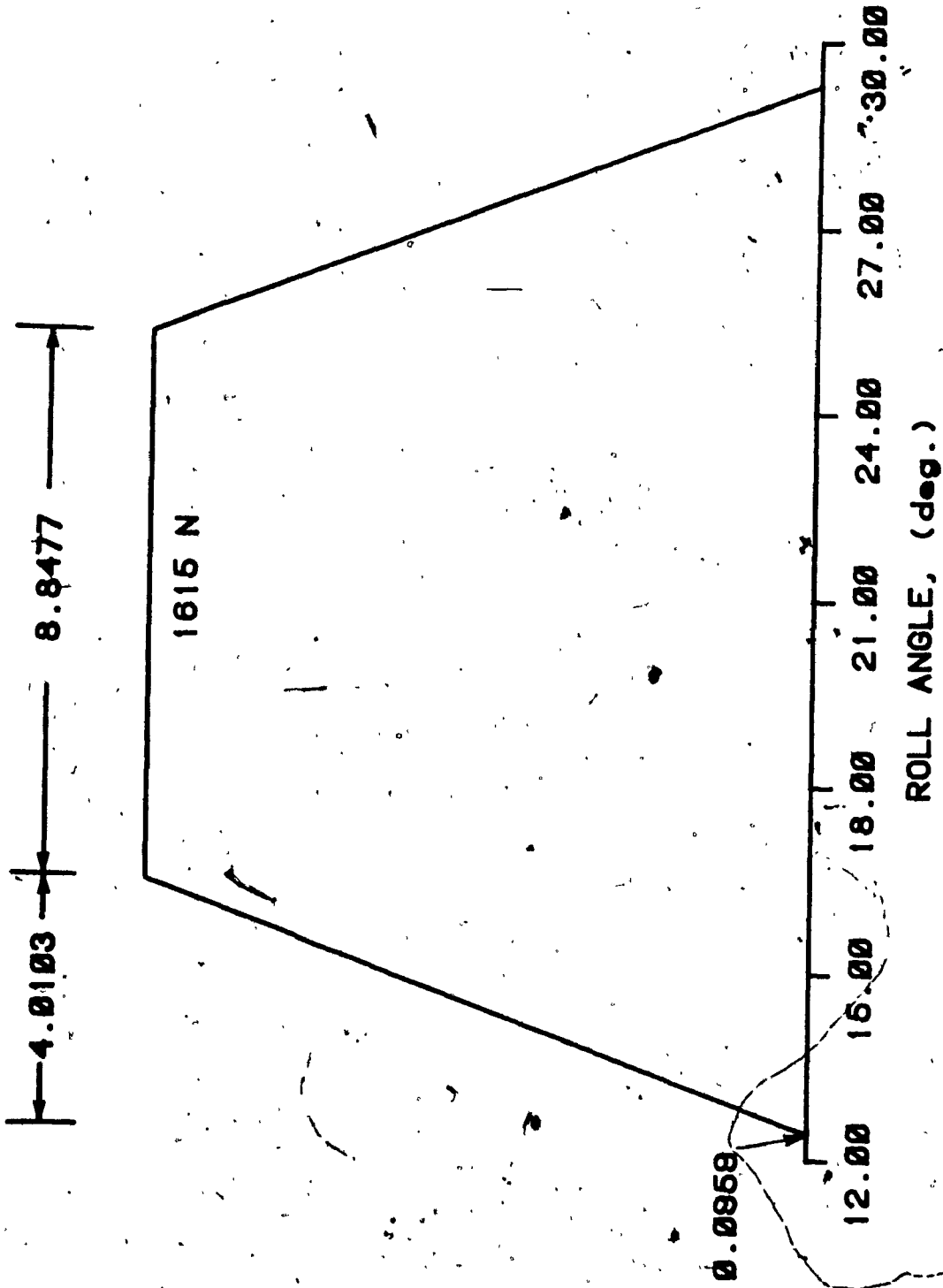


Fig. 2.5: Gear tooth load pattern [42]

Table 2.1: Spur gear data [42]

Number of teeth	28
Diametral pitch	8
Circular pitch, cm	0.9975
Whole depth, cm	0.762
Addendum, cm	0.318
Chordal tooth thickness reference, cm	0.485
Pressure angle, deg.	20
Pitch diameter, cm	8.890
Tooth width, cm	0.625
Outside diameter, cm	9.525
Root fillet, cm	0.102 to 0.152
Measurement over pins, cm	9.603 to 9.630
Pin diameter, cm	9.549
Backlash reference, cm	0.0254
Tip relief, cm	0.001 to 0.0015
Young's modulus, N/m^2	2.07×10^{11}
Poisson's ratio	0.30

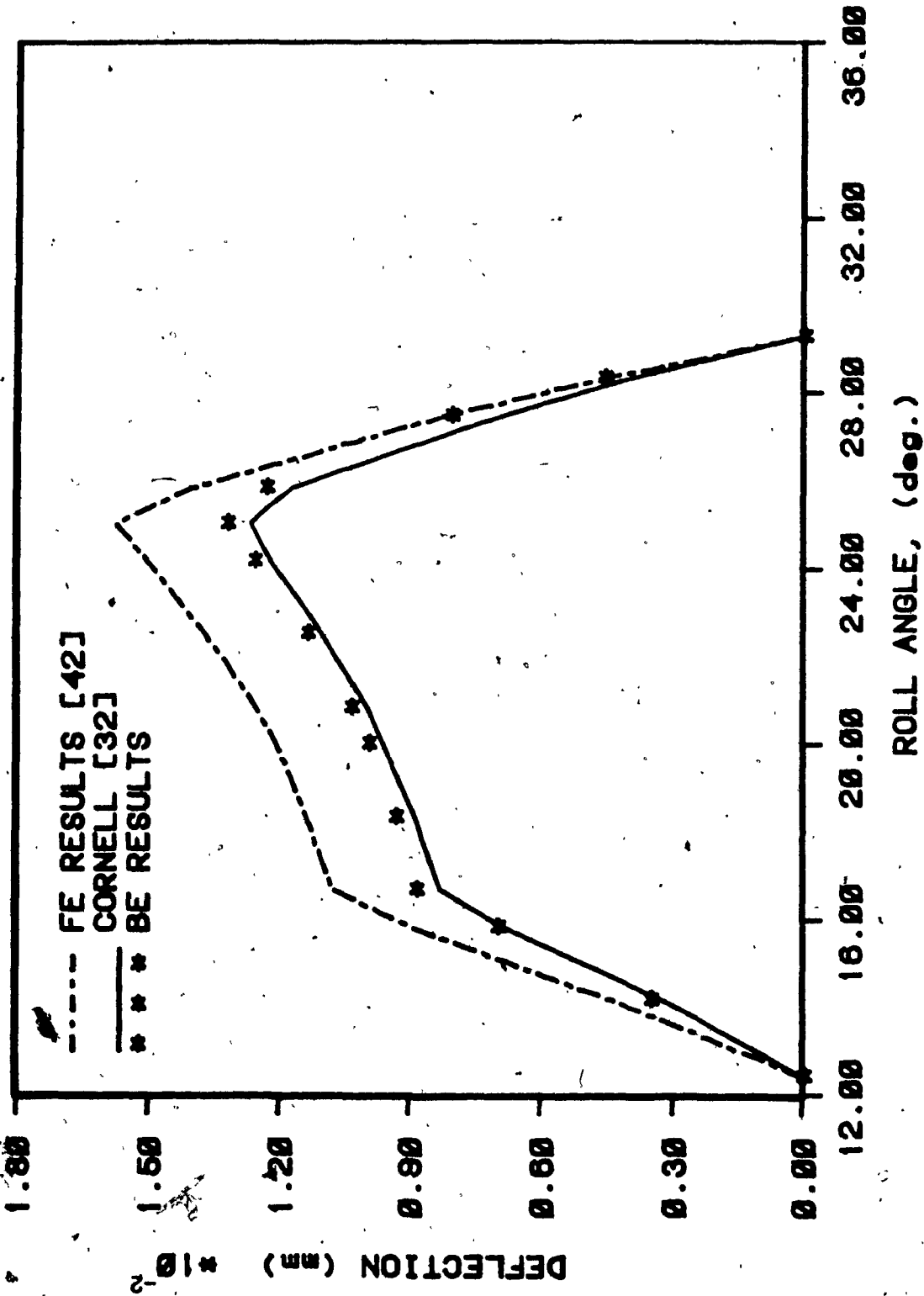


Fig. 2.6: Comparison of tooth deflection values computed by various methods

approximately same reference radius. Cornell's method once formulated, requires less computation time and gives the component deflections due to various participating factors. But, different formulation is required for different types of gear tooth type and thus is not versatile for applications. In contrast, both FEM and BEM give good results as well as they have the advantage of being flexible. But, FEM requires more computation time than BEM, thereby validating the choice of BEM in the present investigation.

2.2.3 Non-linear backlash element

Tooth backlash, which is present in any practical gear system, is also a contributing factor to the dynamics of the gear system. With lightly loaded gears at higher speeds tooth separation and subsequent reverse or forward impact can occur resulting in higher dynamic overloads [18,19]. In addition, the mechanism of backlash was also found to have significant influence on the system stability [116]. In this study, the tooth backlash is modelled as a non-symmetric non-linear element as shown in Fig. 2.7 and is defined by the following equations.

For $(u+e) > 0$,

$$W_d = k_{pg}(t).(u+e) \quad (2.7)$$

For $-BL < (u+e) < 0$,

$$W_d = 0 \quad (2.8)$$

For $(u+e) < -BL$,

$$W_d = k_{pg}(t).(u+e+BL) \quad (2.9)$$

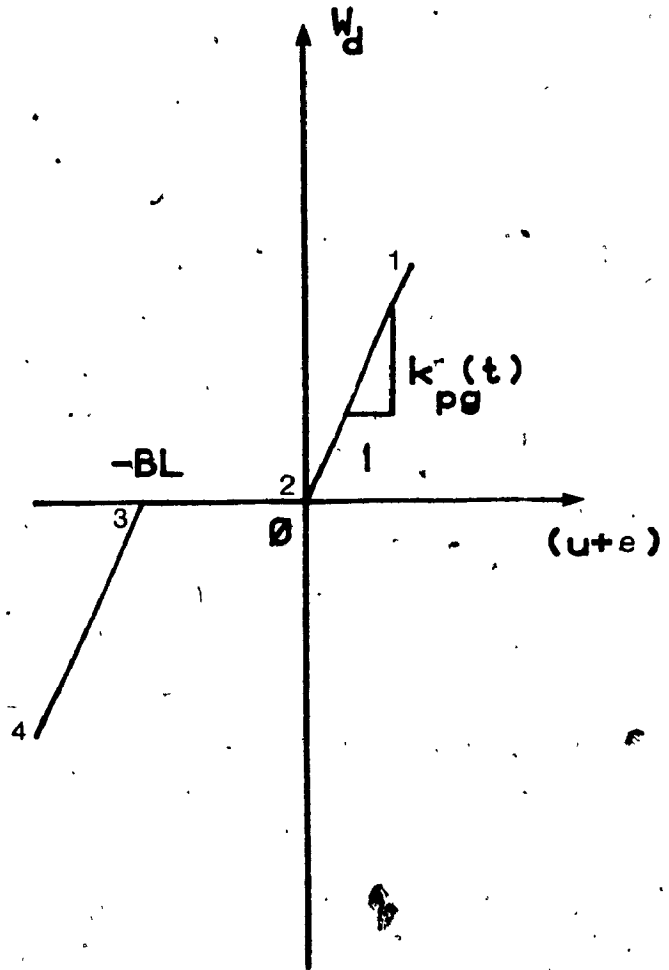


Fig. 2.7: Gear tooth backlash model

where,

u = relative displacement along the line of contact,

e = transmission error,

BL = backlash.

Here, the gears are assumed to be in contact at the start of the analysis. Between points 1 and 2, normal meshing takes place, and between 2 and 3 loss of contact occurs. And region 3 to 4 corresponds to meshing at rear flanks.

2.2.4 System inertias and shaft elasticities

In general, for a given tooth configuration, the variation in the system inertias and shaft elasticities shift the system natural frequencies and thus the subharmonic response peaks of the system. In particular, the shaft elasticities determine the amount of influence other components in the drive have on the gear dynamics. For example, when the shaft elasticities are very small compared to the mesh stiffness, then the gear pair is effectively decoupled from the rest of the gear system and hence its dynamics can be studied with relative ease. Most of the earlier studies on gear dynamic loads [14-18,20] made this assumption and used a single degree of freedom system to evaluate the dynamic loads. But, in reality this may not be the case always. Also, since the proposed simulator is to be used for simulating existing gear systems as well, a

provision to consider the effects of the shaft elasticities and system inertias, if required, is provided.

2.2.5 Damping in the system

Whereas the primary factors and the system inertias determine the critical regions, the severity of the response at these critical regions is determined by the damping in the system. As is shown in a later chapter, for any gear system there is a minimum requirement on damping to prevent Mathew-Hill type of parametric instabilities. In this study, the values of damping ratio used in the numerical examples are chosen based on the experimental results [55,127].

2.2.6 Input torque fluctuations

It is customary in gear dynamic studies to assume constant input torque. In reality, however, the input torque is rarely static. Benton and Seireg [36] studied the effect of torque fluctuation on gear dynamics. They considered an ideal case, wherein the torque fluctuations are assumed to be sinusoidal, and showed that the torque fluctuations have significant influence on system stability. But, under realistic operating conditions the torque fluctuations need not be purely sinusoidal due to the dynamic characteristics of the prime movers. Thus, in the proposed simulator provision is made to include any complex variation in the input torque by way of discretization.

2.2.7 Variation in contact ratio

The design contact ratio, which is defined as the ratio of length of the path of contact to the base pitch, indicates the average number of pairs of teeth in contact. According to this definition, and with reference to the Fig. 2.1, the contact ratio (CR) will be,

$$CR = \frac{A-B}{P_b} \quad (2.10)$$

This ratio is a constant for a given pair of gears. Basically, this ratio provides important information on load sharing between teeth, namely, how many tooth share load and for how long during one mesh period. Thus, this parameter has primary influence on the mesh stiffness fluctuations. Conventional gears, known as Normal Contact Ratio (NCR) gears, have a contact ratio value between 1 and 2. AGMA standards specify a minimum value of 1.2. This value of 1.2 means that for 20% of the time at least two teeth pairs are in mesh. In recent years to increase the load capacity of gears, High Contact Ratio (HCR) gears having a contact ratio value between 2 and 4 have been increasingly used. Here the higher load capacity is achieved by reducing the dynamic load acting on each tooth.

In contrast to the design contact ratio, the instantaneous contact ratio, again defined as given earlier is not constant. This is due to the fact that under

operating load conditions the tooth deflection advances the point of contact and delays the point of losing contact, thereby effectively changing the length of contact.

$$CR_i = \frac{A'B'}{P_b} \quad (2.11)$$

The quantities A', and B' are defined in Fig. 2.8. Thus in reality, a complex situation exists wherein, the stiffness variation determines the contact ratio, which in turn influences the stiffness variation. To solve this statically indeterminate problem, Kasuba, et.al. [19] proposed a search and compute procedure which they referred to as large scale digitized method. As the name implies, their method involves digitizing the gear and pinion profiles and using a search procedure to find the contact points between the deflected tooth pairs in contact.

In this study, however, it is decided to use the design contact ratio, rather than the instantaneous contact ratio. It is felt that since the transmission error signals used as an input to the simulator includes the effect of all the contributing factors, including the change in contact ratio, resulting in non-conjugate action, it will be redundant to include the variation in contact ratio once again.



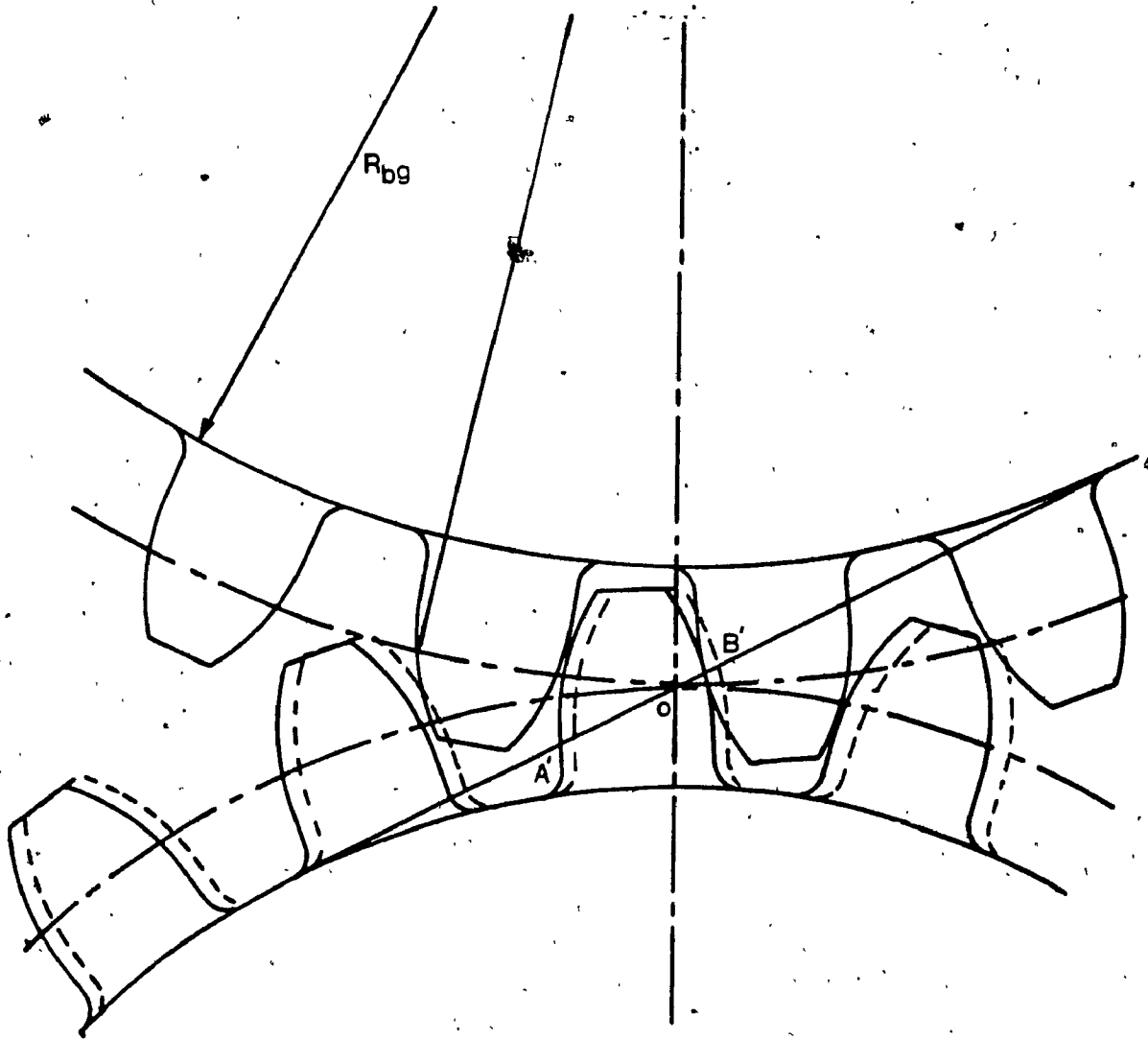


Fig. 2.8: Gear tooth deflection under load

2.2.8 Coupling between torsional and lateral modes

Even though coupling between torsional and lateral modes is usual in practical gear systems, it is also usual to ignore the effect of lateral vibration of gear shafts in gear dynamics studies. Thus almost all the earlier investigations on gear dynamic loads assume that the lateral vibration of gear shafts does not occur. This assumption can be expected to be valid, when the operational speed of the gear pair is not very high. However, with increasing demands on high speed machinery and hence high speed gearing, it becomes necessary to include the effect of coupling between modes for achieving a proper simulation. In addition, since it is well known that gear dynamics is influenced by factors such as misalignment, mass unbalance, bearing characteristics, gyroscopic effects, etc., it is important to include the coupling between modes for obtaining a proper simulation.

Some works on the vibration and whirl of geared rotor systems have been reported in the literature [23-29]. However, because of the simplifying, and non-realistic assumptions made in these studies regarding backlash, and variable mesh stiffness characteristics, these models are not realistic or can be considered complete. To overcome these shortcomings of the earlier models, the coupling between the two vibration modes is included in the proposed simulation model without sacrificing the effects of other important factors.

2.2.9 Effect of friction

The effect of friction between teeth in mesh is normally neglected as a simplification in gear dynamic analysis. This simplification was considered to be necessary, in the past, because of the lack of clear understanding of the related topic of gear lubrication. But, recent advances in lubrication studies [117,118] make this simplification unnecessary any more. Also, as was shown in [58], the presence of friction between teeth may introduce self-excitation resulting in non-linearly determined limit cycle and discontinuous behaviour in gear system response. In addition, the presence of friction also alters the stress pattern radically [58,59].

In the proposed simulation model, the mechanisms of sliding and rolling friction are included with the restriction that the gears operate in elastohydrodynamic lubrication (EHD) regime. This restriction is proposed, because, of the various types of lubrication regimes that can occur in gear trains, only EHD lubrication is clearly understood in terms of predictions [118]. However, this condition is not as restrictive as it appears, since many gears do operate in EHD regime under normal operating conditions. It is suggested that when there is uncertainty about this restriction of EHD lubrication regime the friction elements should be neglected.

Forces acting on gear tooth

Fig. 2.9 shows the normal force, the rolling friction force W_r and the sliding friction force W_s acting on a pair (j^{th} pair) of teeth in contact at various positions along the line of contact. The normal force acting between the teeth in mesh is nothing but the dynamic load under operating conditions and is a direct function of the gear teeth response, variable mesh stiffness, transmission error, and backlash. Its formulation is carried out in detail in the next chapter. The formulation of the sliding friction force and the rolling friction force is carried out here as follows.

The sliding friction force W_{sj} is a function of the coefficient of friction, between the sliding surfaces and the normal load acting between them. And it always acts opposite to the relative motion of the sliding surfaces. Thus,

$$W_{sj} = \mu \cdot W_{dj} (\text{sgn}(V_s)), \quad (2.12)$$

where,

- μ = coefficient of friction,
- W_{dj} = normal load acting between sliding surfaces,
- V_s = sliding velocity.

and,

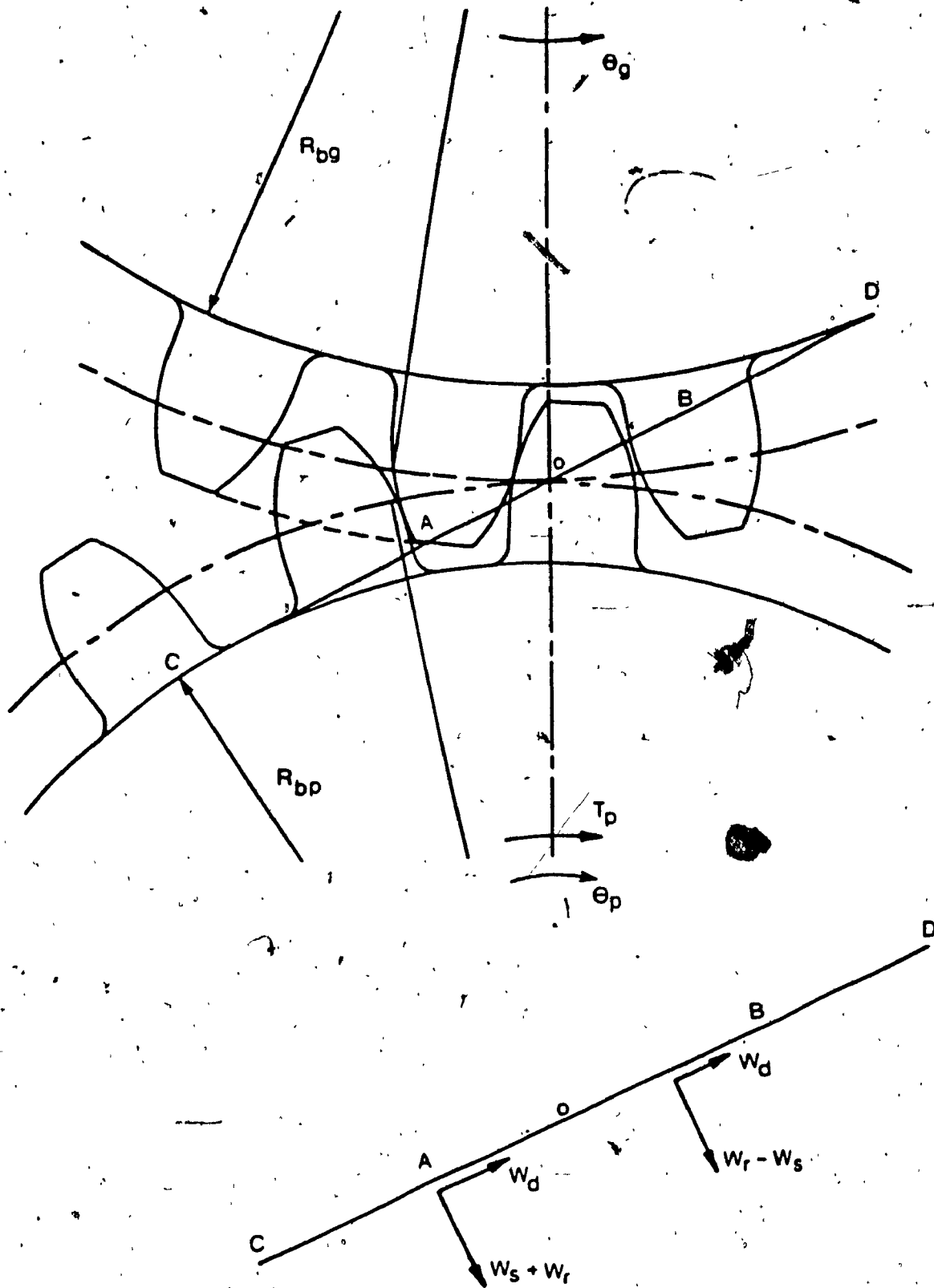


Fig. 2.9:— Forces acting between tooth pair in contact

$\text{sgn}(V_S) = +1$, when V_S is +ve,
 $= -1$, when V_S is -ve.

The coefficient of friction μ , in general, is not a constant and varies along the path of contact. In this study, the empirical relationship, equation (2.13), developed by Benedict and Kelly [119] based on disc machine data is used to account for the variation, in μ .

$$\mu = 0.0127 \log \frac{C_1 W_d / B}{\eta_o V_s V_r^2} \quad (2.13)$$

Here,

C_1 = 29.66 = proportionality constant,
 W_{dj} = normal load, N,
 B = face width of the gears, m,
 η_o = lubricant absolute viscosity, 10^{-3} N s/m²,
 V_r = rolling velocity, m/s,
 V_s = sliding velocity, m/s.

And the rolling friction force in EHD regime of lubrication is directly proportional to the lubrication film thickness [120].

That is,

$$W_{rj} = 8.96 \times 10^7 h_j \quad (2.14)$$

where, the film thickness h_j in metres is calculated by the method of Dowson and Higginson [118] as given in the following equation.

$$h_j = \frac{1.6\eta^{0.6} (\eta_0 V_m)^{0.7} E_e^{0.03} R_e^{0.43}}{W_d^{0.13}} \quad (2.15)$$

where,

- W_d = normal load, N,
- η = pressure viscosity coefficient, m^2/N ,
- η_0 = lubricant viscosity,
- V_m = mean surface speed, m/s,
- E_e = equivalent modulus of elasticity, N/m^2
- R_e = effective radius of curvature at contact point, m.

The total friction force W_s , and the total rolling friction force W_r and the corresponding torques T_s and T_r are obtained by direct summation of the individual components as given below.

$$W_s = \sum_{j=1} W_{sj} \quad (2.16)$$

$$W_r = \sum_{j=1} W_{rj} \quad (2.17)$$

$$T_s = \sum_{j=1} W_{sj} R_j \quad (2.18)$$

$$T_r = \sum_{j=1} W_{rj} R_j \quad (2.19)$$

where,

R_j = radius of curvature at the contact point of the j^{th} tooth pair

j = index denoting the number of tooth pairs in contact at any given time.

It should be noted that the equations (2.13) and (2.15) used here for the computation of the friction coefficient and the film thickness respectively are used here without any rigorous evaluation based on the useful results obtained with these in gear system power loss studies [120-124]. If and when, new improved formulations for these parameters are available the new expressions can be used without any major modifications to the methodology.

2.3 Summary

In this chapter, the primary and secondary factors that affect the gear dynamics are first stated and then reviewed. Also, expressions relating the influence of these factors are derived to facilitate their inclusion into the mathematical models developed subsequently in the following chapters.

CHAPTER 3

DYNAMIC LOAD ESTIMATION - DETERMINISTIC APPROACH

3.1 Introduction

The concern of designers and analysts with dynamic loads acting on gear teeth goes back at least to the eighteenth century. For over a century now, gear dynamic factors or speed factors defined as the ratio of the dynamic load to the statically transmitted load have been used in gear designs to account for the dynamic effects. By this definition the dynamic factor can be viewed as the gear's tooth load magnifying factor.

This factor is intended to account for,

1. the effects of tooth spacing and profile errors,
2. the effect of pitch line speed and RPM,
3. the inertia and stiffness of all rotating elements,
4. the transmitted load per face width,
5. the tooth stiffness.

But in reality, the empirical dynamic factor formulas used in AGMA standards [1] as well as in many other standards are functions of gear pitch line speed and the gear manufacturing quality only. No account is made of the possible variation resulting from specific tooth error pattern, inertias, loading effects and other system

dependent characteristics. Thus, even with increasingly tightened restrictions on the applicability range, the existing empirical dynamic factor formulas may either overestimate or greatly underestimate the actual gear dynamic load amplitudes under certain conditions. In addition, to be able to predict possible failure of a gear during operation not only the maximum stress but also the stress excursion at the critical locations within the gear be known. This requires that the dynamic load history along the entire path of contact and not just the maximum dynamic load as computed in the conventional design process be known. Also, contrary to the concept of fatigue process which is induced by the alternating as well as the mean loads, the current gear design procedures consider only a single value of design load as given by the application of dynamic load factors. Thus quite obviously, the existing gear design practice, which uses a very loosely defined application factor as the only compensation to many important dynamic effects, is inadequate for the design of modern gears.

Such inconsistencies and inadequacies indicate clearly the need for a more concrete analytical basis. Towards this end, many researchers [12-19] have developed analytical models based on the torsional vibrational behaviour of two gear wheels. Generally their results agree well with dynamic loads measured using strain gauges at the root of a

gear tooth, which suggests that such analytical approaches can be refined to give an accurate method for determining dynamic loads. A more complete mathematical model for the configured, typical gear system incorporating the actual measured transmission error record, the variable mesh stiffness, non-linear backlash element, friction between the teeth, and coupling between the torsional and lateral modes, is formulated in the following sections. Fig. 3.1 shows schematically the steps involved in dynamic load simulation process, referred to as the dynamic load simulator hereafter, proposed in this investigation.

3.2 Modelling of the gear system

Depending upon the size of the system and the refinement required, two different modelling and solution schemes are presented in this study. For preliminary design of a new spur gear set, wherein the influences of the other components in the gear system are not known, the two gears and the two supports close to it are the only elements considered. That is, it is assumed that gear set is effectively decoupled from the rest of the system [18,20]. With this assumption, the equations of motion are set up and solved using the state-space method. Even though the same methodology can be used without any change for larger systems with more number of degrees of freedoms, the matrices involved become larger making the analysis prohibitively costly and hence impractical. Thus, for large

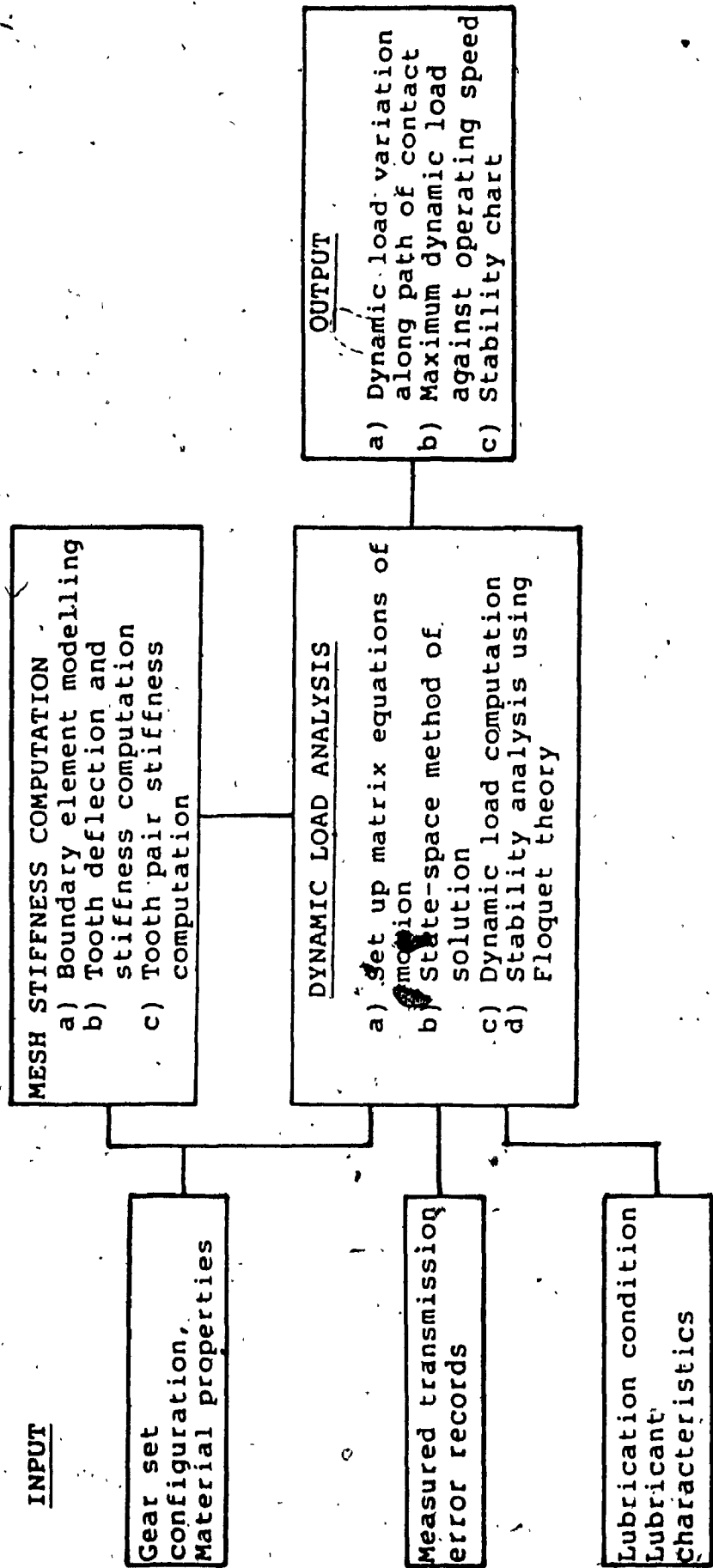


Figure 3.1: Schematic of the dynamic load simulator

systems such as multi-stage gear trains with other associated driveline elements such as couplings, bearings, etc., a new simulation methodology based on the transfer matrix methods and the numerical integration procedures is introduced in chapter 5.

3.2.1 Schematic configuration of the gear system

In this section, a single stage spur gear system, shown in Fig. 3.2, which represents one of the practical cases in gearing applications, is considered to develop the simulation methodology. This system consists of a driving motor, a driven machine, two intermediate shafts, two flexible couplings, four support bearings and two gears. Based on the assumption stated in the preceding section, only the gear set and the supports are configured for modelling.

3.2.2 Modelling of the configured gear system

To develop mathematical models and associated equations of motion of any dynamic system, it is first necessary to generate a substitute vibration system based on the real system. This new system will then be the basis of the response and the dynamic load simulation procedure. Fig. 3.3 shows the equivalent vibration system for the configured gear set system shown in Fig. 3.2. The variable mesh stiffness and damping are denoted as $k_{pg}(t)$, and $c_{pg}(t)$ respectively. The backlash BL between the gears is modelled

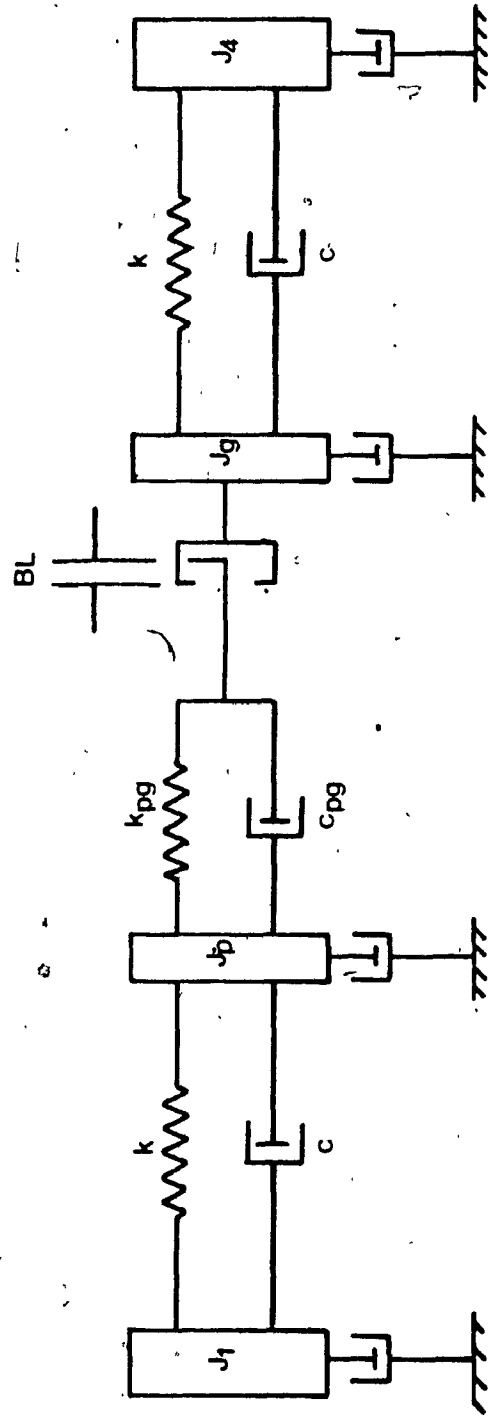
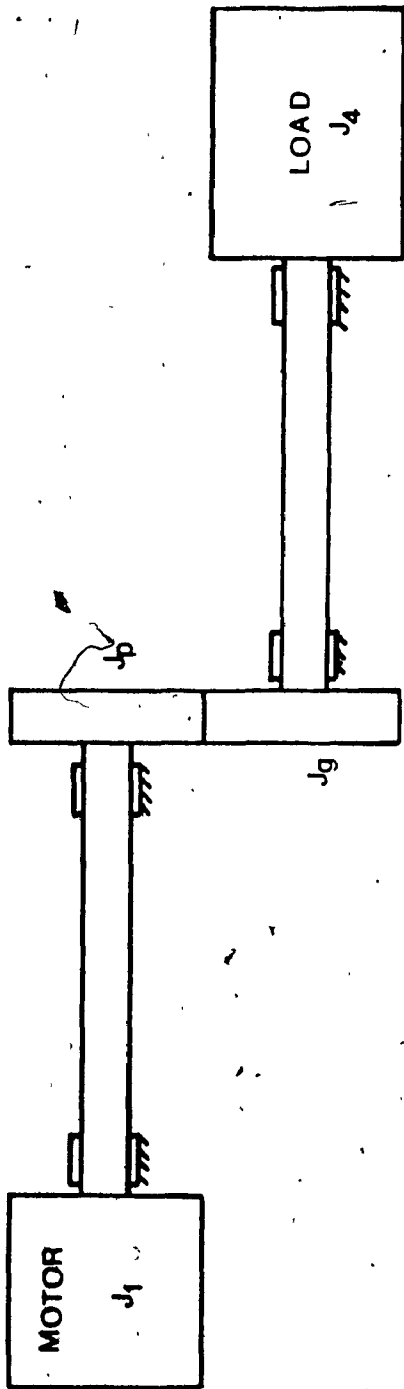


Fig. 3.2: A typical spur gear system

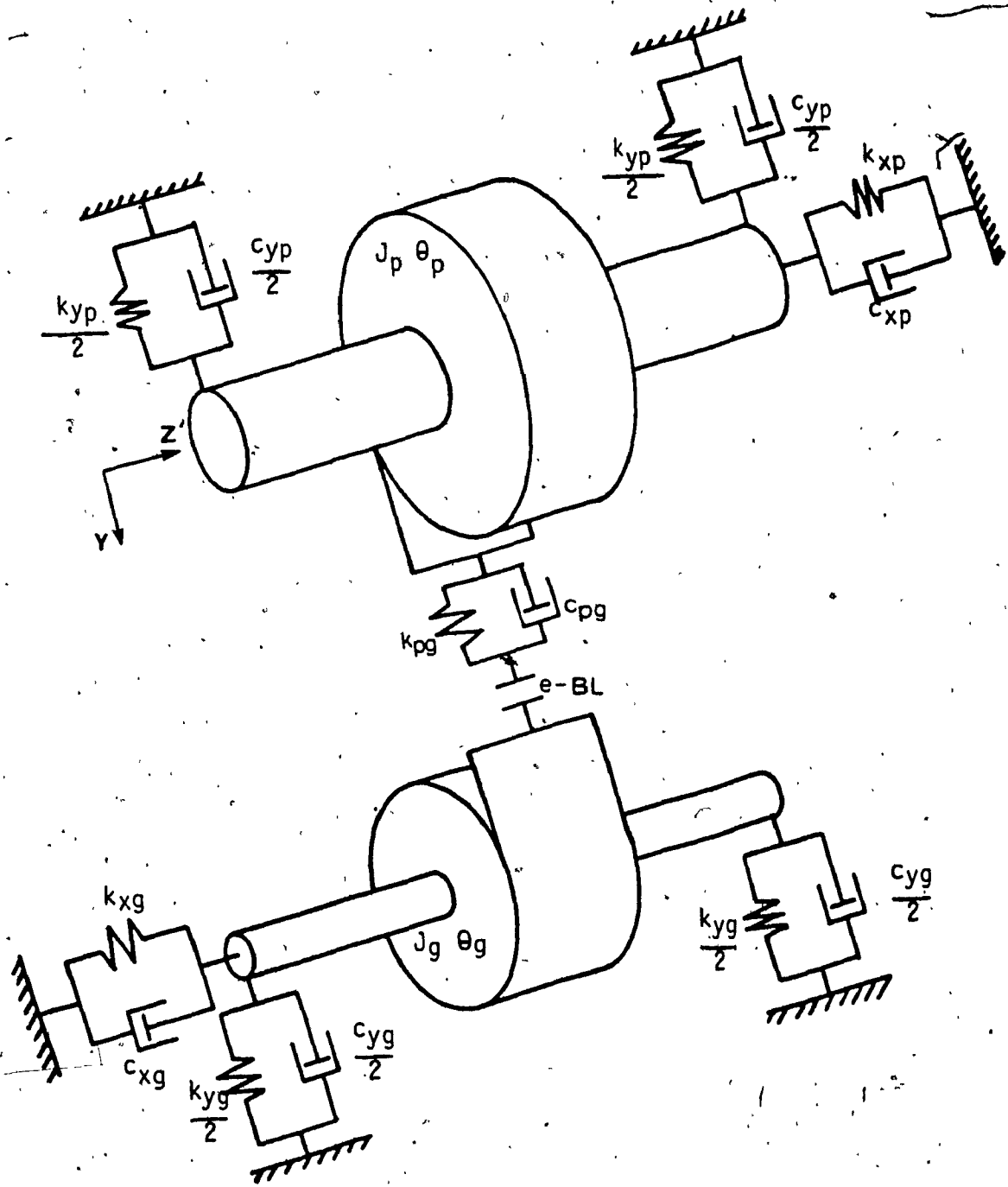


Fig. 3.3: Equivalent vibration system

as shown in Fig. 2.7. Between points 1 and 2, normal meshing takes place and between 2 and 3 there occurs a loss of contact. Region 3 to 4 corresponds to meshing at the rear flanks. The governing equations of motion for the gear pair system considered can be derived using the standard procedures as given below.

Equations of motion

Torsional mode:

$$J_p \ddot{\theta}_p + W_d R_{bp} - T_{sp} + T_{rp} = T_p \quad (3.1)$$

$$J_g \ddot{\theta}_g - W_d R_{bg} - T_{sg} - T_{rg} = -T_g - n T_p \quad (3.2)$$

Lateral mode:

$$m_p \ddot{x}_p + c_{xp} \dot{x}_p + k_{xp} x_p + W_d \sin(\alpha-\beta) - (W_s + W_r) \cos(\alpha-\beta) = 0 \quad (3.3)$$

$$m_p \ddot{y}_p + c_{yp} \dot{y}_p + k_{yp} y_p + W_d \cos(\alpha-\beta) - (W_s + W_r) \sin(\alpha-\beta) = 0 \quad (3.4)$$

$$m_g \ddot{x}_g + c_{xg} \dot{x}_g + k_{xg} x_g - W_d \sin(\alpha-\beta) - (W_s + W_r) \cos(\alpha-\beta) = 0 \quad (3.5)$$

$$m_g \ddot{y}_g + c_{yg} \dot{y}_g + k_{yg} y_g - W_d \cos(\alpha-\beta) - (W_s + W_r) \sin(\alpha-\beta) = 0 \quad (3.6)$$

Here,

J = polar moment of inertia,

m = mass,

- c_x = damping coefficient of the bearing along X direction,
- k_x = stiffness of the bearing along X direction,
- c_y = damping coefficient of the bearing along Y direction,
- k_y = stiffness of the bearing along Y direction,
- θ = torsional displacement,
- x = displacement along X direction,
- y = displacement along Y direction,
- T = external torque applied,
- n = gear ratio,
- α = pressure angle,
- β = angle used to locate the centre line of the gear set,

and the subscripts p and g are used to denote the pinion and gear quantities respectively.

Depending upon the operational situation, with reference to Fig. 2.7, the gear dynamic load W_d , and the dynamic load on each tooth pair in contact W_{dj} are defined in the following manner.

For $(u+e) > 0$,

$$W_d = [c_{pg}(t) \dot{u} + k_{pg}(t)\{u+e\}]. \quad (3.7)$$

For $-BL < (u+e) < 0$,

$$W_d = 0. \quad (3.8)$$

For $(u+e) < -BL$,

$$W_d = [c_{pg}(t) \dot{u} + k_{pg}(t)\{u+e+BL\}]. \quad (3.9)$$

with,

$$W_{dx} = \frac{k_{PG,j}(t)}{k_{PG}(t)} W_d \quad \text{for } j = 1, 2, \dots \quad (3.10)$$

where,

j = index denoting the number of pairs of teeth in mesh at any given time.

e = gear transmission error along the line of action

u = displacement along the line of action

BL = backlash

The displacement along the line of action u is given by,

$$u = R_{bp} \theta_p - R_{bg} \theta_g + (x_p - x_g) \sin(\alpha - \beta) + (y_p - y_g) \cos(\alpha - \beta) \quad (3.11)$$

which can be rewritten concisely as,

$$u = u_1^T u_2 \quad (3.12)$$

where,

$$u_1 = \{ \theta_p, \theta_g, x_p, x_g, y_p, y_g \}^T \quad (3.13)$$

and

$$u_2 = \{ R_{bp}, -R_{bg}, \sin(\alpha - \beta), -\sin(\alpha - \beta), \cos(\alpha - \beta), -\cos(\alpha - \beta) \}^T \quad (3.14)$$

Here the variable mesh stiffness $k_{pg,j}(t)$ is expressed as a five term power series as given in equation (2.6). And $c_{pg}(t)$ is expressed in terms of the critical damping ratio,

the variable mesh stiffness $k_{pg}(t)$ and the equivalent moment of inertia J_e , as,

$$c_{pg}(t) = 2 \xi \sqrt{k_{pg}(t) \frac{J_e}{R_{bp}^2}} \tag{3.15}$$

with,

$$J_e = \frac{J_p J_g}{J_g + n^2 J_p} \tag{3.16}$$

The sliding friction force W_s and the rolling friction force W_r and the corresponding torques T_{sp} , T_{sg} , T_{rp} , and T_{rg} are given by equations (2.12) to (2.19).

By choosing the state vector v as,

$$v = \begin{Bmatrix} u_1 \\ \dot{u}_1 \end{Bmatrix} \tag{3.17}$$

the system equations can be rewritten in terms of the state vector v as,

$$\dot{v}(t) = A(t) v(t) + b(t) \tag{3.18}$$

where,

$$A(t) = \begin{bmatrix} 0 & I \\ -K(t) & -C(t) \end{bmatrix} \tag{3.19}$$

and

$$b(t) = \begin{Bmatrix} 0 \\ f(t) \end{Bmatrix} \tag{3.20}$$

with $f(t) = \{T_p, -T_g, 0,0,0,0\}^T - k_{pg}(t) (e) u_2$, for $(u+e) > 0$,

$$f(t) = \{T_p, -T_g, 0,0,0,0\}^T, \quad \text{for } -BL \leq (u+e) \leq 0, \quad (3.21)$$

$$f(t) = \{T_p, -T_g, 0,0,0,0\}^T - k_{pg}(t) (e + BL) u_2, \text{ for } (u+e) < -BL.$$

And the matrices $K(t)$ and $C(t)$ are respectively given by the equations (3.22) and (3.23) shown in Fig. 3.4, for the case of no friction.

3.3 Solution procedure

The time varying non-linear equation of motion given by equation (3.18) can be solved in a straight forward manner using any suitable numerical integration technique. In this study, however, the state-space method which is widely used in modern control system design for time domain analysis is chosen to solve the system equation (3.18). The advantages of using the state-space technique are:

- a. As a numerical procedure, this approach is less sensitive to the choice of time step [125], and for a given time step, the accuracy of the solution at each time instant can easily be specified and controlled.
- b. In particular, with respect to the problem considered here, the overall transition matrix obtained with the application of state-space

$$\begin{aligned}
 & \mathbf{K}(t) = \begin{bmatrix} \frac{R_{bp}^2}{J_p} & -\frac{R_{bp} R_{bg}}{J_p} & \frac{R_{bp} \sin(\alpha-\beta)}{J_p} & -\frac{R_{bp} \sin(\alpha-\beta)}{J_p} & \frac{R_{bp} \cos(\alpha-\beta)}{J_p} & -\frac{R_{bp} \cos(\alpha-\beta)}{J_p} \\ -\frac{R_{bg} R_{bp}}{J_g} & \frac{R_{bg}^2}{J_g} & -\frac{R_{bg} \sin(\alpha-\beta)}{J_g} & \frac{R_{bg} \sin(\alpha-\beta)}{J_g} & -\frac{R_{bg} \cos(\alpha-\beta)}{J_g} & \frac{R_{bg} \cos(\alpha-\beta)}{J_g} \\ \frac{R_{bp} \sin(\alpha-\beta)}{m_p} & -\frac{R_{bg} \sin(\alpha-\beta)}{m_g} & \sin^2(\alpha-\beta) + \frac{k_{xp}}{k_{pg}} & -\sin^2(\alpha-\beta) & \sin(\alpha-\beta) \cos(\alpha-\beta) & -\sin(\alpha-\beta) \cos(\alpha-\beta) \\ -\frac{R_{bp} \sin(\alpha-\beta)}{m_g} & \frac{R_{bg} \sin(\alpha-\beta)}{m_g} & -\sin^2(\alpha-\beta) & \sin^2(\alpha-\beta) + \frac{k_{yg}}{k_{pg}} & -\sin(\alpha-\beta) \cos(\alpha-\beta) & \sin(\alpha-\beta) \cos(\alpha-\beta) \\ \frac{R_{bp} \cos(\alpha-\beta)}{m_p} & -\frac{R_{bg} \cos(\alpha-\beta)}{m_g} & \sin(\alpha-\beta) \cos(\alpha-\beta) & -\sin(\alpha-\beta) \cos(\alpha-\beta) & \cos^2(\alpha-\beta) + \frac{k_{yp}}{k_{pg}} & -\cos^2(\alpha-\beta) \\ -\frac{R_{bp} \cos(\alpha-\beta)}{m_g} & \frac{R_{bg} \cos(\alpha-\beta)}{m_g} & -\sin(\alpha-\beta) \cos(\alpha-\beta) & \sin(\alpha-\beta) \cos(\alpha-\beta) & -\cos^2(\alpha-\beta) & \cos^2(\alpha-\beta) + \frac{k_{yg}}{k_{pg}} \end{bmatrix} \\
 & \quad (3.32)
 \end{aligned}$$

$$\begin{aligned}
 & \mathbf{C}(t) = \begin{bmatrix} \frac{R_{bp}^2}{J_p} & -\frac{R_{bp} R_{bg}}{J_p} & \frac{R_{bp} \sin(\alpha-\beta)}{J_p} & -\frac{R_{bp} \sin(\alpha-\beta)}{J_p} & \frac{R_{bp} \cos(\alpha-\beta)}{J_p} & -\frac{R_{bp} \cos(\alpha-\beta)}{J_p} \\ -\frac{R_{bg} R_{bp}}{J_g} & \frac{R_{bg}^2}{J_g} & -\frac{R_{bg} \sin(\alpha-\beta)}{J_g} & \frac{R_{bg} \sin(\alpha-\beta)}{J_g} & -\frac{R_{bg} \cos(\alpha-\beta)}{J_g} & \frac{R_{bg} \cos(\alpha-\beta)}{J_g} \\ \frac{R_{bp} \sin(\alpha-\beta)}{m_p} & -\frac{R_{bg} \sin(\alpha-\beta)}{m_g} & \sin^2(\alpha-\beta) + \frac{c_{xp}}{c_{pg}} & -\sin^2(\alpha-\beta) & \sin(\alpha-\beta) \cos(\alpha-\beta) & -\sin(\alpha-\beta) \cos(\alpha-\beta) \\ -\frac{R_{bp} \sin(\alpha-\beta)}{m_g} & \frac{R_{bg} \sin(\alpha-\beta)}{m_g} & -\sin^2(\alpha-\beta) & \sin^2(\alpha-\beta) + \frac{c_{yg}}{c_{pg}} & -\sin(\alpha-\beta) \cos(\alpha-\beta) & \sin(\alpha-\beta) \cos(\alpha-\beta) \\ \frac{R_{bp} \cos(\alpha-\beta)}{m_p} & -\frac{R_{bg} \cos(\alpha-\beta)}{m_g} & \sin(\alpha-\beta) \cos(\alpha-\beta) & -\sin(\alpha-\beta) \cos(\alpha-\beta) & \cos^2(\alpha-\beta) + \frac{c_{yp}}{c_{pg}} & -\cos^2(\alpha-\beta) \\ -\frac{R_{bp} \cos(\alpha-\beta)}{m_g} & \frac{R_{bg} \cos(\alpha-\beta)}{m_g} & -\sin(\alpha-\beta) \cos(\alpha-\beta) & \sin(\alpha-\beta) \cos(\alpha-\beta) & -\cos^2(\alpha-\beta) & \cos^2(\alpha-\beta) + \frac{c_{yg}}{c_{pg}} \end{bmatrix} \\
 & \quad (3.33)
 \end{aligned}$$

Fig. 3.4: Composition of matrices $\mathbf{K}(t)$ and $\mathbf{C}(t)$

technique provides very useful information on the stability of the gear system, which is one of the major requirement in any gear dynamic analysis.

c. In addition, as will be explained later, the overall transition matrix can be used to choose the proper initial conditions so as to reach the steady state condition immediately after the start of the analysis. This results in considerable reduction in computational time.

To solve the continuous-time state equation (3.18) on digital computer, it is first converted to an equivalent discrete-time state equation, with the assumption that, the forcing vector $b(t)$ and the control matrix $A(t)$ change only at equally spaced sampling time instants.

Thus,

$$v(t_{i+1}) = \Phi(t_{i+1}, t_i) v(t_i) + b_d(t_i) \quad (3.24)$$

$i=0,1,2,\dots$

where,

$$\Phi(t_{i+1}, t_i) = \exp(A(t_{i+\frac{1}{2}})(\Delta T)), \quad (3.25)$$

and,

$$b_d(t_i) = \int \Phi(t_{i+1}, t) b(t_{i+\frac{1}{2}}) dt. \quad (3.26)$$

Equation (3.24) is a discrete-time state equation, which has identical solution as that of equation (3.18) at discrete time instants $t_0, t_1, t_2, \dots, t_m$. In the discrete-time state equation (3.24), the state transition matrix Φ and the vector b_d are assumed to be constant and have a value corresponding to $t_{i+1/2}$ in each time interval $(t_i - t_{i+1})$. Such piecewise constant approximations are valid, if the total number of sampling instants is sufficiently large and if the time interval chosen is sufficiently small [126] compared with the time constants of the system. In the present study a time interval smaller than one tenth of the smallest system natural period is used based on an empirical rule [132], commonly used with state-space technique in control system applications.

Equation (3.24) is a recurrence relationship and hence starting from initial condition $v(t_0)$ at time $t=t_0$, the state variables at subsequent time instants can be computed by time marching. This procedure is best suited for implementation on a digital computer. The exponential matrix Φ and the vector b_d are approximated by truncated Taylor's series as given below.

That is,

$$\Phi(t_{i+1}, t_i) = \sum_{r=0}^{\infty} \frac{(\Delta T)^r A(t_{i+1/2})^r}{r!} \quad (3.27)$$

$$b_d(t_i) = \Delta T \sum_{r=0}^{\infty} \frac{(\Delta T)^r A(t_{i+1/2})^r}{(r+1)!} b(t_{i+1/2}) \quad (3.28)$$

where,

ΔT = time step = $(t_{i+1} - t_i)$,

r = the number of terms used to truncate the Taylor series.

3.3.1 Selection of initial conditions

In order to start the solution procedure, it is essential to know the initial values of the state variables at time $t = t_0$. The usual practice is to start with arbitrary initial values and go through a multi-iterative process so as to reach the steady state conditions. This procedure takes up a lot of computational time. However, with initial conditions properly chosen, the steady state response "begins almost immediately" without having to go through the transient response decay period. The proper choice of initial conditions is achieved by the following procedure which is based on the fact that after the passage of one gear mesh, the displacements and velocities must be the same as that for the starting condition when no gear errors are involved. Thus, the procedure is to start with zero initial conditions with the assumption that there are no errors, and no friction, and calculate sequentially the gear motion till the end of mesh cycle. In this process the overall state transition matrix $\Phi(t_m, t_0)$ will also be computed, which in turn can be used to choose the proper initial conditions as follows.

Using the recurrence relationship (3.24), the state of the system at the end of the mesh cycle $v(t_m)$ can be written in terms of the state at the beginning of the mesh cycle $v(t_0)$ as,

$$v(t_m) = \Phi(t_m, t_0) v(t_0) + d(t_m) \quad (3.29)$$

Here, the overall transition matrix $\Phi(t_m, t_0)$ which relates the state variables at the end of the mesh cycle to the state variables at the beginning of mesh cycle, is given by,

$$\Phi(t_m, t_0) = \prod_{i=0}^{m-1} \Phi(t_{i+1}, t_i), \quad (3.30)$$

and,

$$d(t_m) = \sum_{i=0}^{m-2} \prod_{j=i+1}^{m-1} \Phi(t_{j+1}, t_j) b_d(t_i) + b_d(t_{m-1}) \quad (3.31)$$

Since, in the absence of gear errors, under steady state condition,

$$v(t_m) = v(t_0), \quad (3.32)$$

the equation (3.29) can be written as,

$$v(t_0) = \Phi(t_m, t_0) v(t_0) + d(t_m) \quad (3.33)$$

Rearranging the terms in the above equation, the state of the system at the initial time t_0 or the initial conditions will be given by,

$$v(t_0) = [I - \Phi(t_m, t_0)]^{-1} d(t_m) \quad (3.34)$$

Starting with these known initial conditions the solution procedure is repeated with the inclusion of specified gear errors. As can be seen, this procedure requires only two iterations, one to choose the proper initial conditions and one to run the analysis with the proper initial conditions. This results in considerable savings in computations and this is one of the major advantages of using state-space method for the gear dynamics problem.

However, the procedure given above is valid only when the gear teeth in mesh are in one of the three linear portions of mesh stiffness non-linearity curve shown in Fig. 2.7, for the entire mesh cycle. This will be the case in the regions away from the resonances. When the operational situations change the gear mesh conditions during one mesh cycle, the overall state transition matrix $\Phi(t_m, t_0)$ of the system will itself depend on the choice of the initial conditions and hence the given procedure will not be valid. In such cases the computer program has been designed to enter automatically into a multi-iterative mode to reach the steady state conditions.

3.4 Dynamic load estimation

Once the state of the system, namely, the relative velocities and the relative displacements at different time instants have been computed using the numerical procedure

described in the section 3.3, then the dynamic load on each tooth pair and the total dynamic load on the gears can be computed at different time instants and hence at different contact positions by using the equations (3.7) to (3.10).

3.5 Verification of the simulator

In order to validate the proposed dynamic load simulator, a comparison of the simulator results with available experimental results is carried out. For this purpose, experimental results from two recently published studies [55,127], each using different measuring techniques, are considered.

Case I:

Of these, the study by Umezawa et.al. [127] is of more value since complete details of the experimental set up, shown in Fig. 3.5, including the measured transmission error records are provided. In addition to the experimental results, which were obtained by strain gauge measurements and acceleration pick-ups, results of numerical simulation based on torsional motion of the gears are also given in [127]. Since, in the proposed simulator, the coupling between the lateral and torsional modes is included, the stiffness of the base supports of the gears need be known. For this purpose, a finite element deflection analysis of the supports is conducted and the stiffness properties of the supports in the vertical direction, namely k_{yp} and k_{yg}

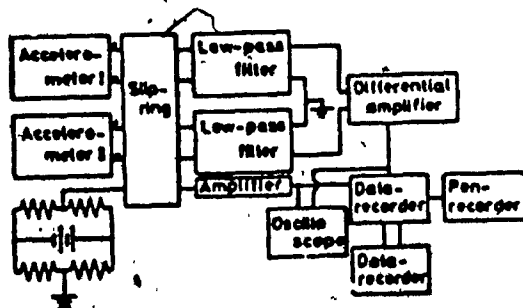
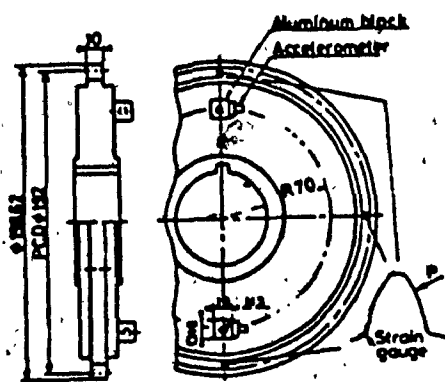
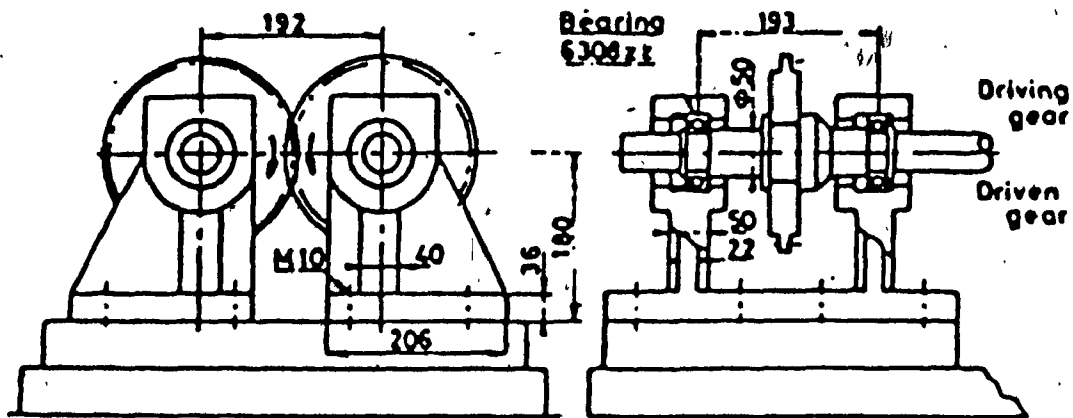


Fig. 3.5: Experimental set-up [127]

are obtained. Table 3.1. gives the various parameters that are required to define the considered gear system. As was suggested in [127], the damping ratio is taken to be 0.07. And because of the lack of knowledge about the lubrication condition during the experiments [127], the frictional non-linearities are not included in the simulation.

Fig. 3.6 shows the results from the proposed simulator superimposed on the results from [127]. As can be seen from Fig. 3.6, the results of the proposed simulator compares very well with the experimental results over the entire frequency range, except that the peak at the support resonance is slightly shifted to the right. This could be attributed to the difference in the computed and the actual values of the support stiffnesses.

Case II:

To further confirm the validity of the simulator and to check the suitability and versatility of the simulator to analyse the dynamics of non-metallic gears, a second comparative study is carried out. For this purpose, the experimental results from the study by Kuske [55] is considered. Kuske [55] showed the dynamic stress and load measurement on meshing gear teeth as an example to establish the viability of the dynamic photoelasticity technique. The photoelastic experimental gear set parameters [55] are given in Table 3.1. The frictional non-linearities are neglected,

Table 3.1: Parameters of the experimental set-up

Parameter	Case I [127]	Case II [55]
Tooth profile	STD.	STD.
Module, mm.	4	8
Number of teeth, Gear 1, mm.	48	25
Number of teeth, Gear 2, mm.	48	25
Pressure angle, deg.	14.5	20
Pitch diameter, Gear 1, mm.	192	200
Pitch diameter, Gear 2, mm.	192	200
Face width, mm.	10	10
Contact ratio	1.80	1.87
Backlash, mm.	0.25	0.25
Material	3SCM steel	FRP
Torque, N-m.	196	1.433 1.933

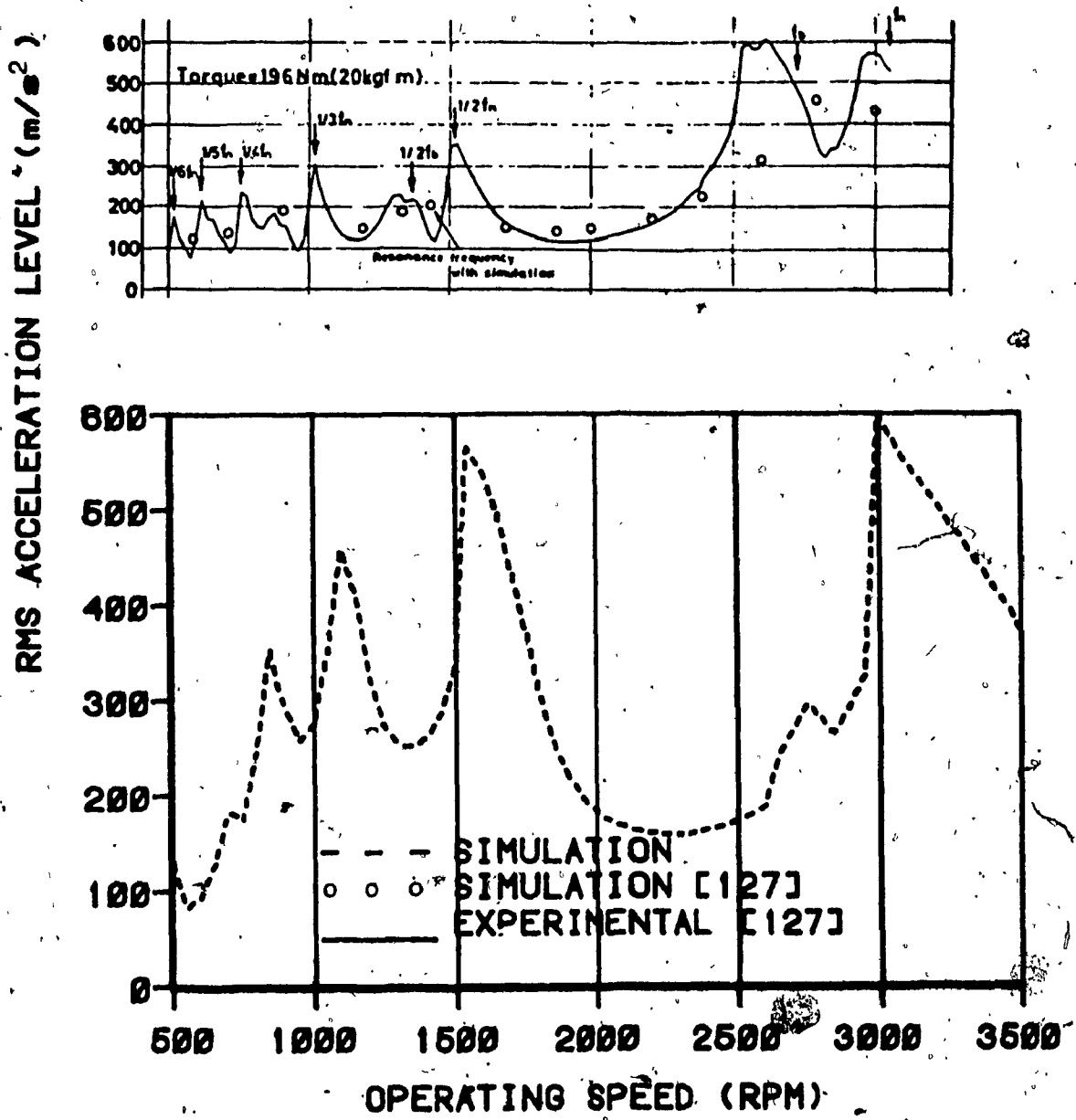


Fig. 3.6: Comparison of simulator and experimental results

because the photoelastic measurements are taken without any lubrication. In addition, the supports had to be excluded for the simulation, because of the lack of complete knowledge of the experimental set up used in [55]. However, inspite of these limiting approximations, the simulator results compare very well with the photoelastic results. Figs. 3.7 and 3.8 show the dynamic load amplitude plotted against time during a mesh period at two different operating conditions. The simulator results follow the trend of the experimental results for the entire time period considered. The location of the peaks and the points at which loss of contact between the mating teeth occurs are found to be the same in both the cases. But the magnitude of the load levels computed by the simulator are different from those given by the photoelastic study. This difference is due to the presence of large amount of friction at the mesh contacts. Because of the rough finish introduced by the machining of photoelastic material and because of the absense of lubrication in photoelasticity tests, the coefficient of friction at the point of contact is typically three to six times higher than those of for gears made of metals [59]. Also, the sliding friction forces reverse their direction across the pitch point, thus increasing the load on the tooth before the pitch point and reducing the load after the pitch point. The photoelasticity results clearly show this trend. However, as mentioned earlier, the frictional characteristics are excluded in the simulation of

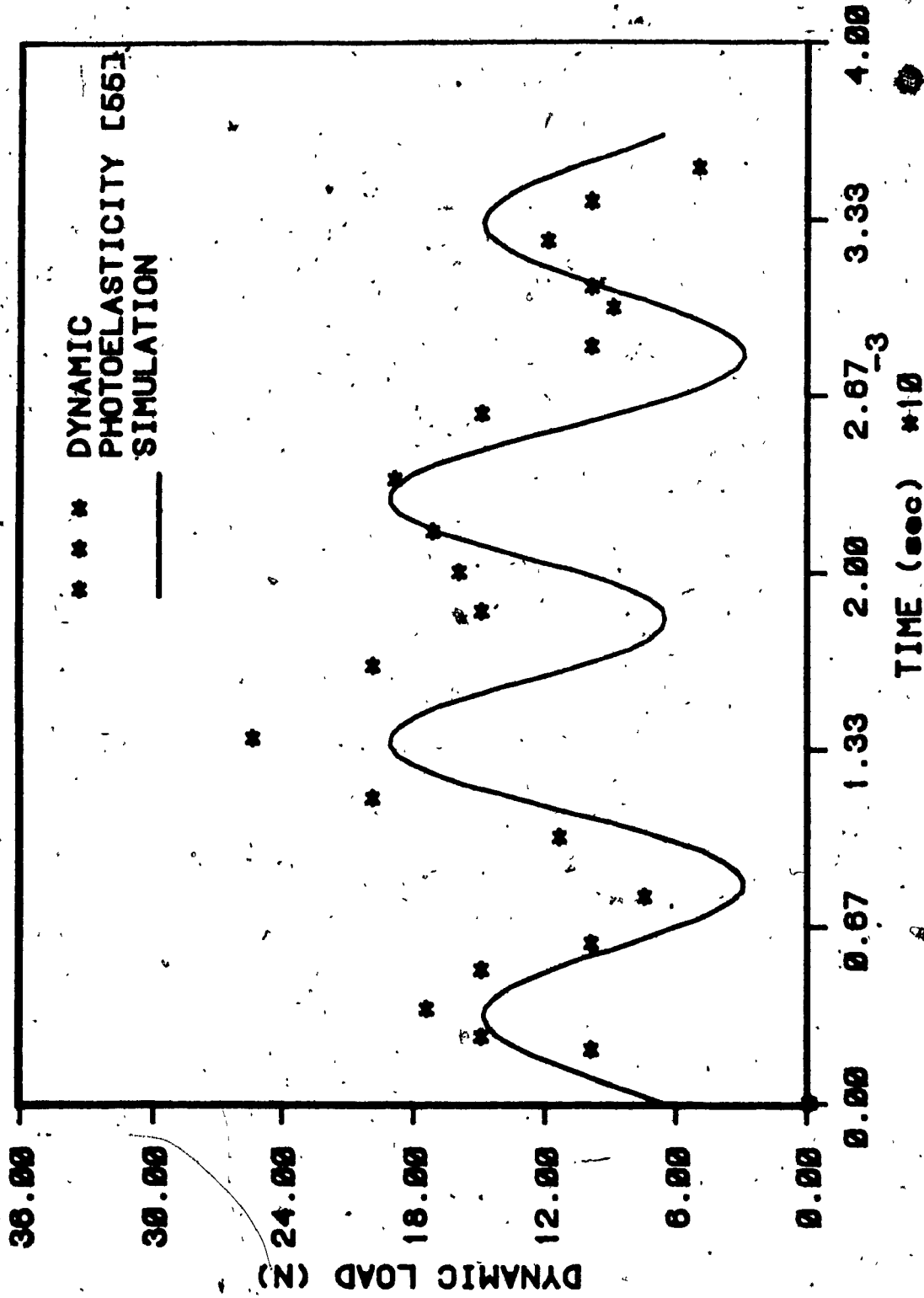


Fig. 3.7: Comparison of simulator and photoelasticity results

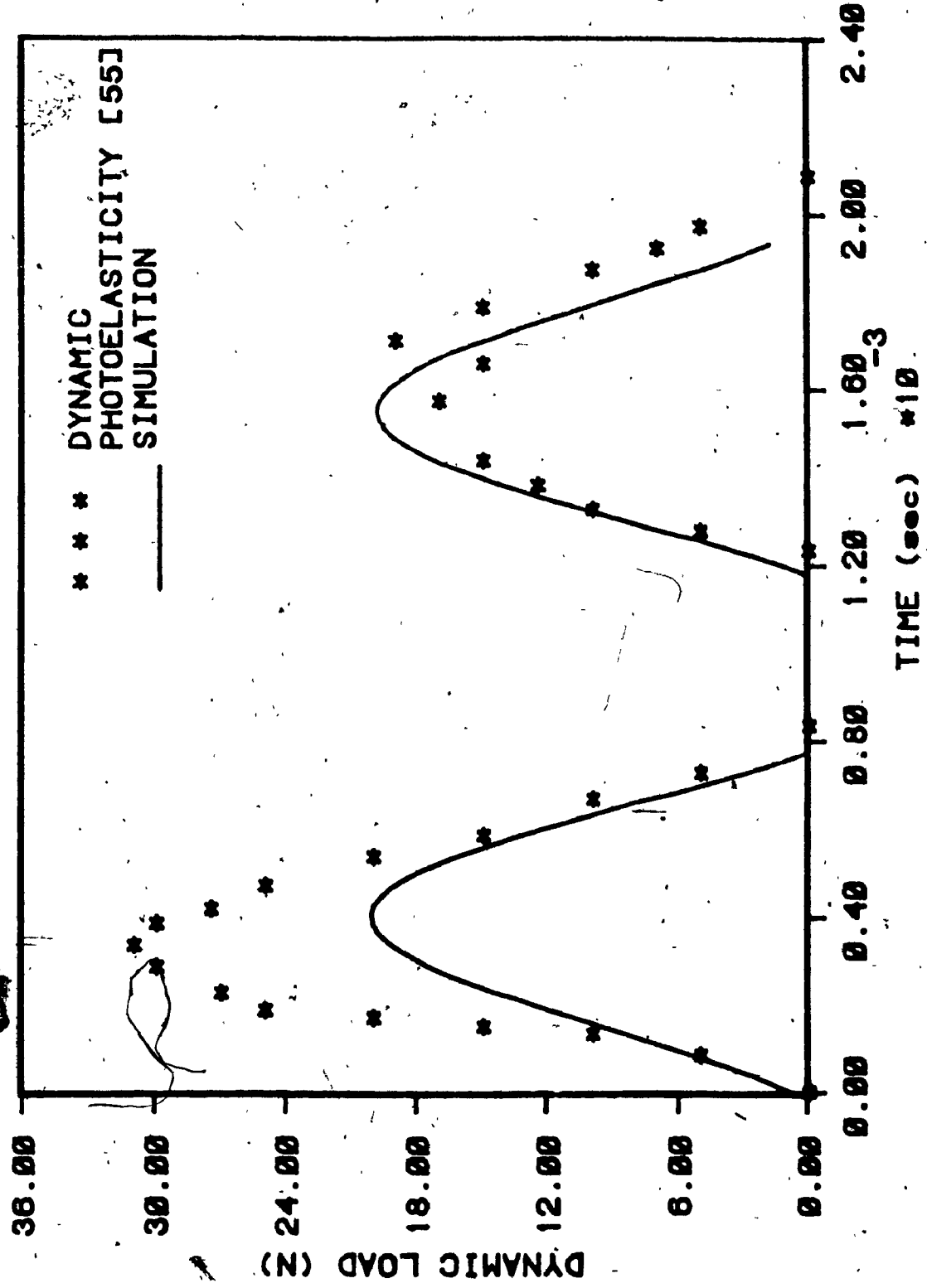


Fig. 3.8: Comparison of simulator and photoelasticity results

the particular case considered here and hence the difference.

3.6 Dynamic load variation

In this section, a parametric study of limited scope is carried out to show that the dynamic load is strongly dependent on gear system parameters and not just the pitch line velocity and gear quality as is implied in the currently used gear dynamic factor formulae. In general, the dynamic load and hence the dynamic stress on a gear tooth varies greatly with contact position, operating speed, damping, and with the changes in system inertias and stiffnesses. It is usual practice to use the dynamic factor (D.F.), defined as the ratio of the dynamic load to the static load, to study the variation in dynamic load. Figs. 3.9 and 3.10 show variation in D.F. with various design parameters, for the gear system defined by the parameters given in Table 3.1.

Variation of D.F. along contact path

Fig. 3.9 gives the variation of dynamic factor along the contact position for three different operating speeds. At low speeds (500 R.P.M.), that are well below the resonant speeds, the D.F. is basically in phase with the stiffness change. As the speed increases through sub-resonant (1600 R.P.M.) and resonant speeds (3000 R.P.M.), the D.F. increases in magnitude. Under light damping tooth

separation and subsequent reverse or forward impact may also occur near the sub-resonant and resonant speeds. Also the location of the occurrence of the maximum dynamic load moves within the single tooth pair contact region contrary to the assumption used in the current gear design practice. At low speeds the maximum dynamic load acts near the point where the single tooth pair contact begins. As the speed increases it moves through the pitch point towards the point where the single tooth pair contact ends. This indicates that during the regular operation of any gear pair, the critical locations in a gear tooth will be subjected to complex stress histories which may lead to fatigue failures.

Effect of operating speed

The effect of speed on dynamic load can be studied by plotting the maximum value of the D.F. at each speed versus the operating speed. Fig. 3.10 shows the maximum D.F. as a function of the operating speed in R.P.M.. As can be expected, the variation in mesh stiffness results in several sub-harmonic resonances, in addition to the primary resonance at 3000 R.P.M.. For comparison, the inverse of the dynamic factor values computed according to the AGMA gear design standards [1] are also shown in Fig. 3.10..

Effect of damping

The damping in the system primarily influences the dynamic load level near the response peaks. In addition, as

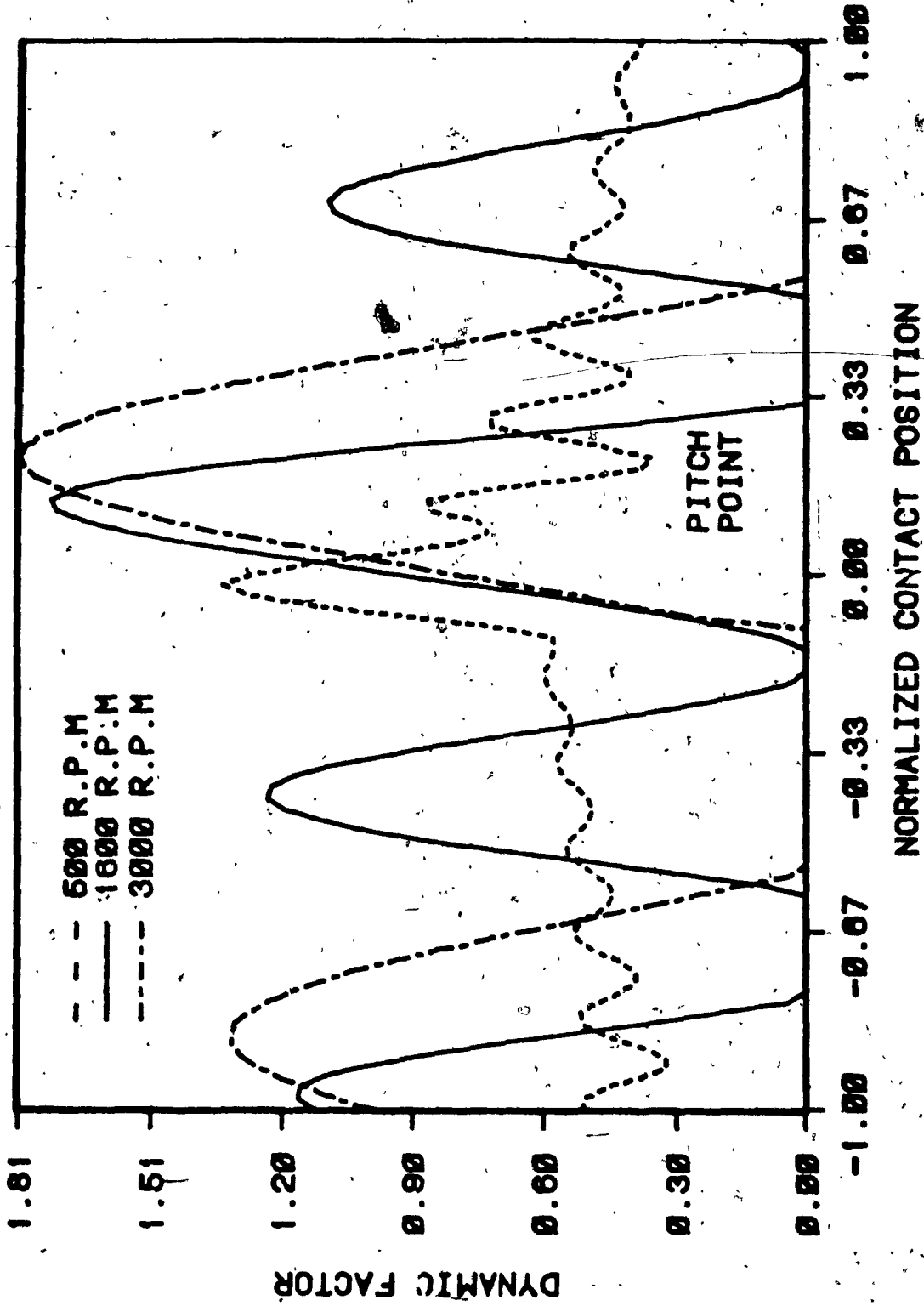


Fig. 3.9: Variation of D.F. along contact position.

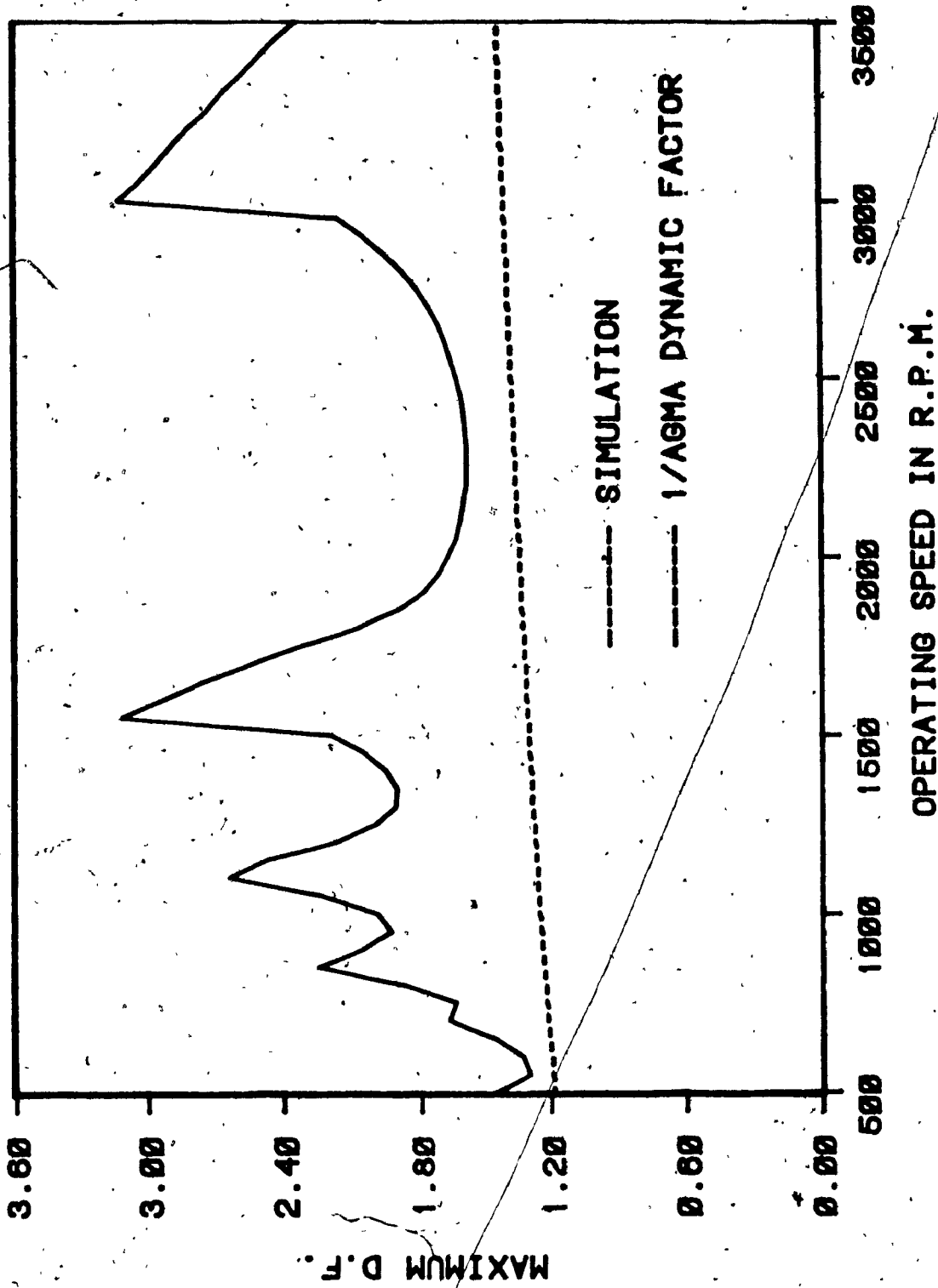


Fig. 3.10: Variation of maximum D.F. with operating speed

is shown in Fig. 3.11, the stability of the system is greatly influenced by the amount of damping and thus there is a need for a minimum amount of damping to avoid instabilities in operating region.

In general, any change in the system inertia and/or stiffnesses will result in a shift in the response peaks.

3.7 Stability analysis

In this section, it is shown that how the stability characteristics of a gear system can be studied easily using the state-space approach employed here. Gear system stability is one of the major design requirements in modern gear design practice since it has been found in practice and in laboratory experiments that operating a gear system in the unstable region leads to excessive dynamic loads and eventually to complete destruction of gear teeth [35]. Many investigators [34-36] have studied this aspect of gear dynamics using the techniques proposed by Bolotin [128]. Even though these techniques are quite general and are applicable to any dynamical system, in practice they tend to be very complex for higher order systems. In this section, it is shown that with the use of state-space method and Floquet theory the stability of the gear system can be carried out in a simple and direct manner.

It is customary in the study of the stability of the gear system to assume that there is no backlash and that there are no gear errors. Though these assumptions are not true in actual gear systems, they simplify the otherwise complex stability analysis procedure. In addition the local stability of a non-linear system can often be inferred from the behaviour of the corresponding linearized system.

Since, for a linear system the stability is not affected by the external forces, the forcing terms can be omitted and it is enough to consider only the homogeneous part of the state equation.

That is,

$$\dot{v}(t) = A(t) v(t) \quad (3.35)$$

where, the matrix $A(t)$ is given by equation (3.19) and is periodic such that,

$$A(t + t_m) = A(t). \quad (3.36)$$

With these conditions, the stability analysis of the gear system, Fig. 3.3, can be carried out in a remarkably simple and general manner as given below.

Converting the equation (3.35) into discrete form, as,

$$v(t_{i+1}) = \Phi(t_{i+1}, t_i) v(t_i) \quad (3.37)$$

and starting from the initial state at the beginning of the mesh period, the state at the end of the mesh cycle can be reached by successive application of equation (3.37).

That is,

$$v(t_m) = \Phi(t_m, t_0) v(t_0) \quad (3.38)$$

According to Floquet theory, the overall state transition matrix $\Phi(t_m, t_0)$ given by equation (3.30), also known as the growth matrix of the system, governs the stability of the system given by equation (3.35) [126]. The given system is asymptotically stable, if and only if, all the eigenvalues of the growth matrix have absolute values less than unity. This condition for asymptotic stability can be checked by using a simple rule [129], which locates the eigenvalues of a difference system in complex plane without actually solving for them. For the present problem, the use of this rule reduces the computational time by more than half.

Fig. 3.11 shows the regions in operating speed range, where at least one of the eigenvalues of growth matrix has an absolute value larger than unity. As can be seen from Fig. 3.11, the damping in the system has a major influence on the stability of the gear system. As the damping is increased, the unstable region becomes smaller and finally

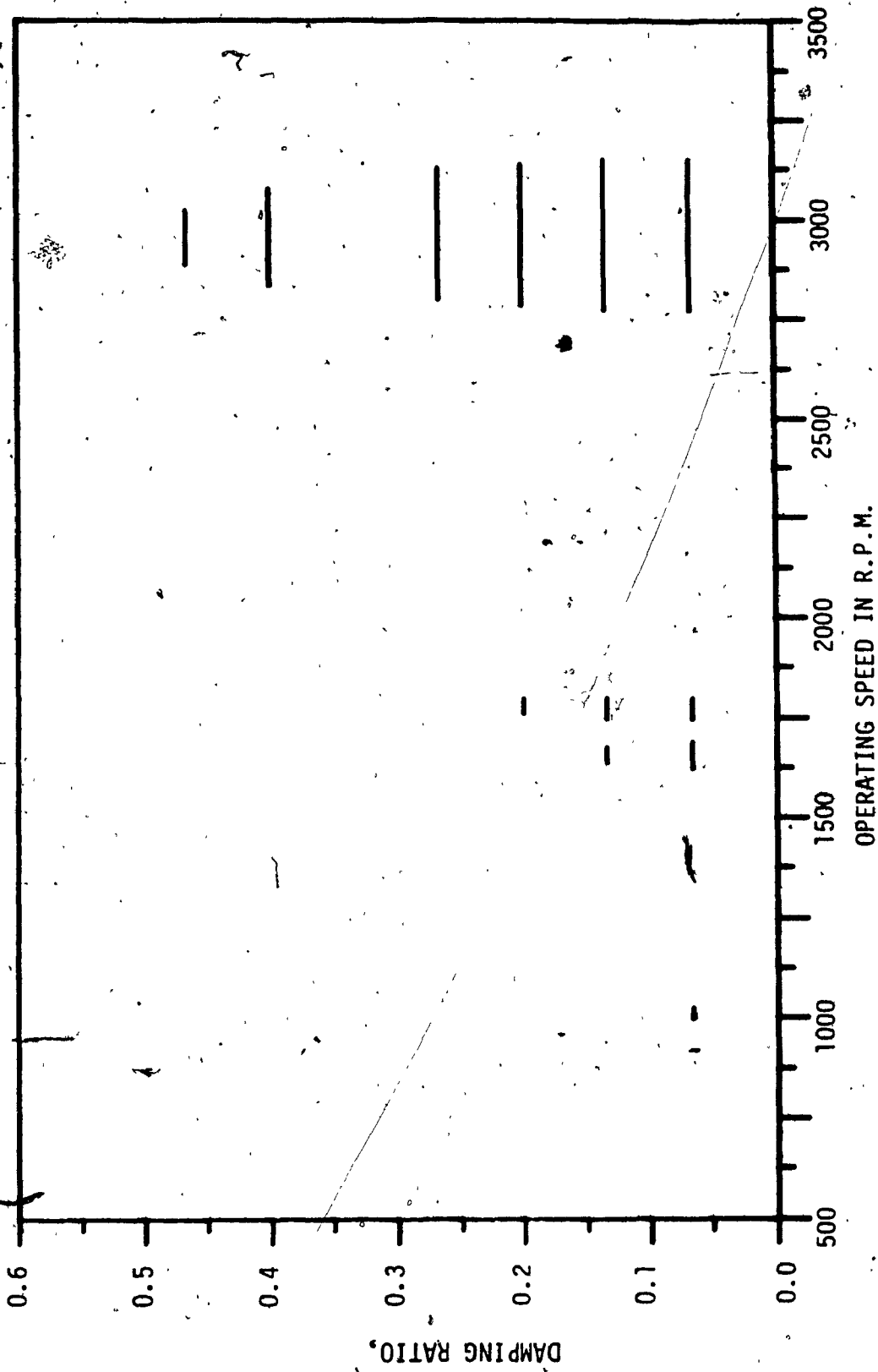


Fig. 3.11: Stability chart for the given gear system

with large enough damping, the system becomes stable for the entire operating speed range. Thus, there is a requirement for a minimum amount of damping to prevent the parametric type instabilities.

3.8 Summary

In this chapter, mathematical models for a spur gear set are formulated incorporating both the torsional motion of the gears and the lateral motion of the supports, with the assumption that the actual transmission error record is available as a continuous time signal. Non-linearities arising from the backlash and the friction between the meshing teeth are included. It is shown that the use of state-space technique to solve the equations of motion is very advantageous both in terms of the amount of useful information that can be obtained from a single analysis and in terms of the computational requirements. A procedure to select proper initial conditions so as to begin the analysis directly in the steady state is given. Verification of the simulator carried out by comparing the results from the simulator with experimental results obtained using both vibration measuring instruments and dynamic photoelasticity technique show the viability of the simulator to simulate both metallic and non-metallic gears. Also, the inadequacies of the currently used design practice and the complexity of the gear dynamic load variation is highlighted with the use of a parametric study. In addition, it is also

shown that the stability of the gear system can be easily studied with the use of state-space technique and Floquet theory.

In the next chapter, the dynamic load simulator described in this chapter is extended so as to use the statistical properties of the transmission error record rather than the actual measured transmission record themselves.

CHAPTER 4

DYNAMIC LOAD ESTIMATION - STOCHASTIC APPROACH

4.1 Introduction

The underlying assumption in the formulation of the dynamic load simulator described in the previous chapter is that the transmission error can be considered and is available as a purely deterministic signal. However in a working gear drive, there are many sources of error such as profile wear, bearing wear, irregularities of clearances in rotating parts, deflection of teeth, dirt in the train, etc., which are random in nature. Also, the availability of measured error signals is possible only after manufacturing and mounting the gear system and not at the design stage. Thus, the simulator presented in the last chapter can be used effectively only to simulate an existing gear system. To overcome this, a new simulation method, wherein the influence of transmission error on gear dynamic loads is studied using a probabilistic approach, is introduced in this chapter. The required statistical and spectral properties of transmission error records can either be obtained from analysing the transmission error recorded from similar gear sets working under similar operating conditions or can be reconstructed from the statistical properties of the component error records [114,115] which can be measured individually with the conventional gear metrology instruments.

Though many researchers [130,131] have investigated the statistical properties of transmission error and their effect on the vibration and noise of gear systems, only Tobe et.al. [20-22] attempted a statistical treatment of the gear dynamic loads. They first formed the Fokker-Planck equation for the non-linear spur gear system and derived the moment equations from it. The non-linear moment equations were then solved for the first two moments of the response using a statistical linearization technique. They also verified their theoretical results with experiments [21]. However, inspite of the sophisticated statistical treatment and good results, their work was not followed or applied by other researchers, because of the large number of equations and complexity involved. Inclusion of other type of non-linearities such as friction between teeth or etc. into the analysis further compounds the complexity even for a smaller degree-of-freedom gear system model. In addition, it is known that under certain dynamic conditions the gear system becomes unstable [19,34-36]. For dynamic systems of this type with discontinuous non-linearities such as backlash, the statistically linearized gains are known to give highly inaccurate results [133].

It is shown, in the following sections, that the statistical analysis of gear dynamic systems can be performed in a more elegant and easier manner using the piecewise-constant approximation and the state-space

approach. The technique proposed here can be readily applied without any modifications to larger degree-of-freedom gear models.

4.2 The mathematical model

Once again, the configured gear system, shown in Fig. 3.3, is used to develop the methodology. This configured gear system is governed by equations of motion given by the matrix equation (3.18). In addition to the assumptions stated in the previous chapter, the following assumptions are made:

1. the transmission error can be regarded as a stochastic process which contains a certain random component due to the random sources of error mentioned earlier as well as a harmonic component due to the eccentricity or pressure angle error.
2. the random component is assumed to be ergodic, stationary, normal and independent of the harmonic component based on physical observations [20].
3. the harmonic component is considered to be deterministic.

Based on these assumptions, the deterministic simulator presented in the previous chapter can be considered as a special case of the stochastic simulator developed here.

4.2.1 Gear transmission error representation

As can be seen from Fig. 4.1, the transmission error signal e_r is an oscillatory random process. Tobe et.al. [20] showed that the random component of gear transmission error records can be generated with good approximation by passing a stationary Gaussian white noise process through a time-invariant shaping filter. Since a second order Markov process provides a good model of oscillatory random phenomena, it is used here as the shaping filter. The shaping filter state equation is:

$$\dot{v}_f(t) = A_f(t) v_f(t) + \Sigma_f w(t), \quad (4.1)$$

Here,

$$A_f = \begin{bmatrix} 0 & 1 \\ -a_2 & -a_1 \end{bmatrix} \quad (4.2)$$

$$\Sigma_f = \begin{bmatrix} 0 \\ 1 \end{bmatrix} \quad (4.3)$$

with,

$$v_f(t) = (e_r, \dot{e}_r)^T \quad (4.4)$$

The coefficients a_1 , and a_2 are functions of the statistical and spectral properties of the transmission error records and are chosen to fit the autocorrelation and PSD plots of the transmission error records as described in Appendix III.

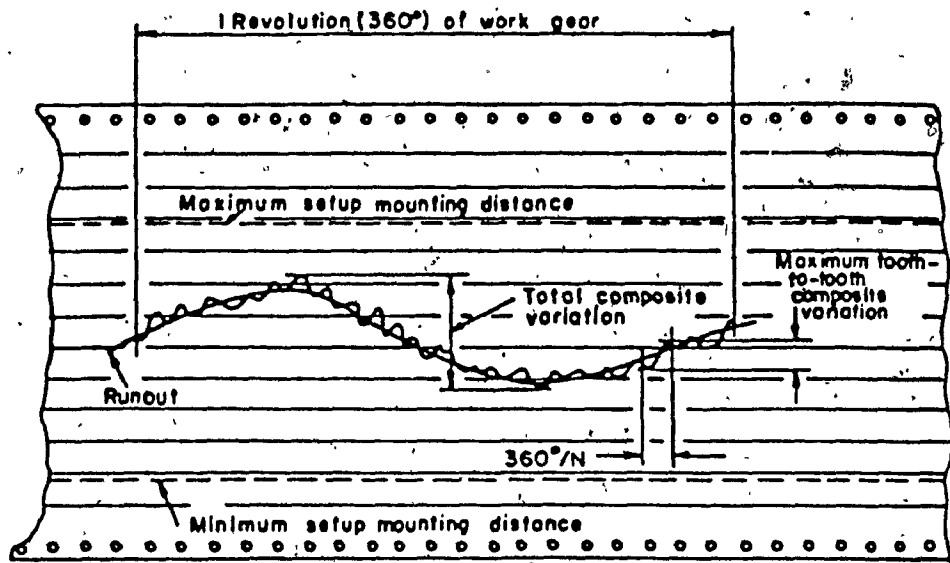


Fig. 4.1: Typical gear transmission error signal

And $w(t)$ is a Gaussian white noise process with the following properties,

$$\langle w(t) \rangle = 0 \quad (4.5)$$

$$\langle w(t)w(t') \rangle = Q(t) \delta(t-t') \quad (4.6)$$

where,

$Q(t)$ = intensity of white noise,

$\delta(\cdot)$ = delta function.

4.2.2 Mathematical model

The state equations of the augmented system can now be obtained by combining the equations (3.18) and (4.1).

That is,

$$\dot{v}_2(t) = A_2(t) v_2(t) + b_2(t) + g_2 w(t), \quad (4.7)$$

where,

$$A_2(t) = \begin{bmatrix} A(t) & G \\ 0 & A_f \end{bmatrix} \quad (4.8)$$

$$b_2(t) = \begin{bmatrix} f(t) \\ 0 \end{bmatrix} \quad (4.9)$$

$$g_2 = \begin{bmatrix} 0 \\ E_f \end{bmatrix} \quad (4.10)$$

$$\mathbf{v}_2 = \begin{Bmatrix} \mathbf{v} \\ \mathbf{v}_f \end{Bmatrix} \quad (4.11)$$

and,

$$\mathbf{f}(t) = \{T_p, -T_g, 0, 0, 0\}^T - k_{pg}(t) \cdot (\text{IN})(\text{BL}) u_2 \quad (4.12)$$

The index IN is set equal to -1, 0, or +1 depending upon the value of $(u+e)$, based on the backlash characteristic curve shown in Fig. 4.2. The vector u_2 and the submatrices $A(t)$, and A_f are given by equations (3.14), (3.19) and (4.2) respectively. And the submatrix G is defined as,

$$G = \begin{bmatrix} 0 & 0 \\ k_{pg}(t) u_2 & 0 \end{bmatrix} \quad (4.13)$$

Even though the excitation is a stationary process, the system given by equation (4.7) is non-stationary because of the time-varying, non-linear function W_d . It is difficult to solve equation (4.7) analytically. However numerical solution of equation (4.7) can be obtained by considering the corresponding equivalent discrete-time system model,

$$\mathbf{v}_2(t_{i+1}) = \Phi(t_{i+1}, t_i) \mathbf{v}_2(t_i) + \mathbf{b}_d(t_i) + \mathbf{w}_d(t_i) \quad (4.14)$$

where, the state transition matrix $\Phi(t_{i+1}, t_i)$ is given by,

$$\Phi(t_{i+1}, t_i) = \exp(\mathbf{A}_2(t_{i+1}) \cdot (\Delta T)), \quad (4.15)$$

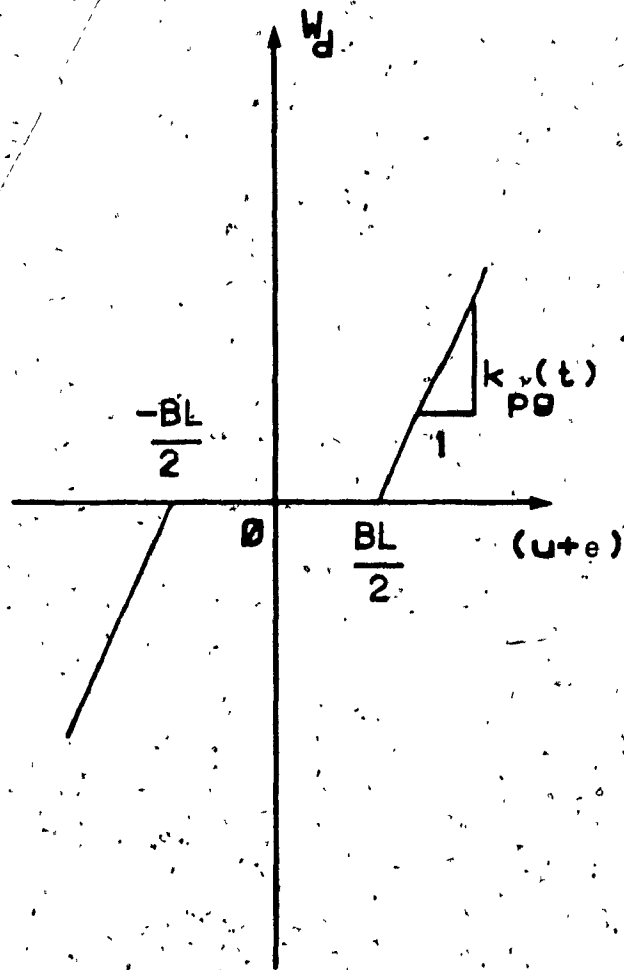


Fig. 4.2: Symmetric backlash characteristics

and, the discrete-time forcing vector $b_d(t_i)$ is given by,

$$b_d(t_i) = \int_{t_i}^{t_{i+1}} \Phi(t_{i+1}, s) b_a(t_{i+1}) ds, \quad (4.16)$$

And $w_d(t_i)$ is a vector valued Gaussian discrete-time stochastic process with statistical properties exactly duplicating those of $w(t)$ for all t_i , such that,

$$\langle w_d(t_i) \rangle = 0 \quad (4.17)$$

$$\langle w_d(t_i) w_d(t_i) \rangle = Q_d(t_i) = \int_{t_i}^{t_{i+1}} \Phi(t_{i+1}, s) \mathbf{g}_a Q(s) \mathbf{g}_a^T \Phi^T(t_{i+1}, s) ds \quad (4.18)$$

$$\langle w_d(t_i) w_d(t'_i) \rangle = 0, \quad \text{for } t_i \neq t'_i. \quad (4.19)$$

Thus, equation (4.14) defines a discrete time stochastic process which has an identical solution process as that of equation (4.7) at discrete times $t_0, t_1, t_2, \dots, t_m$. In the discrete-time state equation presented above, the state transition matrix Φ and the forcing vector b_a are taken to be constant in each time interval $(t_{i+1} - t_i)$. These piecewise-constant approximations are valid, if the total number of sampling instants is sufficiently large and if the time interval is chosen to be sufficiently small compared with the time constants of the system [126]. As was mentioned in the previous chapter, in the present study a time interval smaller than one tenth of the smallest system natural period is used.

The piecewise-constant approximation results in a series of linear stochastic differential equations of the form given by equation (4.14) for each time interval $(t_{i+1}-t_i)$. The corresponding mean and covariance propagation equations are [132]:

$$m_v(t_{i+1}) = \Phi(t_{i+1}, t_i) m_v(t_i) + b_d(t_i) \quad (4.20)$$

$$P_{vv}(t_{i+1}) = \Phi(t_{i+1}, t_i) P_{vv}(t_i) \Phi^T(t_{i+1}, t_i) + Q_d(t_i) \quad (4.21)$$

where,

P_{vv} = covariance matrix,

m_v = mean vector

Equations (4.14), (4.20), and (4.21) are all recurrence relationships and hence starting from the initial conditions $m_v(t_0)$, and $P_{vv}(t_0)$ at time $t=t_0$, the states at other time instants can be computed by the method of time marching. This procedure is best suited for digital computer implementation. The exponential matrix Φ and the vector b_d in the equations (4.15) and (4.16) are obtained by replacing the matrix A in equations (3.27) and (3.28) by A_a . And the integration in equation (4.18) is carried out by using the trapezoidal rule, such that,

$$Q_d(t_i) = 0.5 \Delta T [\Phi(t_{i+1}, t_i) \Sigma_2 Q(t_i) \Sigma_2^T + \Sigma_2 Q(t_i) \Sigma_2^T \Phi^T(t_{i+1}, t_i)] \quad (4.22)$$

where, $\Delta T = (t_{i+1} - t_i)$ is the time step chosen for time marching.

4.2.3 Selection of initial conditions

In the previous chapter, it was shown that, with a choice of proper initial conditions, the steady state response can be reached "immediately" without going through the calculations for the transient response. Also a procedure for choosing such proper initial conditions for the gear dynamic system was introduced, in the last chapter. Here the same procedure is extended to compute the appropriate initial conditions for the mean and covariance propagation equations (4.20) and (4.21). Starting the analysis from the beginning of the mesh cycle ($t=t_0$), and by using the equations (4.20) and (4.21) repetitively, the states at the end of the mesh cycle ($t=t_m$) can be computed as,

$$\mathbf{x}_v(t_m) = \Phi(t_m, t_0) \mathbf{x}_v(t_0) + \mathbf{d}(t_m) \quad (4.23)$$

$$\mathbf{P}_{vv}(t_m) = \Phi(t_m, t_0) \mathbf{P}_{vv}(t_0) \Phi^T(t_m, t_0) + \mathbf{D}(t_m) \quad (4.24)$$

with

$$\mathbf{d}(t_m) = \sum_{i=0}^{m-2} \prod_{j=i+1}^{m-1} \Phi(t_{j+1}, t_j) \mathbf{b}_d(t_i) + \mathbf{b}_d(t_{m-1}) \quad (4.25)$$

$$\mathbf{D}(t_m) = \sum_{i=0}^{m-2} \Phi(t_{i+2}, t_{i+1}) \mathbf{Q}_d(t_i) \Phi^T(t_{i+2}, t_{i+1}) + \mathbf{Q}_d(t_{m-1}) \quad (4.26)$$

Here, the overall transition matrix $\Phi(t_m, t_0)$ is given by,

$$\Phi(t_m, t_0) = \prod_{i=0}^{m-1} \Phi(t_{i+1}, t_i) \quad (4.27)$$

Since the mesh stiffness variation is periodic, the matrix A_a will also be periodic, such that,

$$A_a(t_i + t_m) = A_a(t_i). \quad (4.28)$$

Under this condition, the steady state response of the system at the beginning of the mesh cycle should be nearly equal to response at the end of the mesh cycle.

Thus, under steady state conditions,

$$m_v(t_m) = m_v(t_0), \quad (4.29)$$

$$P_{vv}(t_m) = P_{vv}(t_0). \quad (4.30)$$

Substitution of equations (4.29) and (4.30) into equations (4.23) and (4.24) results in

$$m_v(t_0) = [I - \Phi(t_m, t_0)]^{-1} d(t_m), \quad (4.31)$$

$$\Phi^{-1}(t_m, t_0) P_{vv}(t_0) - P_{vv}(t_0) \Phi^T(t_m, t_0) = \Phi^{-1}(t_m, t_0) D(t_m). \quad (4.32)$$

which can be solved for $m_v(t_0)$, and $P_{vv}(t_0)$. Thus the procedure is to start at the beginning of the mesh cycle with zero initial conditions and to compute the overall transition matrix $\Phi(t_m, t_0)$ and the forcing elements in the vector $d(t_m)$ and matrix $D(t_m)$ at the end of the mesh cycle. Then by solving equations (4.31) and (4.32), the proper

initial conditions can be computed. This procedure needs only two iterations.

However, the above procedure is valid only when the variable mesh stiffness $k_{pg}(t)$ is in one of the three linear segments of the stiffness curve shown in Fig. 4.2 for the entire mesh period. When the operational conditions change the gear mesh status during one mesh period, the overall state transition matrix $\Phi(t_m, t_0)$ of the system will itself depend on the choice of initial conditions and hence the above procedure will not be valid. For these cases the computer program has been designed to enter automatically into a multi-iterative mode to reach the steady state condition.

4.3 Dynamic load analysis

Once the mean and variance of the response states of the gear system have been determined using the numerical procedure described earlier, the statistical properties of the gear dynamic loads can be obtained by substituting the corresponding statistics of the state variables into the following equations.

$$\langle W_d \rangle = W_d(\langle v \rangle, BL, t) \quad (4.33)$$

$$\langle W_d W_d \rangle = k_{pg}^2(t) \langle v^T v \rangle. \quad (4.34)$$

Numerical example

Even though the procedure presented here is applicable to gear systems with both harmonic and random errors, for the numerical example given here, it is assumed that the transmission error consists of only the random component. The parameters of the system to be analysed along with the transmission error statistics are given in Table 4.1. Based on the spectral data given, using the steps described in Appendix III, the values of the constants a_1 , and a_2 in equation (4.2) are respectively set as, 0.11, and 0.102. For the purpose of comparison with Tobe's [20,22] results, the non-linear backlash element is assumed to be of symmetric type as shown in Fig. 4.2 and the supports are not included in the modelling.

In general, the dynamic loads and hence the dynamic stresses on a gear tooth vary considerably with contact position, operating speed, damping, and with the changes in system inertias. Figs. 4.3 to 4.7 show the variation in the mean and variance of the dynamic factor (D.F.) with different design parameters for the gear system shown in Fig. 3.3, and defined in Table 4.1. As can be seen from the Figs. 4.3 to 4.5, the mean value of the dynamic factor (D.F.) does not vary with the random error magnitude, whereas the variance of D.F. increases with the error magnitude. This is due to the fact that the mean value of the random component of error used in the present example is

Table 4.1: Salient parameters of the gear system

Tooth profile	STD.
Diametrical pitch	4
Number of teeth, Gear 1, mm.	20
Number of teeth, Gear 2, mm.	20
Pressure angle, deg.	20
Pitch diameter, Gear 1, mm.	63.5
Pitch diameter, Gear 2, mm.	63.5
Face width, mm.	25.4
Contact ratio	1.56
Backlash, mm.	0.25
Moment of inertia, Gear 1	0.0051
Moment of inertia, Gear 2	0.0051
Load per unit face width, N/mm.	175

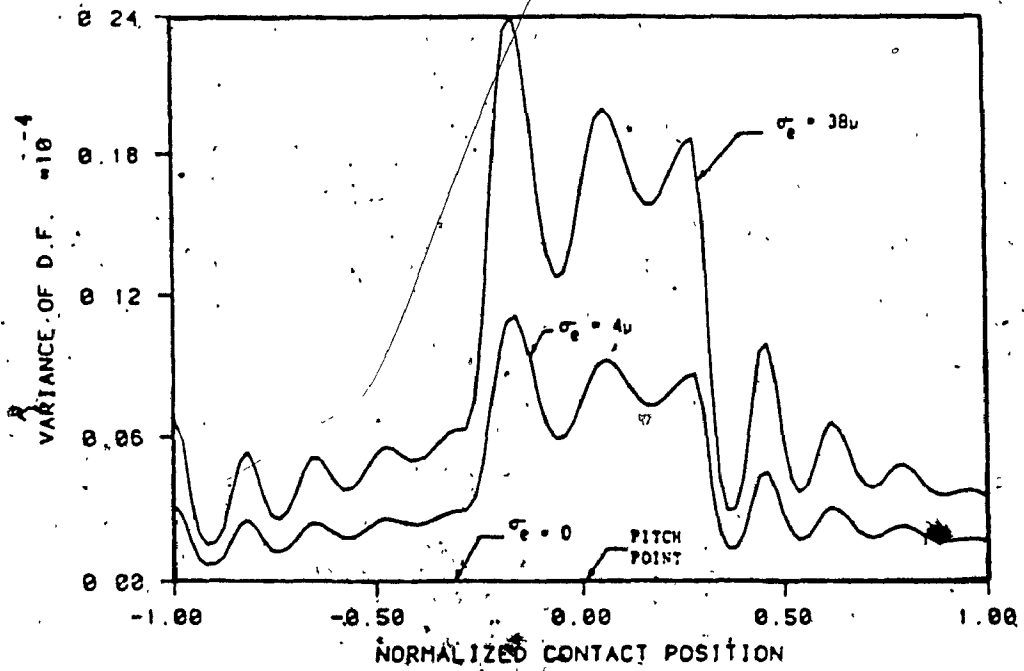
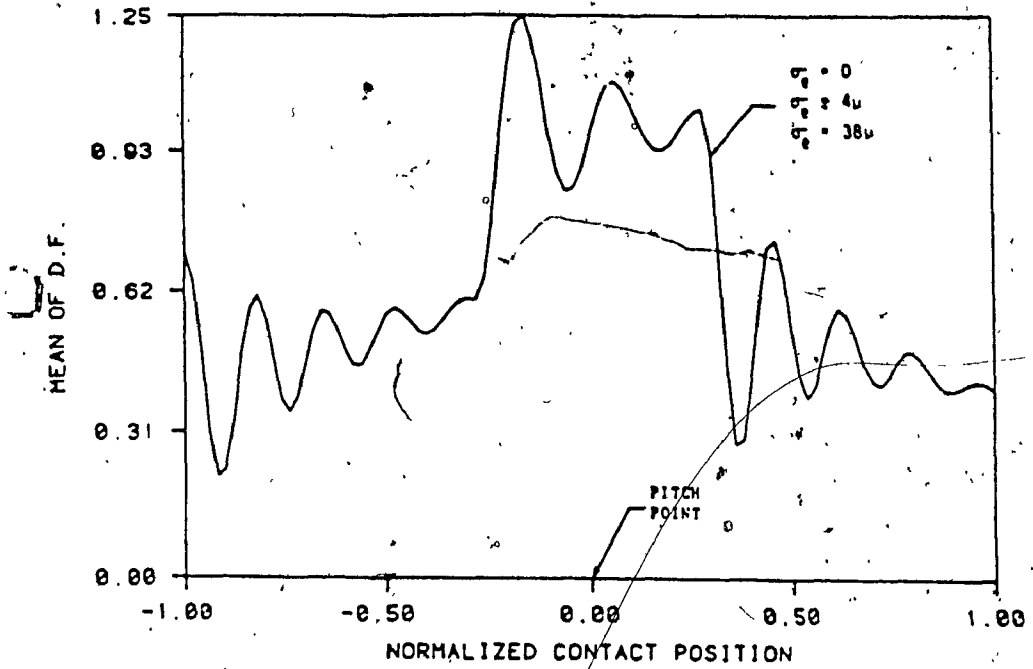


Fig. 4.3: Variation of mean and variance of D.F. with contact position, at 1500 R.P.M.

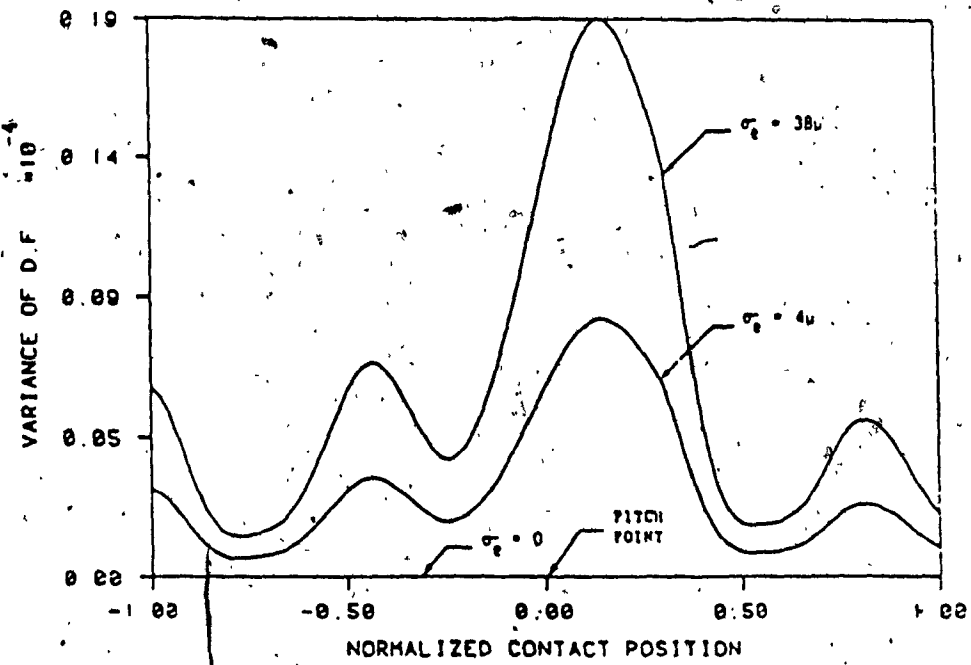
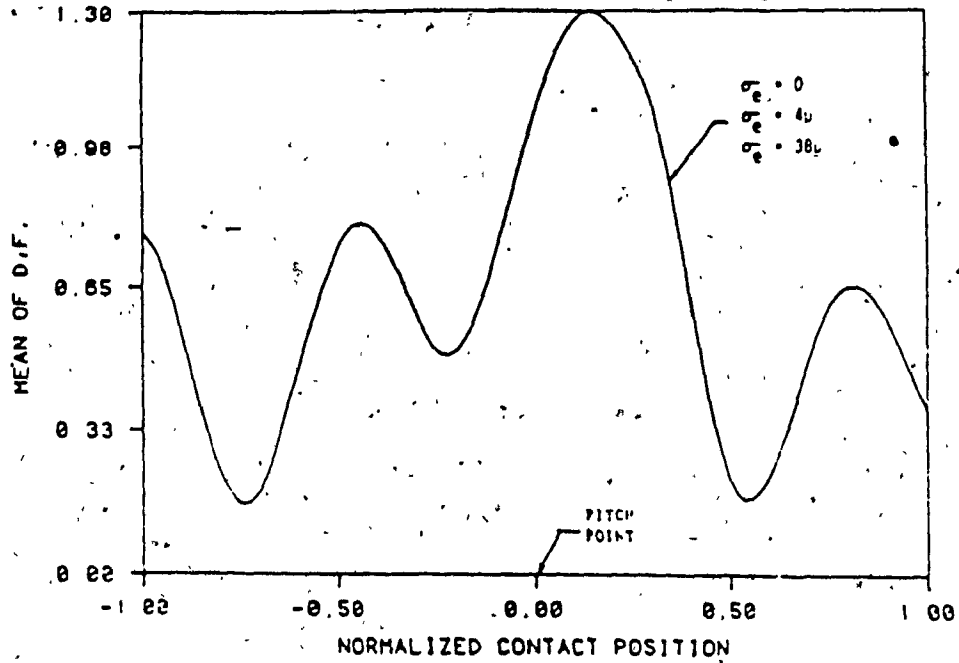


Fig. 4.4: Variation of mean and variance of D.F. with contact position, at 3000 R.P.M.

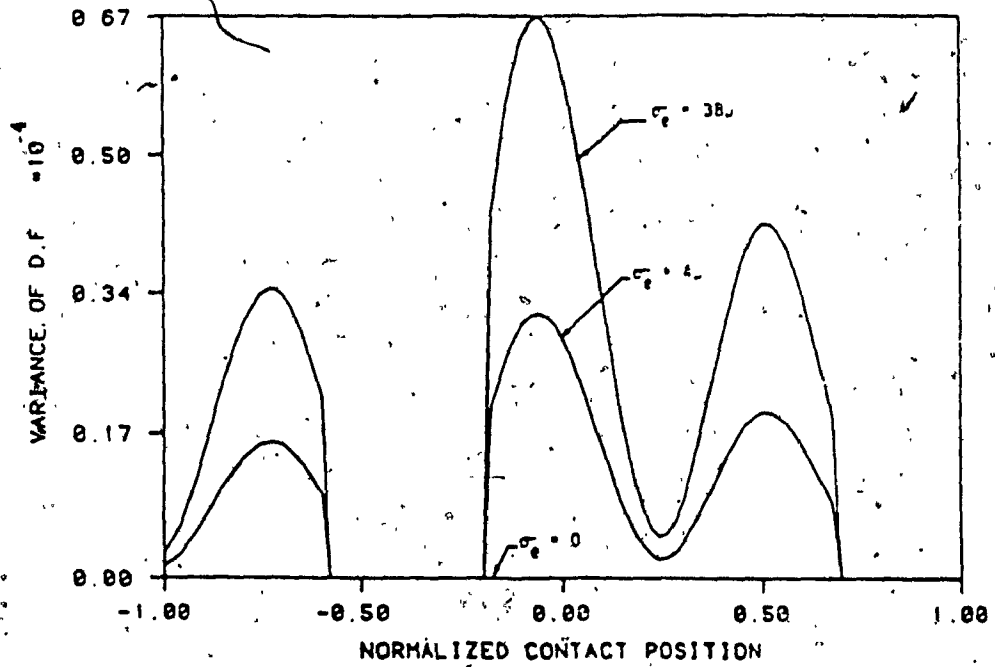
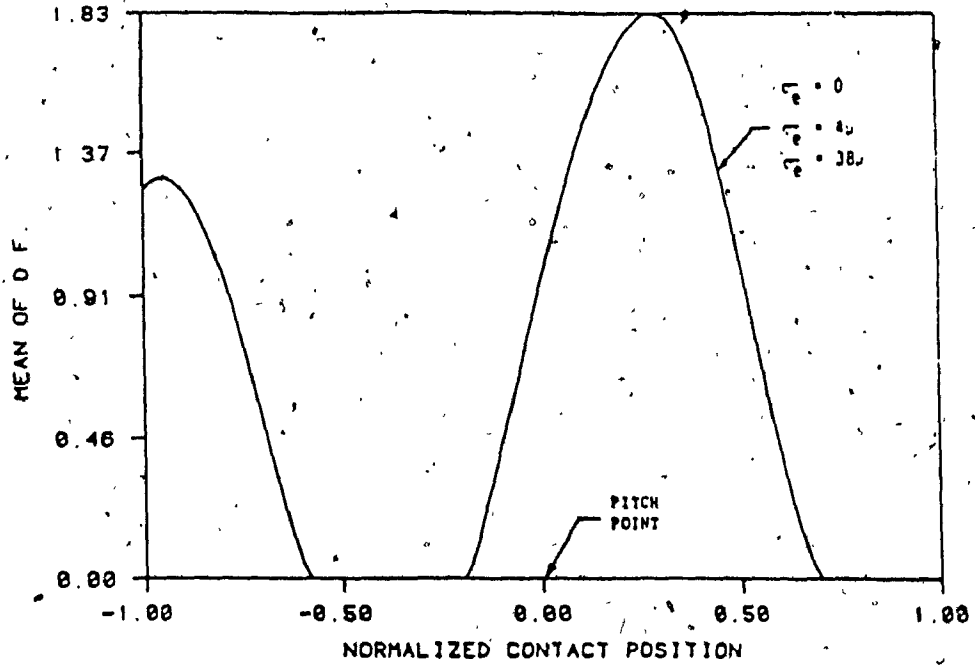


Fig. 4.5: Variation of mean and variance of D.F. with contact position, at 9200 R.P.M.

taken to be zero. However in a more general case, the mean also will increase with error magnitude. Fig. 4.6 shows the effect of random error magnitude and operating speed on the mean and variance of the maximum D.F.. As can be expected the variation in mesh stiffness results in several sub-harmonic resonances, in addition to the primary resonance near 9200 R.P.M..

The limitation of the statistical linearization technique as applied to the gear dynamic problem can be seen from Fig. 4.7. In this figure, the mean of the maximum D.F. computed using three different techniques is plotted against the operating speed. The curve designated as NS is obtained by numerical simulation wherein the actual digitized error signal is used as input. This curve is taken to be the basis for comparison of the results from the other two techniques. The curve designated as PWC is obtained with the approach presented here, and the curve SL is obtained with the use of statistical linearization. It is obvious from this figure that the piecewise constant approximation results compare very well with the simulation results for the entire operating speed range. Whereas the results obtained with statistical linearization compare well with the simulation results only in the speed regions near the system resonances. This can be expected since the gear system behaves essentially in a linear manner in the regions away from the resonance and the equivalent linear system

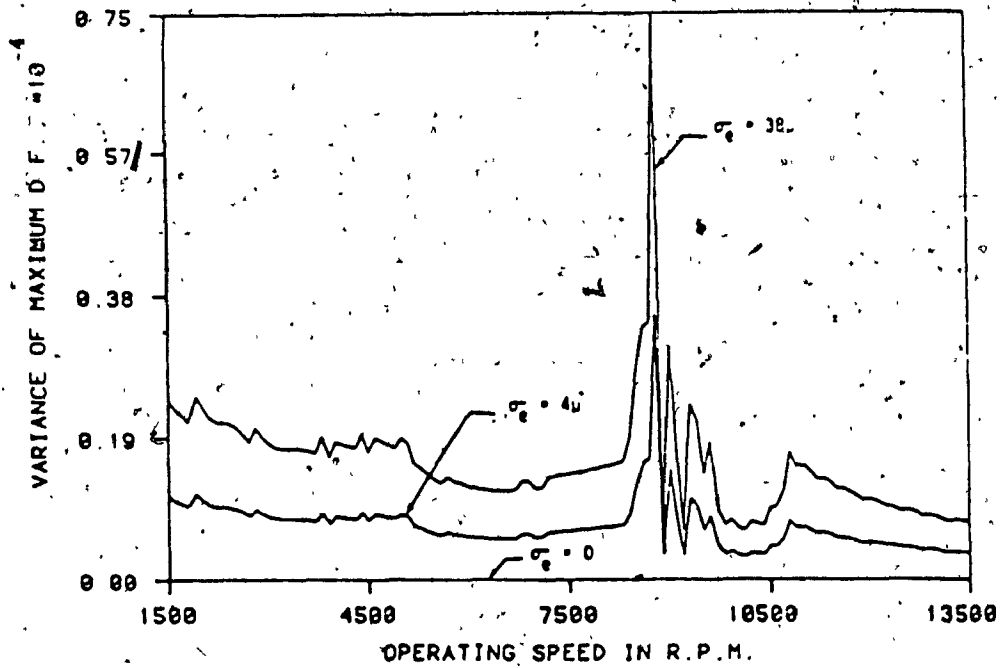
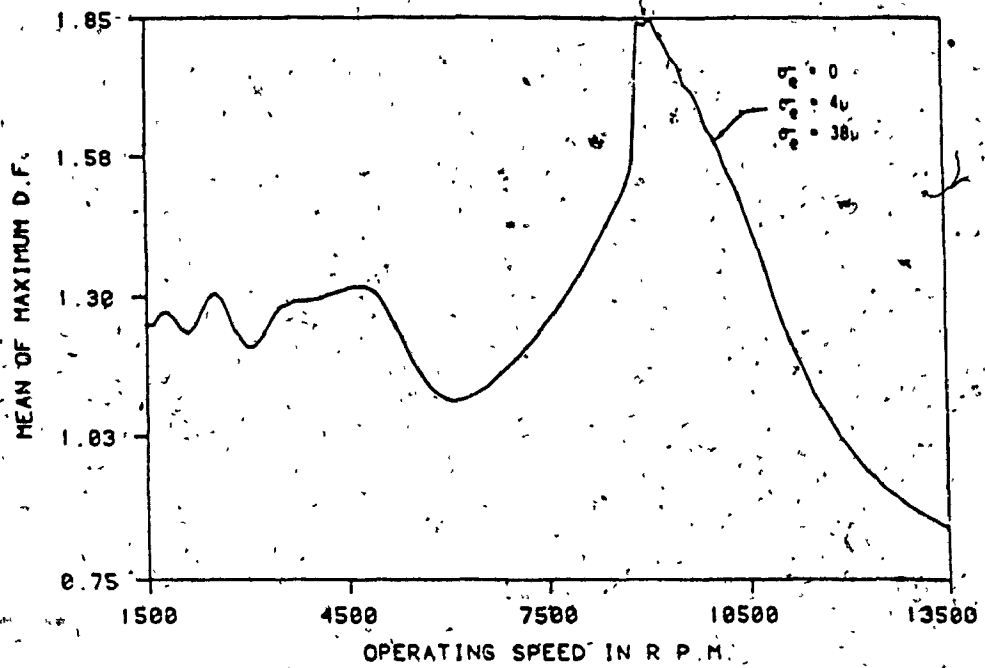


Fig. 4.6: Variation of mean and variance of D.F. with operating speed

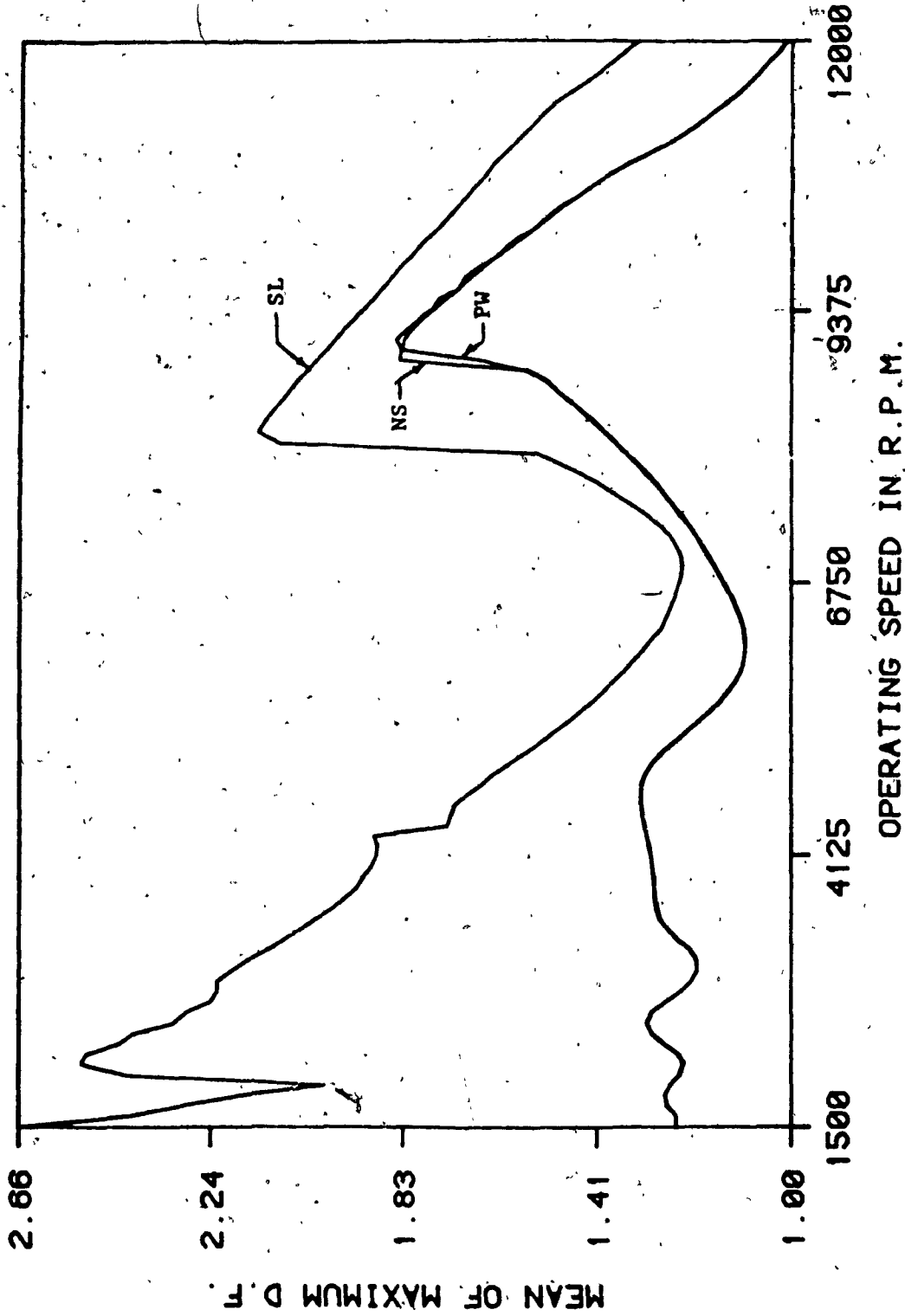


Fig. 4.7: Comparison of mean of D.F. computed using different methods

will not correctly represent the actual system in such cases. In addition it can also be seen from the Fig. 4.7 that the equivalent gains given by the statistical linearization also shifts the system resonances.

4.4 Summary

In this chapter, it is shown that the statistical analysis of the gear dynamic load can be carried out in a simple and direct manner using piecewise constant mesh stiffness approximation and the mean and covariance propagation equations of linear difference system. It is also shown that the statistical linearization technique used by Tobe et.al. [20,22] does not give correct results both in terms of the magnitude and the location of the occurrence of the maximum dynamic load under certain dynamic conditions. In contrast, the piecewise constant approximation used here gives truer results provided the time interval chosen is sufficiently small. Moreover the procedure developed here has the advantage that it can be applied with ease to higher order systems and to systems with complex mesh stiffness and torque fluctuations. Also it is shown that by proper selection of initial conditions using the procedure given earlier, the computation time required for the analysis can be considerably reduced.

CHAPTER 5

DISCRETE - TIME TRANSFER MATRIX METHOD AND ITS APPLICATION TO GEAR SYSTEM DYNAMICS

5.1 Introduction

Even though the dynamic load on gears is primarily the result of gear pair dynamics, the influence of other elements in the gear system is not necessarily minimal. For example, a complete gear system such as that shown in Fig. 5.1, which includes the mating gear pairs, the shafts, the support bearings, seals and the housing may fail in different ways. But most such failures manifest themselves as increased dynamic loads on gears leading to the failure of the gear teeth. Thus, in order to estimate or simulate the dynamic load on gears accurately or truly, the entire gear system including the dynamics of the individual components should be modelled and studied. However, it is customary in gear dynamic load analysis [12-29] to neglect the effect of other system components, since inclusion of these components makes the model very large and complex.

To study such large systems, using straight forward numerical simulation techniques by formulating the equation of motions and solving them numerically is a cumbersome and tedious process. In addition, even though most of the gear systems are mainly made of same type of individual components, their numbers and locations within the system

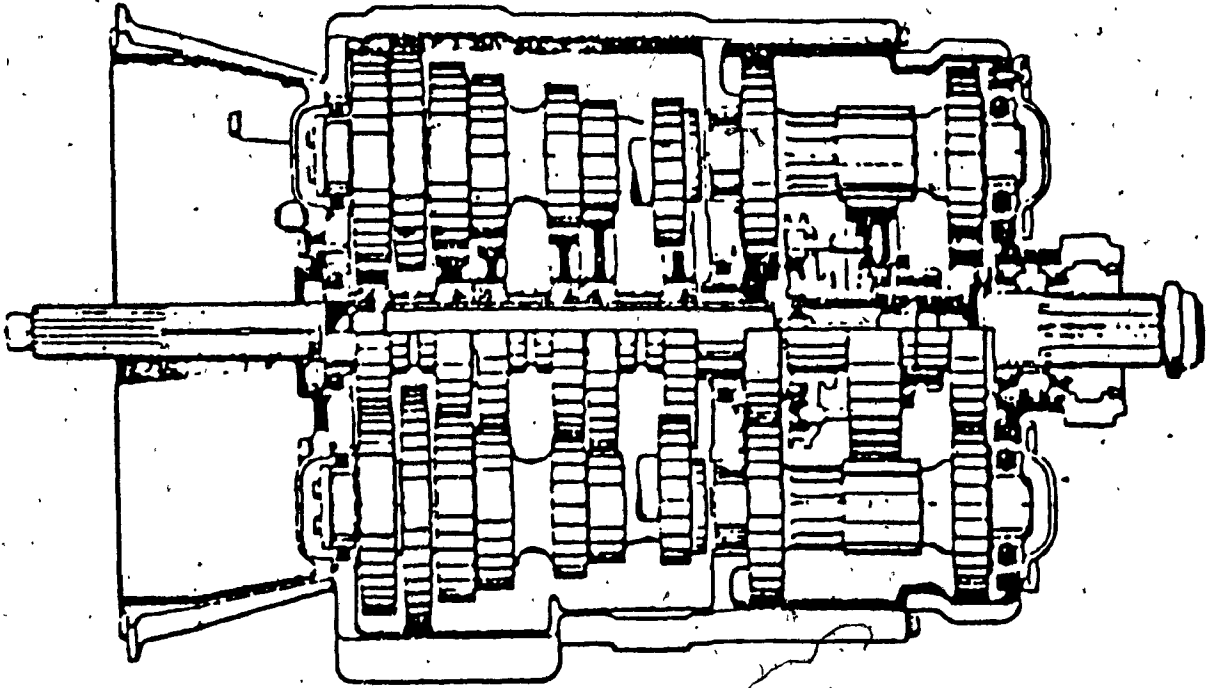


Fig. 5.1: A typical gear system

vary from system to system. Thus, for each gear system configuration, the entire simulation process starting from formation of equations of motion has to be done anew. These deficiencies of the straight forward numerical simulation procedures can be avoided by using a modular approach such as the transfer matrix methods (TMM) [23,27,135] or the dynamic finite element methods (FEM) [37,44] wherein analytical models defining the dynamic properties of each of the components in the gear system are first constructed and then assembled in such a way to attain the required gear system configuration. With such modular approaches once a library of analytical modules of the components are constructed, any required system configuration can be simulated by properly assembling these modules. These techniques are quite powerful and yet flexible. However, finite elements having combined torsional and lateral degrees of freedom are not yet commonly available, thus making FEM unusable for the coupled gear dynamics problem. The TMM on the other hand can accommodate such coupling between torsional and lateral motions. But it is restricted to only linear time-invariant systems under harmonic excitation or free vibration problems. Therefore, many important characteristics of gear systems such as gear tooth backlash, time-varying mesh stiffness, input torque fluctuations as well as non-linear characteristics of other gear system components like friction clutches, and hysteresis damping in the shafts can not be included in the

simulation. Recently, to overcome some of these deficiencies, Daws [25] introduced a new TMM formulation based on harmonic balance method wherein the periodically time-varying characteristics of the gear mesh can be included. But, inspite of his emphasis on improved representation of gear mesh properties, some of the very important non-linear characteristics of the gear mesh such as tooth backlash could not be included in their modelling methodology. Thus it appears that none of the currently available numerical techniques can be used effectively for accurate simulation of gear system dynamics and that there is a significant need for an analysis procedure which treats the system components in a more realistic fashion and provides for a physically realistic assembly of those components.

To achieve such objective, a new modular approach is introduced in this investigation. This modular approach, called Discrete-Time transfer matrix method (DT-TMM), is based on the conventional TMM and the numerical integration procedures. This method combines the advantages of both TMM and numerical integration procedures in that the size of the matrices are small and can be applied to a wide range of problems including linear time-varying and non-linear systems. Basically it involves splitting any system in to a number of simple modules and allowing modelling of these modules. Then, as in the case of conventional TMM, the

modules are connected together to represent the required system configuration. The proposed method is simple, straight forward and provides a powerful tool for dynamic analysis of any general dynamic systems.

In the following sections, the new simulation methodology is described and then applied to gear system dynamic analysis.

5.2 Formulation of the DT-TMM

5.2.1 Basis of the methodology

The DT-TMM is based on the assumption that at any given time instant, t_i , the acceleration and velocity in any given degree of freedom, say x , can be expressed as a linear function of the displacement x with reasonable accuracy. That is,

$$\ddot{x}_n(t_i) = A_n(t_i)x_n(t_i) + B_n(t_i) \quad (5.1)$$

$$\dot{x}_n(t_i) = D_n(t_i)x_n(t_i) + E_n(t_i) \quad (5.2)$$

These types of relationships can be obtained from most of the step-by-step integration procedures employed normally in structural response computations. Derivation of these expressions based on truncated Taylor series can be carried out as follows.

The starting point for most of the numerical integration schemes used in structural response analysis is the truncated Taylor series of order 3. That is,

$$x(t_i) = x(t_{i-1}) + \Delta T \dot{x}(t_{i-1}) + \frac{\Delta T^2}{2} \ddot{x}(t_{i-1}) + \frac{\Delta T^3}{6} \dddot{x}(t_{i-1}) \quad (5.3)$$

where, interval $\Delta T = (t_i - t_{i-1})$.

Different integration schemes with varying sophistication and accuracy can then be derived by replacing the derivatives in equation (5.3) by finite differences. There exists a large body of literature on this subject of how derivatives can be approximated by finite differences. Here, one of the simplest finite difference schemes available is chosen to explain the methodology proposed. That is, the derivatives \ddot{x} , \dot{x} , and x are replaced by the following primitive difference approximations:

$$\ddot{x} = \frac{\ddot{x}(t_i) - \ddot{x}(t_{i-1})}{\Delta T} \quad (5.4)$$

$$\dot{x} = \frac{\dot{x}(t_i) - \dot{x}(t_{i-1})}{\Delta T} \quad (5.5)$$

$$x = \frac{x(t_i) - x(t_{i-1})}{\Delta T} \quad (5.6)$$

In addition, it is assumed that the acceleration is constant during the time interval $(t_i - t_{i-1})$ and is equal to the average of the acceleration values at t_i and t_{i-1} .

Thus,

$$\ddot{x} = 0 \quad (5.7)$$

$$\bar{x} = \frac{\bar{x}(t_i) + \bar{x}(t_{i-1})}{2} \quad (5.8)$$

$$\dot{x} = \bar{x}\Delta T = \frac{\bar{x}(t_i) + \bar{x}(t_{i-1})}{2} \Delta T \quad (5.9)$$

Substitution of equations (5.7) and (5.8) back into equation (5.3) will result in,

$$x(t_i) = x(t_{i-1}) + \Delta T \dot{x}(t_{i-1}) + \Delta T^2 \frac{\ddot{x}(t_i) + \ddot{x}(t_{i-1})}{4} \quad (5.10)$$

Equation (5.10) can be rewritten in the form of equation (5.1), as,

$$\bar{x}_n(t_i) = A_n(t_i)\bar{x}_n(t_{i-1}) + B_n(t_i) \quad (5.11)$$

where,

$$A_n(t_i) = \frac{4}{\Delta T^2} \quad (5.12)$$

and

$$B_n(t_i) = -A_n(t_i) [x(t_{i-1}) + \Delta T \dot{x}(t_{i-1}) + \frac{\Delta T^2}{4} \ddot{x}(t_{i-1})] \quad (5.13)$$

Similarly, by combining equations (5.9) and (5.11), a relationship in the form of equation (5.2) can be obtained, such that,

$$\dot{x}_n(t_i) = D_n(t_i)x_n(t_i) + E_n(t_i) \quad (5.14)$$

where,

$$D_n(t_i) = \frac{2}{\Delta T} \quad (5.15)$$

and,

$$E_n(t_i) = -D_n(t_i) [x(t_{i-1}) + \frac{\Delta T}{2} \dot{x}(t_{i-1})] \quad (5.16)$$

The coefficients $A(t_i)$, $B(t_i)$, $D(t_i)$, and $E(t_i)$ are all definable for any sub-system n for the time interval $(t_i - t_{i-1})$, since these coefficients are all functions of the time interval ΔT and the response quantities $x(t_{i-1})$, $\dot{x}(t_{i-1})$, and $\ddot{x}(t_{i-1})$ at the previous time instant which are all known at time instant t_i . Once these coefficients are computed starting from the specified initial conditions, the discrete time transfer matrix equations can then be formulated on the basis of equations (5.11) and (5.14), as explained in the following sections. It should be noted here that the simple finite difference scheme and the constant acceleration assumption used here in the formulation are only for explanatory purposes and cannot be used in practice, because of the inaccuracies that would be introduced. Instead, any of the many accurate, and commonly available numerical integration procedures can be used. Table 5.1 provides the coefficients A_n , B_n , D_n , and E_n for different numerical integrating procedures.

Table 5.1: Table of coefficients for different integration schemes

METHOD	$A_n(t_1)$	$B_n(t_1)$	$D_n(t_1)$	$E_n(t_1)$
Conventional TMM	$-\omega^2$	0	0	0
Fox-Euler	$\frac{2}{\Delta T^2}$	$-\frac{2}{\Delta T^2} [x(t_{1-1}) + \Delta T \dot{x}(t_{1-1})]$	$\frac{2}{\Delta T}$	$-\left[\frac{2}{\Delta T} x(t_{1-1}) + \dot{x}(t_{1-1})\right]$
Newmark β	$\frac{1}{\beta \Delta T^2}$	$-\frac{1}{\beta \Delta T^2} [x(t_{1-1}) + \Delta T \dot{x}(t_{1-1}) + (0.5 - \beta) \Delta T^2 \ddot{x}(t_{1-1})]$	$\frac{7}{\beta \Delta T}$	$\dot{x}(t_{1-1}) + \Delta T [(1 - \gamma) \ddot{x}(t_{1-1}) + \gamma B_n]$
Wilson θ	$\frac{6}{(\theta \Delta T)^2}$	$-\frac{6}{(\theta \Delta T)^2} [x(t_{1-1}) + \theta \Delta T \dot{x}(t_{1-1}) + (\frac{\theta \Delta T}{3})^2 \ddot{x}(t_{1-1})]$	$\frac{3}{\theta \Delta T}$	$-\frac{3}{\theta \Delta T} [x(t_{1-1}) + \frac{2\theta \Delta T}{3} \dot{x}(t_{1-1}) + (\frac{\theta \Delta T}{3})^2 \ddot{x}(t_{1-1})]$
Houbolt for $l \geq 3$	$\frac{2}{\Delta T^2}$	$-\frac{1}{\Delta T^2} [5x(t_{1-1}) - 4x(t_{1-2}) + x(t_{1-3})]$	$\frac{11}{6\Delta T}$	$-\frac{1}{6\Delta T} [18x(t_{1-1}) - 9x(t_{1-2}) + 2x(t_{1-3})]$
for $l=2$	$\frac{2}{\Delta T^2}$	$-\frac{1}{\Delta T^2} [4x(t_{1-1}) - 2x(t_{1-2}) + 2\Delta T^2 \ddot{x}(t_{1-2})]$	$\frac{11}{6\Delta T}$	$-\frac{1}{6\Delta T} [18x(t_{1-1}) - 5x(t_{1-2}) + \Delta T^2 \ddot{x}(t_{1-2})]$
for $l=1$	$\frac{6}{\Delta T^2}$	$-\frac{3}{\Delta T^2} [3x(t_{1-1}) + 3\Delta T \dot{x}(t_{1-1}) + \Delta T^2 \ddot{x}(t_{1-1})]$	$\frac{3}{\Delta T}$	$-\frac{1}{2\Delta T} [6x(t_{1-1}) + 4\Delta T \dot{x}(t_{1-1}) + \Delta T^2 \ddot{x}(t_{1-1})]$

5.2.2 Formulation of the method

For modelling purposes, following the conventions used in the TMM, a continuous structure may be divided into a certain number of sub-systems as shown in Fig. 5.2. A sub-system can be represented by two parts. One part is defined as a station where the mass of the sub-system is lumped and the external force $f(t)$ and the external displacements $x(t)$ are to take place. The other part is defined as massless span segment having all the properties of the sub-system flexibility and the viscous damping connecting the two adjacent mass stations. Thus, the n^{th} sub-system consists of spring stiffness k_n , damper element c_n , and mass m_n with displacement x_n , and velocity \dot{x}_n . The ends of the spring-damper element have displacements x_n and x_{n-1} . The superscripts L and R are used for designating quantities to the left and right of the elements.

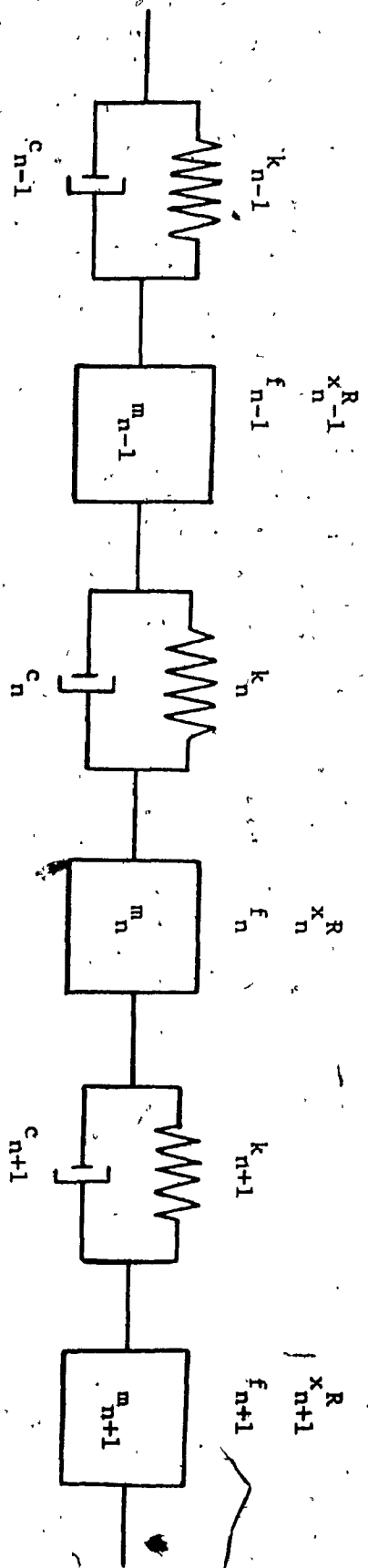
For the n^{th} sub-system, at the time instant t_i , the equation of motion is given by,

$$m_n(t_i) \ddot{x}_n(t_i) = x_n^R(t_i) - x_n^L(t_i) + f_n(t_i) \quad (5.17)$$

with

$$x_n^L = k_n(t_i) [x_n^L(t_i) - x_{n-1}^R(t_i)] + c_n(t_i) [\dot{x}_n^L(t_i) - \dot{x}_{n-1}^R(t_i)] \quad (5.18)$$

In addition, since the displacement on either side of m_n is the same, and since the internal forces x acting on either end of a massless spring-damper element should be the same,



$$x_{n-1}^R = x_n^L$$

$$x_n^R = x_n^L$$

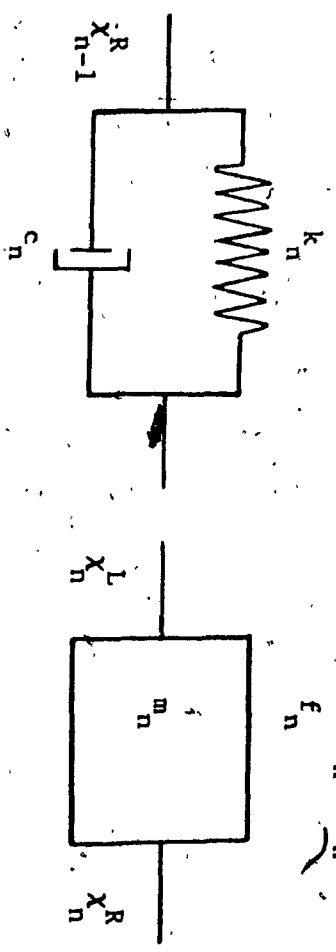


Fig. 5.2: Discretization of a continuous structure into sub-systems

the following identities are valid.

$$\dot{x}_n^R = \dot{x}_n^L \quad (5.19)$$

$$\ddot{x}_n^L = \ddot{x}_{n-1}^R \quad (5.20)$$

In the conventional TMM, because of the assumption of harmonic motion, the acceleration \ddot{x}_n and the velocity \dot{x}_n are expressed as $-\omega^2 x_n$, and ωx_n , respectively. But for a system which is not under harmonic motion, these substitutions are not valid and hence the limitation of the conventional TMM. Here, it is proposed that, by using the approximate relationships of the form given by equations (5.1) and (5.2) the equations (5.17) and (5.18) can be written as,

$$m_n [A_n \ddot{x}_n + B_n] = \dot{x}_n^R - \dot{x}_n^L + f_n \quad (5.21)$$

and

$$\ddot{x}_n^L = k_n [x_n^L - x_{n-1}^R] + c_n [(D_n \dot{x}_n + E_n)^L - (D_{n-1} \dot{x}_{n-1} + E_{n-1})^R] \quad (5.22)$$

Equations (5.19) and (5.21) can now be assembled into a single matrix equation, as,

$$\begin{Bmatrix} \ddot{x} \\ \dot{x} \\ 1 \end{Bmatrix}_n^R = \begin{bmatrix} 1 & 0 & 0 \\ m_n A_n & 1 & m_n B_n - f_n \\ 0 & 0 & 1 \end{bmatrix} \begin{Bmatrix} \ddot{x} \\ \dot{x} \\ 1 \end{Bmatrix}_n^L \quad (5.23)$$

or

$$\ddot{v}_n^R = P_n \ddot{v}_n^L \quad (5.24)$$

Here, following the convention used in the TMM, the square

matrix P_n is called the point matrix and the vector v is called the state vector.

Next, combining equations (5.20) and (5.22),

$$\begin{Bmatrix} x \\ X \\ 1 \end{Bmatrix}_n^L = \begin{bmatrix} \frac{k_n + c_n D_{n-1}^R}{(k_n + c_n D_n^L)} & \frac{1}{(k_n + c_n D_n^L)} & \frac{-c_n (E_n^L - E_{n-1}^R)}{(k_n + c_n D_n^L)} \\ 0 & 1 & 0 \\ 0 & 0 & 1 \end{bmatrix} \begin{Bmatrix} x \\ X \\ 1 \end{Bmatrix}_{n-1}^R \quad (5.25)$$

or

$$v_n^L = F_n^R v_{n-1}^R \quad (5.26)$$

Here, once again following the conventions used in TMM, the square matrix F_n is named as field matrix.

The transfer matrix T_n , which relates the state vectors at either end of the sub-system can then be formulated by combining equations (5.24) and (5.26) as given below.

$$v_n^R = P_n F_n^R v_{n-1}^R \quad (5.27)$$

or

$$v_n^R = T_n^R v_{n-1}^R \quad (5.28)$$

where

$$T_n^R = P_n F_n^R \quad (5.29)$$

Using equation (5.28) repetitively, the overall transfer matrix T , which relates the state vectors at either end of the system can be computed.

That is,

$$T = \prod_{n=0} T_n \quad (5.30)$$

Once the overall transfer matrix of the system is known, the boundary conditions of the system can then be applied and the unknown quantities in the left most end state vector can be computed. Now, knowing the left most end state vector completely, the state vector and hence the response at each sub-system at time t_i can be computed by the repeated use of equation (5.28). The velocity and acceleration quantities at time t_i are then computed using equations (5.1) and (5.2) respectively. The entire procedure can then be repeated for time t_{i+1} and so on.

5.2.3 Algorithm for response computation

Following the formulation given above, the dynamic response at different time instants for different sub-systems can now be computed as follows:

- 1) set $i = 1$.
- 2) knowing the initial conditions $x(t_{i-1})$, $\dot{x}(t_{i-1})$, $\ddot{x}(t_{i-1})$ and the system properties at time t_i , compute the quantities A_n , B_n , D_n , and E_n for each sub-system.

- 3) formulate the transfer matrix for each sub-system and the overall transfer matrix using equations (5.28) and (5.30), respectively.
- 4) apply boundary conditions to the end state vectors of the system and compute the unknown quantities in the left most end state vector as a function of the elements of the overall transfer matrix.
- 5) now, knowing all the elements in the left most end state vector, the response at each sub-system at time instant t_i can be computed by successive multiplication of the transfer matrices, using equation (5.28).
- 6) using the computed values of the displacement at t_i , compute the values of $\dot{x}(t_i)$, and $\ddot{x}(t_i)$ using equations (5.1) and (5.2).
- 7) let, $i=i+1$, use the computed values of the previous step as initial conditions and return to step 2, till the time required for complete analysis.

The algorithm is also given as a flow chart in Fig. 5.3.

5.2.4 Time step selection

Since numerical integration procedures are very sensitive to the integration time step used, proper care should be taken in the choice of the time step. Different integration schemes are sensitive to the time step used in

INITIALIZE: I=0

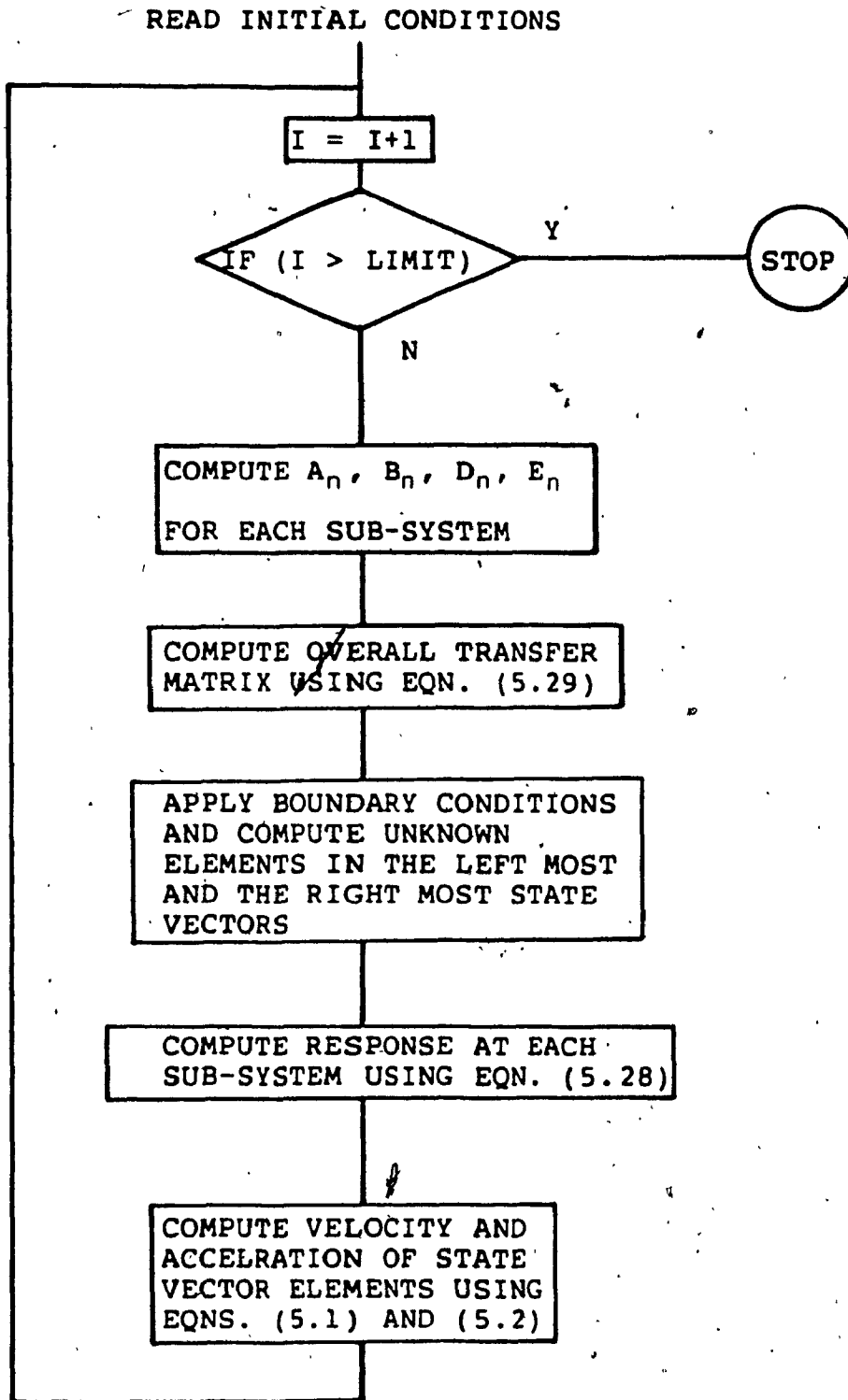


Fig. 5.3: Algorithm for DT-TMM formulation

various degrees. Thus the time step selection depends on the scheme chosen for the formulation. In addition, since the forcing terms and other varying system parameters are discretized in time, the time interval chosen should also be small enough so as not to miss any significant features of the time-varying functions.

5.2.5 Sources of error

Any numerical solution procedure, wherein an approximate solution is assumed, will lead to some errors in the computed solution. In the present case, because of the use of truncated Taylor series as an approximate solution at each sub system, the errors could accumulate both in time as well as in space domains. There is no general method of exactly estimating the accumulated errors involved in a computed solution. However, since the local truncation errors are a function of the time step chosen as well as the finite difference scheme used to approximate the derivative terms in the assumed solution, a general idea of the severity of the accumulated truncation errors can be obtained by using different time steps and different difference schemes and by evaluating the quality of the computed results. So far in the author's experience with DT-TMM in solving problems of varied sizes, with time step properly chosen, the truncation error accumulation was not detrimental to the accuracy of the computed solution.

On the other hand, the effect of propagation of roundoff error, which is a function of the word length of the computing system as well as the number of sub-systems to be modelled, was very significant. Thus it should be noted that even though the DT-TMM requires smaller core requirements and smaller computing time to solve a given problem, these advantages can be offset by the accumulation of roundoff error, especially when analysing very large systems on small computing systems. A detailed study of these errors on the accuracy of DT-TMM solutions is yet to be undertaken.

5.2.6 Highlights of the method

1. Irrespective of the size of the system, the matrices involved in the analysis are always small which reduces the core size requirements.
2. Unlike the conventional TMM, which is restricted to harmonic motion analysis alone, the proposed method is capable of analysing linear time-invariant, linear time-varying, and non-linear systems.
3. In contrast with the conventional TMM, the matrices involved are always real, even when the damping is included. This simplifies numerical computation algorithms involved.

4. Provides flexibility in modelling systems with varying configurations. That is, by creating a library of transfer matrices for commonly occurring sub-systems and by assembling these at the required locations, different configurations can be modelled easily.
5. Natural frequency analysis can also be performed along the lines of the conventional TMM without much effort.
6. Any suitable numerical integration scheme can be included in the formulation, thus providing the analyst the maximum flexibility.
7. It is highly amenable to model chain-like and branching systems such as gear trains with large number of components.

5.2.7 Validation of the proposed methodology

In order to validate the proposed simulation procedure, a comparative study of the results obtained using different techniques is undertaken. For this purpose, two dynamic systems, one linear and the other time-varying and non-linear, are chosen.

Consider the undamped linear multi-degree of freedom spring mass system configured as shown in Fig. 5.4. The salient parameters of the system are defined in Table 5.2. The response of the system is first computed by integrating

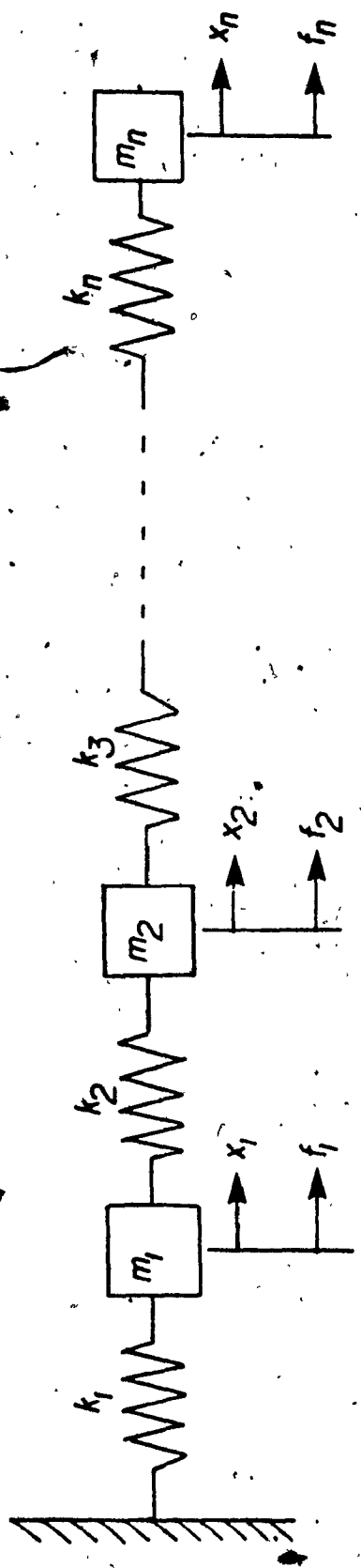


Fig. 5.4: Model of an undamped system with multi degrees of freedom

Table 5.2: Parameters of the system shown in Fig. 5.4.

Station	Mass (Kg)	Stiffness (N/m)	Force (N)	Initial Conditions
n	m_n	k_n	f_n	$x_n(t_0)$ $\dot{x}_n(t_0)$
1	10	55000	0	0 0
2	9	50000	0	0 0
3	8	45000	0	0 0
4	7	40000	0	0 0
5	6	40000	0	0 0
6	6	35000	0	0 0
7	5.5	30000	0	0 0
8	5	25000	0	0 0
9	4.5	20000	0	0 0
10	4	15000	0	0 0
11	3.5	10000	0	0 0
12	4	9000	0	0 0
13	2.5	8000	0	0 0
14	2	7000	0	0 0
15	2	6000	1	0 0

the equations of motion using the Newmark β method with $\beta=1/6$ and $\gamma=1/2$, and is plotted as dotted lines in Fig. 5.5. Then the same system is modelled and solved using the presented DT-TMM procedure and the results are shown in Fig. 5.5 as solid line. For both the cases, the integration time step is taken to be 0.02 sec. As can be seen from Fig. 5.5, the response of the system obtained with DT-TMM is almost identical to the response computed using direct numerical integration. However, as indicated by Fig. 5.6, the computation time required for response calculation is much smaller with DT-TMM. Thus, the use of DT-TMM results in reduced computation time as well as smaller storage requirements for the given problem. The computation time shown in Fig. 5.6 correspond to the execution time based on double precision arithmetic operations on a Vax 11/780 computer.

The suitability of DT-TMM for response calculation of non-linear and/or time varying dynamic systems is studied with the second numerical example. For this purpose, a more practical system configuration such as the spur gear pair system considered in chapter 3 and shown in Fig. 3.3 is chosen. The gear mesh is not only non-linear because of the tooth backlash, but also has time-varying stiffness characteristics. Table 5.3 lists the salient parameters of the system. In chapter 3, the equations of motion of the gear pair system considered are formulated and solved for

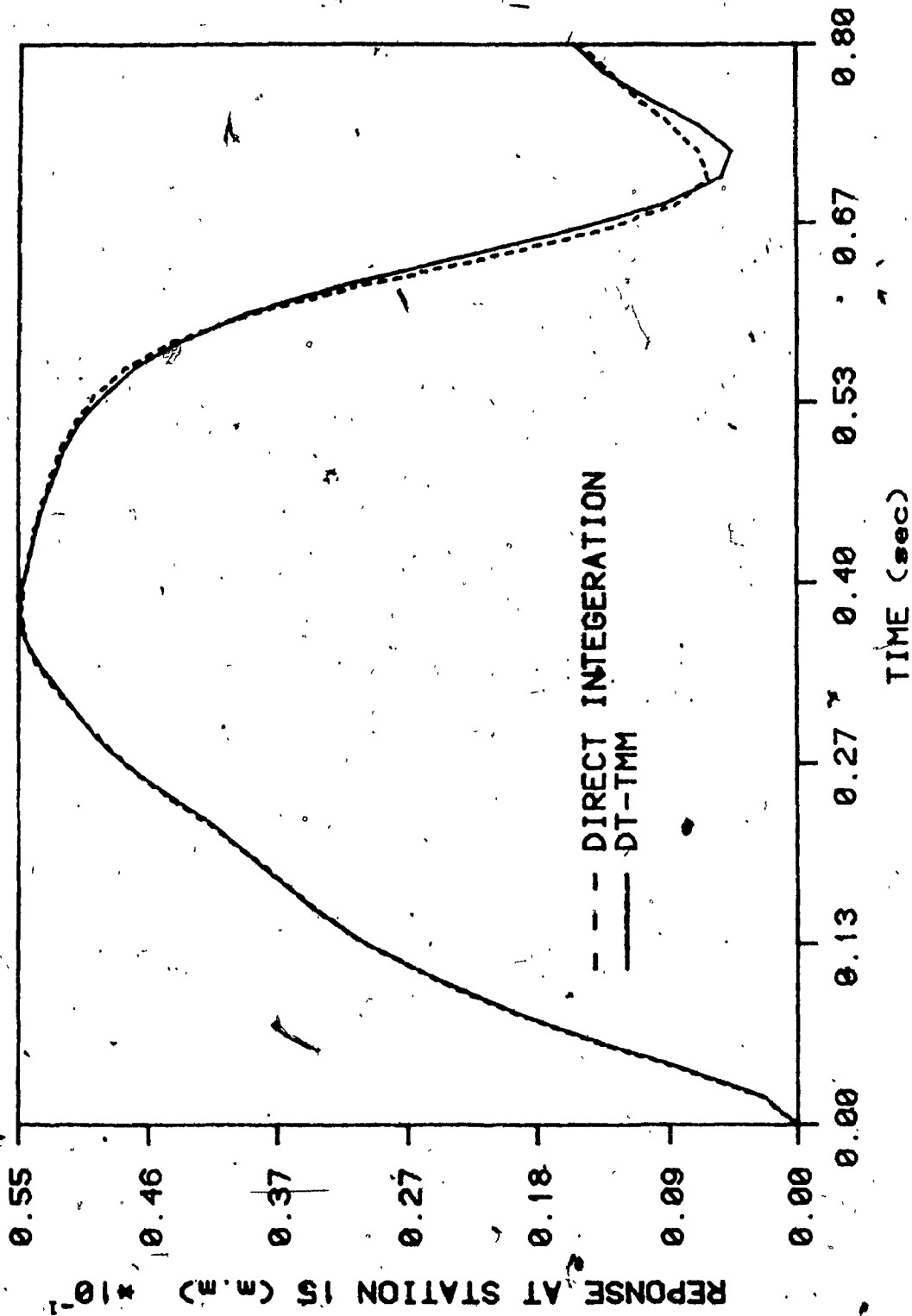


Fig. 5.5: Comparison of response values computed using direct integration and DT-TMM

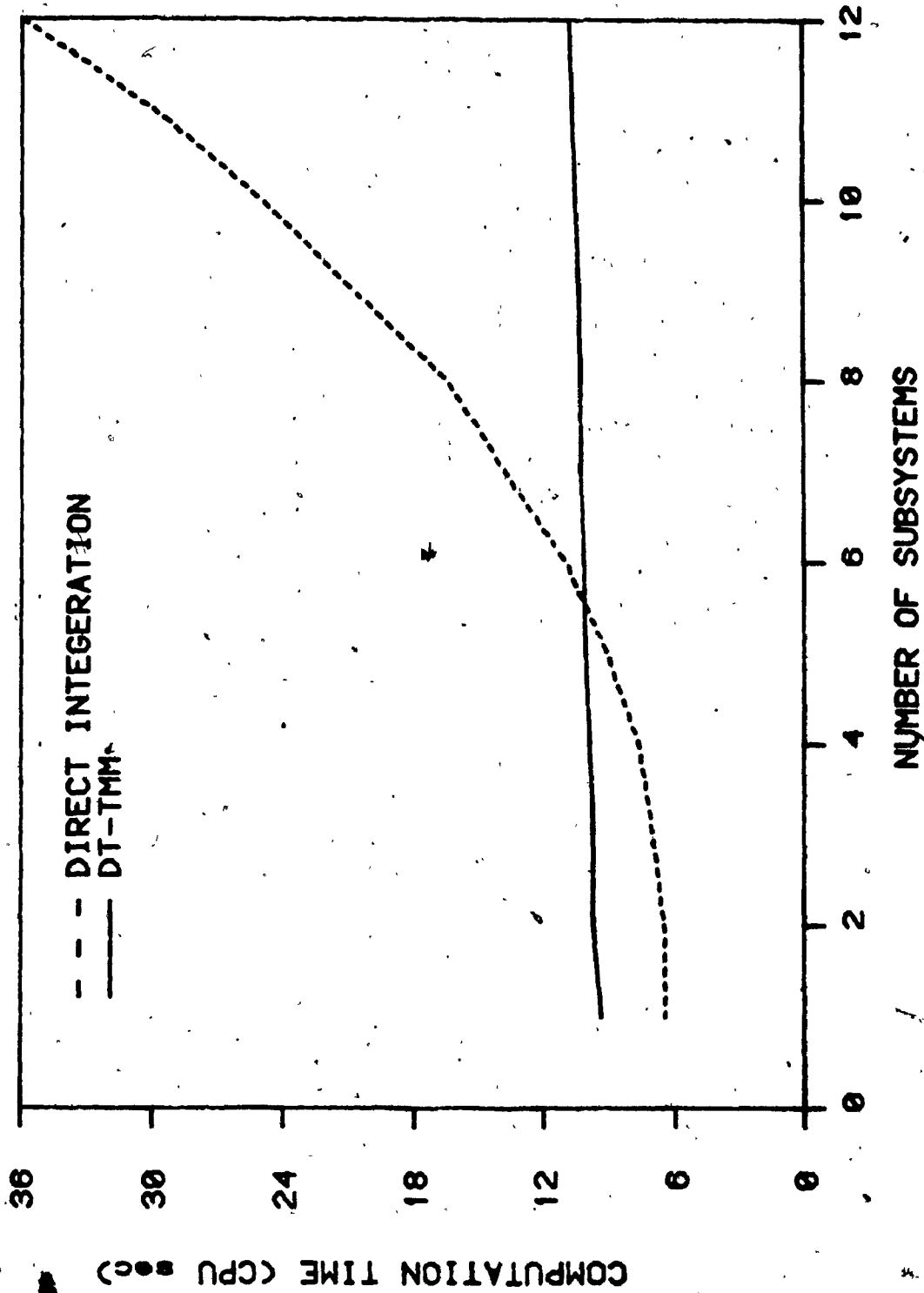


Fig. 5.6: Comparison of computing time of DT-TMM and numerical integration

Table 5.3: Parameters of the gear system shown in Fig. 3.3.

Tooth profile	STD.
Module, mm.	4
Number of teeth, Gear 1, mm.	48
Number of teeth, Gear 2, mm.	48
Pressure angle, deg.	14.5
Pitch diameter, Gear 1, mm.	192
Pitch diameter, Gear 2, mm.	192
Face width, mm.	10
Contact ratio	1.80
Backlash, mm.	0.25
Torque, N-m.	196
Material	3SCM steel
Damping ratio	0.07

the dynamic response of the gear pair using state-space technique. Here, for comparison, the torsional response of the two gears in mesh are first computed using lumped mass model described in chapter 3 and then with DT-TMM. Identical time step and loading conditions are used in both the cases. Fig. 5.7, which shows the relative response of the two gears in mesh, confirms the suitability of DT-TMM for analysis of non-linear and time-varying systems. The maximum deviation between the two curves is about 0.2%. It should be noted here that under certain dynamic conditions the gear teeth may lose contact altogether for short durations. At these conditions the two shafts are essentially uncoupled and will behave as if they are two separate systems. For proper modelling using DT-TMM, this phenomena has to be accounted for.

5.3 DT-TMM as applied to gear dynamics

In the following sections, the DT-TMM formulation proposed in the previous sections is extended to include the coupling between torsional and flexural modes which is usually present in gear train dynamics. The transfer matrix relationships for various modules in the gear system are formulated by considering the equilibrium condition of each module under the action of internal as well as external forces, moments, and torques acting on it. The various assumptions and approximations used in the modelling of some commonly used modules are first stated and then the state

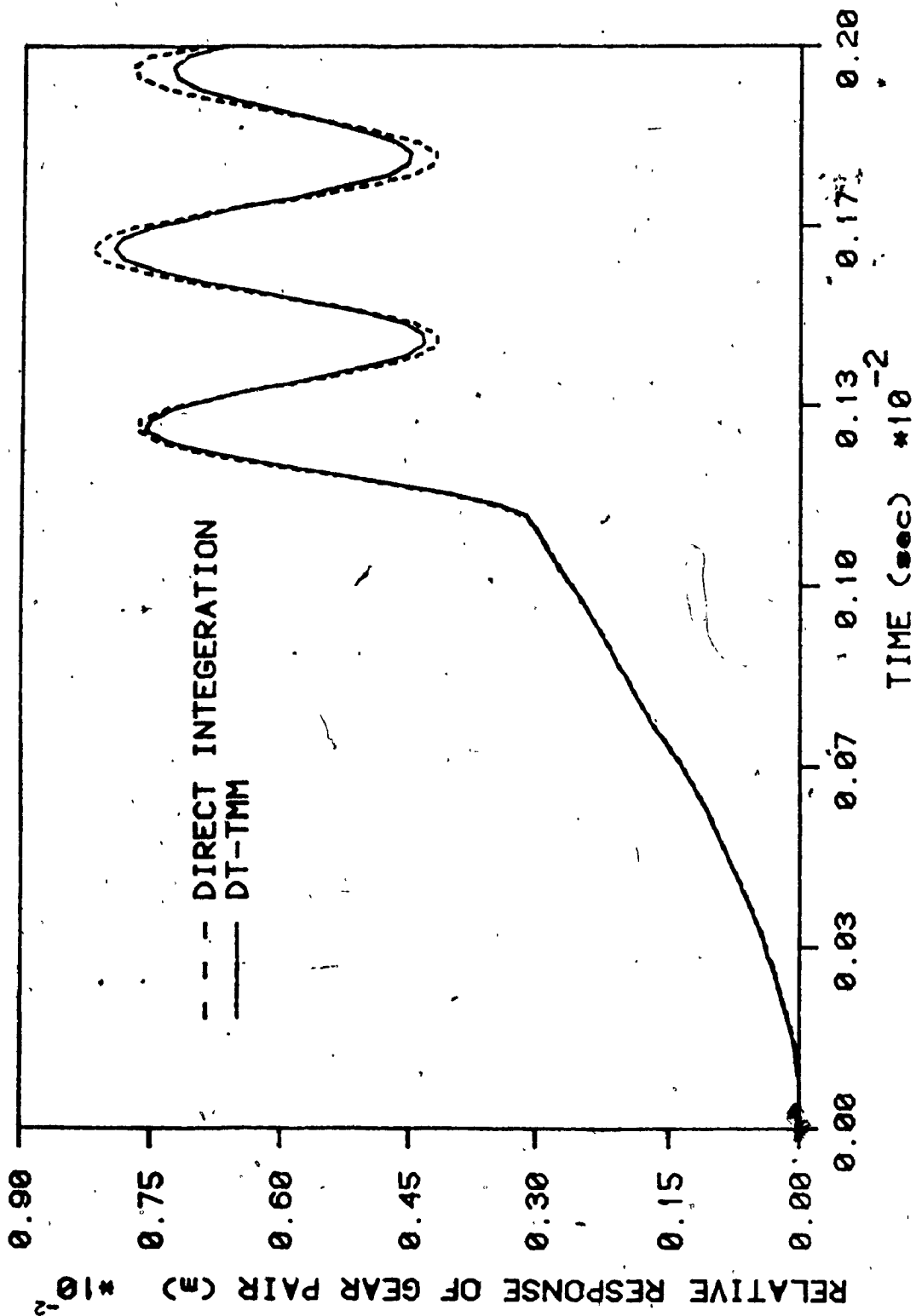


Fig. 5.7: Relative response between two gears modelled

equations describing the state of these modules at any given time instant are formulated.

5.3.1 Massless shaft module

Even though physically the mass of the shaft is distributed over the length of the shaft, for modelling purposes the elastic and dynamic properties of the shaft are considered separate. This lumped mass approximation is widely used in rotor dynamics studies because it is computationally less expensive and provides reasonably accurate results when the mass point locations are well chosen. Also, the shaft modules are assumed to have no inertia in the present formulation. However, modelling of the shaft module with inclusion of distributed mass and inertia is also possible [134].

5.3.2 Lumped mass module

The lumped mass module is used to represent the mass of the shafts and other elements in the gear system. It has only mass properties and no inertial or elastic properties.

5.3.3 Disc module

Disc modules having polar moment of inertia and mass properties is used to model large rotating elements of the gear system such as gears, flywheels, clutch plates etc.. Mass unbalance, and the gyroscopic moments are also considered. As was explained in chapter 2, the dynamic

coupling introduced by the gyroscopic moments are not included in the modelling.

5.3.4 Bearing module

The bearings of the rotors on which the gears are mounted are modelled as shown in Fig. 5.8. Irrespective of the bearing type, its characteristics can be expressed as a function of the stiffness coefficients k_{xx} , k_{xy} and k_{yy} and damping coefficients c_{xx} , c_{xy} , and c_{yy} . Evaluation of these coefficients for different type of bearings is the subject matter of many studies [135] and is beyond the scope of this investigation. The support stiffness can also be included in the model, if required.

General TM relations

Based on these assumptions and observations, the state equation of each module describing the state of the module in the two lateral directions and the torsional direction can be formulated. Fig. 5.9 shows for each of the modules discussed so far the forces, moments, and torques acting on them.

Combining the state equations of all these individual modules, a single set of transfer equations can be set up as given below. By including or ignoring the appropriate quantities in these equations, the transfer matrix relationships of various different modules can be derived.

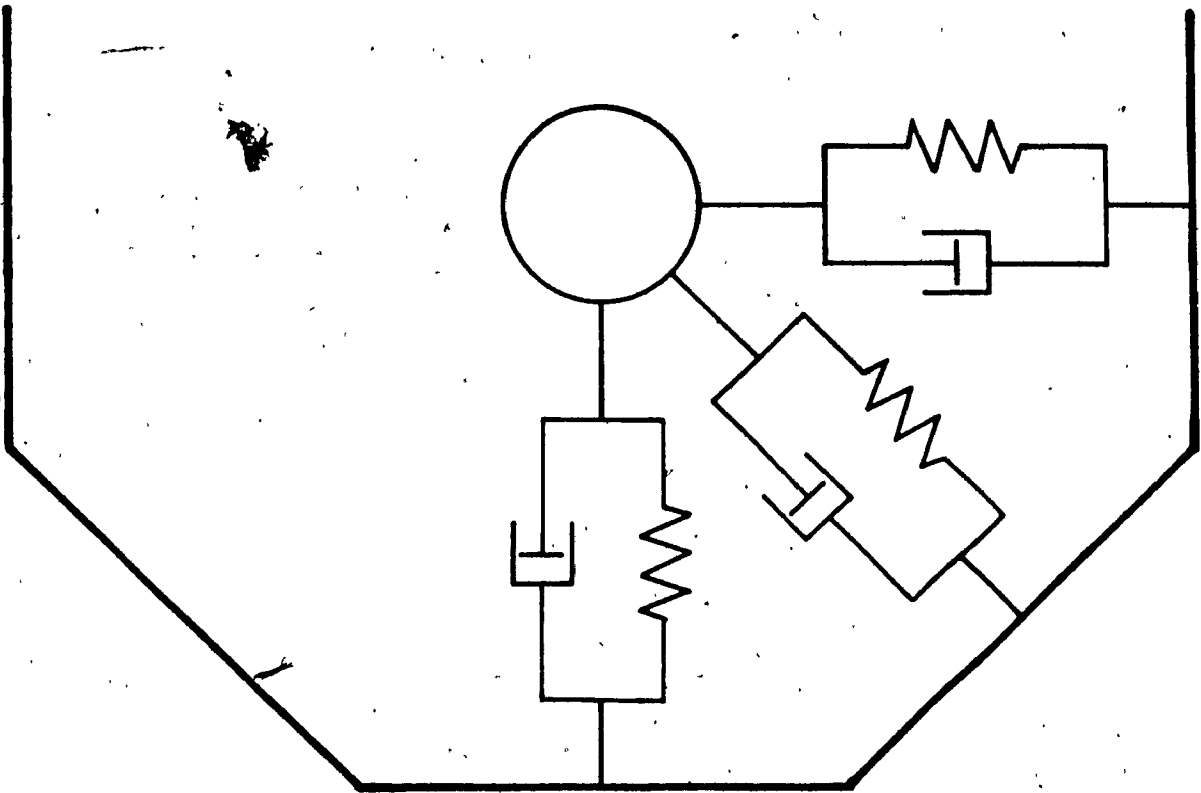


Fig. 5.8: Model of the support bearings

Torsion

$$\tau_n^R = \tau_n^L$$

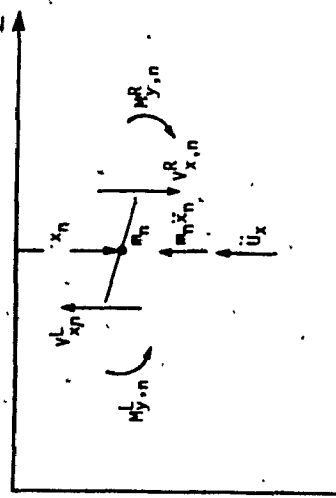
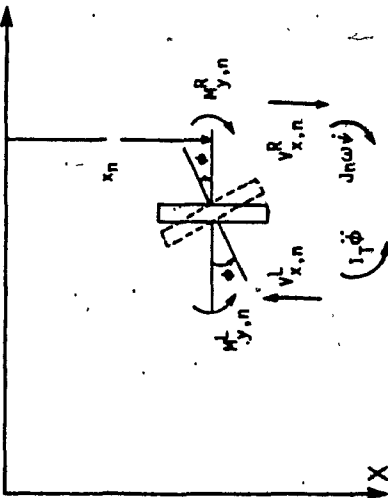
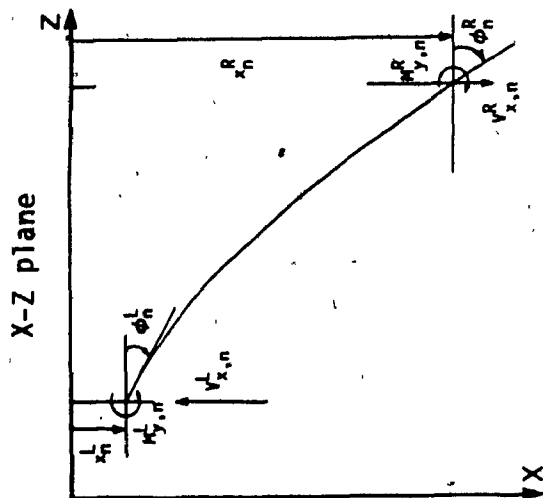
$$\tau_n^L = k_n(\theta_n^R - \theta_n^L) + c(\theta_n^R - \theta_n^L)$$

$$\theta_n^R = \theta_n^L$$

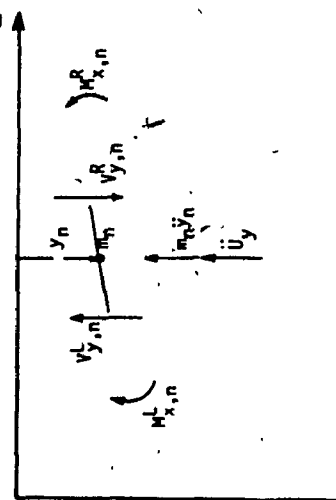
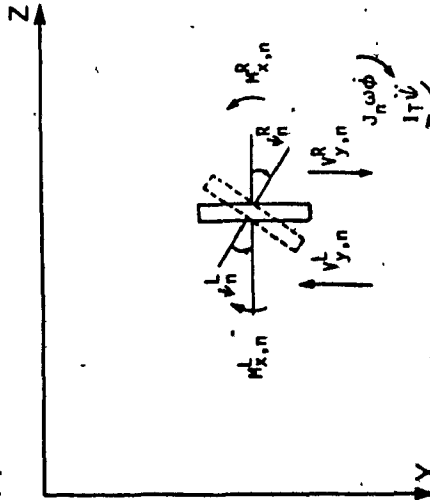
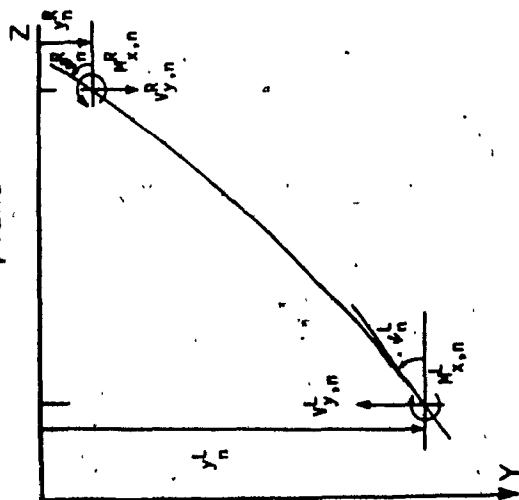
$$\tau_n^R = \tau_n^L + J_n \theta_n$$

$$\theta_n^R = \theta_n^L$$

$$\tau_n^R = \tau_n^L$$



Y-Z plane



Massless Shaft

Disk

Lumped mass

Fig. 5.9: Schematics of different modules

For example, letting $m, J, U, k_{xx}, k_{xy}, k_{yy}, c_{xx}, c_{xy},$ and c_{yy} equal to zero will result in the field equations of the massless shaft module. Similarly, by letting L_n equal to zero will yield the point equations of the disc module and so on.

Lateral motion in the X-Y plane

$$-y_n^R = -y_n^L + L_n \phi_n^L + M_{x,n}^L \frac{L^3}{2EI} + V_{y,n}^L \frac{L^3}{6EI} \quad (5.31)$$

$$\phi_n^R = \phi_n^L + M_{x,n}^L \frac{L}{EI} + V_{y,n}^L \frac{L^2}{2EI} \quad (5.32)$$

$$V_{y,n}^R = V_{y,n}^L + m_n \ddot{y}_n^L + \ddot{U}_{y,n} + k_{yy,n} y_n^L + k_{yx,n} x_n^L + c_{yy,n} \dot{y}_n^L + c_{yx,n} \dot{x}_n^L \quad (5.33)$$

$$M_{x,n}^R = M_{x,n}^L + J_n \omega \phi_n^L + I_T \ddot{\phi}_n^L + V_{y,n}^L L_n \quad (5.34)$$

Lateral motion in the X-Z plane

$$x_n^R = x_n^L + L_n \phi_n^L + M_{y,n}^L \frac{L^3}{2EI} - V_{x,n}^L \frac{L^3}{6EI} \quad (5.35)$$

$$\phi_n^R = \phi_n^L + M_{y,n}^L \frac{L}{EI} - V_{x,n}^L \frac{L^2}{2EI} \quad (5.36)$$

$$-V_{x,n}^R = -V_{x,n}^L - m_n \ddot{x}_n^L - \ddot{U}_{x,n} - k_{xx,n} x_n^L - k_{xy,n} y_n^L - c_{xx,n} \dot{x}_n^L - c_{xy,n} \dot{y}_n^L \quad (5.37)$$

$$M_{y,n}^R = M_{y,n}^L - J_n \omega \phi_n^L + I_T \ddot{\phi}_n^L - V_{x,n}^L L_n \quad (5.38)$$

Torsional motion

For massless shaft module

$$\tau_n^R = \tau_n^L \quad (5.39)$$

$$\tau_n^R = k_n (\theta_n^R - \theta_n^L) + c_n (\dot{\theta}_n^R - \dot{\theta}_n^L) \quad (5.40)$$

For other modules

$$\tau_n^R = \tau_n^L + J_n \ddot{\theta}_n^L \quad (5.41)$$

$$\theta_n^R = \theta_n^L \quad (5.42)$$

Up to this point in the formulation the steps taken are all essentially same as those taken in the conventional TMM procedure. The difference between the TMM and the present formulation lies in the way the time derivative quantities are expressed. In contrast to the conventional TMM procedure wherein, because of the assumption of harmonic displacements, the acceleration and velocity quantities are written as function of the frequency of oscillations, DT-TMM uses the approximate relations of the type given in equations (5.1) and (5.2).

Replacing the time derivative quantities in equations (5.31) to (5.42) by relationships of the form given by equations (5.1) and (5.2) will result in the following equations:

Lateral motion in the X-Y plane

$$-y_n^R = -y_n^L + L_n \psi_n^L + M_{x,n}^L \frac{L}{2EI} + V_{y,n}^L \frac{L^2}{6EI} \quad (5.43)$$

$$\psi_n^R = \psi_n^L + M_{x,n}^L \frac{L}{EI} + V_{y,n}^L \frac{L^2}{2EI} \quad (5.44)$$

$$V_{y,n}^R = V_{y,n}^L + m_n [A_y y + B_y]_{y_n}^L + [A_{U_y} U_y + B_{U_y}]_{y_n}^L + k_{yy,n} y_n^L + k_{yx,n} x_n^L + c_{yy,n} [D_y y + E_y]_{y_n}^L + c_{yx,n} [D_x x + E_x]_{x_n}^L \quad (5.45)$$

$$M_{x,n}^R = M_{x,n}^L + J_n \omega [D_\phi \phi + E_\phi]^L + I_T [A_\psi \psi + B_\psi]^L + V_{y,n}^L L_n \quad (5.46)$$

Lateral motion in the X-Z plane

$$x_n^R = x_n^L + L_n \phi_n^L + M_{y,n}^L \frac{L_n^2}{2EI} - V_{x,n}^L \frac{L_n^3}{6EI} \quad (5.47)$$

$$\phi_n^R = \phi_n^L + M_{y,n}^L \frac{L_n}{EI} - V_{x,n}^L \frac{L_n^2}{2EI} \quad (5.48)$$

$$\begin{aligned} -V_{x,n}^R = -V_{x,n}^L - m_n [A_{xx} x + B_{xx}]^L - [A_{Ux} U_x + B_{Ux}]^L - k_{xx,n} x_n^L - k_{xy,n} y_n^L \\ - c_{xx,n} [D_x x + E_x]^L - c_{xy,n} [D_y y + E_y]^L \end{aligned} \quad (5.49)$$

$$M_{y,n}^R = M_{y,n}^L - J_n \omega [D_\psi \psi + E_\psi]^L + I_T [A_\phi \phi + B_\phi]^L - V_{x,n}^L L_n \quad (5.50)$$

Torsional motion

For massless shaft module

$$\tau_n^R = \tau_n^L \quad (5.51)$$

$$\tau_n^R = k_n (\theta_n^R - \theta_n^L) + c_n [(D_\theta \theta + E_\theta)^R - (D_\theta \theta + E_\theta)^L] \quad (5.52)$$

For other modules

$$\tau_n^R = \tau_n^L + J_n [A_\theta \theta + B_\theta]^L \quad (5.53)$$

$$\theta_n^R = \theta_n^L \quad (5.54)$$

which can be put into a single matrix equation as;

$$v_n^R = T_n v_n^L \quad (5.55)$$

Here, the state vector v is defined as,

$$v = \{y, \phi, M_x, V_y, x, \psi, M_y, -V_x, \theta, \tau, 1\}^T \quad (5.56)$$

and the square matrix T_n , known as the transfer matrix n^{th} module, is given in the Fig.5.10. The expressions for the coefficients A_n , B_n , D_n , and E_n for various commonly used integration schemes are given in Table 5.1.

5.3.5 Gear pair module

The gear pair is modelled as shown in Fig. 5.11. The gear mesh is represented as a non-linear spring-damper element with time-varying stiffness and backlash. The transmission error is introduced as displacement excitation at one end of the non-linear spring-damper element. And the gears themselves are considered as disc modules except that the presence of dynamic load and frictional forces between the gear teeth will introduce additional terms into the state equations. Thus, the equations (5.45), (5.49) and (5.53) will be modified as given below.

For gear 1,

$$V_{y,p}^R = V_{y,p}^L + m_p [A_y y + B_y]_p^L + [A_{Uy} U_y + B_{Uy}]_p^L + k_{yy,p} y_p^L + k_{yx,p} x_p^L + c_{yy,p} [D_y y + E_y]_p^L + c_{yx,p} [D_x x + E_x]_p^L + W_d \cos(\alpha - \beta) \quad (5.58)$$

$$-V_{x,p}^R = -V_{x,p}^L - m_p [A_x x + B_x]_p^L - [A_{Ux} U_x + B_{Ux}]_p^L - k_{xx,p} x_p^L - k_{xy,p} y_p^L - c_{xx,p} [D_x x + E_x]_p^L - c_{xy,p} [D_y y + E_y]_p^L - W_d \sin(\alpha - \beta) \quad (5.59)$$

$$\tau_p^R = \tau_p^L + J_p [A_\theta \theta + B_\theta]_p^L + W_d \dot{R}_{bp} \quad (5.60)$$

T_n	1	1	$\frac{L^3}{2EI}$	$\frac{L^3}{6EI}$	0	0	0	0	0	0	0
	0	1	1	$\frac{L^2}{2EI}$	0	0	0	0	0	0	0
	0	α_1	1	1	0	α_2	0	0	0	0	α_3
	α_4	0	0	1	α_5	0	0	0	0	0	α_6
	0	0	0	0	1	1	$\frac{L^3}{2EI}$	$\frac{L^3}{6EI}$	0	0	0
	0	0	0	0	0	1	1	$\frac{L^2}{2EI}$	0	0	0
	0	α_7	0	0	0	α_8	1	1	0	0	α_9
	α_{10}	0	0	0	α_{11}	0	0	1	0	0	α_{12}
	0	0	0	0	0	0	0	0	α_{13}	α_{14}	α_{15}
	0	0	0	0	0	0	0	0	α_{16}	1	α_{17}
	0	0	0	0	0	0	0	0	0	0	1

$$\alpha_1 = I_T A \phi$$

$$\alpha_2 = J \omega D \phi$$

$$\alpha_3 = J \omega E \phi + I_T B \phi$$

$$\alpha_4 = m A_y + c_{yy} D_y + k_{yy}$$

$$\alpha_5 = c_{yx} D_x + k_{yx}$$

$$\alpha_6 = [m B_y + A_{Uy} U_y + B_{Uy} + c_{yy} E_y + c_{yx} E_x]$$

$$\alpha_7 = -J \omega D \phi$$

$$\alpha_8 = I_T A \phi$$

$$\alpha_9 = -J \omega E \phi + I_T B \phi$$

$$\alpha_{10} = -[c_{xy} D_y + k_{xy}]$$

$$\alpha_{11} = -[m A_x + c_{xx} D_x + k_{xx}]$$

$$\alpha_{12} = -[m B_x + A_{Ux} U_x + B_{Ux} + c_{xx} E_x + c_{xy} E_y]$$

FOR DISC MODULE

$$\alpha_{13} = 1$$

$$\alpha_{14} = 0$$

$$\alpha_{15} = 0$$

$$\alpha_{16} = \frac{J A \phi}{R}$$

$$\alpha_{17} = \frac{J B \phi}{R}$$

FOR SHAFT MODULE

$$\alpha_{13} = \frac{k + c D_{\theta}^L}{k + c D_{\theta}^R}$$

$$\alpha_{14} = \frac{1}{k + c D_{\theta}^R}$$

$$\alpha_{15} = \frac{c[E_{\theta}^R - E_{\theta}^L]}{k + c D_{\theta}^R}$$

Fig. 5.10: Transfer matrix of a gear system component

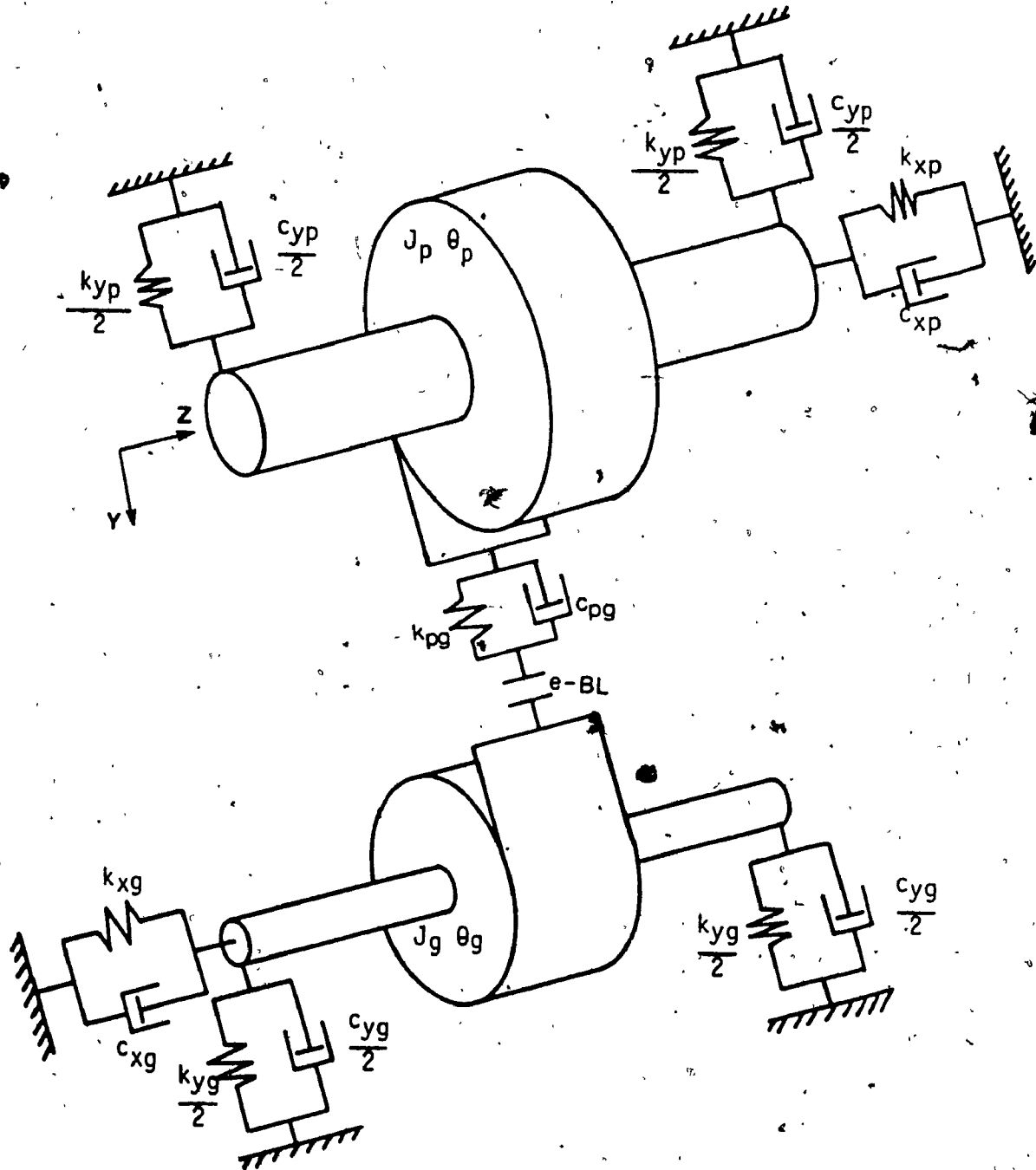


Fig. 5.11: Gear pair module

Similarly for gear 2,

$$V_{y,g}^R = V_{y,g}^L + m_g [A_{y,y} + B_{y,g}]^L + [A_{Uy,y} + B_{Uy,g}]^L + k_{yy,g}^L y_g^L + k_{yx,g}^L x_g^L + c_{yy,g} [D_{y,y} + E_{y,g}]^L + c_{yx,g} [D_{x,x} + E_{x,g}]^L - W_d \cos(\alpha - \beta) \quad (5.61)$$

$$-V_{x,g}^R = -V_{x,g}^L - m_g [A_{x,x} + B_{x,g}]^L - [A_{Ux,x} + B_{Ux,g}]^L - k_{xx,g}^L x_g^L - k_{xy,g}^L y_g^L - c_{xx,g} [D_{x,x} + E_{x,g}]^L - c_{xy,g} [D_{y,y} + E_{y,g}]^L + W_d \sin(\alpha - \beta) \quad (5.62)$$

$$\tau_g^R = \tau_g^L + J_g [A_{\theta,\theta} + B_{\theta,g}]^L - W_d R_{bg} \quad (5.63)$$

Here, the dynamic load is given by equations (3.7) to (3.10) and the torque due to frictional forces under elasto-hydrodynamic lubrication conditions is given by equations (2.12) to (2.19). Replacing the time derivative quantities in the resulting set of equations by the relationships of the form given by equations (5.1) and (5.2) and combining these modified equations along with the rest of disc module equations, the transfer matrix for the gear pair module T_{gp} can be formulated, as given below.

$$\mathbf{v}_n^R = \mathbf{T}_{gp} \mathbf{v}_n^L \quad (5.64)$$

where,

$$\mathbf{v} = \{ -y_p, \phi_p, M_{x,p}, V_{y,p}, x_p, \phi_p, M_{y,p}, -V_{x,p}, \theta_p, r_p, -y_g, \phi_g, M_{x,g}, V_{y,g}, x_g, \phi_g, -V_{x,g}, M_{y,g}, \theta_g, r_g, 1 \}^T \quad (5.65)$$

As can be seen from equation (5.65), the state vector of the gear pair module includes the state variables of both the gears resulting in extended transfer matrix of nearly twice the size of the other module transfer matrices.

5.4 TM for other system components

In addition to the modules defined above, which are absolutely necessary in the construction of any gear system, other driveline components such as clutches, couplings, Hooke's joints, etc. may also be present. Transfer matrices for these components need also be formulated for effective simulation of a gear system. Formulation of the transfer matrices for such components, which is beyond the scope of the present investigation, can be carried out using the same steps as given earlier based on the analytical model of these components.

5.5 Solution procedure

Once the modules are properly defined and assembled to represent the given system, the next step to be taken is to compute the overall transfer matrix of the system. This matrix, which relates the state vectors at either end of the system, is obtained by successive multiplication of the module transfer matrices in the order of occurrence. Then the boundary conditions are applied and the unknown state variables in the left most end state vector are computed as function of the overall transfer matrix elements. Knowing

the left most end state vector, the responses at the individual modules can be obtained by successive application of transfer matrix relations. These steps are, in general, same for any TMM procedure. The difference between various TMM procedures lies in the way the overall transfer matrix is obtained.

Gear systems which are classified as branched rotor systems are normally analysed using TMM by replacing the multi rotor gear system by an equivalent single rotor system. The response of the equivalent system is first computed using the steps given above. Then the actual responses are recomputed from the response of the equivalent system. This procedure requires lot of redundant computations and is not straight forward. Though widely used in rotor dynamic studies [23,135], it is not well suited for gear system analysis [25,136]. To overcome these shortcomings, Mitchell [136] proposed a new branching technique called modified Hibner method. This new technique does not require the formulation of any equivalent system and can easily accommodate the coupling terms introduced by gears. However the size of the matrices involved becomes quite large for multi-stage gear systems, since the state vector consists of the state variables of all the rotors. In addition, it requires that all the rotors in the system be segmented equally so that the total number of modules along each rotor be the same, which may unnecessarily

increase the computation effort. In this investigation, a modification to Mitchell's technique is proposed by which the matrix size and thereby the computation effort can be reduced.

The proposed modification is based on the fact that only the gear pair module of the gear system requires the extended state vector consisting of the state variables of both the rotors. It is proposed here that starting from the left most end of each shaft in the system, transfer matrix of each segment and module be formulated and computed till a gear pair module is encountered. At which point an extended transfer matrix consisting of the transfer matrices of the two shafts connected with the gear pair involved is formed. This extended transfer matrix is then multiplied by the transfer matrix of the gear pair involved to move across the gear pair module. Once past the gear pair module, the extended transfer matrix is decomposed into two matrices each one corresponding to the state variables of the two shafts involved. Then the same procedure is repeated until another gear pair module or end of the shaft is encountered. This procedure reduces the matrix multiplication effort considerably. Also there is no restriction on the number of modules on each rotor. Fig. 5.12 schematically shows the mechanics of the conventional TMM, Mitchell's technique, and the proposed procedure. A measure of the reduction in computation effort can be derived as follows.

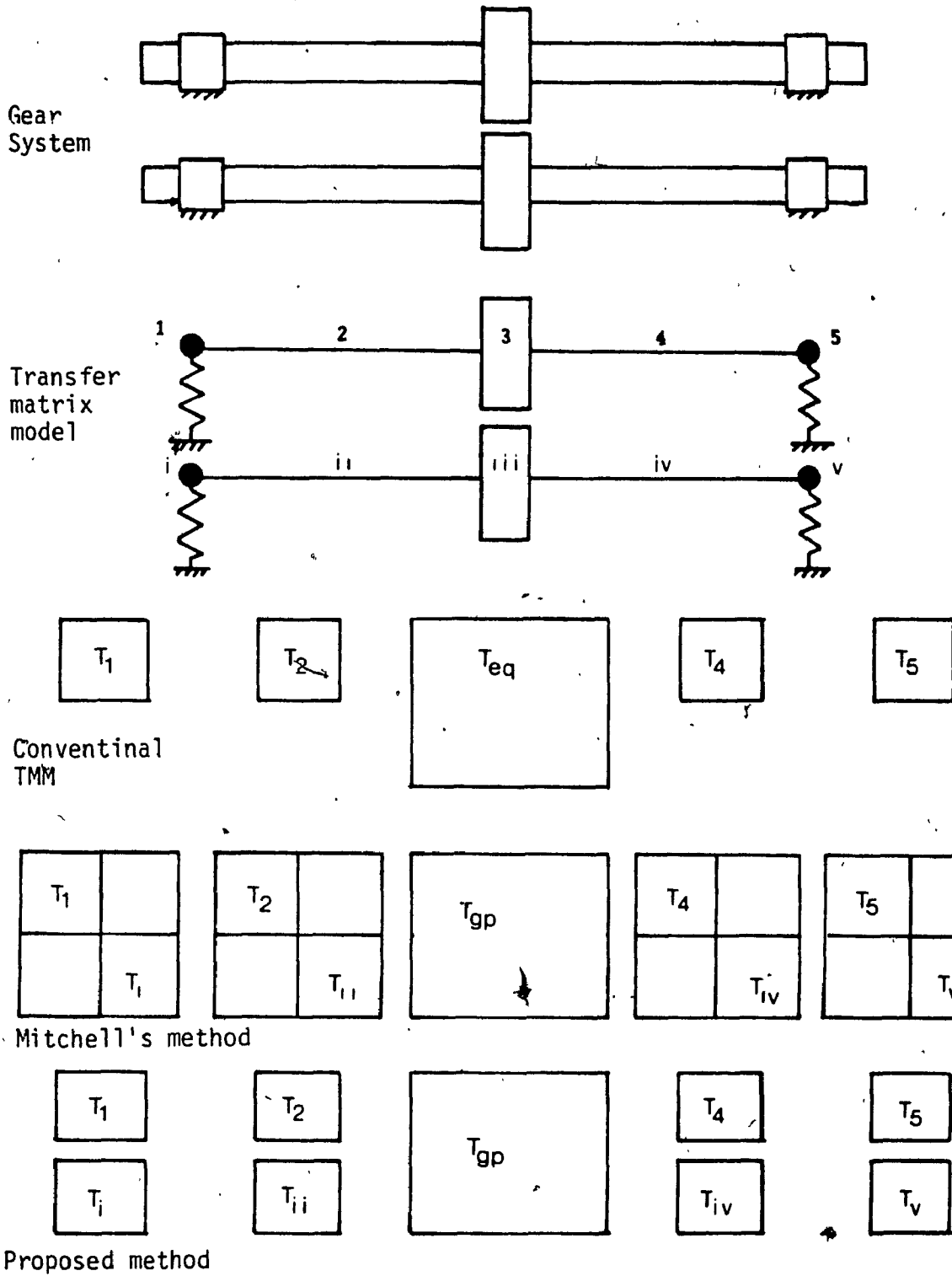


Fig. 5.12: Schematic representations of solution techniques

Consider a multi-stage gear system consisting of N rotors. Let the number of state variables required to describe the state of each rotor be n_s . Assuming that all the rotors are segmented equally, say n modules, the multiplication effort involved with Mitchell's technique will be, approximately, $n(N.n_s)^2$. Whereas for the same system, the proposed modification will require only $(n-1+N)N.n_s^2$ resulting in a reduction of about $N(N-1)(n-1)n_s^2$ multiplications. As can be seen from the given expression, the savings in computational effort increases with the number of rotors N , number of modules n , and the number of state variables n_s .

5.6 Validation of the proposed methodology

In order to examine the suitability of DT-TMM for modelling large practical gear systems consisting of many driveline components, the gear system shown in Fig. 5.13 and defined in Table 5.4, is chosen as a case study. The gear system considered is first analysed using Mitchell's technique with the simplifying assumptions, due to the limitation of Mitchell's technique, of linear and time-invariant mesh behaviour. Then, the same analysis with the same assumptions is carried out using the methodology proposed in this study. Fig. 5.14 shows the results of the present simulation along with the results of Mitchell's technique. As can be seen from this figure, the dynamic factor (D.F.) response results are almost identical under

identical conditions. The maximum difference between the two curves is about 3%, which can be explained as due to the loss of significant digits or truncation error which propagates through successive matrix multiplications involved in DT-TMM. Next, for the same gear system, the same analysis is carried out with the inclusion of tooth backlash and time-varying mesh stiffness and the results are compared to the simplified analysis carried out before. From the comparison study, Fig. 5.15, it can be seen that the simplified assumptions which are currently used are not adequate. For the given problem, it should be noted that the proposed alternative to Mitchell's technique results in about 45% less number of multiplications.

5.7 Summary

A new method of modelling and analysing technique based on the conventional TMM and numerical integration procedures is introduced for dynamic analysis of large practical gear systems. The proposed methodology is unique in the sense that it can accommodate both non-linear and time-varying characteristics of gear system components and at the same time has the modelling flexibility of TMM. All the primary and secondary factors identified in chapter 2 can be easily included in the modelling. It is the most complete model to-date available for the study of gear system dynamics. Comparison of results obtained with the proposed methodology with results obtained from the use of other techniques

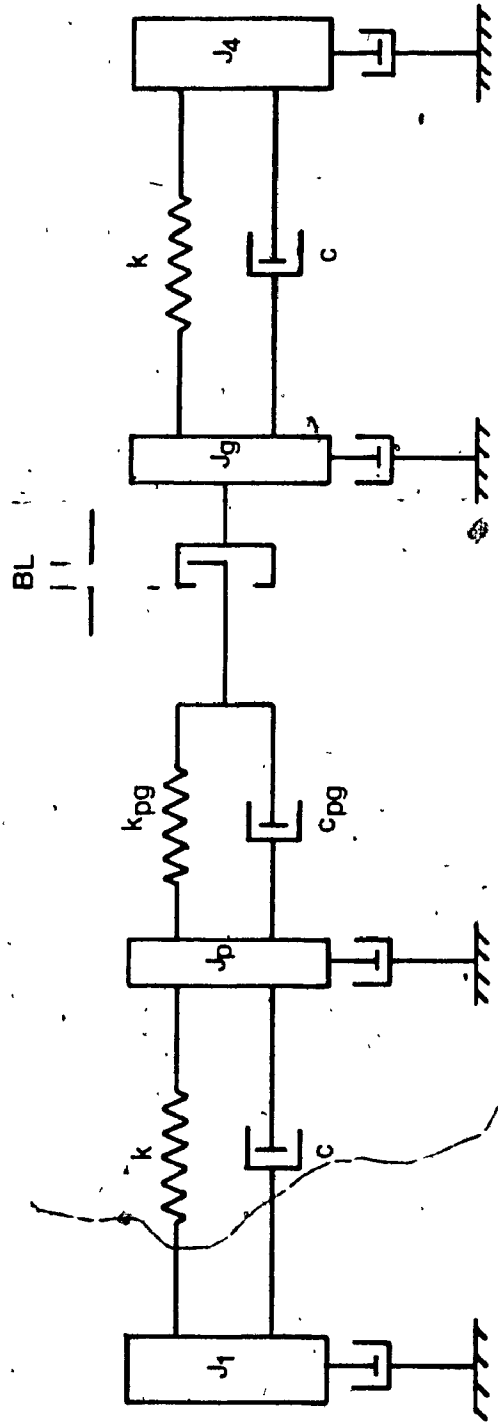
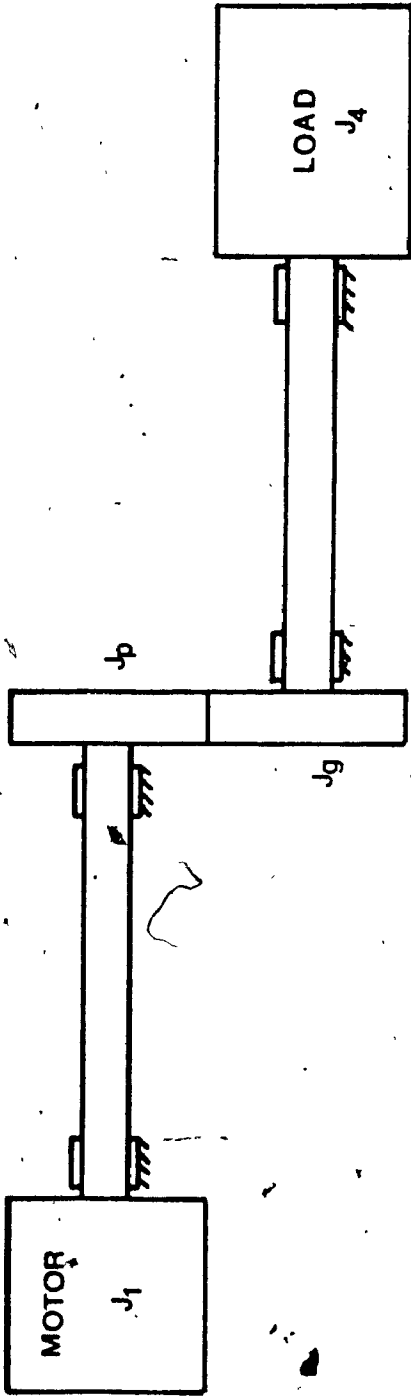


Fig. 5.13: Model of the given gear system

Table 5.4: Parameters of the gear system.

	STD:
Tooth profile	
Module, mm.	4
Number of teeth, Gear 1, mm.	20
Number of teeth, Gear 2, mm.	20
Pressure angle, deg.	20
Pitch diameter, Gear 1, mm.	63.5
Pitch diameter, Gear 2, mm.	63.5
Face width, mm.	25.4
Contact ratio	1.56
Backlash, mm.	0.25
Torque, N-m.	196
Damping ratio	0.07
Moment of inertia, Gear 1, Kg.m ²	0.0051
Moment of inertia, Gear 2, Kg.m ²	0.0051
Moment of inertia, Drive, Kg.m ²	0.026
Moment of inertia, Load, Kg.m ²	0.026
Shaft stiffness, shaft 1, N.m/rad	102,000
Shaft stiffness, shaft 2, N.m/rad	102,000

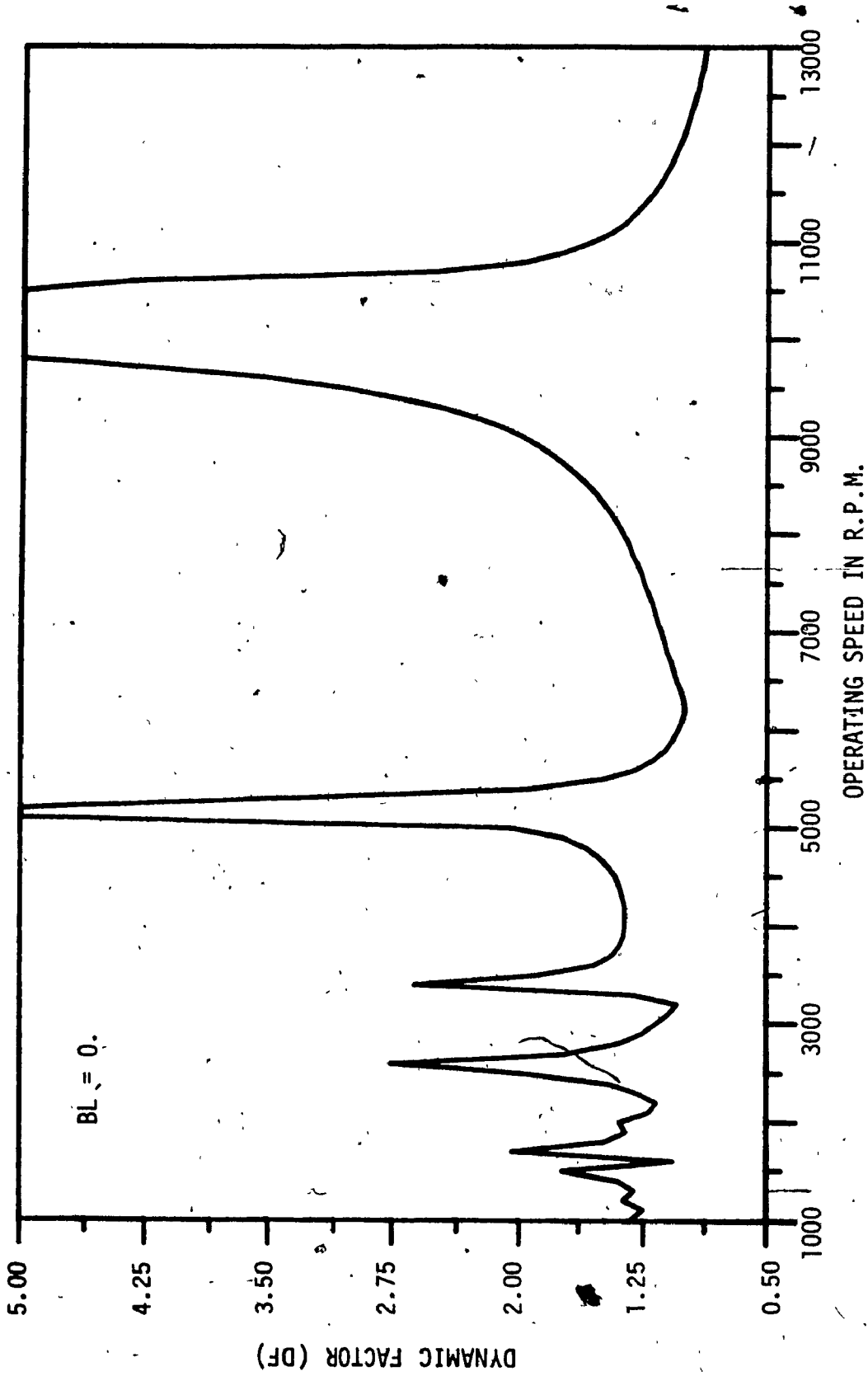


Fig. 5.14: Comparison of simulator results

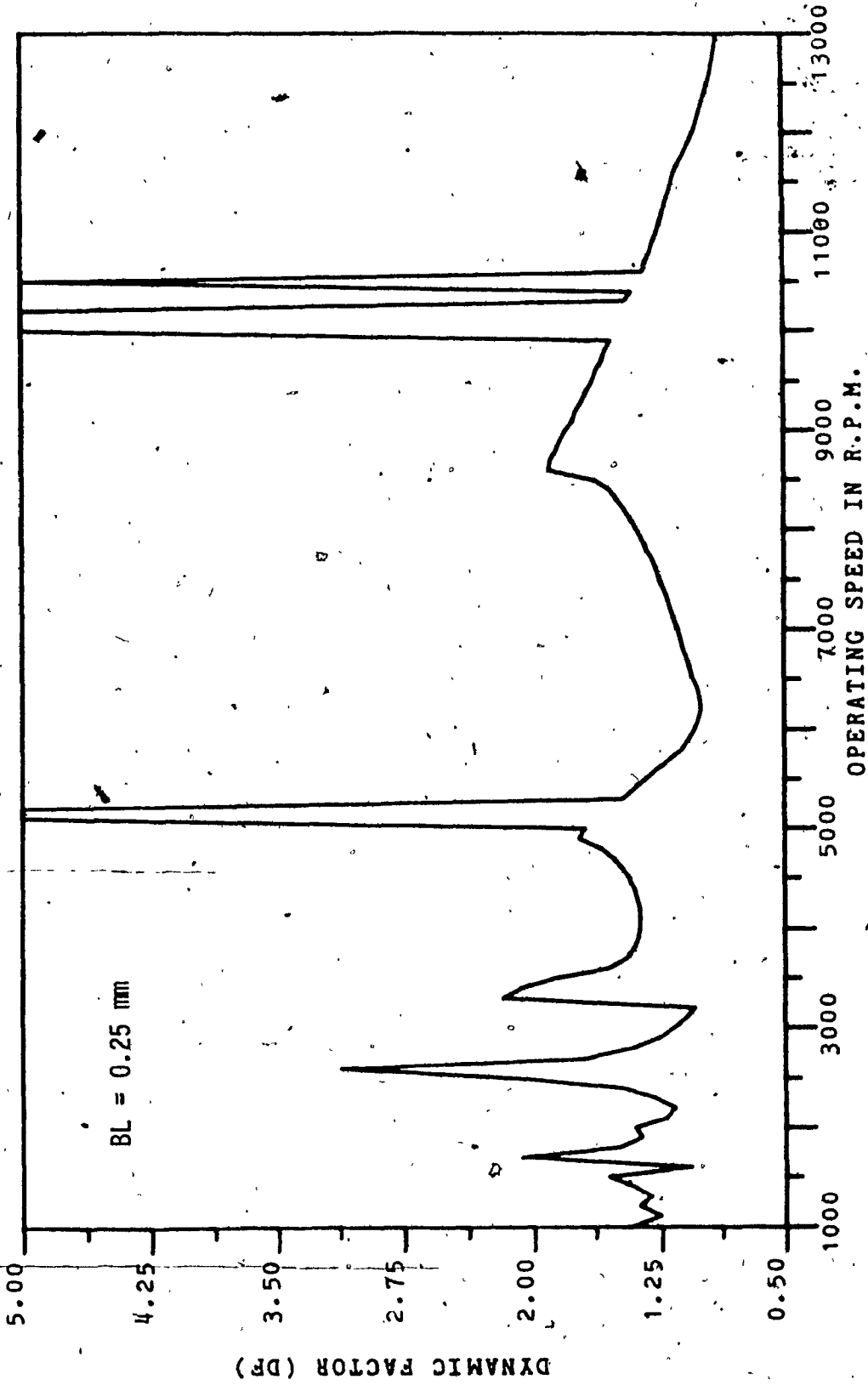


Fig. 5.15: Comparison of simulator results

confirms the potential of the method in gear train applications. With proper care in modelling, not only the conventional multi-stage gear systems but also the other type of complex gear configurations such as planetary gears can also be modelled.

Comparison of the dynamic response and the dynamic load results obtained with the proposed analysis procedure with those of other techniques demonstrates the suitability of the procedure for gear train dynamic analysis.

CHAPTER 6

ESTIMATION OF GEAR FATIGUE LIFE

6.1 Introduction

In recent years, fatigue design technology in general has evolved rapidly due to the introduction of computer aided analysis techniques such as fracture mechanics and local stress-strain concepts. Such advances, however, are not reflected in the fatigue design of gears. The industrial gear design standards such as those proposed by AGMA [1], ISO [2] and others still use a single index value representing the maximum dynamic load as the basis for fatigue design of gears. Such simplified design approaches are found to be adequate for routine design applications since the inadequacies of the analytical descriptions are overcome by the use of empirical service factors and strength reduction factors compiled over a long period of time. However for designs that are outside the range of routine applications, iterative and expensive experimental verifications are required and are heavily relied upon. This is clearly brought about by the fact that majority of the studies on gear fatigue reported in literature are of experimental in nature. Also, the current gear design methods contradict the classical fatigue design concepts and techniques employed in the design of other machine elements. For example, the dynamic load value used in the current gear design methods is assumed to alternate between zero and the

maximum value which requires that the use of mean stress as well as the alternating stress for fatigue design. But, in reality, the current gear design methods use only a single stress value corresponding to the maximum dynamic load as if the gear tooth is subjected to static loading without involving alternating and mean components. In order to overcome such flaws and the uncertainties involved in the current gear design methods as well as to obtain a unified approach which can be used over an extended range of applications and gear types, the use of local stress-strain concepts for the fatigue design of gears is proposed in this study. These have been widely and successfully used [92,96-101] for crack initiation life prediction for different structural members. Fig. 6.1 shows the essential features of this approach.

In essence, this approach involves first an estimation of local stresses and strains at a critical location as a function of the applied load or nominal stress on a reversal by reversal basis. Then, by assuming that both material deformation response and the fatigue life behaviour at the critical location are identical to those of a reference smooth specimen forced through the same critical location deformation history [81], the damage is computed. Here, the specimen is viewed as a filament of material located in the critical location of a complex structure or component, as shown in Fig. 6.2, and the life of the specimen is equated

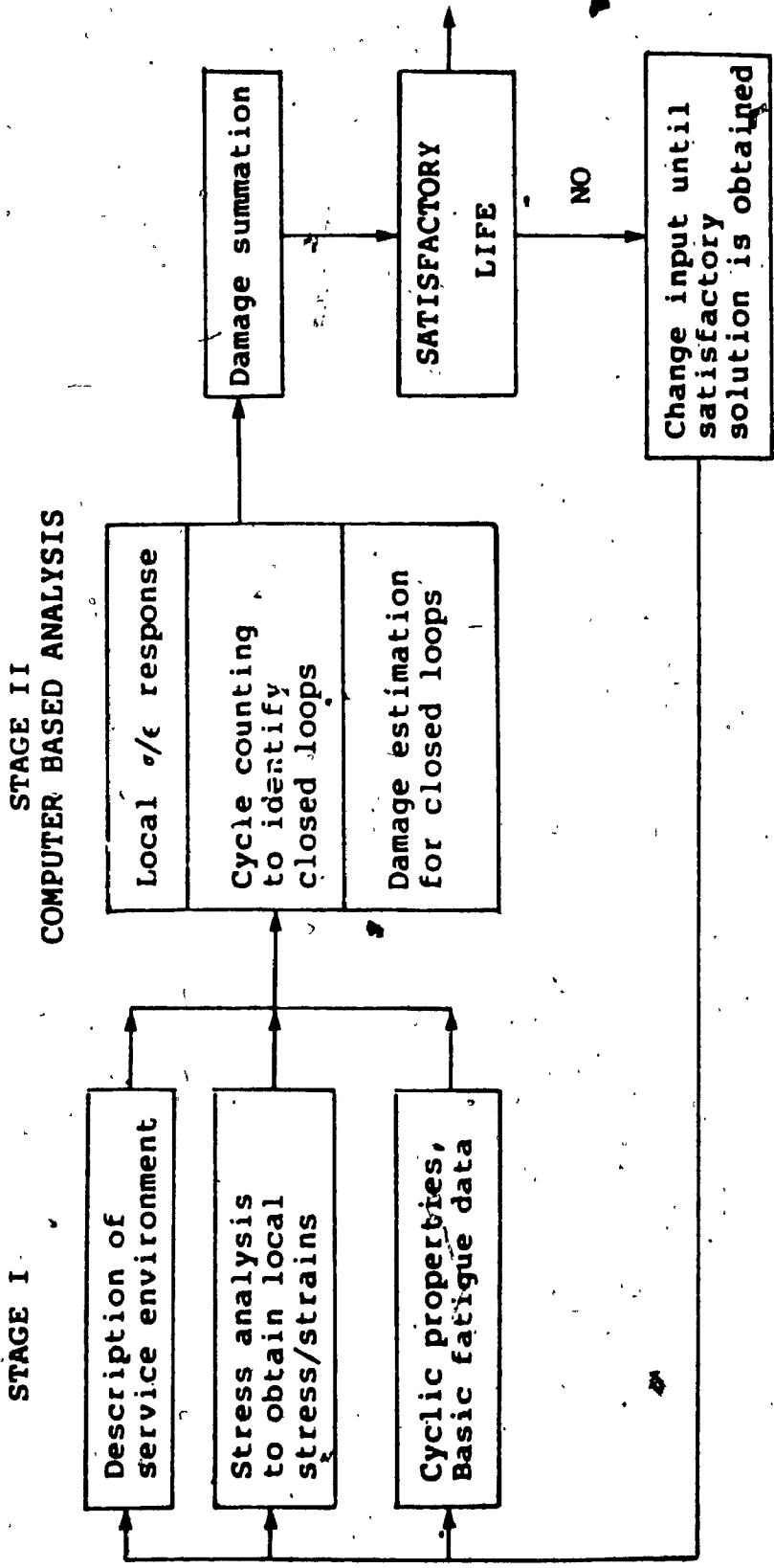


Fig. 6.1: Schematic of local stress-strain fatigue life prediction process

to the life of the component. In the following sections, the first step in the process, namely the computation of stress-strain history at the critical locations within a gear is carried out.

6.2 Computation of the stress-strain history

The knowledge of the stress or strain history at the critical point is essential for the estimation of fatigue life of gears. The conventional gear design methods based on modified Lewis equation, however, provide only a stress index not the stress history. Thus, numerical stress computational procedures such as finite element methods (FEM) [37-45], boundary element methods (BEM) [46-50] and complex potential methods (CPM) [51,52] as well as some analytical formulae [32,59] are increasingly being used for gear tooth stress analysis. Of these, the use of analytical formulae requires less computational effort and they are easy to use. However, the range of applicability of such formulae are restricted usually to only a certain specific type of tooth. On the other hand, the numerical stress analysis procedures such as FEM and BEM are all computation intensive but offer the following advantages:

- a) the ability to model actual gear geometry of both standard and non-standard gears.
- b) adaptability to static as well as dynamic loading conditions,

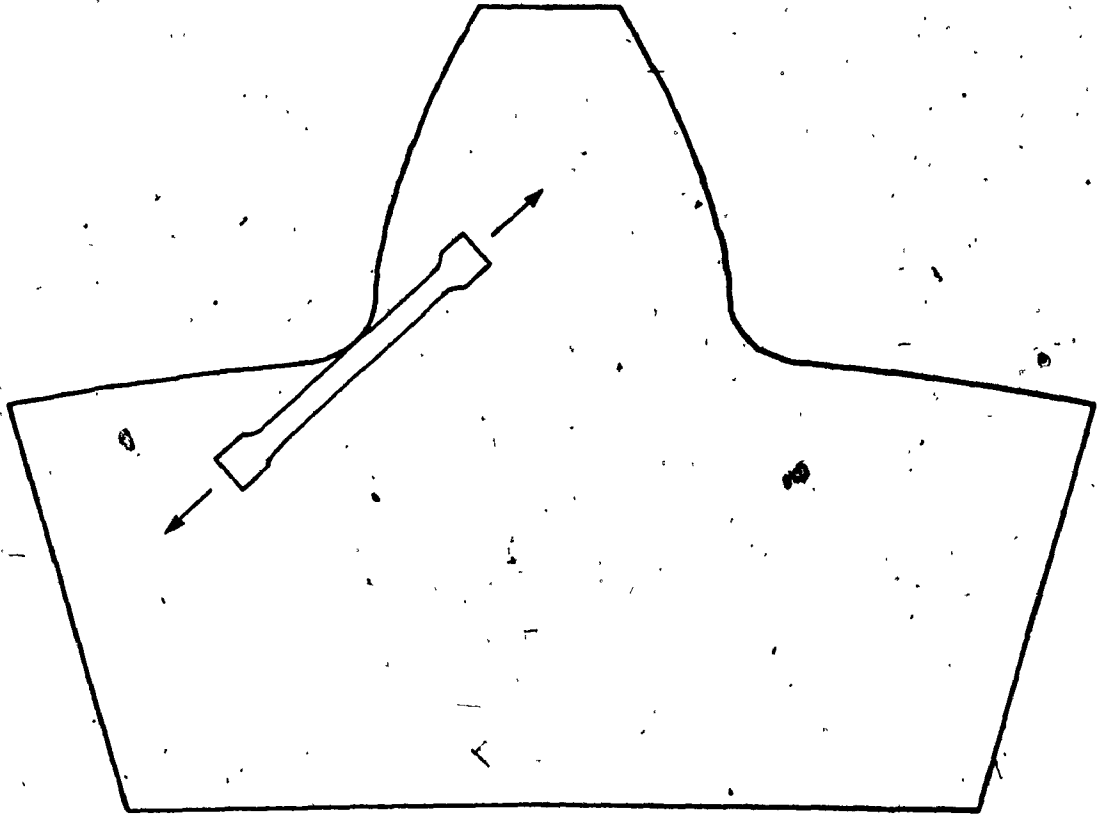


Fig. 6.2: Basis of local stress-strain approach

- c) the flexibility to refine the model easily so as to achieve the required accuracy in stress calculations,
- d) the capacity for inclusion of inelastic material properties as well as variation in these properties within the model.

Also, once sufficient stress data has been generated using the numerical stress analysis procedures, empirical formulae can be derived based on the acquired data-base [45]. In this study, BEM is selected over other methods, based on the observations made in section 2.2.1.

BEM consists in the transformation of the partial differential equation describing the behaviour of the unknown interior and on the boundary of the domain into an integral equation relating only the boundary values, and then finding out the numerical solution of this equation. If the values at internal points are required, they are calculated later from the boundary data. Since all numerical approximations take place only at the boundaries, the dimensionality of the problem is reduced by one. The approach normally consists of the following steps:

- a) The boundary is discretized into a series of elements over which the potential and its normal derivative are assumed to vary according to an interpolation function. The elements could be lines, circular arcs, parabolas, etc..

- b) By the method of collocation, the discretized equation is applied to a number of particular nodes within each element where values of the potential and its normal derivative are associated.
- c) The integrals over each element are carried out by using, in general, a numerical quadrature scheme.
- d) By imposing the prescribed boundary conditions of the problem, a system of linear algebraic equations is obtained. The solution of this system of equations, which can be obtained using direct or iterative methods, produces the remaining boundary data.

In the following sections, the above-listed steps are applied for gear tooth stress analysis. The mathematics of the method are given in Appendix I.

6.2.1 Static Vs Dynamic analysis

Strictly speaking, dynamic analysis should be performed to obtain stress or strain history due to dynamic loads. Dynamic analysis will take care of not only the variation in dynamic load along the contact path but also the speed of travel. Also influence of other dynamic properties such as structural damping can be included. Some work [37,44] on dynamic analysis of gear tooth using FE technique has already been attempted. However, a full dynamic analysis

will require a large amount of computation time and thereby making it impractical for any day to day design use. This is a serious drawback. Instead in this study, a quasi static analysis is utilized for the computation of stress/strain history. This involves discretizing the dynamic load variation along the contact path into a number of finite steps and using the discretized load levels as input to BE analysis at different contact positions.

6.2.2 Boundary element analysis procedure

Broadly the steps involved in the application of BEM are all same as those used in FEM, namely,

- a) construction of a suitable model,
- b) specification of the boundary conditions so as to represent the actual gear under load,
- c) specification of the loading data, namely, the magnitude, direction, and the location of the point of application of the load,
- d) analysis, that is, assembling and solving the system equations,

and

- e) interpretation of the output results.

6.2.3 The boundary element model

The construction of suitable boundary element models involves the selection of proper elements and the discretization of the gear boundary. In this study, simple

line elements with linear interpolation functions are chosen to represent spur gears in plane stress condition. And a specially developed automatic gear mesh generator (AGMG), described in Appendix II, is used for constructing the model based on the input specification, namely, the number of elements required at different parts of the gear boundary and the parameters to define the gear geometry. The generated mesh is then corrected to include the loaded element at the point of load application using the 'user defined element' option in AGMG. Fig. 6.3 shows a boundary element model of gear tooth and the input data required to generate the model. As a compromise between cost and accuracy, usually only the segment of a gear is modelled, exploiting the fact that away from the gear teeth being loaded, the deflections are very small. Here the number of teeth to be modelled is based on the maximum number of teeth in contact during a mesh cycle. That is for gears having contact ratio between 1 and 2, three teeth are modelled and for gear having contact ratio between 2 and 3, five teeth are modelled.

6.2.4 Boundary conditions

Specification of proper boundary conditions is important, since these constraints determine the suitability of the model to represent the actual gear under consideration. In this study, based on the experimental results obtained in a related study [59], two different

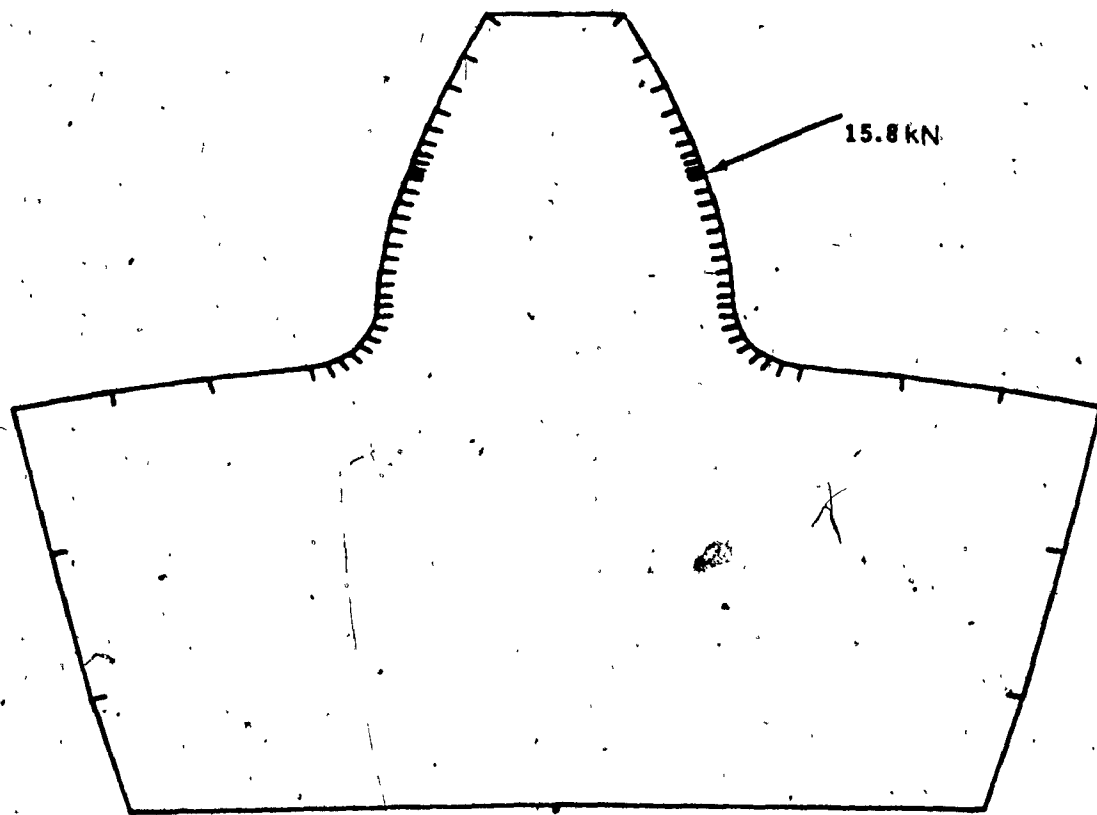


Fig. 6.3: Boundary element model of a spur gear tooth.

schemes are used. For the conventional thick rim or solid blank gears, the deflections along the edges at the side of the gear teeth model and the inner boundary of the model are all set to zero. The inner boundary is formed at the centroid radius of the gear. For thin rim gears, in addition to the deflection of the gear tooth under load the rim also deflects [7,41,43,45]. In order to accommodate these rim deflections the inner boundary is not constrained, as shown in Fig. 6.4.

6.2.5 Loading conditions

The dynamic load simulators described in the previous chapters give the dynamic loads and the friction forces acting on each pair of teeth that come into contact during the mesh cycle as a function of normalized contact position. In order to use these varying loading data for BE analysis, the loading data are discretized along the contact path as shown in Fig. 6.5. Based on these discretized load levels, the equivalent distributed load and the corresponding loaded element size are determined using the frictionless normal contact Hertz equations (2.2). Then employing the 'user defined element' option in AGMG, the loaded element is introduced into the model at the required contact point. This process is then repeated for each discretized load level. The friction forces, if known, are introduced as traction forces on the loaded element. Body forces such as the centrifugal forces are not considered in the present analysis.

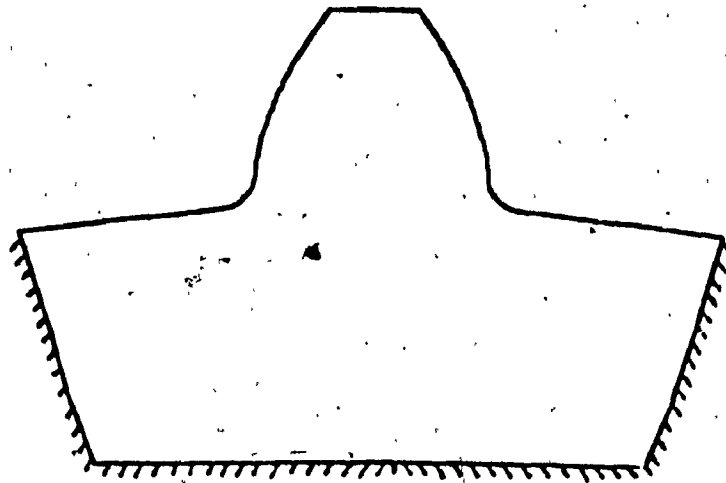
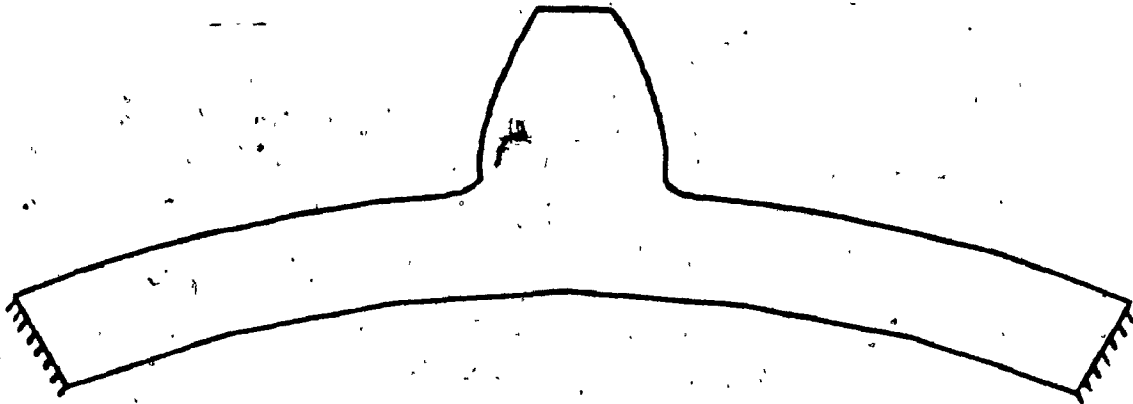


Fig. 6.4: Boundary conditions for thick and thin rim gears

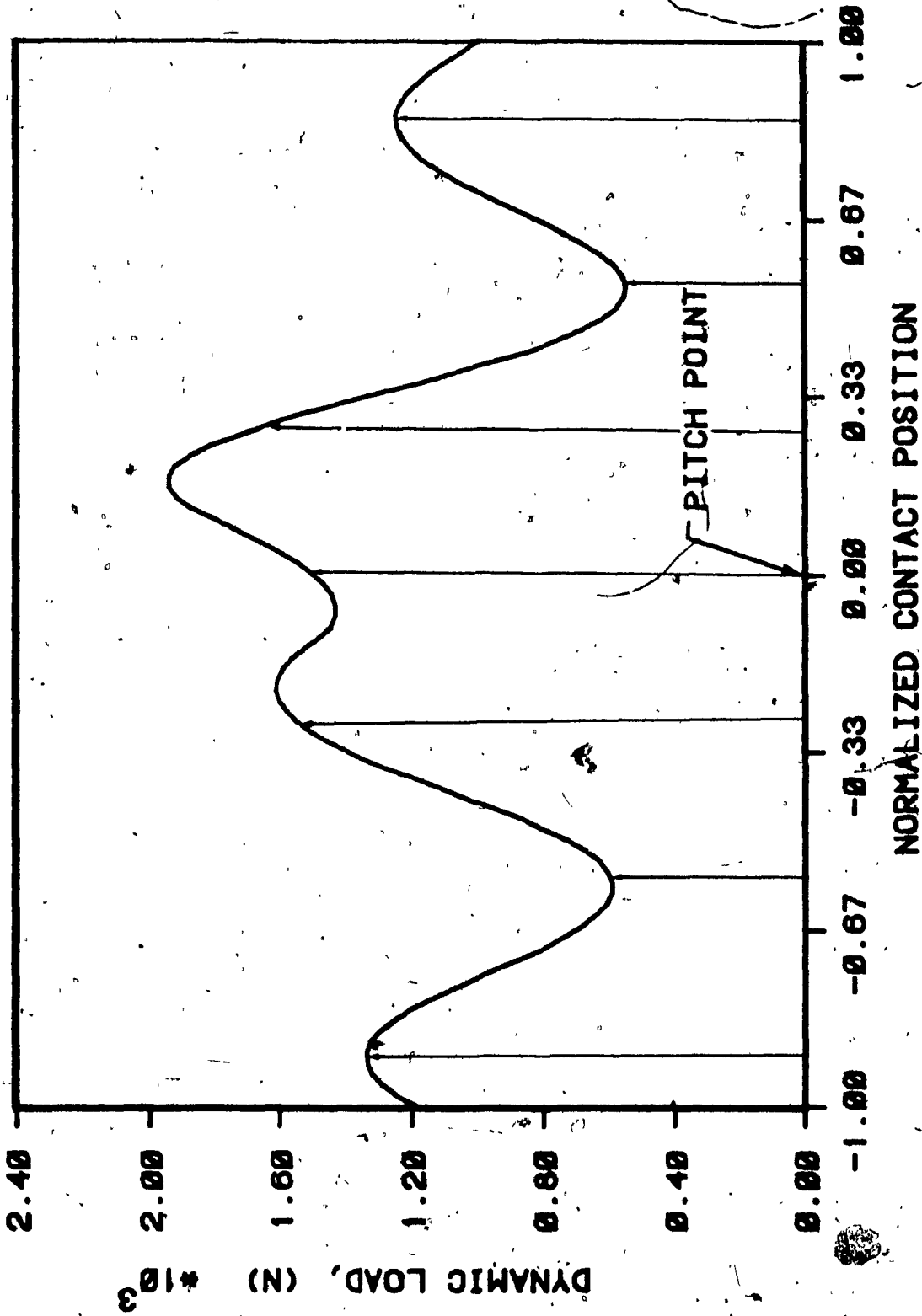
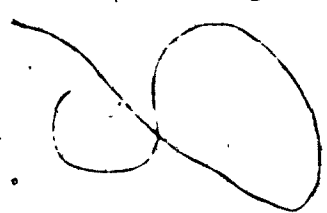


Fig. 6.5: Discretization of dynamic load acting on the tooth

6.2.6 Output from the boundary element analysis

Based on the mathematical formulation given in Appendix I, a fortran program called BE-GEAR was written and implemented on a Vax 11/780 computer. The model data, boundary condition data and loading data prepared according to the preceding steps are then given as input to the program. The output from the program consists of the stress, strain and deflection components at the midpoint of each element on the boundary. It should be noted that in the present investigation only the strain quantities computed by BE-GEAR are used for fatigue damage computations and not the stress quantities. This is due to the fact that the stress quantities computed by BE-GEAR are all based on linear elasticity theory and thus do not take into account the local plasticity which can occur at critical locations. For this reason, in this study, the stress quantities from BE-GEAR, referred to as nominal stresses hereafter, are all used only for validating the BE-GEAR implementation. The stress quantities required for fatigue damage computation are obtained from the cyclic stress-strain relationship [80,82]. Alternatively, a full elasto-plastic analysis could have been carried out using the cyclic stress-strain curve as the governing equation. But such an effort would require more extensive modelling and excessive computation time.



Even though the BE-GEAR program computes the stress/strain quantities at the midpoint of each of the boundary element specified, the points of interest in the present investigation are only a few critical locations on the gear boundary. For bending fatigue analysis, the critical location is considered as the point on the fillet at which the maximum stress occurs. In this study, the Hofer's method [39,59] of finding the weakest section or highly stressed section is employed to locate the critical point in the fillet region. According to this method, the most stressed point on the fillet is the point, the tangent from which makes 30 deg. with the tooth centre line. Fig. 6.6 shows the critical point as defined by the Hofer's method. In reality, however, the critical location is not stationary and varies with the load magnitude and the point of application of the load. Previous numerical [43] and experimental [59] studies on gear tooth stresses of various different types of gears show that the location varies between 24 deg. to 36 deg.. It is claimed [59] that the choice of a constant value of 30 deg. leads to an underestimation of the maximum stress by not more than 5%. Once the critical point has been located, the equivalent strain ϵ' at that point is computed by using the following relationship for each load level applied.

$$\epsilon' = \frac{\sqrt{2}}{3} \sqrt{(\epsilon_1 - \epsilon_2)^2 + (\epsilon_2 - \epsilon_3)^2 + (\epsilon_3 - \epsilon_1)^2} \quad (6.1)$$

where, $\epsilon_{1,2,3}$ are the principal strains at the critical location.

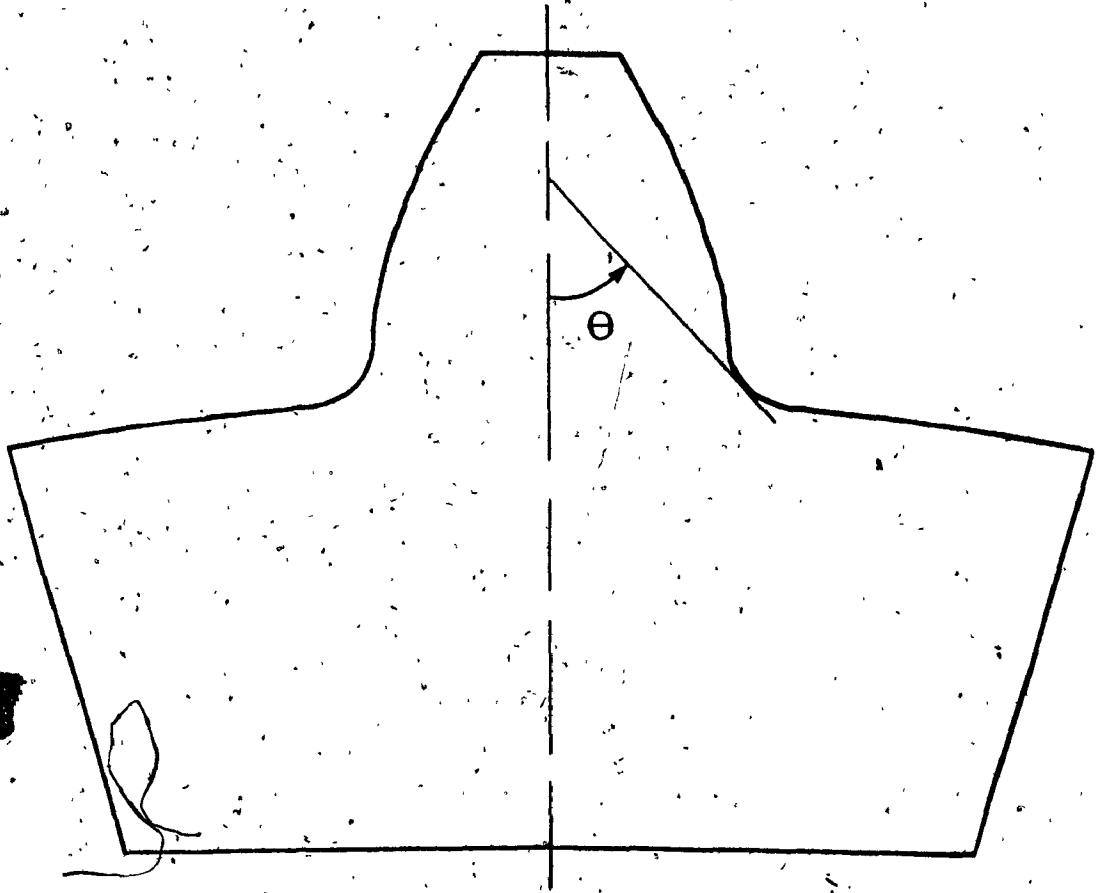


Fig. 6.6: Hofer's angle to define the critical location in the fillet

The equivalent strain quantity, defined as in equation (6.1), cannot be visualized as acting on any specific plane, but has the property that in a state of strain defined by $\epsilon_2 = -\epsilon_1/2$ and $\epsilon_3 = -\epsilon_1/2$, $\epsilon' = \epsilon_1$.

The equivalent strain is used as the controlling variable in this study, since the fatigue damage parameters and failure theories such as S-N diagrams and strain-life diagrams are all developed based on uniaxial constant amplitude loading condition and thus require a single index value to compute fatigue damage. Successful use of the equivalent strain for fatigue damage computation of automotive structural components, and laboratory specimens under multi-axial stressed condition, supports this choice [85,98].

6.2.7 Validation of boundary element results

To check the validity and accuracy of the BE-GEAR results, a comparative study was carried out. In this respect, the results from a related study by Kenedi [59] was used extensively. Kenedi [59] conducted a comprehensive study on gear tooth deflections and stresses in high contact ratio gears using photoelasticity tests, FE analysis, as well as other empirical formulae, thus providing an excellent data-base for validating the BE-GEAR program. Fig. 6.7 shows one such comparison between Kenedi's photoelasticity and FE results and the present BE-GEAR

results for a specific case. As can be seen from this figure, the nominal stress values computed by BE-GEAR agree well with the FE stress values for the entire fillet region. The deviation between the photoelasticity and the numerical stress results was explained by Kenedi as due to the friction that existed in the photoelastic models. In order to check this explanation, frictional forces based on a coefficient of friction value of 0.1 [59] was included in the BE analysis. The results of such a preliminary analysis show that indeed the excessive friction present in photoelasticity models results in reduced stress levels than in actual gear prototypes.

6.3 Construction of duty cycles .

For a gear pair running at constant RPM at steady state conditions, the dynamic load variation, Fig. 6.5, will repeat itself once every mesh cycle, thus resulting in a equivalent strain history, Fig. 6.8, which will also repeat itself once every mesh cycle. Therefore, for a gear pair running at constant speed, the equivalent strain history at that speed can be considered as a typical duty cycle and can be used for computing the fatigue damage and hence the fatigue life in terms of the number of duty cycles.

For the more general case, wherein the gear pair are not running at stationary operating conditions for an extended period of time, the pattern of dynamic load

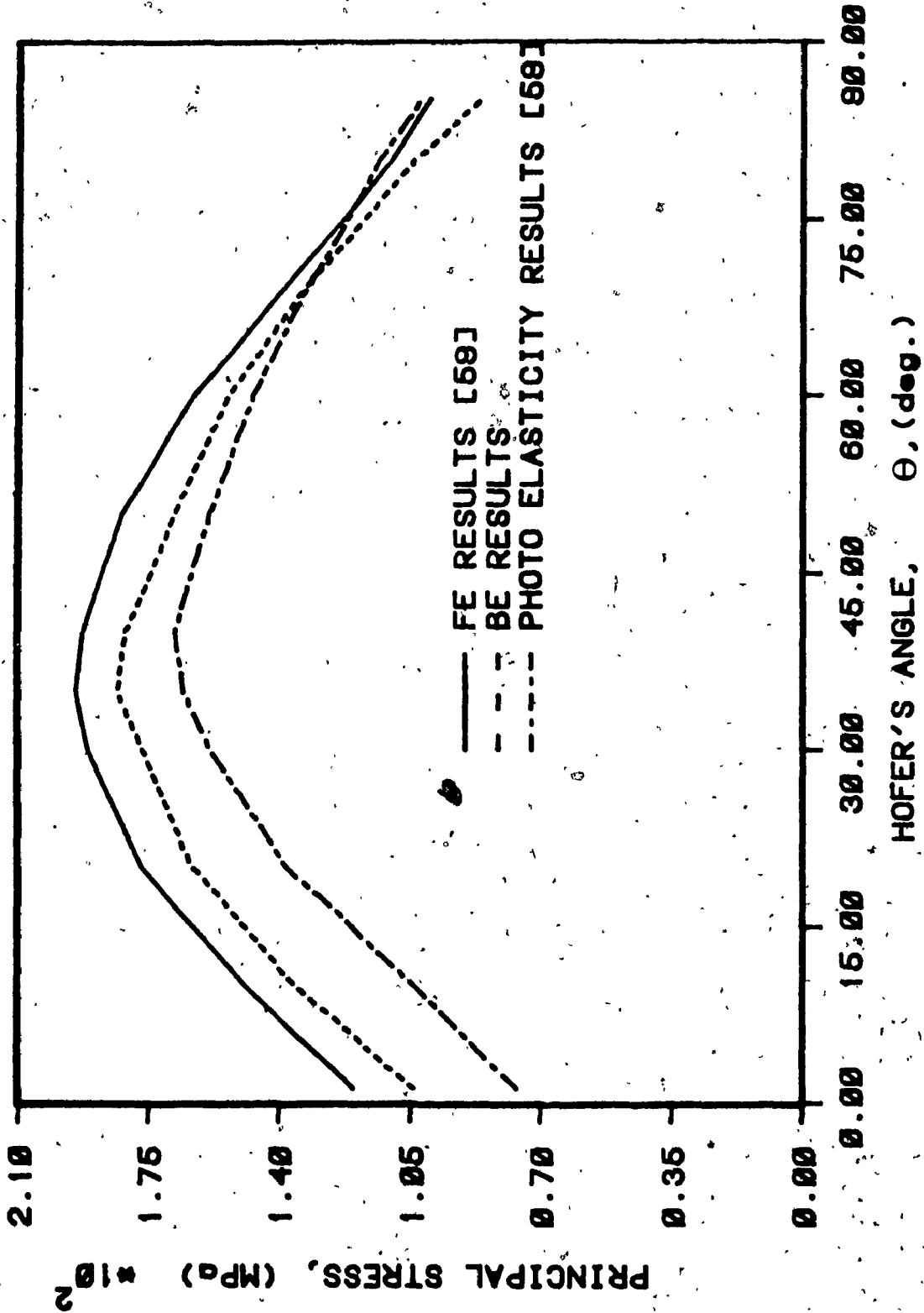


Fig. 6.7: Variation of principal stress values within the fillet region

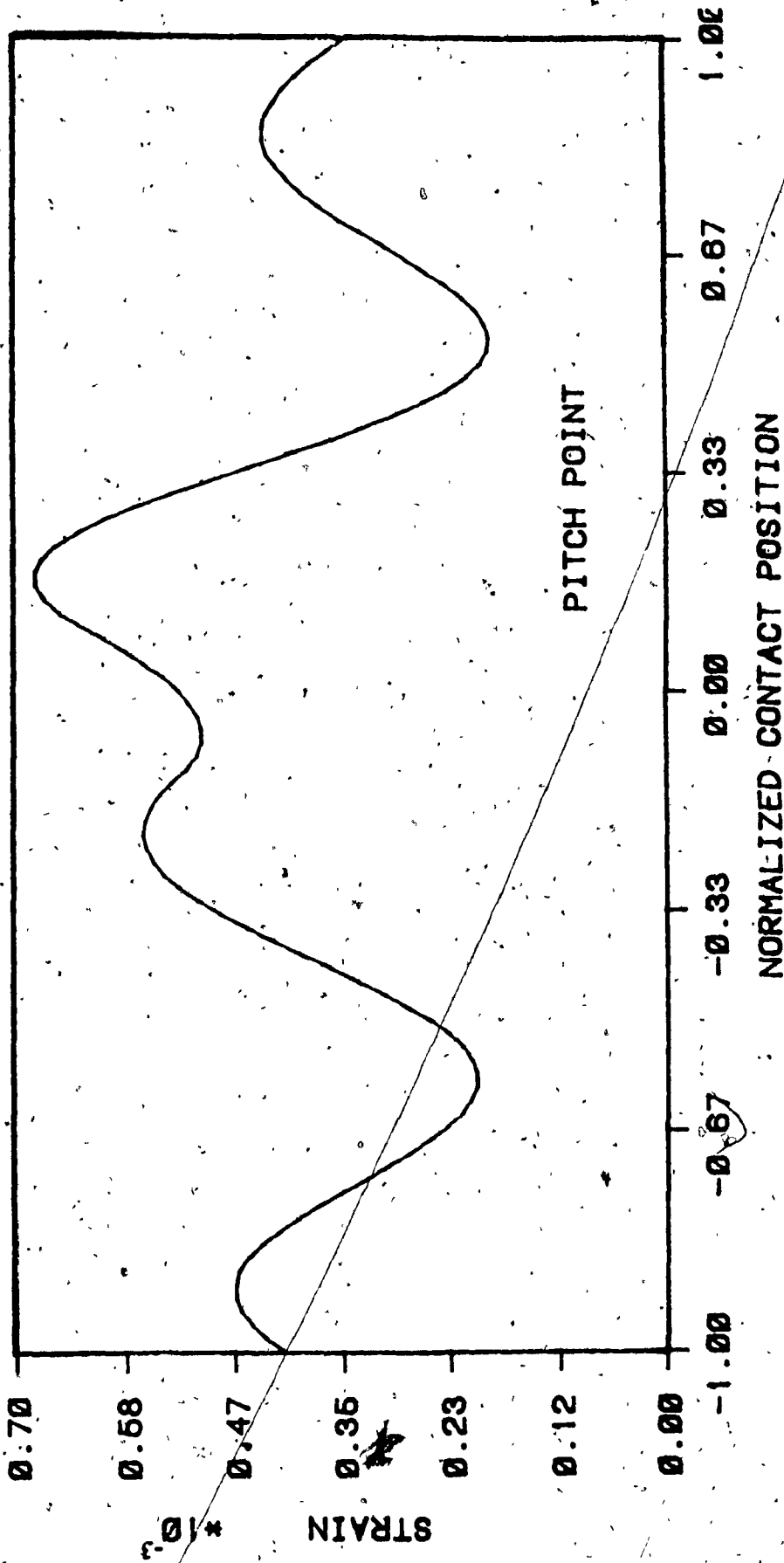


Fig. 6.8: Variation of equivalent strain at the critical location

variation will be constantly changing. But, even in such cases, based on the nature of the application of gears, a typical load history consisting of component load levels arranged in the order of their occurrence can be constructed. While not all inclusive, the constructed load history must represent the typical service condition of the gears to be modelled. Typically such load histories will repeat themselves after certain time intervals.

To obtain the corresponding equivalent strain history using the BE-GEAR program for such long duration load histories will be prohibitively costly. To overcome this problem, it is proposed here that based on the few finite load levels applied at each of the chosen theoretical contact points and the corresponding equivalent strain values at the critical location, non-linear relationship of the form,

$$\epsilon = \frac{W}{d_1} + \left(\frac{W}{d_2}\right)^{\frac{1}{d_3}} \quad (6.2)$$

be constructed. The constants d_1 , d_2 and the exponent d_3 in the equation (6.2) are all chosen to fit the computed data at each theoretical contact position chosen. In this study, ten load levels and ten different contact position are chosen as a compromise between accuracy and cost. Once these non-linear relationships relating the load levels and the equivalent strains has been formulated, then

irrespective of the duration of the load histories, equivalent strain histories can be constructed and thus typical duty cycles can be formulated. Relationships of the form given in equation (6.2) have been used successfully before [96] for analysis of automotive structural components. But in those cases the point of application of the loads were not varying as in the present case.

6.4 Simulation and accumulation of fatigue damage

The work reported in the following sections deals with the stage II of the local stress-strain approach. For this stage, it is assumed that the local strain history is available either as measured strain records or as a result of a stress analysis procedure such as BEM. With this assumption, a computer simulation procedure is developed to model the cyclic stress-strain behaviour of the metals. In the following section, this computer simulation model is explained. For this purpose, a brief introduction of the cyclic behaviour of metals in general is given first.

6.5 Cyclic behaviour of metals

6.5.1 Cyclic stress-strain curve

As mentioned earlier, the local stress-strain approach requires the local stresses and strains prior to performing a cumulative damage evaluation. This requires that the relationships between the cyclic stresses and strains be

defined. The monotonic stress-strain curve used for static load analysis cannot be used for cyclic loadings, since cyclic loading may significantly alter material properties [80]. Either hardening or softening can occur under cyclic loads, depending upon the test condition and the initial state of the material. Hence, the concept of cyclic stress-strain curve was introduced and was defined as the locus of the stable hysteresis loops from several companion tests at different completely reversed constant strain amplitudes [82]. This is illustrated in Fig. 6.9. The curve OABC in Fig. 6.9 gives the cyclic stress-strain curve. Note that this curve gives the relationship between the amplitudes of the stresses and strains.

To obtain a realistic mathematical relationship describing the cyclic stress-strain curve, the total strain range $\Delta\epsilon$ is divided into elastic and plastic components, as,

$$\Delta\epsilon = \Delta\epsilon^e + \Delta\epsilon^p \quad (6.3)$$

or

$$\Delta\epsilon = \frac{\Delta\sigma}{E} + \Delta\epsilon^p \quad (6.4)$$

where,

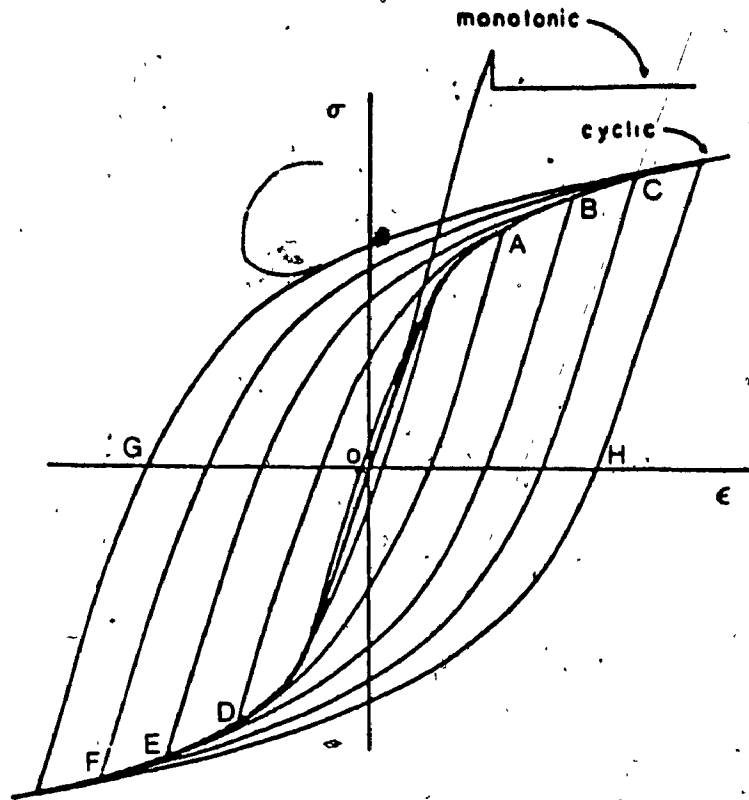


Fig. 6.9: Definition of cyclic stress-strain curve

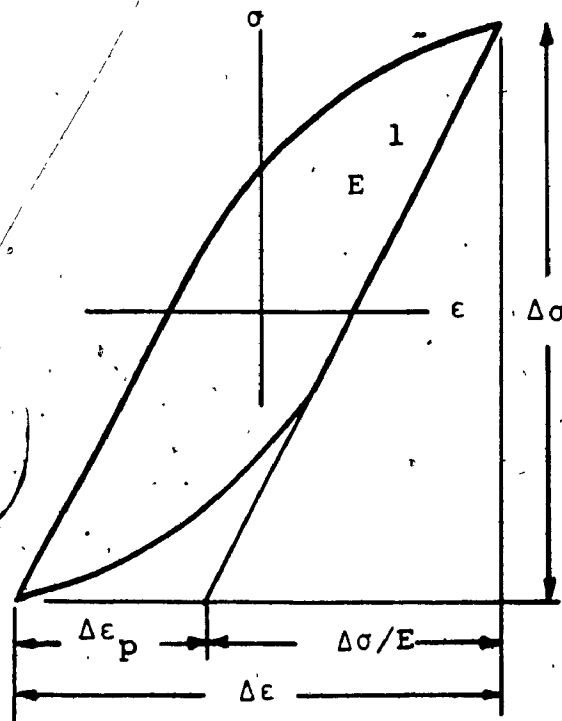


Fig. 6.10: Cyclic stress-strain hysteresis curve

- $\Delta\epsilon^e$ = the elastic strain range
- $\Delta\epsilon^p$ = the plastic strain range
- $\Delta\sigma$ = the stress range
- E = modulus of elasticity

Equation (6.4) can be rewritten in terms of stress and strain amplitudes, as,

$$\epsilon_a = \frac{\sigma_a}{E} + \epsilon_a^p \quad (6.5)$$

where,

$$\epsilon_a^e = \Delta\epsilon^e/2 = \text{the elastic strain amplitude}$$

$$\epsilon_a^p = \Delta\epsilon^p/2 = \text{the plastic strain amplitude}$$

$$\sigma_a = \Delta\sigma/2 = \text{the stress amplitude}$$

On a log-log plot of stress amplitude versus plastic strain amplitude, a straight line usually results, implying a mathematical relationship of the form [80,82,96],

$$\sigma_a = k' (\epsilon_a^p)^{n'} \quad (6.6)$$

where k' and n' are material constants.

Combining equations (6.5) and (6.6), a relationship for total strain can be obtained as,

$$\epsilon_a = \frac{\sigma_a}{E} + \left(\frac{\sigma_a}{k'}\right)^{\frac{1}{n'}} \quad (6.7)$$

The cyclic stress-strain curve OABC in Fig. 6.9 is of this mathematical form. The material constants k' and n' are

defined as cyclic strength coefficient and cyclic strain hardening exponent respectively and are obtained from experiments. These are considered as material properties and the values are reported in literature for different engineering materials [96].

6.5.2 Shape of stress-strain hysteresis loop

It is to be noted that during cyclic loading the material does not follow the cyclic stress-strain curve as a loading path in the sense of a monotonic stress-strain curve. Rather hysteresis loop curves such as CHF and FGC in Fig. 6.9 are formed. This is the most important aspect of cyclic plasticity. In order to truly represent the material deformation, it is necessary to characterize the shape of such hysteresis loop curves.

Fortunately, for most of the engineering materials, the shape of the hysteresis loop curves can be estimated from the cyclic stress-strain curve. This is illustrated in Fig. 6.11, where stable hysteresis loops from Fig. 6.9 are drawn on a shifted axis so that their compressive tips coincide. From the definition of the cyclic stress-strain curve, the tensile tips of loops so plotted must lie on the cyclic stress-strain curve expanded with a scale factor of two. For many engineering materials, this has also been experimentally observed [80,86,87]. Thus, it is reasonable to assume that all stable hysteresis loop traces for a given

material follow a unique curve which may be mathematically described by expanding the cyclic stress-strain curve with a scale factor of two and shifting the origin, [80,96]. Therefore, the loop traces can be expressed as,

$$\frac{\epsilon - \epsilon_r}{2} = \frac{\sigma - \sigma_r}{2E} + \left(\frac{\sigma - \sigma_r}{2k'} \right)^{\frac{1}{n'}} \quad (6.8)$$

where (ϵ, σ) are instantaneous stress and strain, and (ϵ_r, σ_r) are the coordinates of the previous point of strain reversal, such as point F in curve FGC in Fig. 6.9. By appropriate sign changes a similar equation is obtained for hysteresis loop curves during decreasing strain, such as CHF in Fig. 6.9.

$$\frac{\epsilon - \epsilon}{2} = \frac{\sigma - \sigma}{2E} + \left(\frac{\sigma - \sigma}{2k'} \right)^{\frac{1}{n'}} \quad (6.9)$$

Here, (ϵ_r, σ_r) refer to the point C in Fig. 6.9.

There are few engineering metals such as Gray cast iron for which the loop shape approximation just described does not apply. Different relationships has to be formed for these materials.

6.5.3 Memory effect

Another important aspect of material deformation under cyclic loading is the "memory effect". Memory is illustrated in Fig. 6.12 by a portion of a stress strain curve of an engineering material. The specimen was strained

in tension from A to B and then unloaded from B to C and then strained in tension from C through E. In its deformation from point C to D, the material exhibits memory. At point B the metal remembers its previous deformation from A to B and deforms from B to E along the extension of the previous curve A to B. As shown in Fig. 6.13, many reversals of the kind labelled BCD in Fig. 6.12, occur in complex stress-strain histories.

6.5.4 Cycle dependent properties

The third aspect of cyclic plasticity is referred to as cycle dependent hardening or softening. This phenomenon is best illustrated by referring to the test data [92] in Fig. 6.14. copper with three different thermo-mechanical properties was subjected to a constant amplitude of repeated strains. In each case the stress required to enforce this strain amplitude changed from one cycle to the next. The stress on the fully annealed specimen increased rapidly during the first few cycles of the test. This increase in resistance to plastic deformation is cycle dependent hardening. The cold worked copper exhibits cycle dependent softening and the partially annealed copper exhibits mixed behaviour, first hardening and then softening.

As can be seen from the Fig. 6.14 the definition of cyclic stress-strain curve as given earlier will not be valid during hardening or softening. During this process

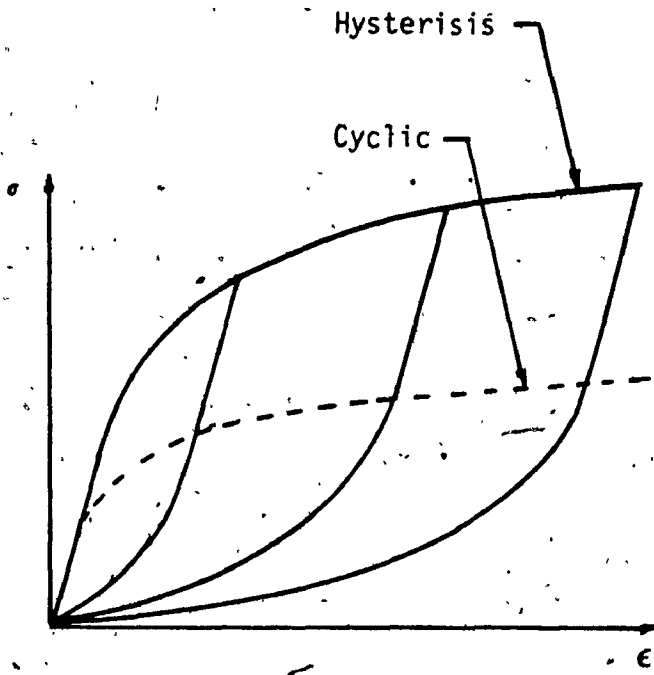


Fig. 6.11: Construction of hysteresis curve

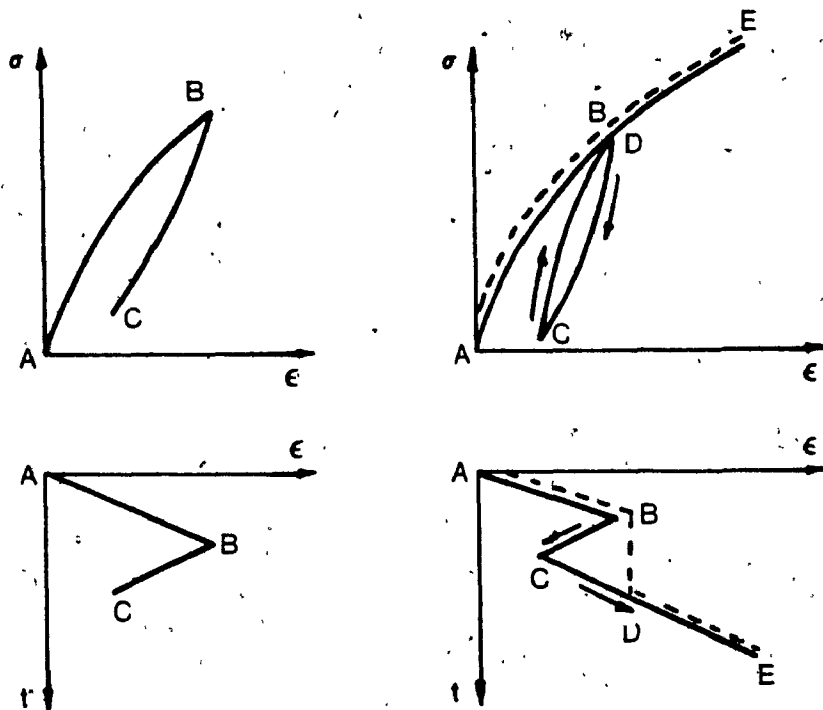


Fig. 6.12: Material memory characteristics

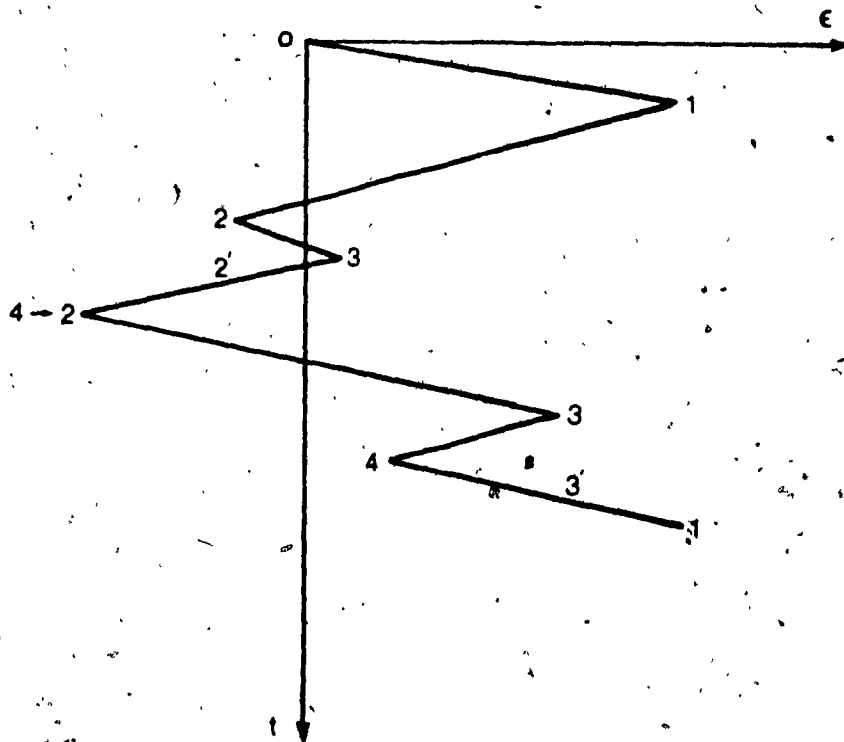
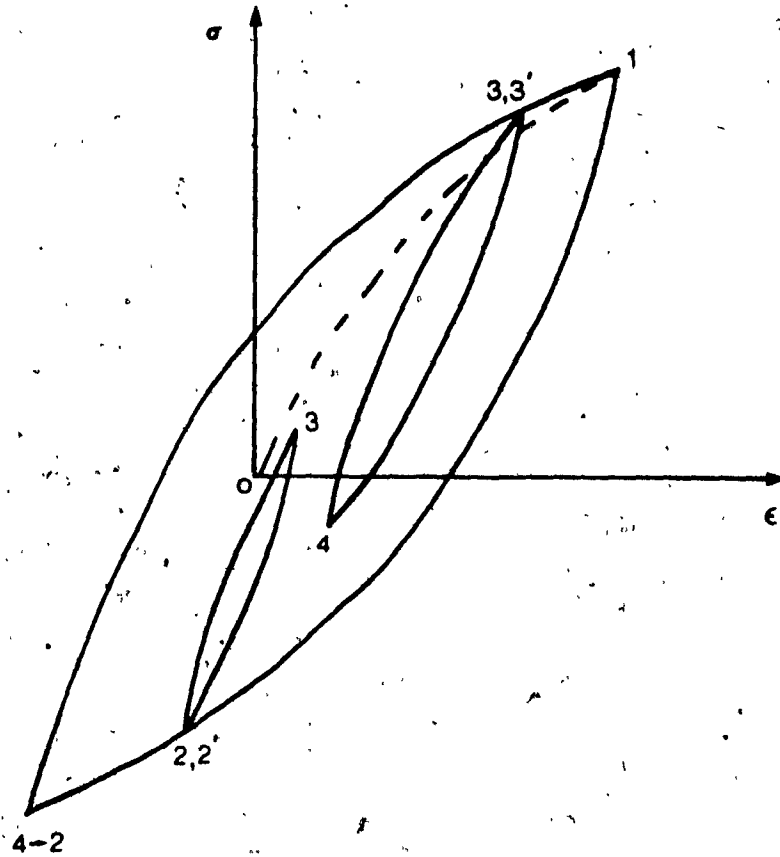


Fig. 6.13: Typical cyclic stress-strain variation corresponding to random strain excursions

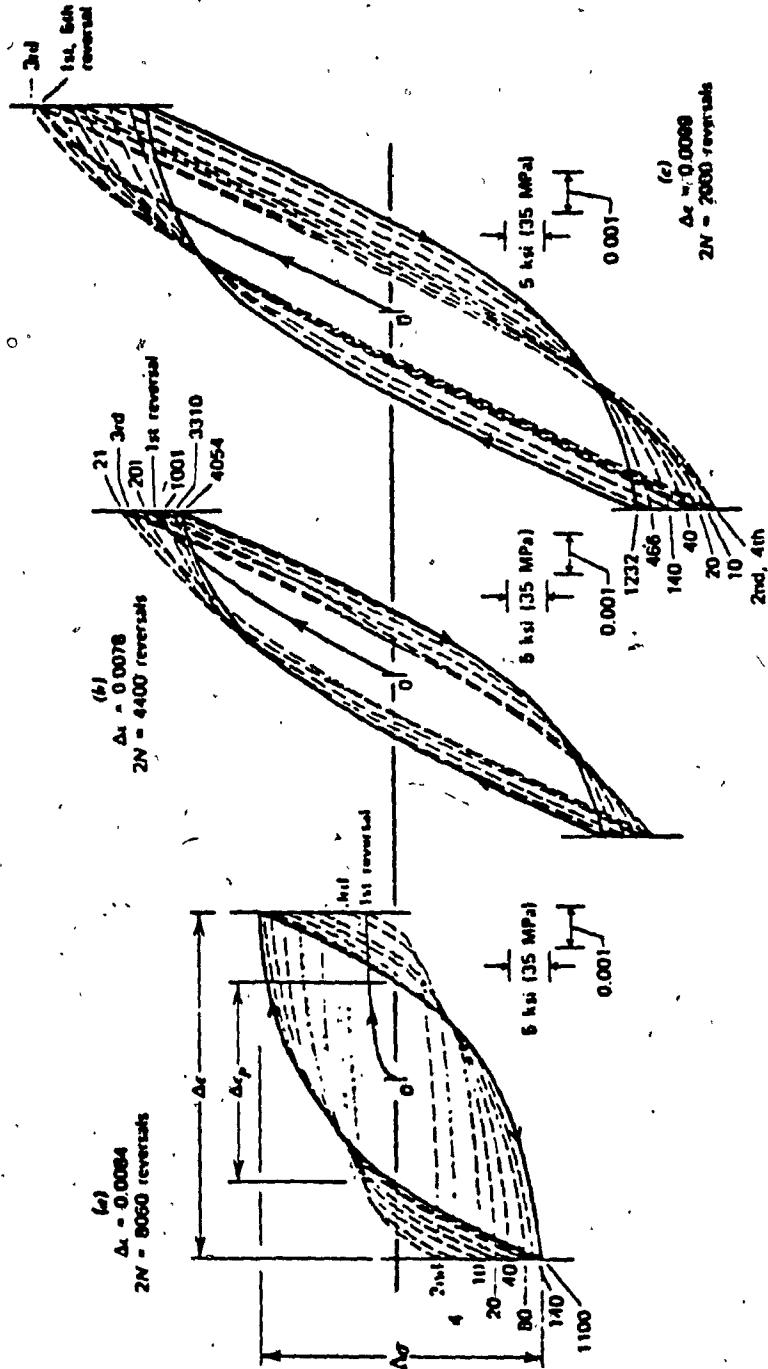


Fig. 6.14: Cyclic Dependent Hardening and Softening [92]
 a) Fully Annealed Copper Showing Cyclic Hardening
 b) Partially Annealed Copper Showing Cyclic Hardening and Softening
 c) Cold-Worked Copper Showing Cyclic Softening.

the material properties are constantly changing. However, hardening and softening are usually transient phenomena which occur at a decreasing rate during the first 20% to 40% of the fatigue life [80,96]. Thus, in most of the fatigue analysis models proposed so far these transient changes in material properties are ignored and the properties that define the steady state of the metal are used throughout the life. The reason for doing so is that the steady state is reached usually in early cycles and the metal remains in the steady state for most of its fatigue life time. In the present analysis too, only the steady state properties are used, because of the above reason. However the cyclic hardening and softening can be introduced into the proposed material model by changing the values of k' and n' for each loop.

6.6 Computer simulation of the material behaviour

One of the earliest models proposed for simulating the material behaviour under cyclic loading is due to Iwan [90]. This rheological model does not include the cyclic hardening or softening behaviour. Later Martin et.al. [91] proposed another model along the same lines including the cyclic hardening and softening phenomena. Their model is composed of springs and frictional sliders. They used a series combination, as shown in Fig. 6.15. By judicious selection and subsequent manipulation of model parameters, their program was made to simulate hysteresis and cycle dependent

changes in the stress-strain response of an aluminum alloy. These models give piecewise linear representation of the cyclic stress-strain curve.

After detailed observations of the responses of several rheological models, Wetzel [92] introduced a set of rules by inductive reasoning, which can describe the responses of these models. These rules can be used directly as a means to simulate the material behaviour of metals. With the introduction of these set of rules, the rheological models were abandoned and most of the current fatigue analysis programs use Wetzel's technique to simulate the material behaviour. A detailed description of Wetzel's technique can be found in references [87,92,96]. Wetzel's technique, as shown in Fig. 6.16, approximates the cyclic stress-strain curve and the hysteresis loop traces by line segments called elements. With this technique, in order to reduce round off errors a large number of elements are required because each element is used to the fullest extent. That is, each element has to be used in full and there is no interpolation to obtain a partial element. And, as the number of elements increase the number of inputs to the simulation program and number of computations within the program increase. In the following sections a new procedure for simulation of material behaviour under cyclic loading is introduced.

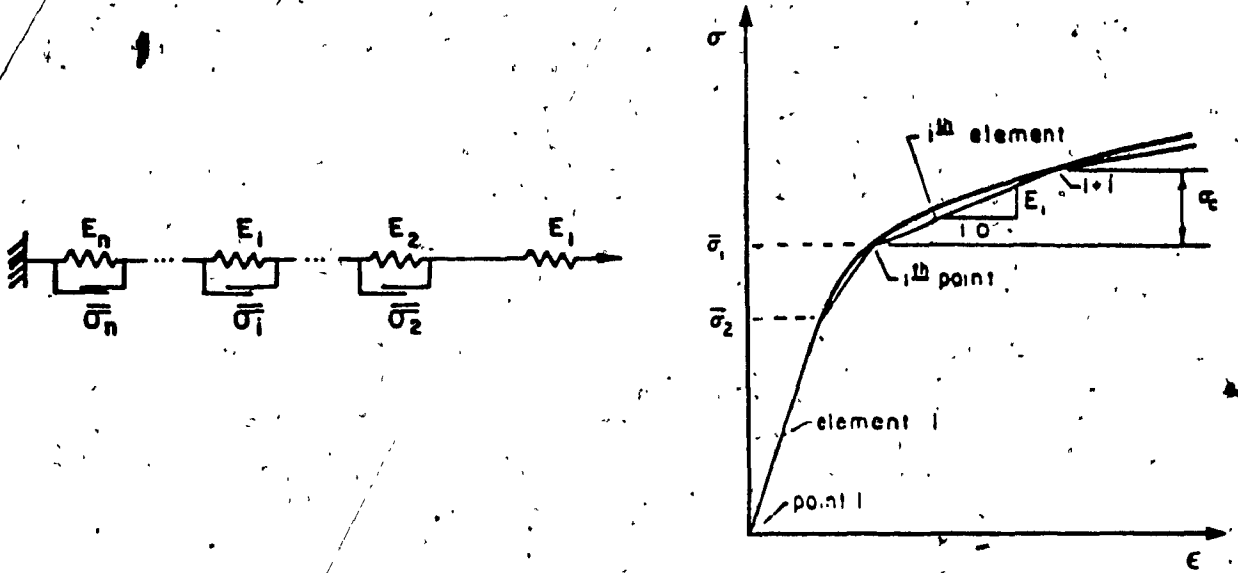


Fig. 6.15: Martin's Rheological Model [91]

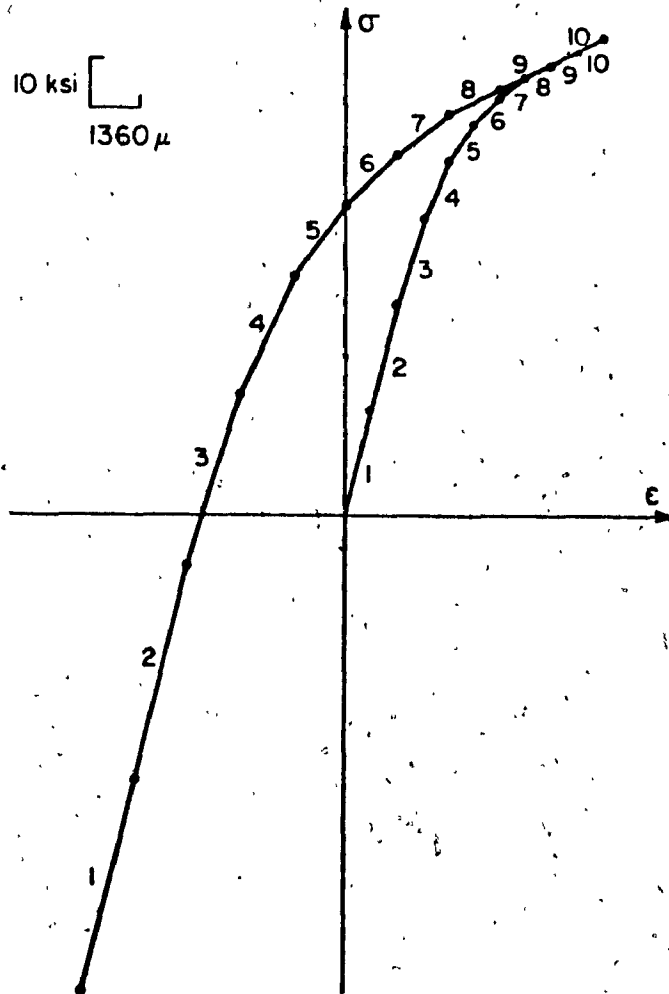


Fig. 6.16: Wetzel's piecewise linear model [92]

6.6.1 Proposed simulation model

In order to avoid these difficulties in the present study the various mathematical relationships, equations (6.7), (6.8) and (6.9), are directly applied in functional form. For this purpose, the equations (6.7), (6.8), and (6.9) are included into the developed computer program as one equation as follows.

$$\text{IN} \frac{\epsilon - \epsilon_r}{k} = \text{IN} \frac{\sigma - \sigma_r}{k E} + \text{IN} \left(\frac{\sigma - \sigma_r}{k k'} \right)^{\frac{1}{n}} \quad (6.10)$$

where,

- IN = index used to denote the slope
- = +1, for increasing strain
- = -1, for decreasing strain
- k = +1 for cyclic strain curve
- = +2 for hysteresis curve

Thus, IN= +1 with k=2 results in equation (6.8), IN= -1 with k=2 results in equation (6.9) and IN= +1 with k=1 results in equation (6.7).

Equation (6.10) can be applied to each hysteresis loop resulting from a irregular strain history, Fig. 6.13, provided (ϵ_r, σ_r) are known for each reversal. Since the shape of the loop curves are known, the stress-strain response can be predicted if it is possible to identify the strain excursions which results in closed loops. This can be easily done using the Rain Flow cycle counting method,

[93-95]. In the present study, however, a new algorithm using the material memory effect described earlier, is introduced to identify the closed loops.

The memory effect of material behaviour can be characterized in a general manner as follows: a) when the strain subsequently reaches a value at which the direction of straining was previously reversed a stress-strain hysteresis loop is closed, and the stress-strain path beyond this point is the same as if the direction of straining had not been reversed. b) once a strain excursion forms a closed loop, this excursion does not affect the subsequent behaviour. In the present computer program for material deformation simulation, these two characteristics of the memory effect and equation (6.10) with appropriate values of k and IN is used to simulate the entire stress-strain response for any strain history.

The simulation starts with the assumption that the loading starts from the unloaded state. The corresponding point (origin) in the stress-strain diagram is designated as 0. Then basically, the simulation procedure involves reading the strain values one by one in sequence, as they occur, into the strain vector E , and checking for loop closure when there are at least three points in the vector E . If there is no closed loop identified between the points present currently in vector E , then more strain points are

read into the vector E until there is a closed loop. Once closed loops are identified the vector E is compressed and reordered by removing those strain points which form the closed loops from the vector E. The corresponding local stress values in vector S are computed using equation (6.10) with appropriate values of k and IN. The reference co-ordinates (ϵ_r, σ_r) for each loop trace are taken to be the preceding points in the strain and stress vectors E and S respectively. Since the point designated as 1 in the stress-strain diagram always lies on the cyclic stress-strain curve, for the stress-strain path 0-1, k is set to unity. Otherwise k is equal to two. The value of the index IN is fixed in the beginning as +1 or -1, depending upon the sign of the first strain value read. Then onwards, the sign of IN is changed every time a new strain value is read. Once all the strain readings are read, the simulation is completed by making the last read strain coordinate equal to the strain coordinate corresponding to the point 1. The logic diagram given in Fig. 6.17 shows the above given procedure in a more organized way. A Fortran program based on the steps described so far is given in Appendix III. The entire procedure can be explained with an example, shown in Fig. 6.13.

In Fig. 6.13, after the first strain coordinate E(1) is read, equation (6.10) is used with IN= +1, k=1 and

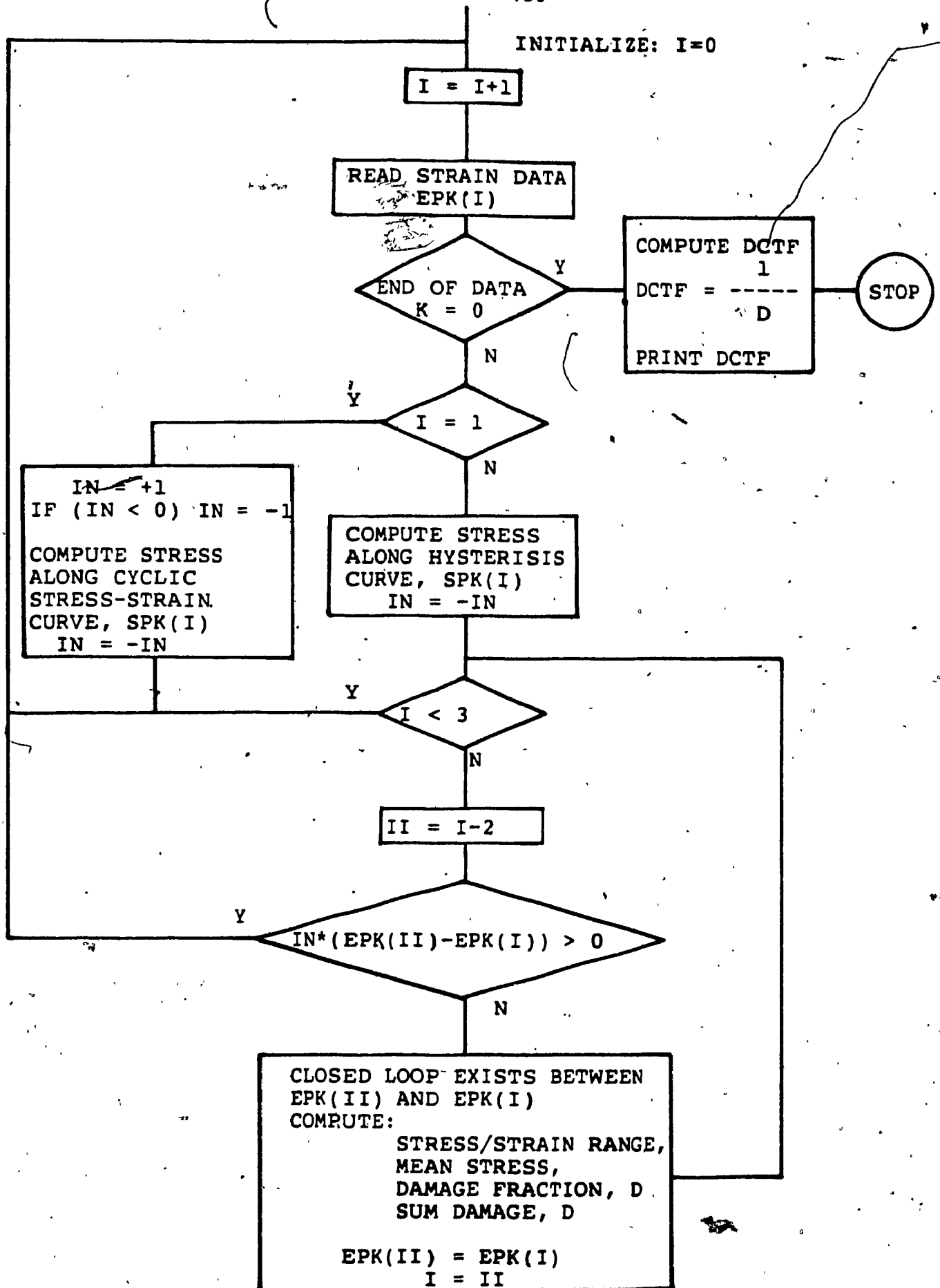


Fig. 6.17: Logic diagram for the fatigue damage simulator

($\epsilon_r=0$, $\sigma_r=0$) for stress-strain path 0-1. Then the next strain value is read into E(2) and the point 2 is reached from point 1 with IN=-1, k=2 and ($\epsilon_r=E(1)$, $\sigma_r=S(1)$). After this the next strain value E(3) is read and since there are now at least three locations in vector E filled, the condition for loop closure is checked for. Since E(3) is greater than E(1), there is a closed loop between 1 and 2.

For damage evaluation, the quantities of interest are only the stress and strain ranges of the loop 1-2-1. Thus, the entire loop 1-2-1 has to be traversed only if a plot of cyclic stress-strain path is needed. This fact is utilized in the present computer program to achieve maximum efficiency. That is, the condition for loop closing at point 1 is checked from point 2 and if it is found that the loop closes at the point 1, then the loop path 2-1 is skipped and the point 3 is reached from point 0. And stress and strain ranges for loop 1-2-1 are computed from the coordinates of points 1 and 2. This "look-ahead" procedure improves the computing efficiency, which is a basic requirement for on line damage evaluation applications. Since, according to the second memory rule stated earlier, once a closed loop is formed it does not have any influence on the subsequent behaviour, the elements E(1), E(2) in vector E and S(1), S(2) in vector S can now be removed. This is achieved by redesignating the last read point 3 as point 1.

Equation (6.10) used in the above procedure is implicit in its variables and hence must be solved by iterative methods. Bisection method with relaxation factor of unity is used here for solving equation (6.10). Convergence is rapid and usually occurs within ten iterations.

For the present problem of gear fatigue damage estimation, knowing the typical duty cycle and the cyclic material properties for the given gear material, the total strain, stress amplitudes and the mean stress level for each of the closed hysteresis loop within the duty cycle can be computed using the steps described in preceding sections.

6.7 Damage computation

Having broken the complex strain history into a series of closed loops, the next step would be to compute the damage corresponding to each of the closed loop. Traditionally, the maximum stress level at the critical location is used as the parameter to measure damage in gear design applications. However, as was pointed out earlier in the section 6.1, the use of maximum stress level without incorporating the alternating and mean components is contrary to the accepted fatigue concepts and is not correct. Furthermore, the use of S-N diagram as the governing criteria excludes the effect of local cyclic plasticity which is considered to be the basis of fatigue

process [80]. To overcome such inadequacies, several new damage parameters have been introduced and experimented with. Nelson [97] conducted an exhaustive evaluation of these parameters in terms of their ability to predict fatigue crack initiation lives of test specimens. He concluded that some of these new damage parameters are found to give better correlation with experimental results than others for some specific types of load histories. In general, none of the parameters resulted in grossly erroneous estimates. That is deviations are found to be within $\pm 3\%$ of the average test life. Such good correlation with experimental results obtained with the test specimens [96,97] as well as actual components [86,98-101] establishes the usefulness of such new damage parameters for crack initiation life predictions. However their usefulness in predicting total fatigue life which consists of both crack initiation life and crack propagation life is yet to be established. Currently, the crack propagation lives are computed with the use of fracture mechanics techniques and added to the crack initiation lives computed with the use of local stress-strain approach. There is no unified approach available yet.

In this study, the total strain amplitude is used as the damage parameter. Equation (6.11) defines the relationship between the total strain amplitude and the life

in number of cycles [80] and Fig. 6.18 shows the same graphically.

$$\epsilon_a = \frac{\sigma'_f}{E} (2 N_f)^{b_1} + \epsilon'_f (2 N_f)^{b_2} \quad (6.11)$$

Here,

- ϵ_a = total local strain amplitude,
- σ'_f = fatigue strength coefficient,
- ϵ'_f = fatigue ductility coefficient,
- E = Young's modulus of elasticity,
- N_f = number of cycles to failure,
- b_1, b_2 = fatigue strength and ductility exponents.

From Fig. 6.18, it can be seen that in low cycle fatigue region the plastic strain component is dominant and in the high cycle fatigue region the elastic strain component is dominant. The commonly used S-N curve can be obtained by multiplying the elastic strain component by a scale factor of E. The effect of mean stresses which are ignored in the current gear fatigue design procedures can be conveniently included into the strain life equation (6.11), such that [80],

$$\epsilon_a = \frac{\sigma'_f - \sigma_0}{E} (2 N_f)^{b_1} + \epsilon'_f (2 N_f)^{b_2} \quad (6.12)$$

where, σ_0 is the mean stress. Substituting the total strain amplitude, and the mean stress level computed for each of the identified closed loops into the equation (6.12), the

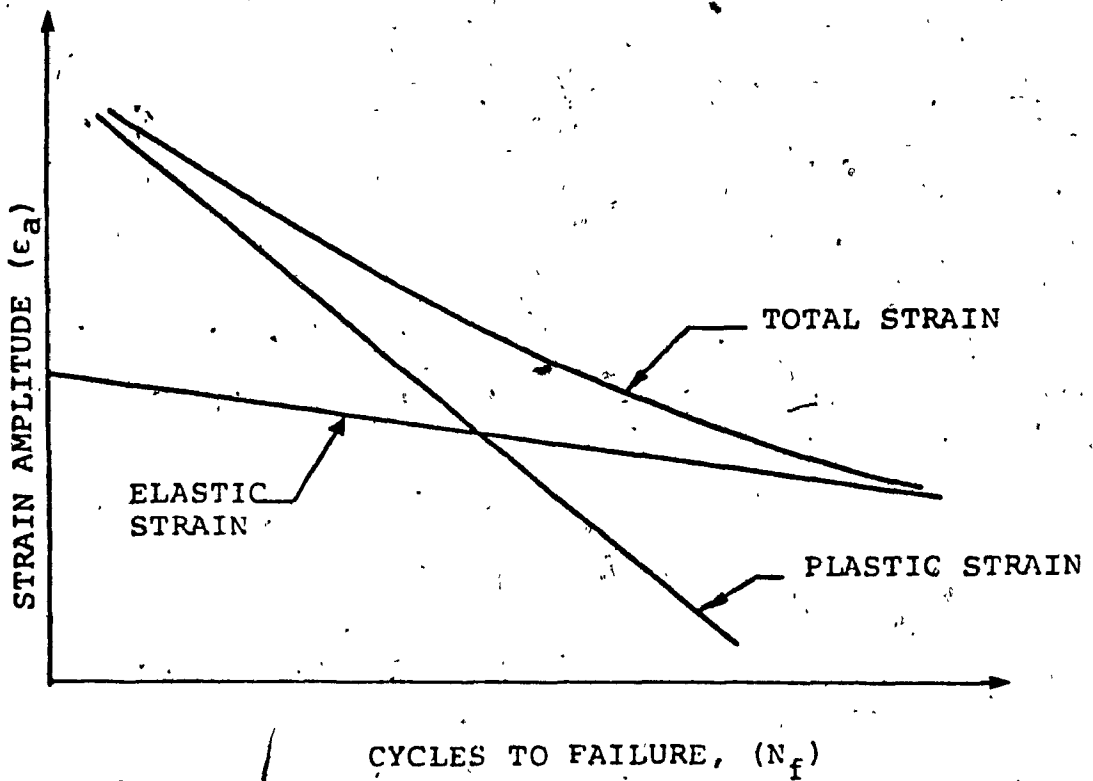


Fig. 6.18: Strain-life characteristics

damage fraction, $D_i = 1/N_f$, associated with each of closed loops can be solved for. And the total damage D occurred within one duty cycle can be computed by summing up the damage fractions of all the loops according to a chosen cumulative damage model.

6.8 Damage accumulation and life estimation

A number of cumulative damage models ranging from the simple, linear Miner's rule [105] to more mathematically complex procedures are available in the literature. Of these, the more complex models such as those reviewed in [97] are mainly of academic interest only since there is either little or no experimental evidence to establish their usefulness. The simpler models, which are usually obtained with the refinement of the Miner's rule are found to give better estimate of fatigue damage accumulation in some specific cases. But, in general none is found to give a better estimate than the simple Miner's rule and hence the Miner's rule is widely used in practice. According to this rule, the component is assumed to have failed when the total cumulative damage is greater than or equal to unity.

That is,

$$D = \sum_{i=1}^n D_i \geq 1 \quad (6.14)$$

where,

D_i = damage fraction due to the i^{th} closed loop
in the duty cycle
 D = accumulated damage

The cumulative fatigue life of the gear under consideration can then be obtained in terms of number of duty cycles to failure, by taking the inverse of the cumulative damage fractions, such that,

$$DCTF = \frac{1}{D} \quad (6.15)$$

where, DCTF denotes the number of duty cycles to failure.

6.9 Summary

In this chapter, a computer method for gear fatigue life prediction based on local stress-strain concepts is introduced. This method of life prediction is significantly more accurate than methods typically used in conventional gear design practices. The superiority of the computer method results from the fact that it evaluates the events that are unique to a complex strain history in a rational way. Also in contrast to the current gear design methods the mean and alternating components of the loading are included in the analysis.

Specifically, the use of BE analysis to obtain strain history at the critical location in the fillet region of the loaded tooth is explained. First, the steps involved in the

application of BEM are stated and applied to gear tooth stress analysis problem. Secondly, the formulation and implementation of the BE-GEAR program is validated by comparing the nominal stress results from BE-GEAR program with FE and photoelasticity test results. Thirdly, the construction of a typical duty cycle is discussed and the use of non-linear relationships of the form of equation (6.2) is proposed to reduce the computations involved in using BEM extensively.

It should be noted that the BEM is used in this study; mainly because of the advantages it offers over FEM by the way of reduction in dimensionality. Any other FE program, either inhouse or commercially available programs can also be used effectively, if a suitable FE model of the gear to be analysed has been created.

Also a fatigue damage computation procedure, with the following features, is presented.

- a) The functional relationships describing stress and strain are used directly without further approximation of the stress-strain equations. This improves the accuracy and the numerical stability.
- b) The present program breaks any complex strain waveform into individual cycles (closed hysteresis loops), so that constant loading data

can be used for damage evaluation.

- c) The cycle counting procedure used in the presented program is more efficient than the other [93-97] counting procedures, since the number of decision points used to identify closed loops as well as the number of arrays required are reduced.
- d) The present program reads the strain peaks and valleys as they occur, in contrast to the existing programs which require the strain history to be rearranged to start at the highest value. This feature, in addition to the conciseness of the presented program makes it best suited for microprocessor based on-line damage evaluation and monitoring applications.
- f) Also, since the closed loops are identified as they occur, any loading order sensitive damage parameter and accumulation model can easily be incorporated.

CHAPTER 7

EXTENSION TO HELICAL AND OTHER TYPES OF CYLINDRICAL GEARS

7.1 General

Involute spur gears have been used extensively so far in this thesis to develop the dynamic load and fatigue damage estimation methodologies. However, the presented methodologies are not restricted to this class of gears alone. The use of matrix equations of motion and solution procedures as well as the use of numerical stress and deflection analysis procedures such as BEM, makes the presented procedures amenable to model and simulate cylindrical gears with different profiles and kinematics. In this respect, the matrix equations of motion and solution procedures described in the chapters 3 to 5 need not be altered for different types of gears. Only the size of the matrices and the composition of the matrices will change. In this chapter, extension of the presented simulation methodologies to helical gear dynamics is presented in detail first, and then the possible application to non-standard cylindrical gears is discussed.

7.2 Helical gear dynamics

The major characteristics that distinguish the helical gear dynamics from spur gear dynamics are the simultaneous surface contact and the oblique nature of the normal load acting on the teeth. These factors cause the contact

condition and the loading on the gear to be three dimensional, resulting in additional degrees of freedom and hence additional equations of motion. As a first approximation, the earlier studies on helical gear dynamics neglected the additional degrees of freedom and used virtual spur gears in the place of given helical gears. Recently, however, a number of coupled lateral-torsional models [25,29] have been introduced to study helical gear dynamics in detail. Of these, the model by Kucukay [29] can be considered to be complete, since it incorporates the effects of additional degrees of freedom as well as the variable mesh stiffness characteristics, the tooth errors, and non-linear characteristics introduced by backlash and load dependent contact ratio. The only draw back of Kucukay's model would be the assumption of Hertz contact theory to estimate the tooth stiffness characteristics. In the following subsections, the additional steps required to extend the presented simulators to simulate helical gears are presented in detail.

7.2.1 Variable mesh stiffness

In principle, the variable mesh stiffness evaluation procedure for helical gear is the same as the procedure described in subsection 2.2.2 for the spur gears. But, in practice, more elaborate steps are needed to compute helical gear tooth stiffness. This due to the fact that, unlike in spur gears, the radius of curvature at the contact is not a

constant. So, the Hertz contact theory, and hence the equations (2.3)' and (2.4) are no longer applicable. To solve such a three dimensional contact problem, normally iterative techniques [50] are employed. Using the iterative techniques the loaded boundary element, dimension and the distributed load on the element are first estimated. Based on the computed load and specified boundary conditions, the deflection δ in the direction of the normal load W is computed using BEM. The tooth compliances C_p , C_g and the tooth pair compliance C_{pg} can then be computed with the use of equations (2.5) and (2.6). From which the tooth pair stiffness in the normal direction $k_{pg,j}$ can be obtained.

That is,

$$k_{pg,j} = \frac{1}{C_{pg,j}} \quad (7.1)$$

$$k_{pg}(t) = \sum_{j=1}^n k_{pg,j} \quad (7.2)$$

7.2.2 Mathematical model

Neglecting the effect of friction between the teeth, the equations of motion for the configured helical gear system shown in Fig. 7.1, can be derived using the standard procedures as given below.

Equations of motion

Torsional mode:

$$J_p \ddot{\theta}_p + W_d R_{bp} = T_p \quad (7.3)$$

$$J_g \ddot{\theta}_g - W_d R_{bg} = -T_g = -n T_p \quad (7.4)$$

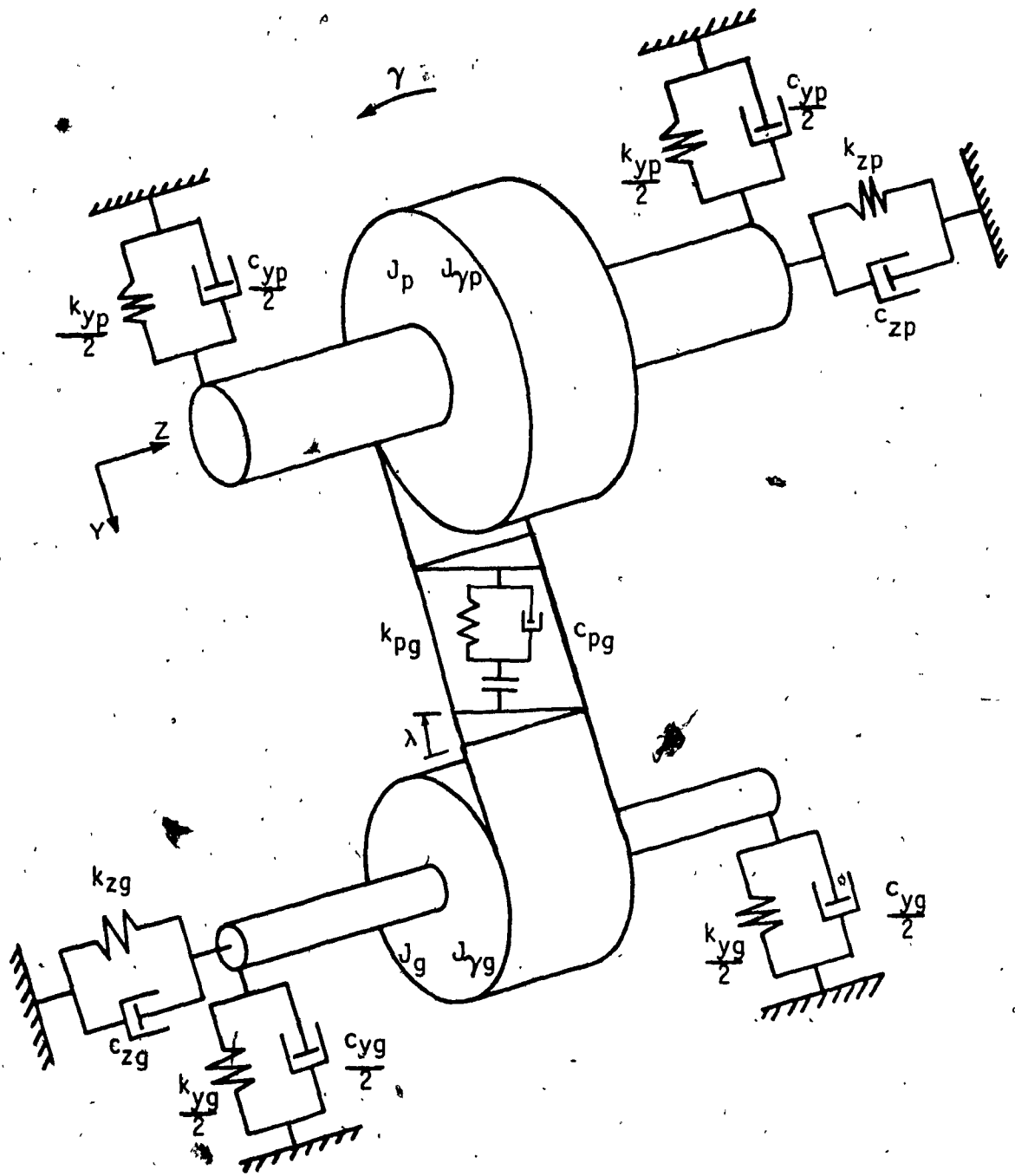


Fig. 7.1: Helical gear set model

Lateral mode:

$$m_p \ddot{x}_p + c_{xp} \dot{x}_p + k_{xp} x_p + W_d \sin(\alpha - \beta) = 0 \quad (7.5)$$

$$m_p \ddot{y}_p + c_{yp} \dot{y}_p + k_{yp} y_p + W_d \cos(\alpha - \beta) = 0 \quad (7.6)$$

$$m_g \ddot{x}_g + c_{xg} \dot{x}_g + k_{xg} x_g - W_d \sin(\alpha - \beta) = 0 \quad (7.7)$$

$$m_g \ddot{y}_g + c_{yg} \dot{y}_g + k_{yg} y_g - W_d \cos(\alpha - \beta) = 0 \quad (7.8)$$

Axial mode:

$$m_p \ddot{z}_p + c_{zp} \dot{z}_p + k_{zp} z_p + W_d \tan(\lambda) = 0 \quad (7.9)$$

$$m_g \ddot{z}_g + c_{zg} \dot{z}_g + k_{zg} z_g - W_d \tan(\lambda) = 0 \quad (7.10)$$

Tipping mode:

$$J_{\gamma p} \ddot{\gamma}_p - W_d \tan(\lambda) R_{\gamma p} = 0 \quad (7.11)$$

$$J_{\gamma g} \ddot{\gamma}_g + W_d \tan(\lambda) R_{\gamma g} = 0 \quad (7.12)$$

Here,

- J = polar moment of inertia in torsional mode,
- J_γ = polar moment of inertia in tipping mode,
- m = mass,
- c_x = damping coefficient of the bearing along X direction,

- k_x = stiffness of the bearing along X direction,
- c_y = damping coefficient of the bearing along Y direction,
- k_y = stiffness of the bearing along Y direction,
- c_z = damping coefficient of the bearing along Z direction,
- k_z = stiffness of the bearing along Z direction,
- c_γ = damping coefficient of the gear in the tipping mode,
- k_γ = stiffness of the gear in the tipping mode,
- θ = torsional displacement,
- γ = angular displacement about the X axis,
- x = displacement along X direction,
- y = displacement along Y direction,
- z = displacement along Z direction,
- T = external torque applied,
- n = gear ratio,
- R_b = base circle radius,
- R = radius of the tipping moment,
- α = pressure angle,
- β = angle used to define the relative location of shafts,
- λ = helix angle on the base cylinder shown in Fig. 7.1, and defined in equation (7.17);

and the subscripts p and g are used to denote the pinion and gear quantities respectively.

With reference to the backlash characteristic curve shown in Fig. 2.7, the dynamic load W_d along the plane of action will be,

$$W_d = \frac{1}{\cos^2(\lambda)} [c_{pg}(t) \dot{u} + k_{pg}(t) \cdot (u+e)] \quad (7.13)$$

for $-BL < (u+e) < 0$,

$$W_d = 0 \quad (7.14)$$

for $(u+e) < -BL$,

$$W_d = \frac{1}{\cos^2(\lambda)} [c_{pg}(t) \dot{u} + k_{pg}(t) \cdot (u+e+BL)] \quad (7.15)$$

where the displacement along the plane of action u , is

$$u = R_{bp} \theta_p - R_{bg} \theta_g + (x_p - x_g) \sin(\alpha - \beta) + (y_p - y_g) \cos(\alpha - \beta) + (r_p - r_g + R_{\gamma p} \gamma_p - R_{\gamma g} \gamma_g) \tan(\lambda) \quad (7.16)$$

with,

$$\tan(\lambda) = \tan(\lambda_0) \cos(\alpha) \quad (7.17)$$

Here,

- λ_0 = helix angle,
- α = pressure angle,
- e = gear transmission error along the line of action

BL = backlash

j = index denoting the number of pairs of teeth in mesh at any given time.

Here the variable mesh stiffness $k_{pg,j}(t)$ is computed as described in the preceding section. And $c_{pg}(t)$ is expressed in terms of the critical damping ratio, the variable mesh stiffness $k_{pg}(t)$ and the equivalent moment of inertia J_e , as in equation (3.15).

By choosing the state vector v as,

$$v = \{ \theta_p, \theta_g, x_p, x_g, y_p, y_g, \dot{x}_p, \dot{x}_g, \dot{y}_p, \dot{y}_g, u_p, u_g, \dot{x}_p, \dot{x}_g, \dot{y}_p, \dot{y}_g, \dot{x}_p, \dot{x}_g, \dot{y}_p, \dot{y}_g \}^T \quad (7.18)$$

the system equations can be rewritten in terms of the state vector v as,

$$\dot{v}(t) = A(t) v(t) + b(t) \quad (7.19)$$

where,

$$A(t) = \begin{bmatrix} 0 & I \\ -K(t) & -C(t) \end{bmatrix} \quad (7.20)$$

and

$$b(t) = \begin{bmatrix} 0 \\ f(t) \end{bmatrix} \quad (7.21)$$

$$f(t) = \{ T_p, -T_g, 0, 0, 0, 0, 0, 0, 0, 0 \}^T - k_{pg}(t) \left(e \pm \frac{BL}{2} \right) u_2 \quad (7.22)$$

Once the equations of motion (7.1) to (7.12) are written in the state-space form as equation (7.19), then the solution procedure described in section 3.3 can be directly applied to solve for the response and hence the dynamic load along the plane of action $W_d(t)$. The resulting dynamic load in the direction normal to the tooth flank can then be obtained from the following relation.

$$W_{dn} = \frac{W_d}{\cos(\lambda)} \quad (7.23)$$

Letting λ equal to zero in the above equations, and neglecting the additional degrees of freedom z and γ , will reproduce the spur gear simulation models explained in chapters 3 to 5.

The stochastic model for helical gears can be constructed by combining equation (7.19) with the shaping filter equation (4.1). The mean and covariance propagation equations can then be formed as described in section 4.2.2 and solved for. Similarly, using the modelling procedure described in chapter 5, based on the additional equations of motion (7.9) to (7.12), the discrete-time transfer matrix for helical gear pair module can be formulated. Due to the additional degrees of freedom introduced, the state vector size and the transfer matrix size will increase. However, the solution procedure will remain the same.

7.3 Extension to other types of cylindrical gears

In addition to the involute spur and helical gears, which are the most widely used in industrial applications, a number of other types of cylindrical gears such as harmonic drives, circular profile gears, non-circular gears, etc. are used in special applications. Conceptually, the presented gear dynamic load estimation and fatigue damage estimation methodologies can be easily applied to all the different types of cylindrical gears without any change. In this respect, the modelling flexibility of the BEM and the presented matrix solution procedures become very useful. The said versatility of the presented methodologies can be easily seen by taking a closer look at the input information required for simulation.

The information required as input to the dynamic load and fatigue damage simulators described so far can be classified into the following categories.

1. Gear system configuration: gear type, gear tooth type, kinematic relations of the gear pair and the dimensions of the system components.
2. Operating conditions: gear ratio, operating speed, applied torque, transmission error information, backlash, etc.
3. Material properties: both monotonic and cyclic properties of gear materials and other system component materials.

and

4. Variable mesh stiffness characteristics.

Of these, the variable mesh stiffness characteristic is the only quantity which may not be readily available for different cases considered. However, this missing information can be easily generated with the use of BEM. Following the procedures described earlier in sections 2.2.2 and 7.2.1 for spur and helical gears, the gear pair stiffness of the gear type considered can be computed. Then, the variable mesh stiffness characteristics for the given gear can be formulated by direct summation of the individual tooth pair stiffnesses for the number of tooth pairs in contact at any given time. Once the variable mesh stiffness characteristic is obtained, the equations of motions can then be set up in state-space form such as equations (3.18) and (7.19) and solved for dynamic load using the solution procedures described in chapters 3 to 5.

In order to use the fatigue damage simulator presented in chapter 6, the local stress/strain history be known. Once again using the BEM, based on the geometry of the gear and the computed normal dynamic loads, the equivalent strains at the critical locations of the gear can be solved for.

7.4 Summary

In this chapter, the additional steps and modelling considerations required to extend the simulation procedures presented in the preceding chapters to the case of helical gears and non-standard cylindrical gears such as circular profile gears etc., are presented. The construction of the helical gear dynamic model is dealt with in detail. And the possible application to other types of cylindrical gears is discussed.

CHAPTER 8

CONCLUSIONS AND RECOMMENDATIONS FOR FUTURE WORK

8.1 General

The procedures described in this thesis provide powerful tools for dynamic analysis of an important class of industrial gears, namely the cylindrical gears such as spur and helical gears. Specifically, the procedures presented eliminate the empiricism involved in the current gear design methods and introduce a sound and rational approach. The techniques presented also have the necessary flexibility to deal with a wide variety of gear types and gear failures. All the three basic modes of failures that constitute gear fatigue failures, namely the tooth bending fatigue, the surface fatigue, and the excessive tooth deflection and overloading caused by resonance, can be easily accounted for in the proposed design methodology.

8.2 Specific conclusions

8.2.1 Gear dynamic load estimation

Mathematical models for a gear set are formulated incorporating both the torsional motion of the gears and the lateral motion of the supports, first with the assumption that the actual transmission error record is available as a continuous time signal. Non-linearities arising from the backlash and the friction between the meshing teeth are

included. It is shown that the use of state-space technique to solve the equations of motion is very advantageous both in terms of the amount of useful information that can be obtained from a single analysis and in terms of the computational requirements. A procedure to select proper initial conditions so as to begin the analysis directly in the steady state is given. Verification of the simulator carried out by comparing the results from the simulator with experimental results obtained using both vibration measuring instruments and dynamic photoelasticity technique show the viability of the simulator to simulate both metallic and non-metallic gears. Also, the inadequacies of the currently used design practice and the complexity of the gear dynamic load variation is highlighted with the use of a parametric study. In addition, it is also shown that the stability of the gear system can be easily studied with the use of state-space technique and Floquet theory.

8.2.2 Stochastic estimation of gear dynamic load

Next, the dynamic load simulator described is further extended so as to use the statistical properties of the transmission error record rather than the actual measured transmission record themselves. It is shown that the statistical analysis of the gear dynamic load can be carried out in a simple and direct manner using piecewise constant mesh stiffness approximation and the mean and covariance

propagation equations of linear difference system. It is also shown that the statistical linearization technique commonly used [20] does not give correct results both in terms of the magnitude and the location of the occurrence of the maximum dynamic load under certain dynamic conditions. In contrast, the piecewise constant approximation presented in this thesis gives truer results provided the time interval chosen is sufficiently small so as to not miss any significant events. Moreover the procedure presented here has the advantage that it can be applied with ease to higher order systems and to systems with complex mesh stiffness and torque fluctuations. Also it is shown that by proper selection of initial conditions using the procedure given in section 4.3, the computation time required for the analysis can be considerably reduced.

8.2.3 Discrete time transfer matrix method

A new method of modelling and analysing technique based on the conventional transfer matrix methods (TMM) and numerical integration procedures is introduced for dynamic analysis of large practical gear systems. The presented methodology is unique in the sense that it can accommodate both non-linear and time-varying characteristics of gear system components and at the same time has the modelling flexibility of TMM. All the primary and secondary factors identified in chapter 2 can be easily included in the

modelling. It is the most complete model to-date available for the study of gear system dynamics. Comparison of results obtained with the presented methodology with results obtained from the use of other techniques confirms the potential of the method in gear train applications. With proper care in modelling, not only the conventional multi-stage gear systems but also the other type of complex gear configurations such as planetary gears can also be modelled. Comparison of the dynamic response and the dynamic load results obtained with the presented analysis procedure with those of other techniques demonstrates the suitability of the procedure for gear train dynamic analysis.

8.2.4 Estimation of gear fatigue life

A computer method of gear fatigue life prediction based on local stress-strain concepts is introduced. This method of life prediction is significantly more accurate than methods typically used in conventional gear design practices. The superiority of the computer method results from the fact that it evaluates the events that are unique to a complex strain history in a rational way. Also in contrast to the current gear design methods the mean and alternating components of the loading can be included in the analysis.

Specifically, the use of boundary element (BE) analysis to obtain strain history at the critical location in the fillet region of the loaded tooth is explained. First, the steps involved in the application of BEM are stated and applied to gear tooth stress analysis problem. Secondly, the formulation and implementation of the BE-GEAR program is validated by comparing the nominal stress results from BE-GEAR program with finite element (FE) and photoelasticity test results. Thirdly, the construction of a typical duty cycle is discussed and the use of non-linear relationships of the form of equation (6.2) is presented to reduce the computations involved in using BEM extensively. Also a fatigue damage computation procedure is presented. The presented simulation procedure uses the functional relationships describing stress and strain directly without further approximation of the stress-strain equations. This improves the accuracy and the numerical stability. The cycle counting program breaks any complex strain waveform into individual cycles or closed hysteresis loops, so that constant loading data can be used for damage evaluation. The cycle counting procedure used in the presented program is more efficient than the existing [8] counting procedures, since the number of decision points used to identify closed loops as well as the number of arrays required is reduced. In contrast to the existing program, the presented program reads the strain values as they occur and is therefore best suitable for loading order sensitive damage parameters.

This feature along with the conciseness of the presented program, makes it best suited for microprocessor based on-line damage evaluation and monitoring applications.

Also, the possible extension of the presented simulation methodologies to helical and non-standard gears such as circular profile gears is discussed.

Finally, since the ultimate usefulness of the procedures presented in this thesis depend upon the ease and cost of using them in day to day applications, a single, menu driven computer software incorporating the three gear dynamic load simulation methodologies presented in this thesis is developed as part of this investigation.

Some of the results of this investigation have also been presented and published in journals [139-141].

8.3 Recommendations for future work

- 1) Even though the simulation procedures presented are versatile enough to analyse both bending fatigue and surface fatigue in gears, only the bending fatigue problem is considered in detail in this thesis. Thus, there is a need for further work to validate the methods for the case of surface fatigue in gears.

- 2) The method of using the equivalent strain ϵ' for computing fatigue damage under multi-axial stress conditions is selected on the basis of the successful use of such parameters in some limited laboratory tests. To be more rigorous, the method of describing the relation between uniaxial stresses and strains should be generalized to include multi-axial stress states.
- 3) Design and implementation of a micro-processor based on-line damage monitoring system based on the fatigue simulation program presented in chapter 6, will be very useful.
- 4) Since, the fatigue damage assessment procedure presented here identifies the significant events in the stress/strain history event by event as they occur, the use of more rigorous stochastic damage accumulation model is possible and should be investigated.
- 5) The apparent versatility of the procedures described to simulate non-standard types of cylindrical gears should be further investigated and validated.
- 6) Finally, the computer software developed as a part of this thesis need be further enhanced so as to achieve a comprehensive, easy to use computer aided gear design package.

REFERENCES

- [1] American Gear Manufacturers Association, AGMA standard 218.01: "AGMA Standard for Rating the Pitting Resistance and Bending Strength of Spur and Helical Involute Gear Teeth", AGMA, Arlington, VA, Dec. 1982.
- [2] International Organization for Standardisation, ISO/DIS 6336, Parts 1-3: "Calculation of Load Capacity of Spur and Helical Gears", Switzerland, 1983.
- [3] German Institute for Standardisation, DIN 3990, Parts 1-4: "Basic Principles for the Calculation of Load Capacity of Spur and Helical Gears", Berlin, Nov. 1980.
- [4] American Gear Manufacturers Association, AGMA standard 110.03: "Nomenclature of Gear-Tooth Wear and Failures", AGMA, Arlington, VA, 1962.
- [5] DUDLEY, D.W.: "Gear Handbook", McGraw-Hill, N.Y., 1962.
- [6] SHIGLEY, J.E., and MITCHELL, L.D.: "Mechanical Engineering Design", McGraw-Hill, N.Y., 1983.
- [7] DRAGO, R.J., BROWN, F.W., and FAUST, H.S.: "Recent Advances in the Evaluation of Stresses in Light Weight, High Speed, Heavily Loaded Gearing", Reliability, Stress Analysis and Failure Prevention Methods in Mechanical Design, A Century 2 Publication, ASME, N.Y., 1980, pp. 225-235.

- [8] LEWIS, W.: "Investigation of the Strength of Gear Teeth", Proc. of the Engineers Club, Philadelphia, 1893, pp. 16-23.
- [9] BUCKINGHAM, E.: "Dynamic Loads on Gear Teeth", ASME Research Publication, N.Y., 1931.
- [10] TUPLIN, W.A.: "Gear-tooth Stresses at High Speed", Proc. of the I.Mech.E., Vol. 163, 1950, p. 162.
- [11] TUPLIN, W.A.: "Dynamic Loads on Gear Teeth", Machine Design, Vol. 25, Oct. 1953, pp. 203-211.
- [12] NAKADA, T., and UTAGAWA, M.: "The Dynamic Loads on Gear Caused by the Varying Elasticity of the Mating Teeth", Proc. of the 6th Japan National Congress for Applied Mechanics, 1956, pp. 493-497.
- [13] ATTIA, A.Y.: "Dynamic Loading of Spur Gear Teeth", Journal of Engg. for Industry, Trans. of ASME, Vol. 81, No. 1, 1959, pp. 1-9.
- [14] UTAGAWA, M., and HARADA, T.: "Dynamic Loads on Spur Gear Teeth Having Pitch Errors at High Speed", Bulletin of JSME, Vol. 5, No. 18, 1962, pp. 374-380.
- [15] TOBE, T., and TAKATSU, N.: "Dynamic Loads on Spur Gear Teeth Caused by Teeth Impact", Bulletin of JSME, Vol. 16, No. 96, June 1973, pp. 1031-1037.
- [16] MAHALINGAM, S. and BISHOP, R.E.D.: "Dynamic Loading of Gear Teeth", Journal of Sound and Vibration, Vol. 36, No. 2, 1974, pp. 179-189.

- [17] ICHIMARU, K., and HIRANO, F.: "Dynamic Behaviour of Heavily-Loaded Spur Gears", Journal of Engg. for Industry, Trans. of ASME, May 1974, pp. 373-381.
- [18] CORNELL, R.W., and WESTERVELT, W.W.: "Dynamic Tooth Loads and Stressing for High Contact Ratio Spur Gears", Journal of Mechanical Design, Trans. of ASME, Vol. 100, Jan. 1978, pp. 69-76.
- [19] KASUBA, R., and EVANS, J.W.: "An Extended Model for Determining Dynamic Loads in Spur Gearing", Journal of Mechanical Design, Trans. of ASME, Vol. 103, April 1981, pp. 398-409.
- [20] TOBE, T., and SATO, K.: "Statistical Analysis of Dynamic Loads on Spur Gear teeth", Bulletin of JSME, Vol. 20, No. 145, July 1977, pp. 882-889.
- [21] TOBE, T., SATO, K., and TAKATSU, N.: "Statistical Analysis of Dynamic Loads on Spur Gear Teeth - Experimental Study", Bulletin of JSME, Vol. 20, No. 148, Oct. 1977, pp. 1315-1320.
- [22] TOBE, T., SATO, K., and TAKATSU, N.: "Statistical Analysis of Dynamic Loads on Spur Gear Teeth - Effect of Shaft Stiffness", Bulletin of JSME, Vol. 19, No. 133, July 1976, pp. 808-813.
- [23] LUND, J.W.: "Critical Speeds, Stability, and Response of a Geared Train of Rotors", Journal of Mechanical Design, Trans. of ASME, Vol. 100, July 1978, pp. 535-538.

- [24] HAMAD, B., and SEIREG, A.: "Whirl of Geared Systems Supported on Hydrodynamic Bearings", Proc. of the Fifth World Congress on Theory of Machines and Mechanisms, Montreal, July 1979, pp. 1109-1112.
- [25] PAWS, J.M.: "An Analytical Investigation of Three-dimensional Vibration in Gear-Coupled Rotor Systems", Ph.D. Thesis, Virginia Polytechnic Institute and State University, Blacksburg, VA, 1979.
- [26] IIDA, H., TAMURA, A., KIKUCHI, K., and AGATA, H.: "Coupled Torsional-Flexural Vibration of a Shaft in a Geared System of Rotors (1st Report)", Bulletin of JSME, Vol. 23, No. 186, Dec. 1980, pp. 2111-2117.
- [27] IWATSUBO, T, ARII, S., and KAWAI, R.: "Coupled Lateral-Torsional Vibration of Rotor System Trained by Gears (Part I - Analysis by Transfer Matrix Method)", Bulletin of JSME, Vol. 27, No. 224, Feb. 1984, pp. 271-277.
- [28] IIDA, H., and TAMURA, A.: "Coupled Torsional-Flexural Vibration of Shaft in a Geared System", Paper No. C272/84, Proc. of the 3rd Intl. Conference on Vibration in Rotating Machinery, IMechE, England, Sept. 1984, pp. 67-72.
- [29] KUCUKAY, F: "The Dynamic Behaviour of High Speed Gears", Paper No. C317/84, Proc. of the 3rd Intl. Conference on Vibration in Rotating Machinery, IMechE, England, Sept. 1984, pp. 81-90.

- [30] PREMILHAT, A., TORDION, G.V., and BARONET, C.N.: "An Improved Determination of the Elastic Compliance of a Spur Gear Tooth Acted on by a Concentrated Load", Journal of Engg. for Industry, Trans. of ASME, Vol. 96, No. 2, May 1974, pp. 382-384.
- [31] CHAKRABORTY, J., and HUNASHIKATTI, H.G.: "Determination of the Combined Mesh Stiffness of a Spur Gear Pair Under Load", ASME paper 74-DET-39, ASME, N.Y., 1974, pp. 1-7.
- [32] CORNELL, R.W.: "Compliance and Stress Sensitivity of Spur Gear Teeth", Journal of Mechanical Design, Trans. of ASME, Vol. 103, April 1981, pp. 447-459.
- [33] CARDOU, A., and TORDION, G.V.: "Calculation of Spur Gear Tooth Flexibility by the Complex Potential Method", ASME paper 84-DET-85, ASME, N.Y., 1984, pp. 1-5.
- [34] TORDION, G.V., and GAUVIN, R.: "Dynamic Stability of a Two-Stage Gear Train Under the Influence of Variable Meshing Stiffnesses", Journal of Engg. for Industry, Trans. of ASME, Aug. 1977, pp. 785-791.
- [35] BENTON, M., and SEIREG, A.: "Simulation of Resonances and Instability Conditions in Pinion-Gear Systems", Journal of Mechanical Design, Trans. of ASME, Vol. 100, Jan. 1978, pp. 26-32.

- [36] BENTON, M., and SEIREG, A.: "Factors Influencing Instability and Resonances in Geared Systems", Journal of Mechanical Design, Trans. of ASME, Vol. 103, April 1981, pp. 372-378.
- [37] WALLACE, D.B., and SEIREG, A.: "Computer Simulation of Dynamic Stress, Deformation, and Fracture of Gear Teeth", Journal of Engg. for Industry, Trans. of ASME, Nov. 1973, pp. 1108-1114.
- [38] WILCOX, L.E., and AUBLE, R.E.: "Three-dimensional Stress Analysis of Meshing Gear Teeth", Proc. of World Congress on Gearing, Paris, France, 1977, pp. 93-107.
- [39] HONDA, H., and CONWAY, J.C.: "An Analysis by Finite Element Techniques of the Effects of a Crack in the Gear Tooth Fillet and its Applicability to Evaluating Strength of the Flawed Gears", Bulletin of JSME, Vol. 22, No. 174, Dec. 1979, pp. 1848-1855.
- [40] WANG, K.L., and CHENG, H.S.: "A Numerical Solution to the Dynamic Load, Film Thickness, and Surface Temperatures in Spur Gears, Part I: Analysis", Journal of Mechanical Design, Trans. of ASME, Vol. 103, Jan. 1981, pp. 177-187.
- [41] SUZUKI, T., CHONG, T.H., AIDA, T., FUJIO, H., and KUBO, A.: "Tooth Fillet Stress of Gear with Thin Rim (1st Report)", Bulletin of JSME, Vol. 25, No. 204, June 1982, pp. 1022-1029.

- [42] COY, J.J., and CHAO, C.H.: "A Method of Selecting Grid Size to Account for Hertz Deformation in Finite Element Analysis of Spur Gears", Journal of Mechanical Design, Trans. of ASME, Vol. 104, Oct. 1982, pp. 759-764.
- [43] CHANG, S.H., HUSTON, R.L., and COY, J.J.: "A Finite Element Stress Analysis of Spur Gears Including Fillet Radii and Rim Thickness Effects", Journal of Mechanisms, Transmissions, and Automation in Design, Trans. of ASME, Vol. 105, Sept. 1983, pp. 327-330.
- [44] LIN, H.H., HUSTON, R.L., and COY, J.J.: "Dynamic Analysis of Straight and Involute Tooth Forms", ASME paper 84-DET-226, ASME, N.Y., 1984, pp. 1-10.
- [45] CHONG, T.H., and KUBO, A.: "Simple Stress Formulae for a Thin-Rimmed Spur Gear, Part 1: Derivation of Approximation Formulae for Tooth Fillet and Root Stresses", ASME paper 84-DET-62, ASME, N.Y., 1984, pp. 1-6.
- [46] BREBBIA, C.A., TELLES, J.C.F., and WROBEL, L.C.: "Boundary Element Techniques", Springer-Verlog, N.Y., 1984.
- [47] FAURE, L.: "Analysis of Tooth Root Stresses in Internal Gears with a Boundary Integral Equation Method", Proc. of Intl. Symposium on Gearing and Power Transmissions, Vol. II, Tokyo, Japan, 1981, pp. 138-145.

- [48] ALEMANNI, M., BERTOGLIO, S., and STRONA, P.: "B.E.M. in Gear Teeth Stress Analysis: Comparison with Classical Methods", Proc. of Intl. Symposium on Gearing and Power Transmissions, Vol. II, Tokyo, Japan, 1981, pp. 177-182.
- [49] RUBENCHIK, V.: "Boundary-Integral Equation Method Applied to Gear Strength Rating", Journal of Mechanisms, Transmissions and Automation in Design, Trans. of ASME, Vol. 105, March 1983, pp. 129-131.
- [50] GAKWAYA, A., CARDOU, A., and DHATT, G.: "Evaluation of Stresses and Deflection of Spur and Helical Gears by the Boundary Element Method", ASME paper 84-DET-169, ASME, N.Y., 1984, pp. 1-11.
- [51] BARONET, C.N., and TORDION, G.V.: "Exact Stress Distribution in Standard Gear Teeth and Geometry Factors", Journal of Engg. for Industry, Trans. of ASME, Vol. 95, Nov. 1973, pp. 1159-1163.
- [52] CARDOU, A., and TORDION, G.V.: "Numerical Implementation of Complex Potentials for Gear Tooth Stress Analysis", Journal of Mechanical Design, Trans. of ASME, Vol. 103, April 1981, pp. 460-466.
- [53] DOLAN, T.J., and BROGHAMMER, E.I.: "A Photoelastic Study of the Stresses in Gear-Tooth Fillets", University of Illinois Experiment Station, Bulletin No. 335, 1942.

- [54] WINTER, H., and HIRT, M.: "The Measurement of Actual Strains at Gear Teeth, Influence of Fillet Radius, on Stresses and Tooth Strength", ASME paper 72-DET-48, ASME, N.Y., 1972.
- [55] KUSKE, A.: "Photoelastic Stress Analysis of Machines Under Dynamic Load", Experimental Mechanics, March 1977, pp. 87-96.
- [56] ALLISON, I.M., and HEARN, E.J.: "A Three-Dimensional Photoelastic Investigation of Stress Distributions in Helical Gears", Strain, July 1979.
- [57] Mc CANN, R.F.: "Measuring Dynamic Stresses on Helicopter Transmission Gear Teeth, Utilizing Telemetry", 26th Intl. Instrumentation Symposium, ISA, Seattle, May 1980, pp. 573-582.
- [58] ALLISON, I.M., and HEARN, E.J.: "A New Look at the Bending Strength of Gear teeth", Experimental Mechanics, Vol. 20, No. 5, July 1980, pp. 217-225.
- [59] KENEDI, L.L.: "An Experimental Investigation of High Contact Ratio Gear Tooth Behaviour", Master's Thesis, Dept. of Mechanical Engineering, Concordia University, Montreal, 1982.
- [60] ERRICHELLO, R.: "State-of-the-Art Review - Gear Bending Stress Analysis", Journal of Mechanisms, Transmissions, and Automation in Design, Trans. of ASME, Vol. 105, Sept. 1983, pp. 283-284.

- [61] "Gear Design and Testing 1972-1982 - Citations from the International Aerospace Abstracts Data Base", NTIS report PB 83-858639, 1983.
- [62] SEABROOK, J.B., and DUDLEY, D.W.: "Results of a Fifteen Year Programme of Fatigue Testing of Gear Teeth", Journal of Engg. for Industry, Trans. of ASME, Aug. 1964, pp. 221-239.
- [63] FUJITA, K., YOSHIDA, A., and AKAMATSU, K.: "A Study on Strength and Failure of Induction Hardened Chromium-Molybdenum Steel Spur Gears", Bulletin of JSME, Vol. 22, No. 164, Feb. 1979, pp. 242-248.
- [64] MOORE, W.L.: "Low-Cycle Fatigue and Ultimate Strength Related to Gear Design", Journal of Mechanical Design, Trans. of ASME, Vol. 101, July 1979, pp. 373-379.
- [65] YURUZUME, I., and MIZUTANI, H.: "Bending Fatigue Tests of High Speed Spur Gears", ASME paper 80-C2/DET-87, ASME, N.Y., 1980, pp. 1-8.
- [66] ODA, S., and TSUBOKURA, K.: "Effects of Addendum Modification on Bending Fatigue Strength of Spur Gears", Bulletin of JSME, Vol. 24, No. 190, April 1981, pp. 716-722.
- [67] ODA, S., TSUBOKURA, K., and NAMBA, C.: "Effects of Addendum Modification on Bending Fatigue Strength of Spur Gears with Higher Pressure Angle", Bulletin of JSME, Vol. 25, No. 209, Nov. 1982, pp. 1813-1820.

- [68] TOBE, T., and MARUYAMA, N.: "Bending Strength of Spur Gear Teeth (1st Report)", Bulletin of JSME, Vol. 25, No. 202, April 1982, pp. 671-678.
- [69] TOBE, T., and MARUYAMA, N.: "Bending Strength of Spur Gear Teeth (2nd Report)", Bulletin of JSME, Vol. 25, No. 209, Nov. 1982, pp. 1797-1804.
- [70] TOBE, T., and MARUYAMA, N.: "Bending Strength of Spur Gear Teeth (3rd Report)", Bulletin of JSME, Vol. 25, No. 209, Nov. 1982, pp. 1805-1812.
- [71] FUJITA, K., YOUSHIDA, A., NAKATA, S., and KOMINAMI, K.: "Study on the Effect of Tooth Fatigue on Dynamic Performance of Gear Pair", Bulletin of JSME, Vol. 26, No. 232, Dec. 1983, pp. 2272-2278.
- [72] ODA, S., and TSUBOKURA, K.: "Bending Fatigue Strength of Spur Gears in Vacuum", Bulletin of JSME, Vol. 23, No. 181, July 1980, pp. 1228-1234.
- [73] CHEN, J.H., and JUARBE, F.M.: "Fatigue Resistance and Noise Generation of Gear Materials: Bronze, Nylon, Cast Iron, and Phenolic", ASME paper 82-DE-3, ASME, N.Y., pp. 1-7.
- [74] YELLE, H., YOUSEF, S.S., and BURNS, D.J.: "Root Bending Fatigue and Cyclic Thermal Softening of Acetal Thermoplastic Spur Gears", Proc. of Fatigue'81, Society of Environmental Engg., England, March 1981, pp. 261-270.

- [75] MANSON, S.S.: "Fatigue: A Complex Subject - Some Simple Approximations", *Experimental Mechanics*, July 1965, pp. 193-226.
- [76] SANKAR, T.S., XISTRIS, G.D., and OSTIGUY, G.: "Reliability of Machinery Using Fatigue Damage Accumulation due to Random Vibrations", *Journal of Mechanical Design*, *Trans. of ASME*, Vol. 100, 1978, pp. 619-625.
- [77] SHIN, Y.S.: "Prediction of Random High-Cycle Fatigue Life of LWR Components", *Journal of Pressure Vessel Technology*, *Trans. of ASME*, Vol. 102, Nov. 1980, pp. 378-386.
- [78] GARIVALTIS, D.S., GARG, V.K., and D'SOUZA, A.F.: "Fatigue Damage of the Locomotive Suspension Elements Under Random Loading", *Journal of Mechanical Design*, *Trans. of ASME*, Vol. 103, Oct. 1981, pp. 871-880.
- [79] SHIN, Y.S., and AU-YANG, M.K. (Eds.): "Random Fatigue Life Prediction", PVP-Vol. 72, ASME, N.Y., 1983.
- [80] SANDOR, B.I.: "Fundamentals of Cyclic Stress and Strain", The University of Wisconsin Press, 1972.
- [81] COLLINS, J.A.: "Failure of Materials in Mechanical Design", John-Willey and Sons, N.Y., 1981.
- [82] LANDGRAF, R.W., JO DEAN MORROW, and ENDO, T.: "Determination of the Cyclic Stress--Strain Curve", *Journal of Materials*, *JMESA*, Vol. 4, No. 1, March 1969, pp. 176-188.

- [83] TOPPER, T., SANDOR, B.I., and Jo DEAN MORROW:
"Cumulative Fatigue Damage Under Cyclic Strain Control", Journal of Materials, JMLSA, Vol. 4, No. 1, March 1969, pp. 189-199.
- [84] TOPPER, T.H., WETZEL, R.M., and MORROW, J.D.:
"Neuber's Rule Applied to Fatigue of Notched Specimens", Journal of Materials, JMLSA, Vol. 4, No. 1, March 1969, pp. 200-209.
- [85] UDOGUCHI, T., ASADA, Y., and YASUHIRO, N.: "An Approach to Investigate Notch Effect on Low-Cycle Fatigue with Finite Element", Paper II-57, Proc. of Intl. Conference on Pressure Vessel Technology, San Antonio, 1973, pp. 785-800.
- [86] LANDGRAF, R.W., and La POINTE, N.R.: "Cyclic Stress-Strain Concepts Applied to Component Fatigue Life Predictions", SAE paper 740280, SAE Trans., 1974, pp. 1198-1207.
- [87] SOCIE, D.F.: "Fatigue Life Prediction Using Local Stress-Strain Concepts", Experimental Mechanics, Feb. 1977, pp. 50-56.
- [88] PARIS, P.C.: "The Fracture Mechanics Approach to Fatigue", Fatigue - An Interdisciplinary Approach, Proc. of 10th Sagamore Conference, Syracuse, N.Y., Syracuse University Press, 1964, p. 107.
- [89] CROOKER, T.W.: "Fracture Mechanics - Fatigue Design", Mechanical Engineering, June 1977, pp. 40-45.

- [90] IWAN, W.D.: "On a Class of Models for the Yielding Behaviour of Continuous and Composite Systems", Journal of Applied Mech., Trans. of ASME, Sept. 1967, pp. 612-617.
- [91] MARTIN, J.F., TOPPER, T.H., and SINCLAIR, G.M.: "Computer Based Simulation of Cyclic Stress-Strain Behaviour with Applications to Fatigue", Materials Research and Standards, MTRSA, Vol. 11, No. 2, 1971, pp. 23-28.
- [92] WETZEL, R.M.: "A Method of Fatigue Damage Analysis", Ph.D. Thesis, Dept. of Civil Engg., University of Waterloo, 1972.
- [93] DOWLING, N.E.: "Fatigue Failure Predictions for Complicated Stress-Strain Histories", Journal of Materials, JMLSA, Vol. 7, No. 1, March 1972, pp. 71-87.
- [94] FUCHS, H.O., NELSON, D.V., BURKE, M.A., and TOOMAY, T.L.: "Shortcuts in Cumulative Damage Analysis", SAE paper 730565, SAE, 1973, pp. 1-16.
- [95] ENDO, T., MITSUNAGA, K., TAKAHARHI, K., KOBAYASHI, K., and MATSUISHI, M.: "Damage Evaluation of Metals for Random or Varying Loading - Three Aspects of Rain Flow Method", Proc. of the 1974 Symposium on Mechanical Behaviour of Materials, Society of Material Science, Japan, 1974, pp. 371-380.

- [96] WETZEL, R.M. (Ed.): "Fatigue Under Complex Loading: Analysis and Experiments", SAE Advances in Engg. Pub., Vol. 6, SAE, 1977.
- [97] NELSON, D.V.: "Cumulative Damage in Metals", Ph.D. Thesis, Dept. of Mechanical Engineering, Stanford University, California, 1978.
- [98] LEIS, B.N.: "Fatigue Life Prediction of Complex Structures", Journal of Mechanical Design, Trans. of ASME, Vol. 100, Jan. 1978, pp. 2-9.
- [99] LAM, T.C., and STEELE, J.M.: "Computer Simulation of Fatigue Damage", Proc. of Intl. Computers in Engineering Conference, Vol. 3, ASME, Chicago, Aug. 1983, pp. 97-103.
- [100] THOMAS, T.J, NAIR, S., and GARG, V.K.: "Elasto-Plastic Stress Analysis and Fatigue Life Prediction of a Freight Car Wheel Under Mechanical and Cyclic Thermal Loads", Computers & Structures, Vol. 17, No. 3, 1983, pp. 313-320.
- [101] CONLE, A., and LANDGRAF, R.W.: "A Fatigue Analysis Program for Ground Vehicle Components", Proc. of Intl. Conference on Fatigue - SEECO'83, Society of Environmental Engg., London, 1983, pp. 1-16.
- [102] MUSIOL, C., DRAPER, J., SYKES, N., and MORTON, K.: "Advances in Computer Aided Design Against Fatigue", Engineering Research and Design - Bridging the Gap, I.Mech.E. Conference Pub 1981-7, 1981, pp. 67-78.

- [103] MORTON, K., MUSIOL, C., and DRAPER, J.: "Local Stress-Strain Analysis as a Practical Tool", Proc. of Intl. Conference on Fatigue - SEECO'83, Society of Environmental Engg., London, 1983, pp. 219-229.
- [104] KNIGHT, F.L.: "Computer Aided Fatigue Design - A Review", Proc. of Intl. Computers in Engineering Conference, Vol. 2, ASME, Los Vegas, Aug. 1984, pp. 431-441.
- [105] MINER, M.A.: "Cumulative Damage in Fatigue", Journal of Applied Mechanics, Trans. of ASME, Vol. 12, 1945, pp. 159-164.
- [106] FARLEY, D.M., and KINZEL, G.L.: "A Comprehensive Procedure for the Interactive Computer-Aided Design of Parallel Shaft Gears", Proc. of the Intl. 1983 Computers in Engineering Conference, Chicago, Aug. 1983, pp. 25-31.
- [107] TAMMA, K.K., and LAMBI, M.A.: "Interactive Computer Aided Design and Analysis of Spur Gears", Proc. of the Natl. Conference on University Program in Computer-Aided Engg., Design, and Manufacturing, Lehigh Univ., Bethlehem, Aug. 1984, pp. 191-196.
- [108] ARABYAN, A., SHIFLETT, G.R., and SUN, C.Y.: "A Simplified, Microcomputer-Based Method for Spur Gear Design", ASME paper 84-DET-207, ASME, N.Y., 1984, pp. 1-7.

- [109] LUK, Y.W., and MITCHELL, L.D.: "Development of an Interactive Computer Program for Fatigue Analysis", ASME paper 79-DE-E-4, ASME, N.Y., 1979.
- [110] SHIN, J.H., and KINZEL, G.L.: "Development of an Interactive Procedure for Fatigue Analysis Using Computer Graphics", Proc. of 2nd Intl. Computers in Engineering Conference, Vol. 1, ASME, San Diego, Aug. 1982, pp. 69-80.
- [111] MARUYAMA, K., and NAKADA, T.: "On Dynamic Measuring Method of Rotating Error of the Master Worm-Wheel", Bulletin of the Tokyo Institute of Technology, No. 94, 1968.
- [112] SHIMOJIMA, M., ISHIKAWA, J., KAJITANI, M., and OSADA, H.: "A Study of Automatic Gear Accuracy Measuring Instrument", Trans. of JSME, Vol. 43, No. 373, p. 3548.
- [113] TODA, A., and TORDION, G.V.: "Dynamic Behaviour of Mechanical Systems with Gear Transmission Error", Proc. of the Fifth World Congress on Theory of Machines and Mechanisms, Vol. 2, Montreal, July 1979, pp. 1130-1133.
- [114] MASSO: "On the Relation Between the Angular Position Error and the Individual Error of the Gear", Bulletin of the Tokyo Institute of Technology, No. 95, 1969.
- [115] TODA, A. and TORDION, G.V.: "Approximation of Gear Transmission Error by standard Gear Errors", ASME paper 80-C2/DET-71, ASME, N.Y., 1980, pp. 1-6.

- [116] MICHALOPOULOS, D., and DIMAROGONAS, A.: "Dynamic Behaviour of Geared Systems with Backlash due to Stick-slip Vibratory Motion", *Wear*, 1983, pp. 135-143.
- [117] MARTIN, K.F.: "A Review of Friction Predictions in Gear Teeth", *Wear*, Vol. 49, 1978, pp. 201-238.
- [118] DOWSON, D., and HIGGINSON, G.R.: "Elastohydrodynamic Lubrication", Pergamon Press Ltd., 1977.
- [119] BENEDICT, G.H., and KELLY, B.W.: "Instantaneous Coefficients of Gear Tooth Friction", *ASLE Trans.*, Vol. 4, No. 1, April 1961, pp. 59-70.
- [120] ANDERSON, N.E., and LOEWENTHAL, S.H.: "Effect of Geometry and Operating Condition on Spur Gear System Power Loss", *Journal of Mechanical Design, Trans of ASME*, Vol. 103, Jan. 1981, pp. 151-159.
- [121] MARTIN, K.F.: "The Efficiency of Involute Spur Gears", *Journal of Mechanical Design, Trans. of ASME*, Vol. 103, Jan. 1981, pp. 160-169.
- [122] ANDERSON, N.E., and LOEWENTHAL, S.H.: "Comparison of Spur Gear Efficiency Prediction Methods", *NASA-CP-2210*, 1983.
- [123] REINHART, W.R., FERGUSON, R.J., and DELANEY, R.G.: "Prediction of the Efficiency of Non-Circular Spur Gears", *Trans. of CSME*, Vol. 8, No. 2, 1984, pp. 96-102.

- [124] ANDERSON, N.E., and LOEWENTHAL, S.H.: "Efficiency of Non-Standard and High Contact Ratio Involute Spur Gears", ASME paper 84-DET-172, ASME, N.Y., 1984, pp. 1-8.
- [125] BAHAR, L.Y., and SINHA, A.K.: "Matrix Exponential Approach to Dynamic Response", Computers & Structures, Vol. 5, 1975, pp. 159-165.
- [126] HSU, C.S.: "On Approximating a General Linear Periodic System", Journal of Mathematical Analysis and Application, Vol. 45, 1974, pp. 234-251.
- [127] UMEZAWA, K., SATO, T., and ISHIKAWA, J.: "Simulation on Rotational Vibration of Spur Gears", Bulletin of JSME, Vol. 27, No. 223, Jan. 1984, pp. 102-109.
- [128] BOLOTIN, V.V.: "The Dynamic Stability of Elastic Systems", Holden-Day Inc., San Francisco, 1964.
- [129] DUFFIN, J.A.: "Algorithms for Classical Stability Problems", SIAM Review, Vol. 11, 1969, pp. 196-213.
- [130] MARK, W.D.: "Analysis of Vibrating Excitation of Gear Systems - part II: Tooth Error Representation, Approximation, and Application", Journal of Acoustical Society of America, Vol. 66, Dec. 1979, pp. 1758-1787.
- [131] LEES, A.W., and PANDEY, P.C.: "Vibration Spectra from Gear Drives", Proc. of IMechE, 1980, pp. 103-108.
- [132] MAYBECK, P.S.: "Stochastic Models, Estimation, and Control", Vol. I, Academic Press, N.Y., 1979.

- [133] BEAMAN, J.J.: "Accuracy of Statistical Linearization", Proc. of Conference on New Approaches to Nonlinear problems in Dynamics, Siam, 1980, pp. 195-207.
- [134] HATTER, D.J.: "Matrix Computer Methods in Vibration Analysis", John Wiley and Sons, N.Y., 1973, p. 135.
- [135] KIKUCHI, K.: "Analysis of Unbalance Vibration of Rotating Shaft System with Many Bearings and Disks", Bulletin of JSME, Vol. 13, No. 61, 1970, pp. 864-872.
- [136] MITCHELL, L.D.: "A New Branching Technique for the Static and Dynamic Analysis of Geared Systems", Paper No. C256/80, Proc. of Second Intl. Conference on Vibration in Rotating Machinery, IMechE, 1980, pp. 37-42.
- [137] CHRISTIANSEN, H.W., and STEPHENSON, M.B.: "MOVIE.BYU - A General Purpose Computer Graphics System", Dept. of Computer Science, Brigham Young Univeristy, Provo, Utah, 1981.
- [138] MITCHNER, R.G., and MABIE, H.H.: "The Determination of the Lewis Form Factor and the AGMA Geometry Factor J for External Spur Gear Teeth", Journal of Mechanical Design, Trans. of ASME, Vol. 104, Jan. 1982, pp. 148-158.
- [139] KUMAR, A.S., SANKAR, T.S., and OSMAN, M.O.M.: "On Dynamic Tooth Load and Stability of a Spur-Gear System Using the State-space Approach", Journal of Mechanisms, Transmissions, and Automation in Design, Trans. of ASME, Vol. 107, 1985, pp. 54-60.

- [140] KUMAR, A.S., OSMAN, M.O.M., and SANKAR, T.S.: "An Automatic Gear Mesh Generator (AGMG) for Finite Element Modelling of Spur and Helical Gears", ASME paper 85-DE-6, presented at the ASME National Design Engineering Conference, Chicago, March 1985.
- [141] KUMAR, A.S., OSMAN, M.O.M., and SANKAR, T.S.: "On Statistical Analysis of Gear Dynamic Loads", Accepted for publication in the Journal of Vibration, Acoustics, Stress and Reliability in Design, Trans. of ASME, 1986.

APPENDIX I
BOUNDARY ELEMENT METHOD

The boundary element analysis program BE-GEAR implemented as a part of this investigation is used extensively in this thesis for gear tooth stress and deflection analysis. Presently, the program is capable of analysing two dimensional plane stress and plane strain elastostatic problems. This appendix gives brief introduction to the boundary element methods and the numerical implementation scheme. Detailed descriptions of the same are available in the recently published texts such as [46].

Basis of BEM

Consider the portion of the gear to be analysed as an elastic body defined by $\Omega + \Gamma$, where Ω is the domain and Γ is the boundary as shown in Fig. I.1. If Ω is a three dimensional domain, then Γ is the boundary surface. If Ω is a two dimensional domain, then Γ is the boundary contour. For such an elastic body to be in equilibrium under the action of prescribed tractions p_i and/or displacements u_i , the wellknown Navier's equation for elastostatic case has to be satisfied.

That is, in Cartesian tensor coordinates,

$$(\lambda + G) u_{j,j} + G u_{i,jj} + b_i = 0 \quad (1.1)$$

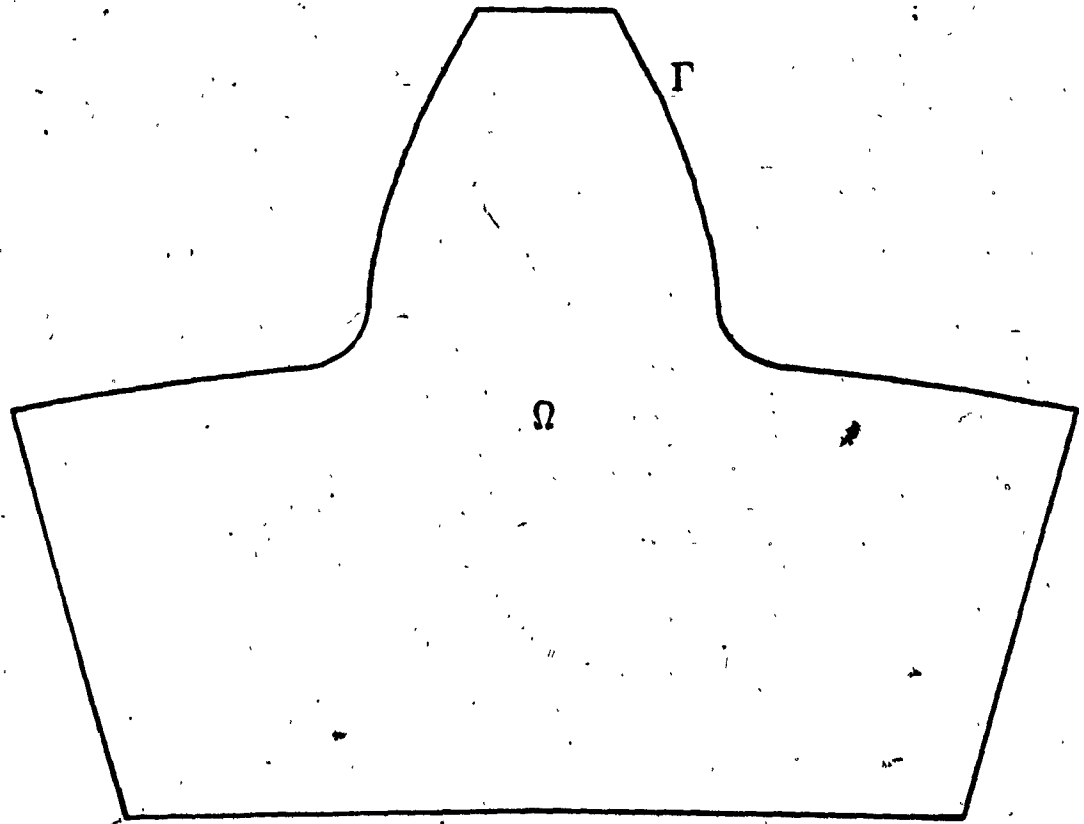


Fig. I.1: Definition of domain and boundary

with, the boundary conditions,

$$p_i = \bar{p}_i - \sigma_{ij} \eta_j \quad (1.2)$$

and

$$u_i = \bar{u}_i \quad (1.3)$$

Here,

- G = bulk modulus of rigidity,
- Λ = Lamé constant,
- b = body forces,
- u = displacements,
- p = tractions,
- \bar{u} = prescribed displacements,
- \bar{p} = prescribed tractions,
- σ_{ij} = stress tensor,
- η_i = unit normal in the i^{th} direction,
- i and j = index used to denote different directions,
- ∂_{ij} = denotes partial differentiation of the variable in the j^{th} direction with respect to the variables in i^{th} and j^{th} direction,
- ∂_{ijj} = denotes partial differentiation of the variable in the i^{th} direction with respect to the variable in the j^{th} direction, twice.

The reformulation of the partial differential equation (I.1) into an integral equation and the numerical solution of such an integral equation is the basis of the BEM. Such

reformulations can be achieved through different techniques [46] such as weighted residual method or Somigliana identity equation, etc., such that,

$$c_{ij}(\xi)u_i(\xi) = \int_{\Gamma} u_{ij}^*(\xi, x) p_j(x) d\Gamma(x) - \int_{\Gamma} p_{ij}^*(\xi, x) u_j(x) d\Gamma(x) + \int_{\Omega} u_{ij}^*(\xi, x) b_j(x) d\Omega(x) \quad (I.4)$$

where,

- ξ = nodal location where the prescribed tractions or displacements occur,
- x = field point,
- $c_{ij}(\xi)$ = coefficient defined through the condition of rigid body motion.

Equation (I.4) provides a relationship between the boundary displacements u , boundary tractions p and body forces b and is valid for both two and three dimensional domains. Here, p^* , and u^* are known and the unknowns are the values of p and u over the boundary. For the present problem of gear tooth stress and deflection analysis, the body force terms in the equation (I.4) can be neglected such that,

$$c_{ij}(\xi)u_i(\xi) = \int_{\Gamma} u_{ij}^*(\xi, x) p_j(x) d\Gamma(x) - \int_{\Gamma} p_{ij}^*(\xi, x) u_j(x) d\Gamma(x) \quad (I.5)$$

The purpose of BEM formulation is to obtain a numerical solution to this equation.

Numerical solution scheme

The basic steps involved in the numerical solution procedure used in BE-GEAR program are listed in the following subsections.

Step I:

The boundary is discretized into a series of elements, say N number of elements. The tractions and the displacements over these elements are assumed to vary according to a chosen interpolation function. The order of the chosen interpolation function determines the type of boundary element to be used in the modelling. That is,

$$p(x) = \Phi^T p^n \quad (1.6)$$

$$u(x) = \Phi^T u^n \quad (1.7)$$

where,

- Φ = interpolation function,
- u^n = displacements at the nodes,
- p^n = tractions at the nodes.

Step II:

Equation (I.5) is then applied in discretized form to each nodal point ξ of the boundary Γ , such that,

$$c_{ij}(\xi)u_i(\xi) = \sum_{j=1}^N \int_{\Gamma} u_j^*(\xi, x) \Phi^T d\Gamma(x) p^n + \sum_{j=1}^N \int_{\Gamma} p_{ij}^*(\xi, x) \Phi^T d\Gamma(x) u^n \quad (1.8)$$

The integrals in the equation (I.8) are computed over each boundary element using a suitable numerical integration scheme. This results in a system of N linear algebraic equations involving a set of N nodal tractions and nodal displacements.

Step III:

Next, as in FEM, boundary conditions are prescribed and the resulting system of N equations is solved for the unknown boundary tractions and displacements.

Step IV:

The values of displacements at any specified internal points are then obtained using discretized integral equations.

Step V:

Once the displacement at different points are known, the strain and stress values at these points are then obtained through the application of strain-displacement relations and stress-strain constitutive relations.

APPENDIX II

AN AUTOMATIC GEAR MESH GENERATOR (AGMG)

This appendix describes a newly developed automatic gear mesh generator which was used extensively during the course of this thesis work to generate Boundary Element (BE) and Finite Element (FE) meshes of gears. The new AGMG has the following features:

- a. Interactive - Menu driven commands.
- b. Minimal input.
- c. Automatic profile definition.
- d. Automatic node numbering and element numbering.
- e. Option to change the numbering scheme.
- f. Ability to model standard and non-standard gear tooth geometry.
- g. Ability to form the mesh with different elements, Fig. II.1.
- h. Ability to model spur as well as helical gears.
- i. Ability to model single tooth, multiple teeth or the whole gear.
- j. Selective mesh refinement and local modification using the 'user defined element' option.
- k. Provides smoother and better distributed elements.
- l. Graphic output and flexible data output format.

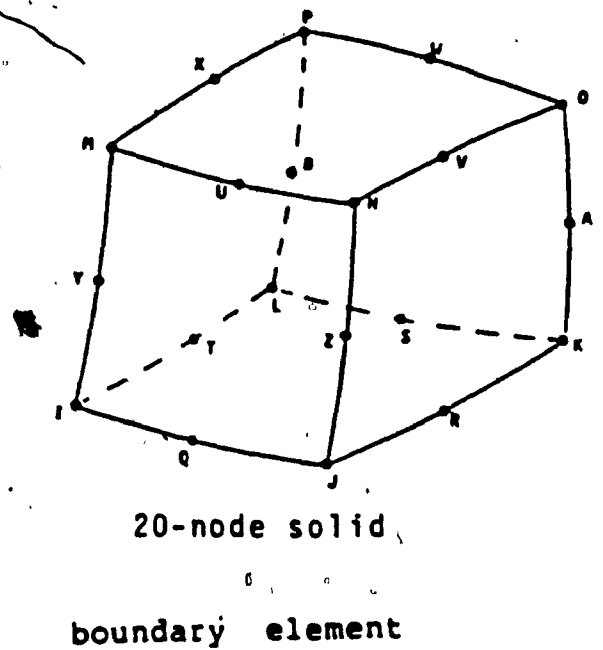
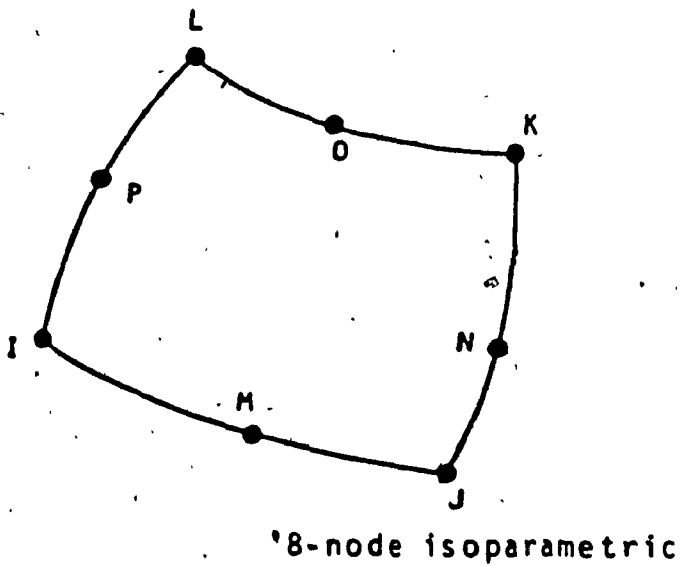
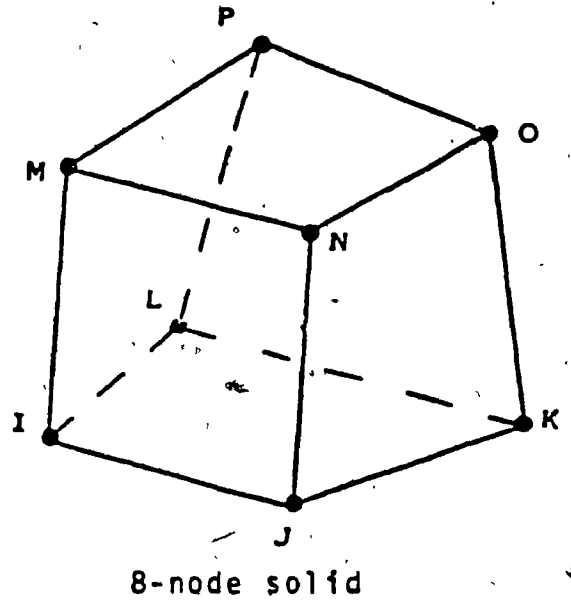
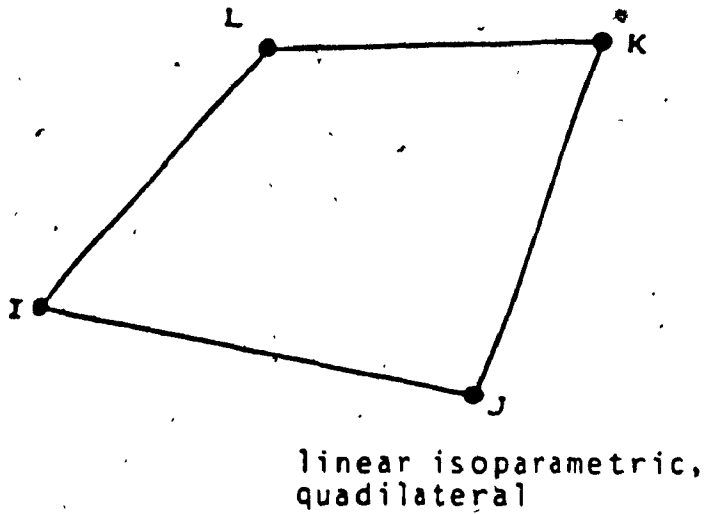
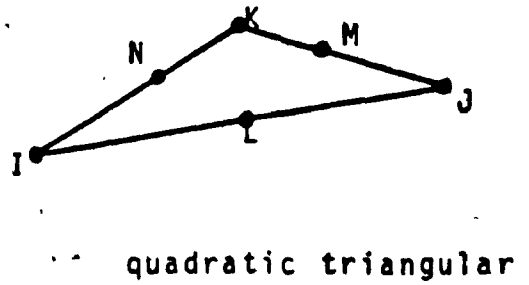
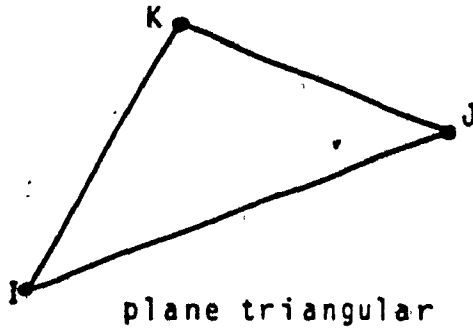


Fig. II.1: Element library in AGMG

- m. Ability to interface with the powerful MOVIE:BYU [137] graphics program.

Basic construction of AGMG

The actual construction of the mesh within AGMG is carried out according to the following scheme:

1. Data input to AGMG - model data, geometry data.
2. Generation of an Equivalent Rectangular Mesh.
3. Element and nodal numbering to reduce frontwidth and/or bandwidth.
4. Mapping of the equivalent mesh on to the profile.
5. Profile generation.
6. Element smoothing, if specified.
7. Solid element mesh generation, if specified.
8. Alteration of the generated mesh locally, if specified.
9. Output - Graphical display of mesh generated, - Data file generation.
10. Repeat steps 1 to 8, with new data, if changes are required. Otherwise exit.

Data input

There are two kinds of inputs, namely model data and geometry data needed for AGMG. Model data consists of the number of divisions in X-direction (NXD), number of divisions in the involute region (NINVD), number of

divisions in the fillet region (NFILD), number of divisions in the rim region (NRIMD), and the type of element (IETYPE). And geometric input consists of diametrical pitch, pitch diameter, pressure angle, face width and the type of gear tooth (e.g. AGMA std., AGMA stub, etc). With these minimal geometry data the AGMG computes all the other required quantities such as root fillet radius, addendum, dedendum etc., according to AGMG tooth type specified. However, the user also has the option to input these parameters manually to obtain non-standard types of gear tooth.

Equivalent rectangular mesh

AGMG first generates an equivalent rectangular mesh, Fig. II.2, with the use of the model data. This equivalent rectangular mesh is conceptually similar to the 'basic mesh' concept introduced by Suzuki et.al. [41]. The major difference between the two concepts is that with Suzuki's basic mesh concept, different basic mesh has to be generated for different types of elements used, whereas with the method proposed here different types of elements can all be generated from the same equivalent mesh. All the mesh data, except the coordinates of the nodes are computed based on the equivalent rectangular mesh. This includes the computation of total number of nodes and elements in the mesh and nodal and element numbering.

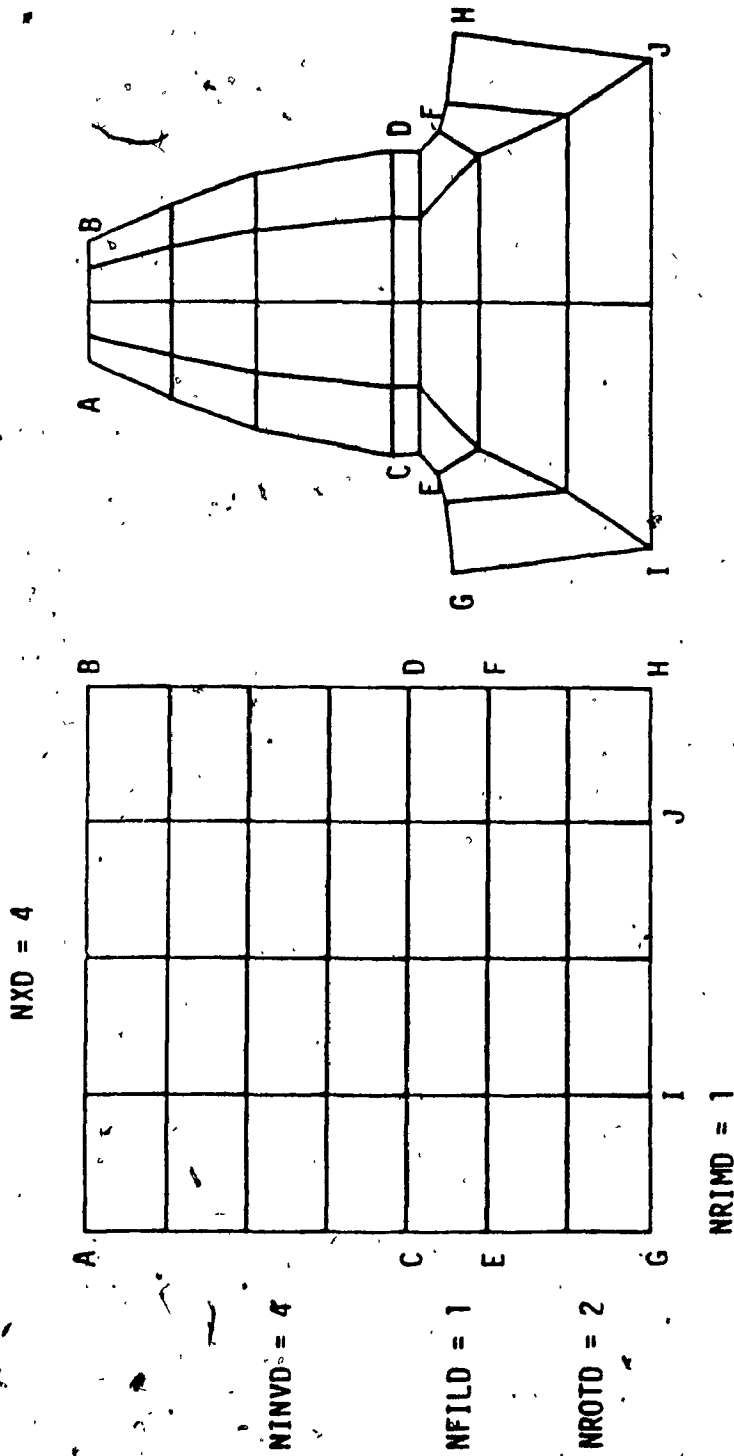


Fig. II.2: Equivalent rectangular mesh

Node numbering

AGMG, by default, numbers the nodes and elements in such a way that it reduces the bandwidth and the frontwidth of the resulting solution matrices during the FEM analysis. Since numbering is done based on the equivalent rectangular mesh, there are only two options, namely numbering along the shorter side of the rectangle or along the larger side of the rectangle. By default AGMG starts the node numbering from the upper left corner and proceeds along the shorter side of the rectangle to optimize the bandwidth. However the user has also been provided with the option to change the numbering direction. In addition, by default AGMG numbers first node as node number 1 and proceeds in ascending order in the specified direction. Once again, the user has the option to define any number as the first node number. This enables the user to model different parts of the gear tooth separately and combine them later.

Element numbering

If the mesh generated is to be analysed with a FE routine which uses a 'front solver' rather than a 'band solver', then node numbering becomes unimportant. In this case, element numbering is very important. By default, AGMG starts element numbering from the upper leftmost element and proceeds along the shorter side of the equivalent rectangle. Once again the user is provided with the option to change the numbering scheme. Depending upon the element type

specified the node and element numbering schemes in AGMG automatically takes care off the midside nodes if they are present. Fig. II.3 shows the different numbering schemes possible with AGMG.

Mapping of the Equivalent mesh

The mesh of the actual gear tooth is obtained by mapping the equivalent rectangular mesh on to the gear tooth profile or contour. For explanation purpose, the equivalent mesh can be considered as a flexible rubber net. Then, the mesh model of the tooth can be generated by stretching the imaginary rubber net (equivalent mesh) and fitting it onto the frame of the tooth profile or contour form. The coordinates of the nodes on the tooth profile required for mapping are generated as follows.

Profile definition

Normally the tooth profile coordinates are either input manually or with the help of a digitizer. But AGMG generates these coordinates using the geometrical input data and mathematical relationships defining the profile. Fig. II.4 shows the coordinate system used for profile generation. The involute part of the profile is generated with equations (II.1) and (II.2) given here.

$$X^P = R_b [\cos(\theta + \beta) + \theta \sin(\theta + \beta)] \quad (II.1)$$

$$Y^P = R_b [\sin(\theta + \beta) - \theta \cos(\theta + \beta)] \quad (II.2)$$

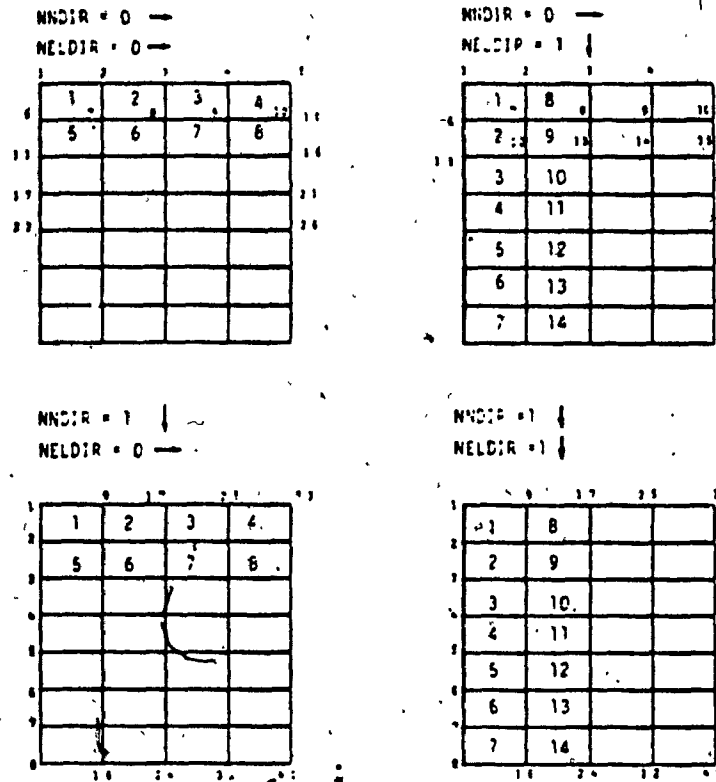


Fig. II.3: Different numbering schemes

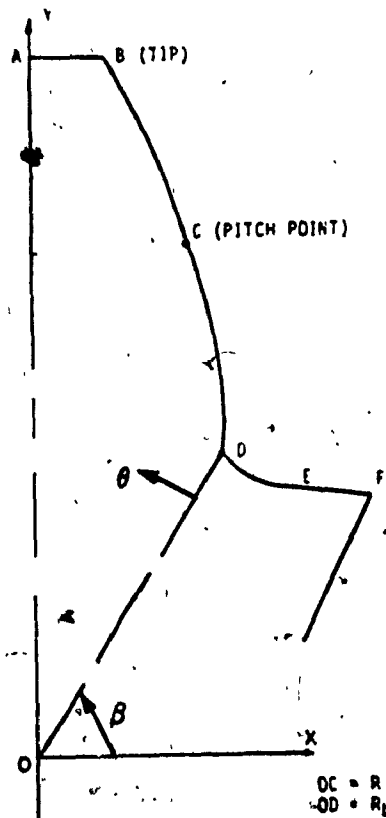


Fig. II.4: Coordinates used for involute profile generation

where,

X = X coordinate value of a point on the involute portion

Y = Y, coordinate value of a point on the involute portion

R_b = base radius of the gear

θ = involute generating angle

β = transformation angle

And the fillet or root portion of the tooth is generated by using the equations given in [138]. Since in AGMG the profile generation and the placement of nodes on the profile are done simultaneously, it is possible to generate only those points where the nodes are located and not the entire profile. This results in considerable saving in computation time.

The required divisions in the involute part of the profile are obtained by dividing the involute generating angle θ by NINVD. To obtain a better control on the element shapes and sizes in this region, the involute portion is divided into two regions. That is, NINVD should be at least equal to two. One region is between the tip of the tooth and the pitch point, and the other one is between the pitch point and the intersection point of fillet and involute portion. Thus there is always a node at these points. These points and the corresponding involute generating

angles are shown in Fig. II.4. The spacing between the involute divisions are varied and controlled by the weighing factor (WN). This factor used in equation (II.3), divides the generating angle in geometric progression. For the upper involute part a smaller weighing factor ($\ll 1$) is suggested, to have smaller divisions near the tip of the tooth and for the lower involute part, a factor value greater than unity is suggested to get finer elements near the fillet region. However, the user has the option to change the value of this weighing factor during the execution of the program to obtain any specific arrangement.

$$\theta_i = (\theta_F - \theta_I) \frac{WN^{i-1}}{WN^{m-1}} + \theta_I \quad (II.3)$$

$i = 1, 2, \dots, m$

where,

- m = number of divisions
- WN = weighing factor used to control the vertical spacing between nodes
- θ_I = initial value of the involute generating angle
- θ_F = final value of involute generating angle
- θ_i = intermediate value of involute generating angle required in the interval θ_I to θ_F

The coordinates of the nodes on the root fillet are obtained by dividing the trochoid generating angle (φ) by NFILD. Similarly the nodes on the rim of the gear are

computed by dividing the rim thickness by NRIMD. As the nodes on the boundary are generated, the program also stores the coordinates of the corresponding nodes on the centre line of tooth, Fig. II.4. Once the coordinates of all the nodes on the profile and centre line are computed, the coordinates of other internal nodes (i.e. nodes between the centre line and outer profile) are computed by using the following equation.

$$X^i = (X^P - X^C) \frac{WF^{i-1}}{WF^{m-1}} + X^C \quad (II.4)$$

$i = 1, 2, \dots, m$

$$Y^i = (Y^P - Y^C) \frac{WF^{i-1}}{WF^{m-1}} + Y^C \quad (II.5)$$

$i = 1, 2, \dots, m$

where,

m = number of elements required between the centre-line and the profile points

= $NXD/2$

X^P = X coordinate value

Y = Y coordinate value

WF = weighing factor used to control the horizontal spacing between nodes.

i = index denotes intermediate values of parameters

p = denotes points on the tooth profile

c = denotes points on the tooth centre-line

By changing weighing factor (WF), the horizontal spacing between the internal nodes can be changed. AGMG uses a

factor value of greater than unity to get a finer mesh near the tooth boundary. Once again, the user has the option to change the value of factor during execution to obtain different meshes. As mentioned earlier the coordinates of the nodes on the other half of the tooth are taken as the mirror image of the coordinates of corresponding nodes computed so far. In the case of elements with midside nodes, the coordinates of the midside nodes are computed as the average of the two adjacent nodes.

Smoothing

It has been found that the shape of elements can be improved by placing internal nodes at the centre of the other surrounding nodal points. This can be achieved efficiently by making the coordinates of an internal node as the average of the coordinates of its neighbouring nodes. This kind of smoothing process is an iterative process, since moving one nodal coordinate will affect the other internal nodal coordinates. The iteration is stopped as soon as none of the internal nodal points change significantly. Fig. II.5 shows the unsmoothed, selectively smoothed and fully smoothed meshes generated with ACGM. Selective smoothing capability is provided to have a better control on the mesh configuration. Also, smoothing can be switched on and off by the user during execution of the program.

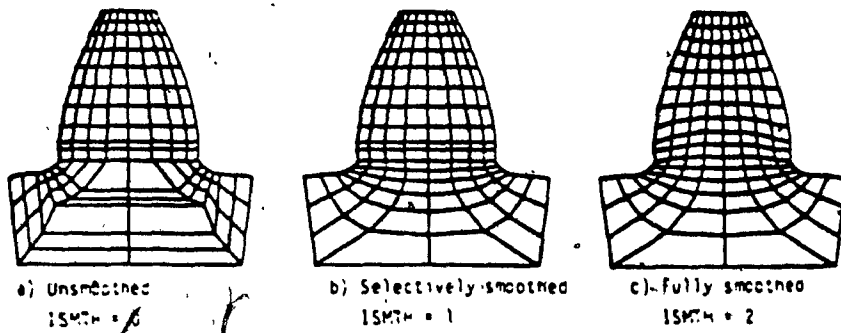


Fig. II.5: Different smoothing schemes

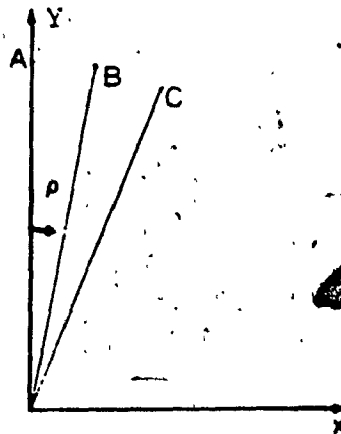
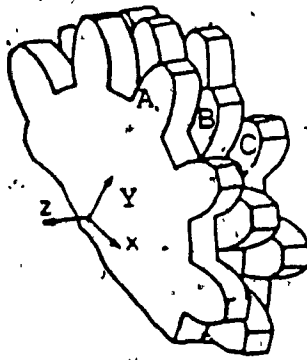


Fig. II.6: Helical gear construction

Solid element modelling capability

The AGMG also has the capability to generate meshes of 3-D solid elements. This is activated by specifying the number of divisions or elements in the gear thickness direction, NZD, a value greater than zero. The 3-D meshes are generated by providing the third dimension (element thickness) to the corresponding 2-D mesh generated by AGMG. The solid element thickness is computed by dividing the facewidth by NZD. The AGMG node numbering schemes are then repeated NZD times to define the solid elements properly.

Meshes for Helical gears

The AGMG solid element generation capability can also be used to create meshes of helical gear tooth. For modelling purpose the helical gears can be represented, as shown in Fig. II.6, by a series of thin spur gear plates which have been displaced angularly in the plane of rotation. As the number of plates approach infinity, the points on the gear tooth form into helices. However, for mesh generation one needs to consider only finite number of plates, given by $(NZD+1)$.

AGMG first generates the mesh of plate 1, Fig. II.6, and then computes the rotation angle of consecutive plates using equation (II.6). Then using this rotation angle, the coordinates of nodes on each plate are computed.

$$\rho = R_p \sin(\lambda_o) \frac{B}{N Z D} (i-1) \quad (II.6)$$

$$i = 1, 2, \dots, N Z D + 1$$

where,

- R = pitch radius of gear
- B = face width of gear
- N Z D = number of elements in the Z direction
- i = index used to increment elements in the Z direction
- ρ = angle to generate helical gear teeth
- λ_o = helix angle of the gear

User defined element option

The mesh generated by the AGMG can be locally altered using this option. The user can instruct the AGMG to place a particular element of specified size at a user specified location in the model. AGMG will automatically rearrange the surrounding elements to accomodate the user specified element.

Output from AGMG

Graphic output capabilities are built into AGMG so that the user can view and evaluate the mesh generated at each stage. All nodal coordinates and element definitions are also written to data files specified by the user. The formats can be easily changed to accomodate different analysis programs. In addition, AGMG also interfaces with the powerful MOVIE.BYU graphics program. This capability,

though not essential for the operation of AGMG, provides the user the ability to display and manipulate (rotate, shrink, section, explode, etc) the graphic image of the mesh generated, to have a better view of the mesh.

Description of AGMG

The operation of AGMG revolves around the 'AGMG - Main Menu', shown in Fig. II.7. All the AGMG functions originate from here and, when executed, also return here. The user can enter any of the given options by typing in the corresponding key value. If the user by mistake, types in any other key AGMG ignores the wrong entry and waits for the correct choice.

The first option in the main menu leads the user to 'AGMG - GEOMETRY DATA' table, shown in Fig. II.8. The geometry data table displays the name of the parameter, and the current value of the parameter in the current unit system chosen in a tabular format and prompts the user to enter new values, if necessary. If the user elects to modify the current data, then the cursor moves to the first parameter in the table. At this point the user can modify the current value of the first parameter by typing in the new value and by pressing the 'RETURN' key. Just pressing the 'RETURN' key without any new values retains the current value unchanged. Then the cursor moves to the next parameter in the table and the same process is repeated

AGMG -- MAIN MENU

1. CHANGE/DISPLAY GEOMETRY DATA
2. CHANGE/DISPLAY MODEL DATA
3. GENERATE THE MESH
4. ENTER USER DEFINED ELEMENT OPTION
5. PLOT
6. EXIT

Fig. II.7: AGMG - main menu

until all the parameters in the table are entered. Once all the parameter values have been entered, AGMG prompts the user to find out any more changes are required. If the user elects to change any of the parameter values then the cursor moves next to the first parameter in the table and the above mentioned process is repeated. Otherwise the control returns to the main menu.

The second option in the main menu leads the user to the 'AGMG - MESH DATA' table, shown in Fig. II.9. This table is used to enter the finite element mesh model parameters, namely, the type of element, the number of elements in the X-direction, the number of the elements in the Y-direction, etc.. The model data can be entered and/or modified in the same manner as in the geometry data table. In addition, the user can also instruct AGMG to read the required data from a data file and then use the data tables to display and to modify the data.

One of the novel features of AGMG is the following: As the cursor moves to each parameter in the tables, the restrictions on that parameter, the available options and the default selections are displayed at the bottom portion of the display. This helps the user to make the right choice. And if the user, despite these messages, enters wrong data then the error message 'ERROR - TYPE IN AGAIN' is flashed at the last line of the display. Till the user

AGMG - GEOMETRY DATA

PITCH DIA (in)	3.50	RIM THICK (in)	0.15
DIA PITCH	0.00	HUB THICK (in)	0.00
PR ANGLE (deg)	20.00	ADDENDUM (in)	0.13
HLX ANGLE (deg)	0.00	DEDENDUM (in)	0.14
FACE WIDT (in)	0.25	WORK DEPT (in)	0.25
ROOT RAD1 (in)	0.05		

DO YOU WANT TO CHANGE ANY GEOMETRY DATA ? (Y/N):

Fig. II.8: AGMG - geometry data table

AGMG - MODEL DATA

NXD	0	IETYP	0
NINVD	0	ISMTH	0
NFIELD	0	NNDIR	0
NROTD	0	NEDIR	0
NRIMD	0	NDIR	0
NZD	0	NFN	0
NCT	0		

NINVD SHOULD BE GREATER THAN THREE AND EVEN

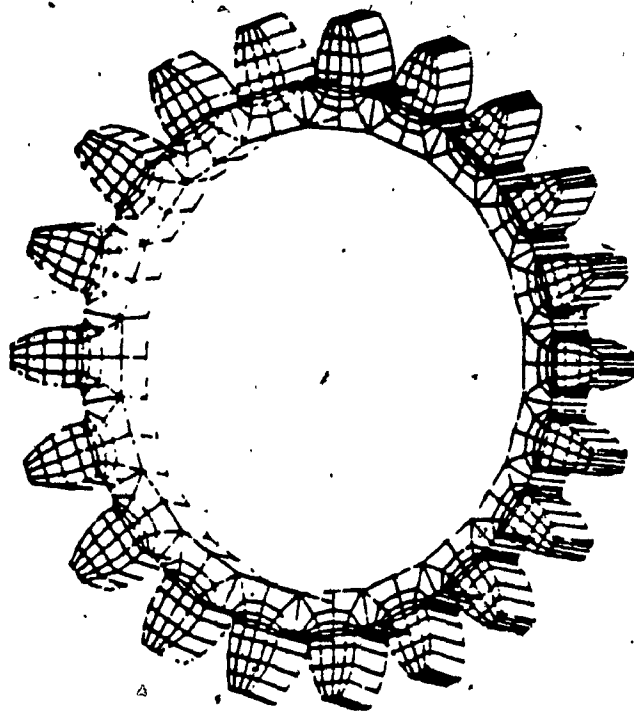
Fig. II.9: AGMG - mesh data table

enters the proper value, the cursor will not move to the next parameter. These self diagnostic messages and graceful error recovery procedures make AGMG less error prone and very easy to use even for the first time user.

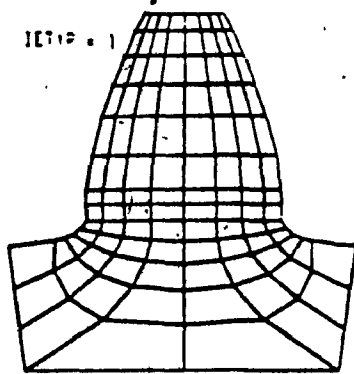
The third option in the main menu instructs AGMG to generate the mesh with the current geometry and mesh data. Once the mesh is generated successfully, the control returns back to the main menu. Also, if the current geometry and/or mesh data tables are incomplete, then an error message is flashed on the display and control returns to the main menu. At this point the user can enter option 1 or 2 to complete the required table and proceed to option 3 again.

The generated mesh can be altered locally by using the fourth option in the main menu, namely the 'user defined element' option.

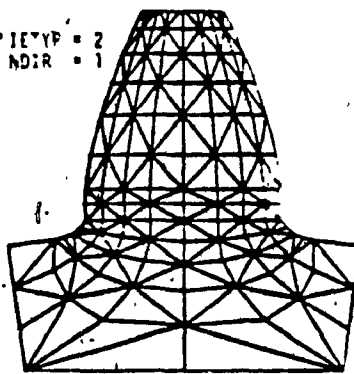
The fifth option in the main menu is used to output the generated mesh data in the form of data files and/or in the form of plots. Once again only if the third option in the main menu is completed successfully, the user can enter the fifth option. Otherwise control is returned to the main menu with an error message. In the plot mode the user has the option to use the basic plotting routines built within the AGMG or to use the powerful MOVIE.BYU graphics program. The routines within AGMG can only plot the mesh generated



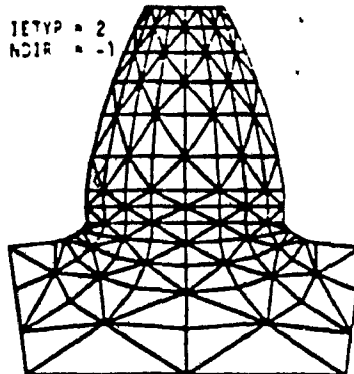
IETYP = 1



IETYP = 2
NDIR = 1



IETYP = 2
NDIR = -1



NID = 8
NINID = 8
NFIELD = 3
NROD = 2
NPRM = 3
ISM = 1

Fig. II.10: Examples of different meshes generated with ~~ACMG~~

and manipulation of mesh model is not currently possible. However, the second option in the plot mode leads the user into the MOVIE.BYU program with the required data already read. The user can use any of the MOVIE.BYU commands to manipulate and display the mesh in color or in monochrome. The control returns to the main menu after exiting from the plot mode. At this point the user has option to choose any one of the first four options to modify the data and regenerate the mesh. Or by choosing option 6 the user can exit AGMG. Fig. II.10 shows some of different meshes generated with AGMG.

APPENDIX III

SELECTION OF SHAPING FILTER PARAMETERS

In chapter 4, a linear, second order shaping filter of the form,

$$\dot{v}_f(t) = A_f(t) v_f(t) + E_f w(t), \quad (\text{III.1})$$

with

$$A_f(t) = \begin{bmatrix} 0 & 1 \\ -a_2 & -a_1 \end{bmatrix} \quad (\text{III.2})$$

$$E_f = \{ 0, 1 \}^T \quad (\text{III.3})$$

$$v_f(t) = \{ e_r, \dot{e}_r \}^T \quad (\text{III.4})$$

is used to generate the random component of the transmission error signal. By varying the filter parameters a_1 , and a_2 , different time correlated error signals can be generated for the same stationary, Gaussian white noise input. In this appendix, a procedure for the proper selection of the filter parameters to obtain an error signal with specified statistics is described.

Equation (III.1) can be rewritten in terms of the damping ratio ξ and the natural frequency ω_n as,

$$\ddot{e}_r + 2 \xi \omega_n \dot{e}_r + \omega_n^2 e_r = w(t) \quad (\text{III.5})$$

Thus,

$$a_1 = 2 \xi \omega_n \quad (\text{III.6})$$

$$a_2 = \omega_n^2 \quad (\text{III.7})$$

The corresponding autocorrelation function will be [20],

$$\psi(t) = \frac{\sigma^2}{\cos(\eta)} e^{-\xi \omega_n t} [\cos(\sqrt{1-\xi^2} \omega_n t - \eta)] \quad (\text{III.8})$$

$$\eta = \tan^{-1} \frac{\xi}{\sqrt{1-\xi^2}} \quad (\text{III.9})$$

$$\omega_d = \sqrt{1-\xi^2} \omega_n \quad (\text{III.10})$$

where,

σ = the standard deviation of the transmission error signal,

The parameters σ , η , ξ , and ω_n are all chosen to fit the estimate of the autocorrelation function of the required transmission error signal. For instance, the ω_n is chosen to fit the observed resonant peak in the power spectral density (PSD) plot. Similarly the frequency at which the PSD plot peaks will give the ω_n . Also from the autocorrelation function plot, the variance σ^2 can be obtained since,

$$\psi(0) = \sigma^2 \quad (\text{III.11})$$

Once these parameters are known, the shaping filter parameters a_1 , and a_2 can be obtained from the equations (III.6) and (III.7).

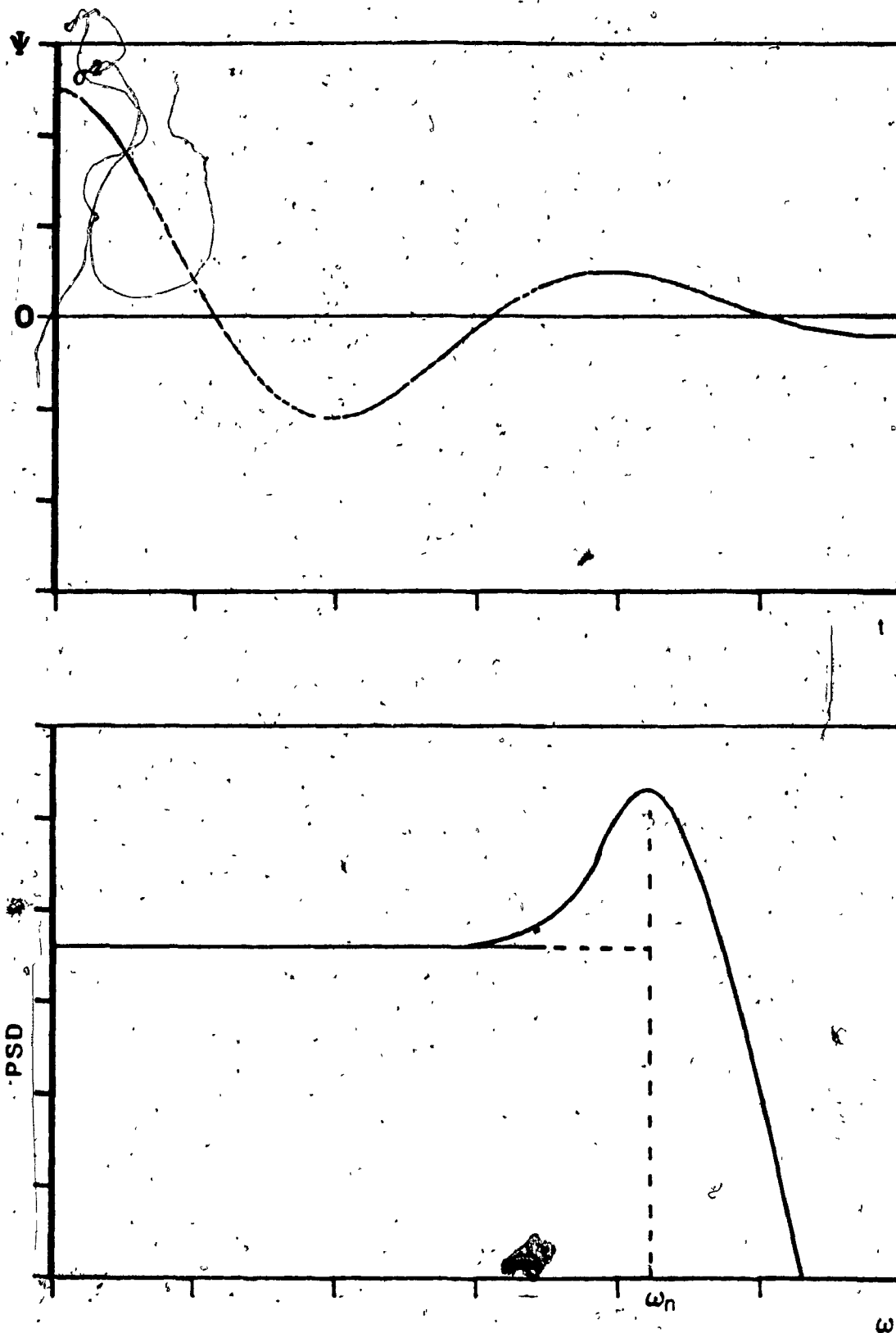


Fig. III.1: Autocorrelation and PSD plots for a second order Markov process

APPENDIX IV

FORTRAN PROGRAM FOR FATIGUE SIMULATION

```

PROGRAM CYCLE COUNT SIMUL
COMMON E(50), S(50)
COMMON /MATER/ FSC, FSE, FDC, FDE, CSC, CSE, EE
I = 1

1  READ IN MATERIAL PROPERTIES
   C C C
   READ *, FSE, FSE, FDC, FDE, CSC, CSE, EE
   C C C
   READ IN STRAIN PEAK VALUES E(I)
   C C C
   K = 0, DENOTES NO MORE DATA TO READ
   C
   CALL DATAIN (E(I), K)
   IN = 1
   IF (E(I).LT.0.) IN=-1
   C C C
   COMPUTE STRESS BASED ON CYLIC STRESS-STRAIN CURVE
   C C C
2  IF (I.EQ.1) CALL STRESS (IN, 0., 0., E(I), S(I))
   I = I+1
   IN = -IN
   C C C
3  CALL DATAIN (E(I), K)
   IF (K.NE.0) GO TO 5
   IF (E(I).EQ.E(I-1)) GO TO 3
   C C C
   COMPUTE STRESS CORRESPONDING TO E(I) BASED ON HYSTERSIS CURVE
   C C C
4  CALL STRESS (IN, E(I-1), S(I-1), E(I), S(I))
   IF (I.LT.3) GO TO 2
   II = I-2
   IF (IN*(E(II)-E(I)).GT.0.) GO TO 2
   C C C C C
   CLOSED LOOP IDENTIFIED BETWEEN E(II) AND E(II+1)
   COMPUTE MEAN STRESS AND DAMAGE FRACTION
   C C C C C
   CALL DAMAGE (II, DAMS)
   E(II) = E(I)
   I = II
   GO TO 4
5  IF (IN*(E(I-1)-E(I))) 7, 8, 6
6  IN = -IN
   I = I-1
7  E(I) = E(I)
   GO TO 4
   C C C
   COMPUTE NUMBER OF BLOCKS TO FAILURE (BTF)
   C C C
8  BTF = 1./DAMS
   PRINT*, 'NUMBER OF BLOCKS TO FAILURE = ', BTF
   CALL EXIT
   END

```

```

SUBROUTINE STRESS(IN, SRE, SRS, EP, ST)
COMMON /MATER/ FSC, FSE, FDC, FDE, CSC, CSE, EE
STRES(ST, K) = (IN*(ST-SRS)/(K*EE)) + (IN*(ST-SRS)/
1 (K*CSC))**(1./CSE) - (IN*(EP-SRE)/K)
K = 1
IF (SRE.NE.0. .OR. SRS.NE.0.) K = 2
ST = SRS
DST = 50.
S2 = STRES (ST, K)
DO 10 I = 1, 500
S1 = S2
S2 = STRES (ST, K)
IF (S1*S2 .LT. 0.) DST = -DST/2.
IF (ABS(S2) .LE. 0.1E-04) GO TO 20
10 ST = ST + IN*DST
PRINT *, ' NO CONVERGENCE'
20 RETURN
END

```

C
C
C

```

SUBROUTINE DAMAGE(NN1, DAMS)

```

COMPUTE DAMAGE ACCORDING TO STRAIN-LIFE CURVE

```

COMMON E(50), S(50)
COMMON /MATER/ FSC, FSE, FDC, FDE, CSC, CSE, EE
NN2 = NN1+1
EA = ABS(E(NN1)-E(NN2))/2.
SA = ABS(S(NN1)-S(NN2))/2.
SM = (S(NN1)+S(NN2))/2.
SA = SA/(1.-(SM/FSC))
DAM = 2.*(FSC/SA)**(1./FSE)
DAMS = DAMS+DAM
RETURN
END

```

- FSC = fatigue strength coefficient
- FSE = fatigue strength exponent
- FDC = fatigue ductility coefficient
- FDE = fatigue ductility exponent
- CSE = cyclic strength coefficient
- CSE = cyclic strength exponent
- EE = modulus of elasticity
- E(I) = strain peak value
- S(I) = stress peak value
- DAMS = accumulated damage
- BTF = number of blocks to failure
- IN = index used to indicate the slope
- K = index used to identify end of data